CRANFIELD UNIVERSITY

Liu, Chengyuan

Turboelectric Distributed Propulsion System Modelling

School of Engineering

PhD Thesis
Academic Year: 2010 - 2013

Supervisor: Prof. Riti Singh;
Dr. Panagiotis Laskaridis; Dr. Georgios Doulgeris
December 2013

CRANFIELD UNIVERSITY

School of Engineering

PhD Thesis

Academic Year 2010 – 2013

Liu, Chengyuan

Turboelectric Distributed Propulsion System Modelling

Supervisor: Prof. Riti Singh;
Dr. Panagiotis Laskaridis; Dr. Georgios Doulgeris
December 2013

This thesis is submitted in partial fulfilment of the requirements for the degree of PhD

ABSTRACT

The Blended-Wing-Body is a conceptual aircraft design with rear-mounted, over wing engines. Turboelectric distributed propulsion system with boundary layer ingestion has been considered for this aircraft. It uses electricity to transmit power from the core turbine to the fans, therefore dramatically increases bypass ratio to reduce fuel consumption and noise. This dissertation presents methods on designing the TeDP system, evaluating effects of boundary layer ingestion, modelling engine performances, and estimating weights of the electric components. The method is first applied to model a turboshaft-driven TeDP system, which produces thrust only by the propulsors array. Results show that by distributing an array of propulsors that ingest a relatively large mass flow directly produces an 8% fuel burn saving relative to the commercial N+2 aircraft (such as the SAX-40 airplane). Ingesting boundary layer achieves a 7-8% fuel saving with a well-designed intake duct and the improved inlet flow control technologies. However, the value is sensitive to the duct losses and fan inlet distortion. Poor inlet performance can offset or even overwhelm this potential advantage. The total weight of the electric system would be around 5,000-7,000 kg. The large mass penalties further diminish benefits of the superconducting distributed propulsion system. The method is then applied to model a turbofan-driven TeDP system, which produces thrust by both the propulsors array and the core-engines. Results show that splitting the thrust between propulsors and core-engines could have a beneficial effect in fuel savings, when installation effects are neglected. The optimised thrust splitting ratio is between 60-90%, the final value depends on the propulsor intake pressure losses and the TeDP system bypass ratio. Moreover, splitting the thrust can reduce the weight of the electric system with the penalty of the increased core-engine weight. In short, if the power density of the superconducting system were high enough, turboshaft-driven TeDP would be preferable to power the N3-X aircraft.

Keywords:

BLI, TeDP, Distortion, NASA N3-X Aircraft, Turbogenerator, Propulsor, thrust split ratio

ACKNOWLEDGEMENTS

I am fortunate to have been surrounded by so many good and brilliant people in my years at Cranfield. The members of my reading committee are prominent in this group. This research would not have been possible if not for tremendous support from Professor Riti Singh. He successfully maintained adequate funding during the course of my work. His guidance and timely advice were necessary to successfully complete my work. His faith in my abilities allowed me to develop my problem-solving skills to the highest level.

Secondly, I would like to sincerely thank Dr. Panagiotis Laskaridis and Dr. Georgios Doulgeris, my supervisor. Their advices and guidance have been helpful during all the duration of the project. Working for and with them has been greatly rewarding and a true pleasure. I also acknowledge gratefully the assistance received from Dr. A.J.B Jackson, who has shared his knowledge on engine performances; Dr. Y. Li, who gave comments on my thesis.

Last but most certainly not least, I must acknowledge two people whom I admire and deeply respect. Without their support, love, and advice, I could never have accomplished any of this work. As a small token of thanks, I dedicate this work to my parents, Liu, Qilin and Yan, Guangming. I owe all that I have and have accomplished to them.

TABLE OF CONTENTS

LIST OF FIGURES

LIST OF TABLES

LIST OF ABBREVIATIONS

Acronyms

AC	=	alternating current
ADP	=	aerodynamic design point
AR	=	Average blade height/Average blade chord
BL	=	boundary layer
BLI	=	boundary layer ingesting
BLT	=	boundary layer thickness
BPR	=	bypass ratio
BSCCO	=	bismuth strontium calcium copper oxide
BWB	=	blended wing body
C.V.	=	control volume
CESTOL	=	cruise-efficient short take-off and landing
CFD	=	computational fluid dynamic
cFPR	=	core engine fan pressure ratio
CMF	=	corrected mass flow rate, defined by Eq.6.8
CN	=	corrected non-dimensional shaft speed
CPF	=	cooling power factor, defined by Eq.6.28
DC	=	direct current
DC(60)	=	circumferential distortion parameter
DP	=	design point
EF	=	efficiency penalty
Eff	=	efficiency
EIS	=	entry into service
EM, E-motor	=	electric motor
FPR	=	fan pressure ratio
HP	=	horse Power
HPC	=	high pressure compressor

HPT	=	high pressure turbine
HTR	=	hub to tip ratio
HTS	=	high temperature superconductor
HWB	=	hybrid wing body
ISA	=	international standard atmosphere
LF	=	loss factor
LH2	=	liquid hydrogen
LPC	=	low pressure compressor
LPT	=	low pressure turbine
Ma	=	Mach number
NDP	=	non-dimensional fan power, defined by Eq.6.11
NMF	=	Non-dimensional mass flow rate
NPER	=	non-dimensional shaft speed, defined by Eq.6.9
NPR	=	nozzle pressure ratio
NPSS	=	numerical propulsion system simulation
OPR	=	overall pressure ratio
PAI	=	propulsor airframe integration
PCM	=	parallel compressor method
PL	=	pressure loss
PMAD	=	power management and distribution
PPR, FPR	=	propulsor fan pressure ratio
PR	=	pressure ratio
PSC	=	power saving coefficient
PSM	=	parallel stream method
R	=	specific gas constant
Re	=	Reynolds number
RPM	=	rotation per minute
RTO	=	rolling take off
SFC	=	specific fuel consumption

SFW = subsonic fixed wing

STOL = short take-off/landing

T/O = take off

TeDP = turboelectric distributed propulsion

TET = turbine enter temperature

TSR = thrust split ratio

TSFC = thrust specific fuel consumption, kg/N/s

WRF = wake recovery factor

Symbols

C_V = nozzle coefficient

C_p = specific heat at constant pressure

H_{avg} = average value of the boundary layer shape factor

LF_{mix} = the mixing loss factor

R_{Ma} = mass-averaged inlet Ma of the boundary layer to a given height

R_{Pt} = mass-averaged inlet total pressure of the boundary layer to a given height

T_N = net thrust

η_{isen} = isentropic efficiency

η_{poly} = polytropic efficiency

A = area

a = *sound speed*

alt = *altitude*

b = *span of ingested boundary layer*

D = drag

d = diameter

F = thrust

f = propulsor fan cap factor

H, h = Propulsor capture height

I	=	current
K	=	Pseudo Energy Factor
K_F, K_F	=	fan proportionality constant
L	=	propulsor intake width
m	=	mass flow
N	=	number of propulsors
p	=	static pressure
P, Pt	=	total pressure
R	=	*splitter ring*
T	=	total temperature
t	=	static temperature
V,U	=	velocity
W	=	weight
W	=	power
ρ	=	density
σ_t:	=	*rotor blade tip solidity*
Φ	=	fuel saving coefficient
r	=	ratio of the specific heat
δ	=	boundary layer thickness
θ	=	boundary layer momentum thickness
μ	=	efficiency
τ	=	torque
ω	=	rotating speed

Subscripts

∞	=	freestream condition
$_A$	=	airframe
$_B$	=	core engine bypass
$_{BL}$	=	boundary layer
$_{C, CE}$	=	core engine

$_{F}$ = fan

$_{FS}$ = free stream

$_{H}$ = high velocity section

$_{j}$ = jet

$_{L}$ = low velocity section

$_{M}$ = maximum

$_{N}$ = net

$_{o}$ = ambient

$_{P}$ = propulsor

$_{S}$ = static conditions

$_{T}$ = tip

$_{w}$ = wake

Chapter I

Introduction

Civil aviation evolution is widely due to the improvements of gas turbine technology over the last fifty years. Principles of gas turbines have been underlying quite a long time before the rise of aviation around the first part of the twentieth century. Indeed, gas turbines principles were described in a British patent took out by John Barber in 1791. Then it took almost 150 years before the principles described in this patent were turned into real products by Frank Whittle in 1943. Gas turbine technologies have been continuously improved by researchers. Since the late 1950s, overall pressure ratio has risen from about 15 to over 40 and take-off turbine inlet temperature has risen from about 1400 K to 1800 K. Increasing passenger numbers over the past decades have widely increased aircraft size, leading to the need for more powerful engines. Meanwhile, growing numbers of emissions requirements have led to pollutant levels released by aero engines being more widely taken into account in the design process. According to IATA, the international air transport association, the world's airlines made a combined loss of $2.8bn (£1.9bn) in 2010 even with a continued growth of passengers and freight air traffic [8]. The main reasons include the 3 – 3.5% increasing rate of annual fuel consumption, increased fuel price, heavy taxes for emissions, etc. So in the foreseeable future, new generation commercial airplane should have lower fuel consumption, lower emission and noise.

Bypass ratio (BPR) of current turbofan engines are unlikely to exceed 12, due to the fan tip speed limitation. That is because, to increase BPR, a larger fan is needed. This leads to higher fan tip speed. Geared turbofans employ a gearbox between the fan shaft and the low pressure turbine shaft in order to reduce the fan shaft speed and thus to reduce the fan tip speed. Its BPR, therefore, can be as high as 20. However, if we keep increasing the BPR, the gearbox efficiency reduces and its weight as well the weight of the engine nacelle increases eliminating the initial benefits. So for higher BPR engine, open rotor concept should be used as it can

dramatically increase the BPR without increasing the weight too much. Higher propulsive efficiencies are achieved for turbofans by increasing the bypass ratio through increasing the fan diameter but there is a diminishing return to this improvement as nacelle diameters and consequently weight and drag also increase. Open rotor engines remove this limitation by operating the propeller blades without a surrounding nacelle, thus enabling ultrahigh bypass ratios to be achieved. However, it is difficult to control its noise, especially at take-off.

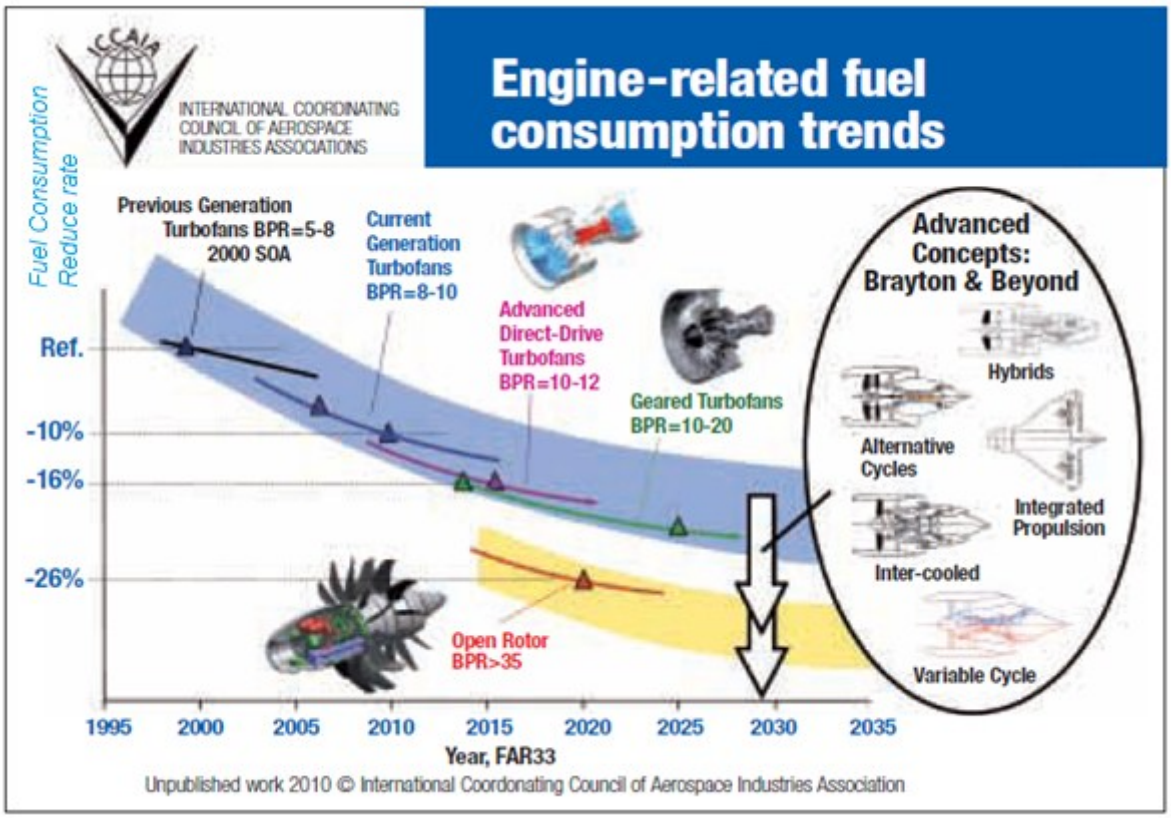

Figure 1.1 Next Generation Engines for Commercial Airplane [17]

In 2005, NASA introduced the concept of turboelectric distributed propulsion system (TeDP) on a bended wing body airframe as the following figure shows. It replaces the fan stage (in turbofans) with a number of small motor driven fans (propulsors). All the propulsors are embedded into the upper rear surface of the airframe with a common nacelle. Turboshaft engine is used to produce power to the motors. Different from turbofans, the TeDP system has two parts: the core-engine, which comprises a turboshaft engine and a generator, is used to generate power; the propulsor, which comprises a propel fan and a motor, is used to produce thrust.

Superconducting technologies are used to transmit the power from the core engine to propulsors.

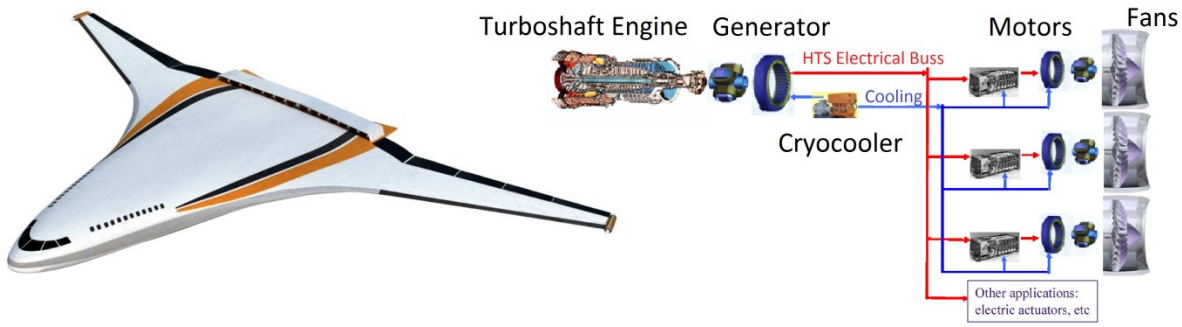

Figure 1.2 NASA N3-X Aircraft with its Propulsion System [17]

Its benefits, firstly, include replacing a single large diameter fan with multiple smaller fans and embedding them into the airframe. This novel design reduces the total propulsive weight and increases the propulsive efficiency and aircraft landing clearance. Secondly, the shaft speed of the fans is independent of the turbine engine shaft speed. The electrical system functions as a gearbox with an arbitrary gear ratio; this allows the turbine in the turbogenerator to be optimised independently without considering the fan tip speed limitation. Moreover, superconducting power transmission technology has higher efficiency than mechanical gearbox, which can save 3% to 4% power. Thirdly, engine noise can be effectively controlled because the core, or turbogenerator, is used to produce electricity but not thrust; the core jet noise can be reduced. If the turbogenerator noise remains too high, its position can be changed without disturbing the location and the performance of the propulsors. Another noise source is the propulsors, located on the upper surface of an airframe. Airframe serves as a noise barrier during take-off and landing. Simple mechanical structure also reduces mechanical noise. Furthermore, the diameter of the turbogenerator is small because of the absence of a fan in the core; larger, high efficiency turbo machinery can be used. The safety and reliability of the system also improved due to more fans used.

1.1 Aims and Objectives

This study is in NASA's N+3 project of subsonic fixed wing body. So the main aim is to find a new propulsion system to meet N+3 technical goals. Distributed propulsion

system with superconducting electric system was chosen due to its potential on fuel reduction. The objectives of this study include:

- Developing the TeDP system design methodology.
- Comparing results with NASA's calculation results.
- Modelling the TeDP system performances on a fixed wing body airframe.
- Modelling the boundary layer ingesting (BLI) and analysing the impacts on engine performances.
- Analysing performance of the electric systems, including the superconducting generator, the motor, and the cooling system; as well as the impacts on the whole propulsion system performance.
- Figuring out the method to match performances of the motor and the fan stage at off-design conditions.
- Developing the method to estimate weight of all the electric components.
- Designing alternative propulsor configurations for the TeDP system.

1.2 Scope

The background of the topic of this thesis is described in chapter 2, which reviews briefly the developing of commercial airplane engine and the future challenges. Also, a few comments are made on the benefits and drawbacks of using a TeDP system, as well as the technical challenges.

The first main technical element presented in chapter 3 is the use of Cranfield tools to model performances of a TeDP system introduced by NASA and to compare with their results. This chapter starts with an introduction of NASA's TeDP system design concept, and their method to model boundary layer ingestion. Then, propulsor modeling methodology by Matlab and core-engine modeling methodology by Turbomatch are given. Finally, a back-to-back comparison with NASA's results is made.

The second main technical element presented in chapter 4, 5 and 6 is the development of our own tools to model the distributed propulsion system with boundary layer ingestion. It includes the method to model boundary layer ingestion

(chapter 4); new TeDP system (whose core engine has its own fan, free power turbine and nozzle and therefore can produce both power and thrust) designing and design point performance analysis (chapter 5); and off-design methodology with BLI (chapter 6). Previous studies are also introduced and explored. The third main element (chapter 6) is the development of methods to analyze the performance of the electrical components, including the motor, the generator, the cryocooler and the inverter. The method to estimate their weights is also introduced.

The last part (chapter 7) puts forward a novel TeDP system propulsor conceptual design to eliminate the negative impacts of intake distortion caused by BLI. The propulsor can be used on both blended-wing-body and tube-and-wing airplanes.

Chapter II

Background

The intricate challenges of meeting future environmental goals in commercial aviation require a cross-disciplinary effort that focuses on: feasible propulsion systems, reduced fuel consumption, aviation safety and reliability, noise reduction, and optimized aircraft design to achieve desirable flight attributes. With a constant increase of air passengers, and the demands for technological innovation to reduce harmful emissions and jet noise, the impact of commercial propulsion systems becomes even more pronounced. Air transport's contribution to climate change represents 2% of human-induced CO2 emissions (and 12% of all transport sources). Flights produce 628,000,000 tonnes of CO2 yearly Worldwide, it is estimated that the equivalent of 1300 new international airports will be required by 2050 with a doubling of the commercial aircraft fleet [2]. The challenge facing aviation is to meet the predicted growth in demand for air travel (increasing 4-5% per annum over the next 20 years) and ensures the environment is protected. In 2005, two leading associations, European Union (EU) and National Aeronautics and Space Administration (NASA), gave their future plans for the next generation airplane.

Clean sky, funded by EU, aims to produce and negotiate constructive proposals that will achieve a significant further reduction in the impact of the noise and emissions of the airplanes. This project includes promoting environmental awareness within the industry; informing the public and Government about the aviation's environmental performance; and establishing and promote best practice in, for example, airport and flight operations. American government provided their technology goals for future timeframe, the N+1, N+2, and N+3 represent the year 2015, 2020 and 2030, targeted at reducing fuel consumption, noise and emissions. Table 2.1 and Table 2.2 list the technical goals. It is widely accepted that to achieve these longer term aims there will need to be a significant step change in the technologies of future aircraft as well as operations.

Table 2.1 The environmental objectives of Clean Sky Plan [1]

Program	Smart fixed wing aircraft	Green regional	Green rotorcraft	Sustainable & green engines	Systems for green operations	Eco Design
Activities	1. Active wing 2. New aircraft configurations	1. Advanced aerodynamics 2. Lower weight structure	1. New power plants 2. Innovative blade and rotor 3. New aircraft configuration	1. Advanced LP & HP system 2. New engine concepts	1. Mission & trajectory management 2. Aircraft engine management	Whole life cycle environmental impact analysis
Targets	CO2 ~ 12 to 20% Noise ~ 10 dB	CO2 ~ 12 to 20% Noise ~ 10 dB	CO2 ~ 26 to 40% NOx ~ 53 to 65% Noise ~10dB	CO2 ~ 15 to 20% NOx ~ 60% Noise ~ 18 dB	CO2 ~ 10 to 15% Noise ~ 9 dB	CO2 ~ 10%

Table 2.2 NASA's technology goal for future subsonic fixed wing body [13]

	N+1 (2015 EIS) Tube and wing	N+2 (2020 EIS) Hybrid wing body	N+3 (2030 EIS) Advanced aircraft concept
Noise	-32 dB	-42dB	55 LDN at average airport boundary
LTO NOx	-60%	-75%	Better than -75%
Fuel burn	-33%	-40%	Better than -70%
Field length	-33%	-50%	Exploit metroplexa [a] concepts

[a] Concepts that enable optimal use of the airports within the metropolitan area.

In order to meet future traffic demand with limited airport access, revolutionary airplane concepts are needed that can utilize smaller airports. For these new concepts to be successful, they must dramatically reduce take-off and landing noise, due to the urban setting of many of these fields, and yet still carry an economically viable number of passengers and freight over transcontinental distances at current jet transport speeds. At the same time, these new aircrafts must dramatically reduce the energy consumption and environmental impacts. In response to growing aviation demands and concerns about the environment, NASA's Subsonic Fixed Wing (SFW) project identified four "corners" of the technical trade space—noise, emissions,

aircraft fuel burn, and field length—for aircraft design. Distributed propulsion system was chosen to power the aircraft. Distributed propulsion is based on dividing up the thrust for the beneficiary gain of noise reduction, shorter take-off and landing, enhanced specific fuel consumption and flight range.

2.1 Historical Review of Distributed Propulsion Technology

It is well known that the jet engine was conceived as a possible means of aircraft propulsion during the 1920s and 1930s. During the 1940s the jet engine was very much in its infancy, in the form of turboprops, powered aircraft in airline service. The 1950s saw the development of the axial compressor into a viable machine, which spawned new turbo-jets and new low bypass ratio turbofans. In 1954, Griffith [4] replaced the earlier propositions of propellers with gas turbines and presented the concept of an aircraft with a master combustion engine unit in combination with numbers of gas turbines that were placed in the span wise direction of the wing (Fig.2.1).

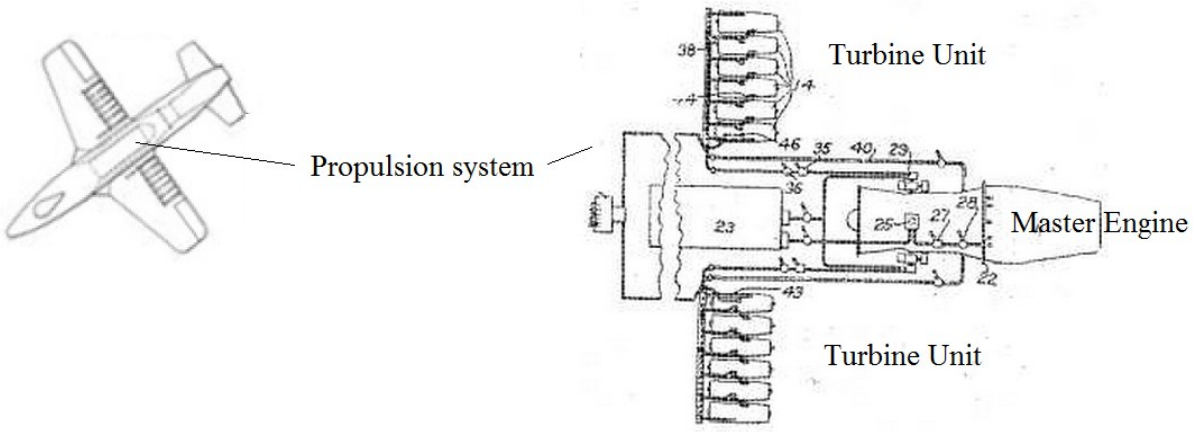

Figure 2.1 Distributed Propulsion Concept by Griffith [4]

In 1964, Reyle's [54] put forward an aircraft concept (Fig.2.2) that could use gas turbine technology for the engine disposed between the ducting surfaces and nuclear engines in the nacelles. Reyle envisioned that this concept would contribute to power-weight ratio enhancements, but did also recognize radiation issues in the event of an aircraft crash. Future nuclear concepts have not entirely been abandoned, but it is not a good choice due to the safety issue.

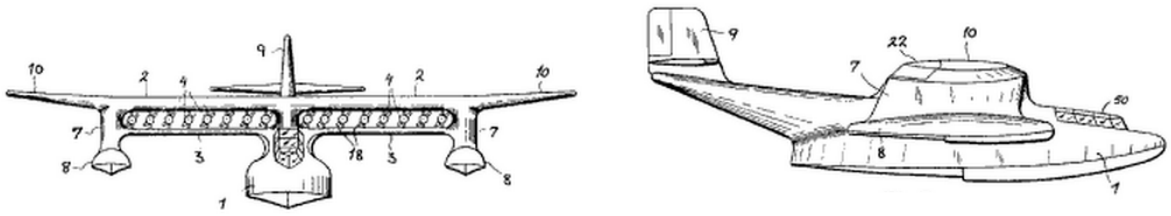

Figure 2.2 The Distributed Propulsion Concept by Reyle [54]

From 1970s to 1990s, NASA proposed a number of distributed propulsion concepts and detailed studies on airframe and propulsion system integration [36, 56]. One of the early concepts was shown in Fig.2.3. The aircraft was based on a conventional ‘tube-and-wing’ airframe configuration with 16 tip-driven fans spread along the top surface near the wing trailing edge. The tip-driven fans with fan pressure ratio of 1.25 were powered by high-pressure discharge air from the low pressure compressor stages and mounted on a hinged flap to achieve high lift via super circulation. In addition, the massive suction effect in front of inlets created additional lift on the airframe and delayed flow separation on the wing upper surface [36].

Figure 2.3 Short Take-off Landing (STOL) Transport Using Low Compressor Discharge Tip-driven Fans [36]

NASA small business innovative research centre conducted a system study of integration and advanced cryogenic electric propulsion system onto a 150-passager STOL airliner as fig.2.4 shows. The airplane is the integration of the superconducting-electric-motor-driven fans within the wing. The inboard wing is therefore separated into top and bottom sections, and all the motor-driven fans are completely embedded into the airframe. This configuration reduces the wing weight and it’s bending moment, because the distributed fans and the use of the common nacelle as wing rib structure provide stress relief to the wing structure. In addition, a

favourable aerodynamic advantage exists such that at low speed, thrust vectoring of a two-dimensional low temperature nozzle may provide super circulation of airflow around the airfoil for a large improvement in lift coefficient. The vehicle used liquid hydrogen both as the fuel and cooling fluid. Liquid hydrogen has a boiling point of 23 K at 2 atm. Boiling it is therefore capable of cooling the electric system. NASA predicted, although the study was very preliminary in nature, the propulsion system features along with the vehicle configuration itself did certainly point toward large reduction in fuel burn.

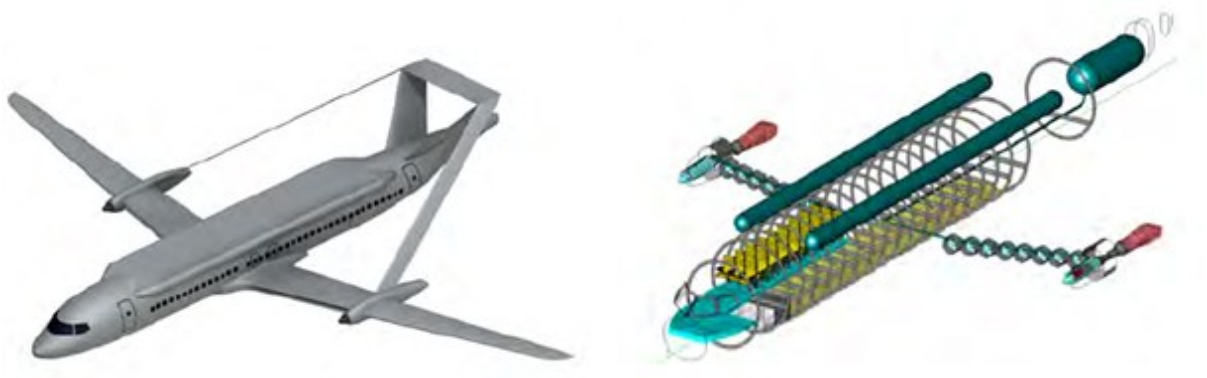

Figure 2.4 The ECO-150 Vehicle Concept by NASA [36]

In 2006, a cruise-efficient STOL aircraft was proposed by NASA (Fig.2.5) based on a high subsonic hybrid wing body, or blended wing body [34]. The HWB configuration was chosen due to its high cruise efficiency, low noise characteristics, and a large internal volume for integrating embedded propulsion system.

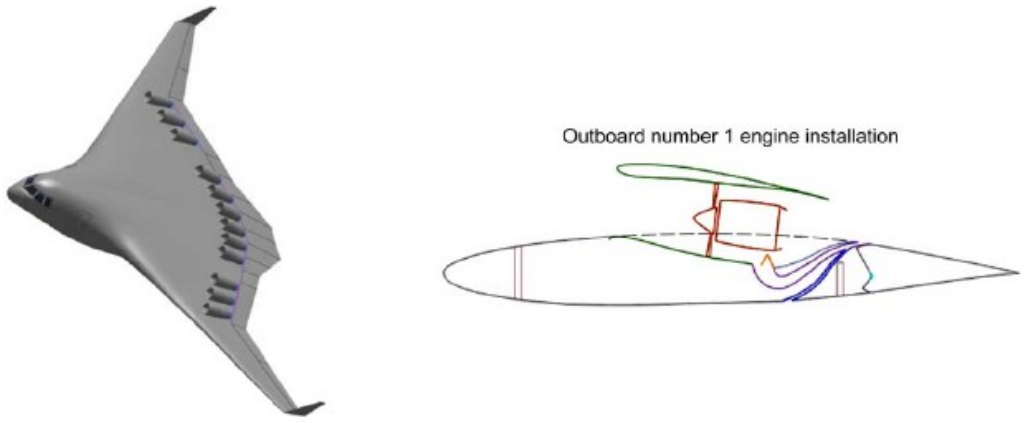

Figure 2.5 Cruise-Efficient Short Take-off and Landing Configuration [34]

The propulsion system employs 12 small low bypass ratio engines partially embedded within the wing structure and mounted along the wing upper rear surface. This configuration enables short take-off and landing, as well as low noise. These

characteristics of the aircraft may enable 24-hour use of the underutilized regional and city-centre airports to increase the capacity of the overall airspace while still maintaining efficient high subsonic cruise flight capability [17]. Embedded distributed propulsion enables the use of low pressure fan-bypass engines, wherein a high-aspect-ratio slot nozzle is used in conjunction with a slotted airfoil with the nozzle exhaust pumping through the slot to increase circulation and lift. The small diameter engines with a bypass ratio of 9.4 have forward noise shielding and employ mixer nozzles to increase the jet noise frequency and move the jet noise source locations forward. The forward jet source noise can then be shielded by airframe surfaces to reduce aft and side line noise.

In 2004, a distributed propulsion concept employing a dual fan driven by one engine core on a HWB airframe was studied by NASA [31]. The Fig.2.6 shows the concept. The propulsion system utilizes a core engine to drive two large-diameter fans via gears and shafts. In this configuration, the core engine is outside the airframe boundary layer flow with almost 100% inlet total pressure recovery, and the dual fans ingest full boundary layer flow to improve propulsive efficiency.

Figure 2.6 The HWB Configuration Using Dual Fans Single Engine Core Propulsion system [31]

The Cambridge-MIT institute future developed this concept and developed the SAX-40 conceptual HWB aircraft using a similar gear-driven multi-fan propulsion concept [51,59]. This aircraft, shown in Fig.2.7, employs three engines and each engine has three fans that are driven by a single core engine. Similar to NASA's studies, this propulsion system has ultra-high bypass ratio and low engine noise, as well as improved propulsive efficiency by ingesting boundary layer.

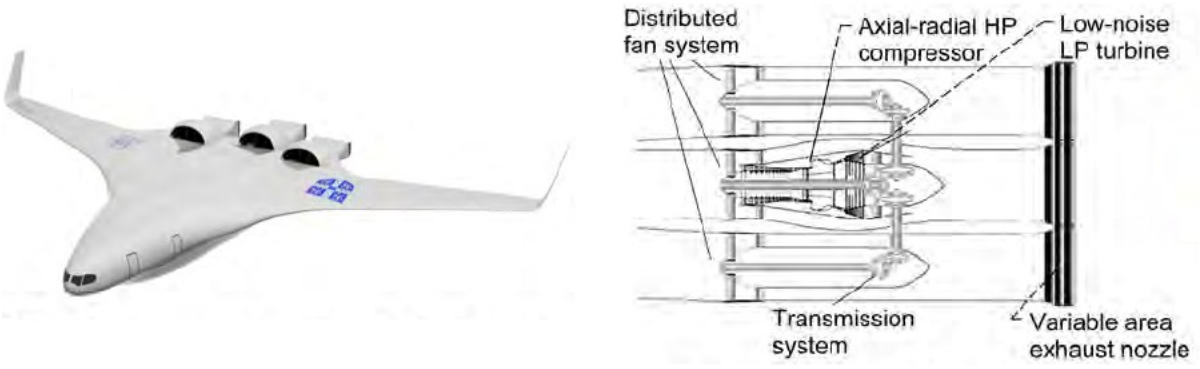

Figure 2.7 the SAX-40 Concept by Cambridge-MIT Institute [52]

2.2 Turboelectric Distributed Propulsion (TeDP) Technology

Drastic changes in the power transmission of the distributed propulsion system for a large transport aircraft was proposed and studied on HWB to improve performance and to reduce environmental impacts even further [33]. This propulsion system uses a new concept called 'turboelectric distributed propulsion'. The Fig.2.8 shows one of the NASA's designing and fig.2.9 is the propulsion system it uses. The vehicle uses 16 distributed electric fans driven by superconducting motors with power coming from two wing-tip mounted turbo-generators. This arrangement allows the utilisation of many small partially embedded fans while retaining the superior efficiency of large core engines, which are physically separated but connected to the fans through electric power lines.

Figure 2.8 A NASA HWB Vehicle Concept Using the TeDP System [33]

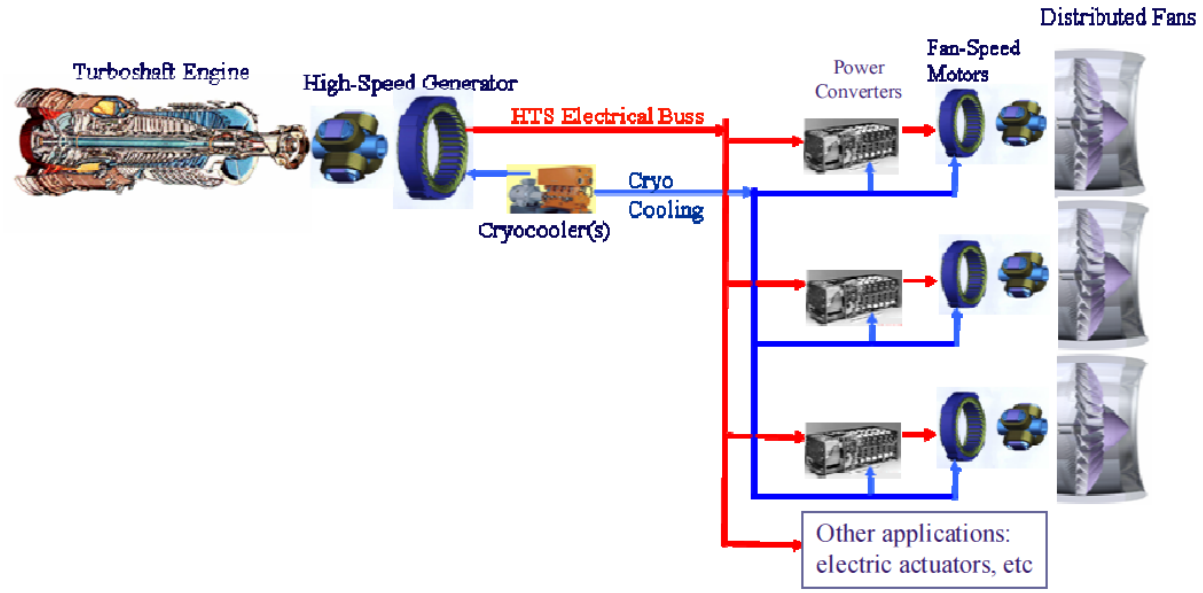

Figure 2.9 Components in a TeDP System [33]

The six major components of a TeDP system are the generator, the motors, the turboshaft engine, the fans, the cooling system, and the cables to transmit power from the generators to motors. It is necessary to use superconducting electric system rather than conventional motors and generators to achieve ultra-high power density, therefore to reduce the weight. Two cooling methods, using liquid hydrogen or cryocooler, can be used to maintain the low running temperature of the superconducting electric system. Although the TeDP system can also be used on a 'tube-and-wing' airframe, the concept is most naturally applied to a BWB body aircraft. The following are identified as possible advantages of using the TeDP system (information comes from technical meeting with NASA and Cranfield in Apr. 2011: ref. [17]):

- Decoupling of the propulsive device from the power producing device. This is the major departure from the current aircraft engine. It is possibly enabling unprecedented performance and design flexibility of the vehicle. The propulsors (motor-driven fans) and the core-engines (turbogenerator) can be located at any locations to optimise aircraft performance and operation.
- The speed of the power turbine shaft is independent of the fan (in the propulsor) shaft speed. The electric system functions as a gearbox with arbitrary gear ratio. This allows the power turbine shaft speed be optimised without considering the fan tip speed limitation.

- Improved fuel efficiency due to ultra-high bypass ratio. The bypass ratio here refers to the ratio of mass flow through all propulsors to the mass flow through all the turbogenerators.
- Integration of large fan areas into the aircraft. Numbers for small fans are used to replace the single large diameter fan of equal area.
- Low power loss due to superconducting technology. Comparing to 4-5% loss for a geared turbofan engine, the transmit power loss of a TeDP system is less than 1%.
- Minimal engine core jet noise. The designed core engine should be as small as possible in order to extract maximum power for the free power turbine, therefore, reduced the core jet exhaust gas temperature and velocity and hence the jet noise. Moreover, if the jet noise remains too high, the turbogenerator can be moved without impacting location of fan nacelle.
- Only cold fan air in the propulsors exhaust nozzle, this enables using low temperature material for the nozzle.
- Improved safety: all the fans can continue operating at a reduced but symmetric thrust while one of the core-engine failed.
- Allows fan power to be provided by devices, such as battery, other than a turbine.
- The turbogenerators could be oversized with regard to the power needs of propulsion to provide significant amounts of electrical power for none propulsion uses while in flight. The full generator capacity would be available for none propulsion uses while on the ground.
- The small fans in the TeDP system have a rotational inertia that is much smaller than that of the single fan stage in a turbofan engine. This low rotational inertia enables the motor changing its rotating speed almost instantly.
- Relatively inexpensive fan blades can be used.
- Improved propulsive efficiency by ingesting boundary layer flow.

However, using a TeDP system may bring following drawbacks:

- High system complexity.
- Increased weight: the cooling system, motor, inverter, generators may weight more than gear box.
- Propulsor intake pressure loss due to BLI

The main objective of the distributed propulsion concept is to achieve optimum vehicle benefits through the integration of aerodynamic, propulsive, structural, and/or operational elements. The concept could be applied to various vehicle configurations such as the traditional tube and wing, the hybrid-wing-body aircraft, and the supersonic aircraft. However, in order to achieve maximum benefits, it will be necessary to design an aircraft with greater emphasis on propulsion airframe integration right from the conceptual design stage [21]. The concept uses superconducting turboelectric generators, motors, and transmission lines as a means of transferring power from the turbines to the fans. In addition, the use of electrical power transmission allows a high degree of flexibility in positioning the turboelectric generators and fan modules to best advantage.

2.3 Advances in TeDP Technology

2.3.1 Superconducting machines

Superconducting technology is one of the most important technologies to enable the development of turboelectric distributed propulsion. Conventional motors exhibit a maximum torque density for low speed applications; the value is reached by increasing current density in the copper winding and therefore leads to a significant decrease of the efficiency. Superconducting machines can be designed to exhibit both high torque and high power density (Fig.2.10). For example, the 36.5 MW HTS (high temperature superconducting) motor developed by American Superconductor has a maximum output torque around 38 N.m/kg.[17] Even high torque is not necessarily needed in airborne applications, the superconducting motors can exhibit both high torque and high power density. Siemens in Germany also built a 4 MW HTS generator rotating at 3600 RPM [43]. AMSC developed a 36.5 MW HTS generator rotating at 120 RPM. However, both generators fail to satisfy the N+3 TeDP system requirement (motor: 3.6 MW @4500-5000 RPM; generator: 27.3 MW @ 3600 RPM). The other technical challenge of superconducting machine is the low running temperature. Cooling devices are needed to maintain the temperature. In the last 40 years, the temperature has been increased from almost 0 K to 92 K [63]. The Fig.2.11 shows the timeline of superconducting materials. Since about 1993, the

highest temperature superconductor was a ceramic material consisting of thallium, mercury, copper, barium, calcium and oxygen (HgBa2Ca2Cu3O8+δ) with Tc = 133–138 K [1]. The development of HTS motors is rapid, ultra-high power density HTS generator and motor with high running temperature will be available in foreseeable future.

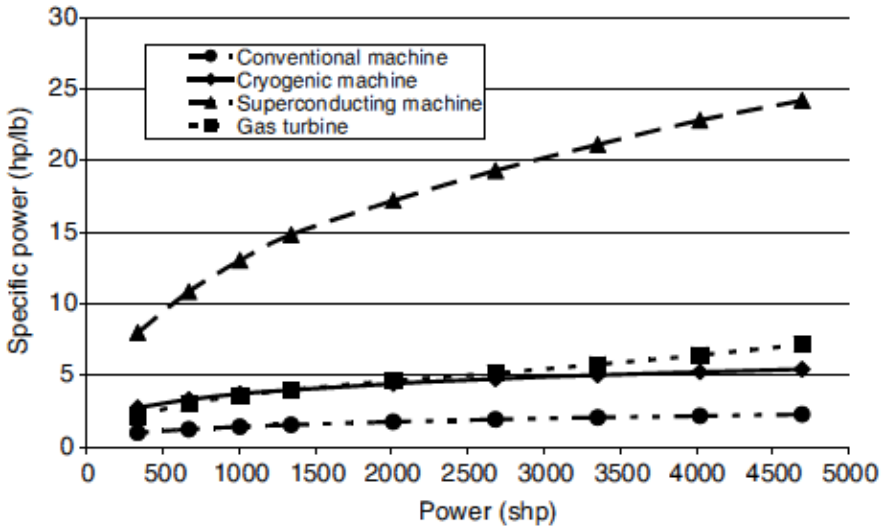

Figure 2.10 Power Density Comparison [42]

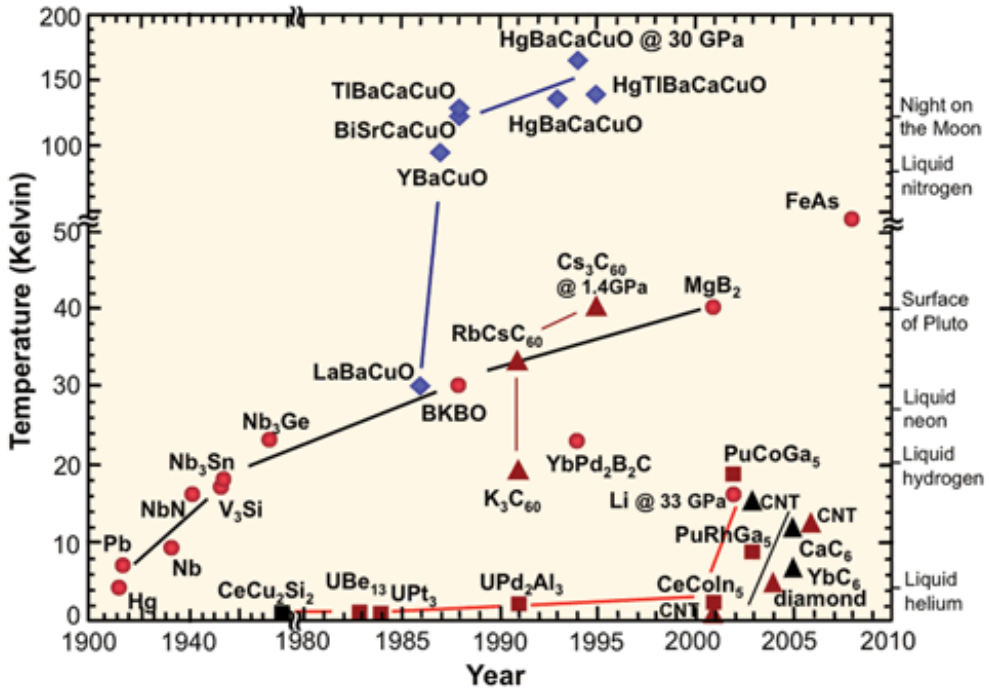

Figure 2.11 Timeline of Superconducting Materials and Their Working Temperature [63]

2.3.2 Liquid Hydrogen (LH2) Powered Aircraft

Natural resources are becoming less available and alternative energy sources will have to be considered very soon [23]. Comparing to Methanol and Gasoline, LH2 has about twice energy density. Hydrogen can be cleanly converted into electrical energy through fuel-cells or burnt with very low emissions in high speed turbo-generators. Moreover, hydrogen can be efficiently stored in its liquid form at cryogenic temperatures and could therefore provide a very convenient cooling system at 20K for superconducting devices.

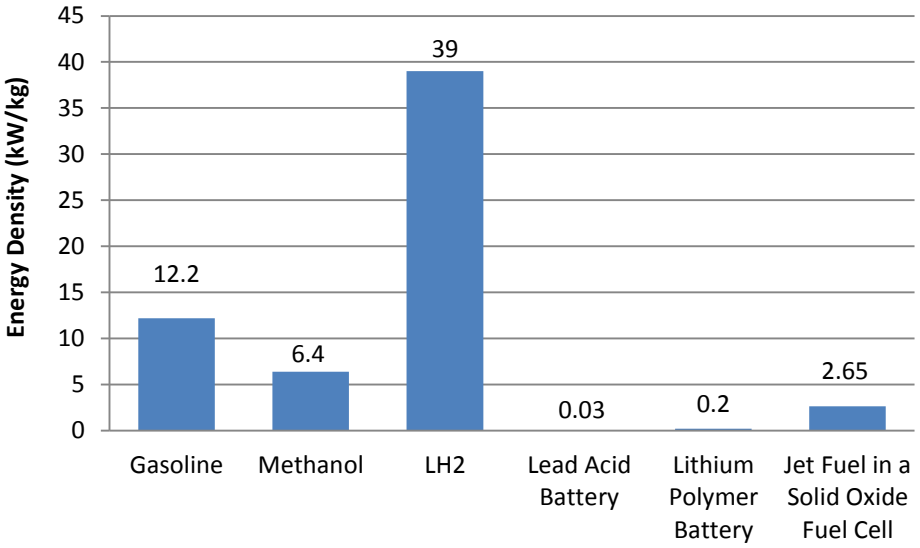

Figure 2.12 Energy Densities of Difference Fuels

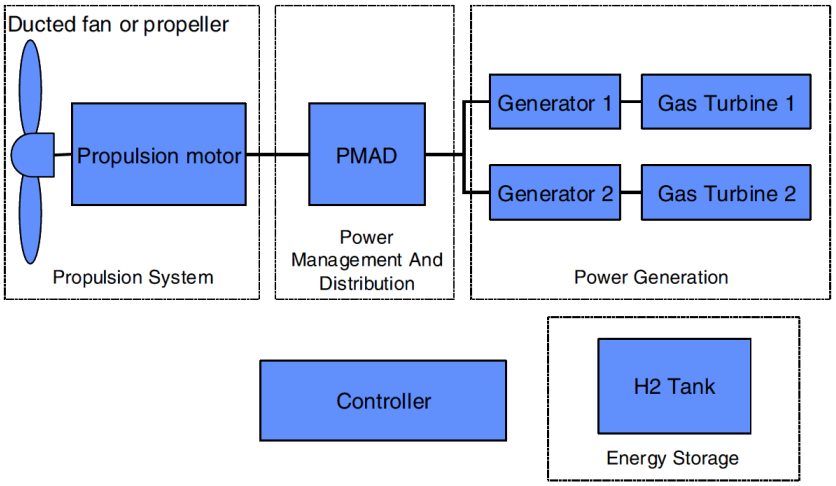

Figure 2.13 GE LH2 Powered Aircraft Power System Concept [42]

A typical LH2 powered aircraft configuration is presented in Fig.2.13. Turbogenerators use high speed turbines rotating at their optimum speed to maximize efficiency coupled to high speed superconducting generators. In this case, LH2 should flow from the tank to the propulsion motors and generators that could be fully superconducting. Then power converters can be used to heat up the LH2 before entering the fuel cell or combustor. LH2 as the energy source and superconducting cooling fluid is in very good synergy and represent one of the most promising technologies in future aircraft.[6]

2.3.3 Propulsion

Current technology of propulsion system in aircrafts is based on gas turbines. The most advanced engine is the high bypass ratio turbofan engine that generates thrust through exhaust hot gas and through the rotation of a large duct fan. The most recent turbofan has bypass ratio above 8-10; hence most of their thrust is produced by the fan and only a small fraction by the exhaust of hot gas, typically less than 10%. The turbine is then acting primarily as a turbo-shaft engine and is used to rotate the fan. The relative low turbine rotating speed limits (due to the tip speed limitation) its efficiency. Also, torque and rotation speed are strongly coupled in gas turbine, thus limiting its controllability. Therefore, there would be great advantages in replacing the gas turbine with motors. Fig.2.14 shows the concept. Distributed propulsion further improves this concept by replacing the big fan stage with numbers of small fans, and each fan is driven by a small HTS motor. [35]

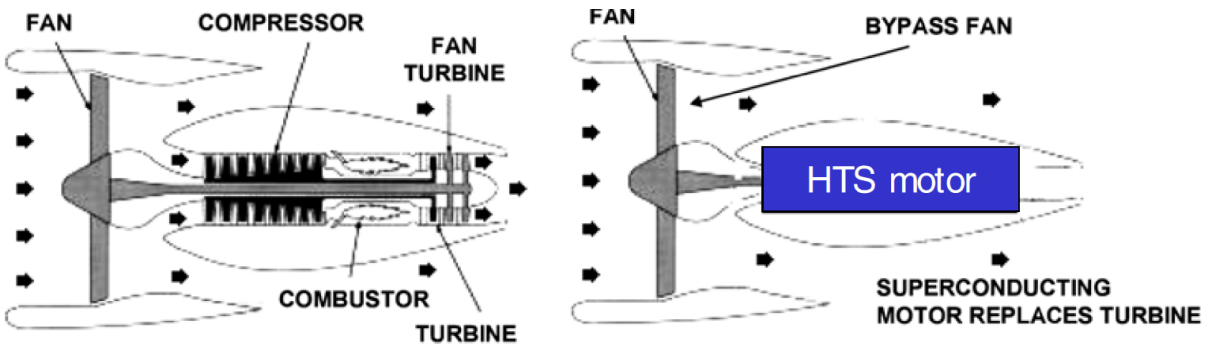

Figure 2.14 Motor-driven Fan Concept [9]

More technical background on components of the TeDP system is given in following chapters.

Chapter III

A Design Method of the Embedded Turboelectric Distributed Propulsion (TeDP) System on a Hybrid-Wing-Body Airframe

Meeting future goals for aircraft and air traffic system performance will require a fundamental shift in approach to aircraft and engine design. In 2005, NASA released plans of next generation commercial airplane for 2030 related with the hybrid wing body (HWB) and superconducting distributed propulsion system. The HWB concept adapts NASA's cruise-efficient short take-off and landing (CESTOL) airframe. The propulsion system employs distributed electric fans, which are embedded on the upper surface of the airframe, driven by superconducting motors with power provided by two wing-tip mounted turboelectric generators.

This chapter, firstly, put forward a preliminary design method of an embedded TeDP system for hybrid-wing-body aircrafts. The method includes the way to choose the number of core-engines, the Turbomatch model of the core-engine, the way to choose the number of propulsors, their pressure ratio and their diameter. It provides the first step to design a TeDP system on the NASA N3-X Aircraft. The core-engine used in this chapter is powered by a turboshaft engine. This means that the embedded propulsor array provide all the thrust. A turbofan-driven TeDP system will be introduced in chapter 5. Secondly, a TeDP system was developed based on NASA's assumptions, and a back-to-back comparison with NASA's results is made. Thirdly, a new turboshaft-driven TeDP system was introduced to power the NASA N3-X Aircraft. This TeDP system has 16 propulsors powered by two turboshaft-driven core-engines. Finally, the propulsor intake loss due to BLI was examined. It has been found that if the loss was sufficiently high, the embedded configuration is not preferred.

3.1 Introduction

Historically, civil aircraft and propulsion system design has evolved to meet the demands of higher efficiency, better reliability, and lower running cost. To specify those goals, the NASA Subsonic fixed Wing project defined targets for the next three generations of aviation (N+1, N+2, and N+3) [17]. To meet these requirements, fundamental changes are needed on both airframe and propulsion system designs. One of the vehicle and propulsion concepts that NASA has explored for N+2 was a hybrid-wing-body (HWB) airframe with 12 small conventional high bypass ratio turbofan engines [17]. The HWB was the main object of study to meet NASA's N+2 goals. Meanwhile, the Cambridge-MIT institute developed the SAX-40 conceptual design [14, 30] and Boeing with NASA developed the N2 aircraft [24]. Both SAX-40 and N2 aircrafts utilized HWB, but different propulsion modules.

To improve vehicle performance enough to satisfy NASA's N+3 goals, the HWB airframe designed for N+2 was used but the propulsion system should be replaced by turboelectric distributed propulsion (TeDP) system. A concept currently analysed at NASA is N3-X shown in Fig.3.1. This vehicle utilizes low pressure electrically driven fans with power from electric generators driven by turboshaft engine. The fans of N3-X were put in a continuous nacelle cross the upper/rear surface of the HWB aircraft, and two wing-tip mounted turbogenerators were each combined by a turboshaft engine and a superconducting generator [31].

The concept of a TeDP system consists in driving a large number of small fans, usually more than ten, with a small number of cores, usually fewer than four. The fans, or propulsors, are used to produce thrust and the cores only generate electricity. The power is transmitted electrically rather than mechanically, which makes the fan shaft speed independent of turbogenerator shaft speed. One other benefit is ingesting boundary layer flow to improve propulsive efficiency. The average inlet velocity is reduced due to boundary layer flow, and if the fan nozzle is un-choked, the slower inlet flow also results in a slower exit jet velocity.

The first TeDP engine design and cycle analysis for HWB aircraft was introduced by NASA (2009) at 47th AIAA Aerospace Sciences meeting. In the thesis, a range of fan pressure ratios were examined at the aerodynamic design point (ADP) of the vehicle (31,000ft/Mach 0.84) [31,41]. They found the minimum thrust specific fuel

consumption (TSFC) at the ADP to be between 1.3 and 1.35 and a detailed engine thermodynamic cycle calculation was made at propulsor pressure ratio equals 1.35 with 14 fans. In 2011, an examination of the effects of BLI on TeDP systems was presented by NASA at 49th AIAA Aerospace Sciences meeting. In this meeting, they tested the effects of BLI on TeDP system performance at different PPRs. And a design fan pressure ratio of 1.3 with 15 fans was selected to explore the performance of a TeDP system by Numerical Propulsion System Simulation (NPSS) [17, 19]. Two parameters, mass average inlet pressure and mass average inlet Mach number, were introduced to calculate BLI inlet conditions. The BLI model introduced in this chapter was very simple; a more detailed analysis of BLI propulsion systems was presented in reference 12, which defined a control volume to calculate thrust of BLI propulsion system with or without a transonic shock in front of the inlet, as well as to analysis the benefit of BLI. They found electrically driven propulsion system benefits most from the BLI and the presence of transonic waves [32].

3.1.1 The Thrust Requirements

A new airframe concept, N3-X, with TeDP system, was introduced at AIAA Aerospace Science Meeting. The N3-X aircraft is designed to carry a 53,570 kg payload 12200m at Mach 0.84. These mission requirements need 400kN maximum thrust at take-off. Table 3.1 summaries the thrust requirements at DP, RTO and T/O.

Table 3.1 NASA N+3 Airplane (N3-X) Thrust Requirements

Flight Condition	Thrust Requirements
Aerodynamic Design Point (30,000 ft / Ma=0.84 / ISA)	30,000 lbf (133 KN)***
Rolling Take-Off (SL / Ma=0.25 / ISA+27 R)	65,000 lbf (289 KN)
Sea Level Static Take-Off (SL / Ma=0.0 / ISA)	90,000 lbf (400 KN)

***: the value is obtained based on the aircraft with podded engine; NASA estimates ingesting boundary layer will reduce the value by 7%.

3.1.2 The NASA N3-X Aircraft TeDP System

The TeDP system has 15 motor-driven propulsors powered by two core-engines. The motor driven propulsors are assumed to be positioned in a continuous array across the upper rear surface of the fuselage section with the inlet as close to trailing edge as possible. The propulsor array forms a V-shape with the bottom of the V at the centre line and the arms moving forward to follow the trailing edge. The maximum span-wise distance available for the array is 64 feet (19.5 meters). There is always a single centreline propulsor with an equal number of propulsors on either side. However, in this model, the propulsors are put in a straight line. So both odd and even number of fans can be used. The structure of one propulsor unit was combined by a fan, an electric motor (EM) and nozzle with shared nacelle.

Figure 3.1 NASA N3-X Aircraft with the TeDP System [17]

The two core-engines (turbogenerator) are assumed to be mounted on the wing-tips. This is an unusual location for turbomachinery. The reason for this, as NASA explained, is potential in reducing damages due to the failure of turbine rotor. They explained it is because the wing-tip location leads to a very narrow angle that any debris resulting from engine failure could impacts the rest of the aircraft. Other potential advantages include some span loading relief in the normal upward lift direction. However, dramatically increment on the wing strength is needed. This will lead to expensive material. So where to mount the turbogenerator needs further evaluation. Each turbogenerator consists of a two spool gas generator feeding a power turbine which in turn drives a superconducting generator. The key turboshaft

engine design parameters are listed in Table 3.2. These parameters were used in modelling the core-engine performance with our own tools.

The electric system consists of superconducting motors and generators with superconducting cables connecting them. Superconducting devices have ultra-high power density and the overall efficiency (shaft power into the generator to shaft power out of the motor) exceeds 99%. There are two ways of cooling in order to maintain the low working temperature of the superconducting devices: using liquid hydrogen or cryocoolers. In this chapter, only using cryocoolers was examined. The electric power to drive the cooling system was obtained from NASA's results. More studies will be introduced in chapter 7.

Table 3.2 Turbogenerator Design Parameters [19]

Component	Parameter	Design Value
Low Pressure Compressor (LPC)	Polytropic Efficiency	0.9325
High Pressure Compressor (HPC)	Polytropic Efficiency	0.9325
LPC & HPC	Pressure ratio	OPR varied to equal max T3 with an equal Δh split between compressors
	OPR	74.8
	PR of the LPC	16.44
	PR of the HPC	4.55
Burner	Inlet Temperature (T3)	934 K @ ADP
		1005 K @ RTO
	Exit Temperature (T4)	1811 K @ ADP
		1922 K @ T/O
High Pressure Turbine	Polytropic Efficiency	0.93
Low Pressure Turbine	Polytropic Efficiency	0.93
Power Turbine	Polytropic Efficiency	0.924

3.1.3 NASA Boundary Layer Ingestion Method

In their method, they use two mass average parameters, R_{Ma} and R_{Pt}, to recalculate the propulsor inlet conditions. Eq.3.1 and Eq.3.2 show the definition. Alternative BLI modelling method will be introduced in next chapter.

$$R_{Ma} = \frac{\sum_0^i (m_i Ma_i)}{\sum_0^i m_i} \tag{3-1}$$

$$R_{Pt} = \frac{\sum_0^i (m_i Pt_i)}{\sum_0^i m_i} \tag{3-2}$$

A profile of the mass-average Ma and Pt was calculated from the boundary layer profiles (Fig.3.2 shows the boundary layer profiles along the centreline 60% to 100% of the fuselage chord length). The mass average Ma and Pt for each distance "i" in the profile was calculated from the Eq.3.3 and Eq.3.4, where m_i is the mass flow through the i_th segment of the boundary layer, Ma_i is the Mach number in the i_th segment, and Pt_i is the total pressure in the i_th segment.

$$Ma_{inlet} = Ma_0 \times R_{Ma} \tag{3-3}$$

$$Pt_{inlet} = Pt_0 \times R_{Pt} \tag{3-4}$$

$$Pt_0 = p_0 \left(1 + \frac{r-1}{2} Ma_0^2\right)^{\frac{r}{r-1}} \tag{3-5}$$

where Ma_0 is the flight Mach number and p_0 is the ambient static pressure

They further assumed that the boundary layer thickness for different design propulsor pressure ratios is the same (0.46 meter) and at the DP the height of the stream tube entering the propulsor inlet is the same as the inlet capture height. So iteration is needed to match the inlet mass flow ratio, and therefore to calculate the value of R_{Ma} and R_{Pt} . The boundary layer velocity profiles along the centreline from 60% to 100% of the fuselage chord length are shown in Fig.3.

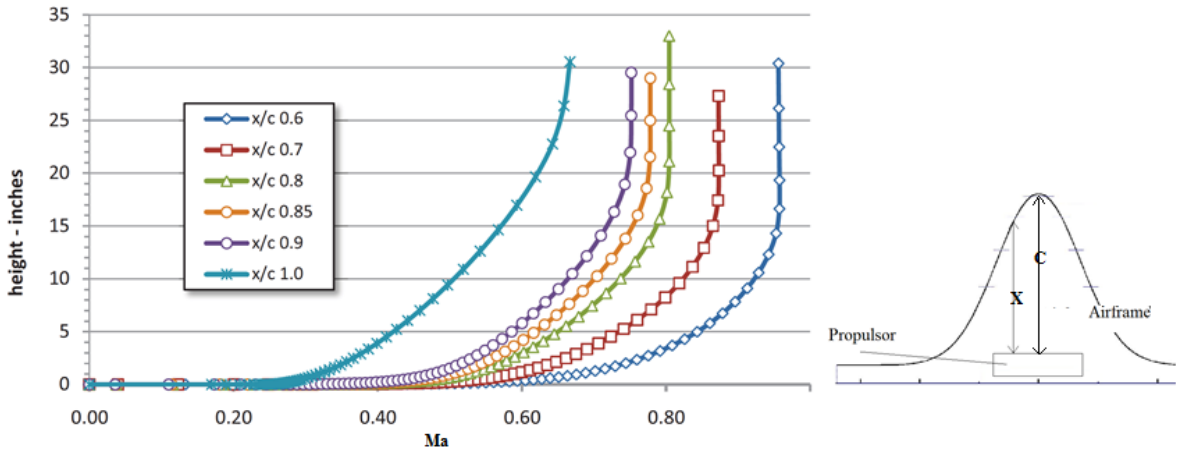

Figure 3.2 Centreline Ma Contours Used by NASA [19]

The inlet for the propulsors is a continuous 2-D “mail-slot” inlet across the 18 meters span recovered by the propulsor array. In order to have insight into the conditions at the physical inlet throat, the model of the inlet was divided into external and internal diffusion. This allows the inlet throat Ma and static pressure to be calculated. However the critical parameter necessary to determine the inlet conditions is not the physical inlet height, rather it is the height of the capture sheet of air as measured at the point just before any external diffusion begins. When a range of different design fan pressure ratios were examined this capture height was varied so that it matched the inlet height on the assumption that the inlet height and capture height will be the same at the design point. During off-design analysis of a given design the capture height was varied such that the air flowing through a sheet of that height contains the mass flow required by the propulsors. It is the R_{Ma} and R_{Pt} of this flow that determine the inlet drag of the propulsor. Any air above this height passes over the top of the propulsor nacelle. The result is that during off design operation the incoming R_{Ma} and R_{Pt} seen by the propulsor is throttle dependent.

3.2 TeDP System Design Methodology

The propulsors and turboshaft engine were modelled separately by Matlab and Turbomatch respectively. Turbomatch platform is an existing component based engine performance tool developed at Cranfield University. This software was used to develop and run representative thermodynamic models of the engine investigated. TURBOMATCH has the ability to perform steady state engine performance

calculations at both design point and off-design conditions. NASA's method to model BLI was used to obtain the inlet conditions and then the number of fans, its shaft speed, its pressure ratio, inlet duct pressure loss, etc. A range of PPR should be examined to find an optimised PPR for the new TeDP system.

3.2.1 Turboelectric Drive Train

The turboelectric approach requires that a number of new electric components are inserted into the aircraft propulsive drive train between the core-engines and the distributed fans. These components include superconducting generator, transmission lines, cooling system and motors. Different from other traditional propulsion system, such as turbofan, turboprop, etc., power was transmitted electrically rather than mechanically. So the propulsors and turbogenerators should be modelled separately to optimise their performance at different rotational speeds. In the first step, the behaviours of superconducting system were represented by efficient factors, μ. Detailed analysis of their performance and impacts on TeDP system design will be introduced in the following chapter. So the overall system model can be expressed in Fig.3.3. Efficiency of the motor and the generator is 0.9999 and the transmission efficiency is 0.999. In this figure, *W* is the power. [38]

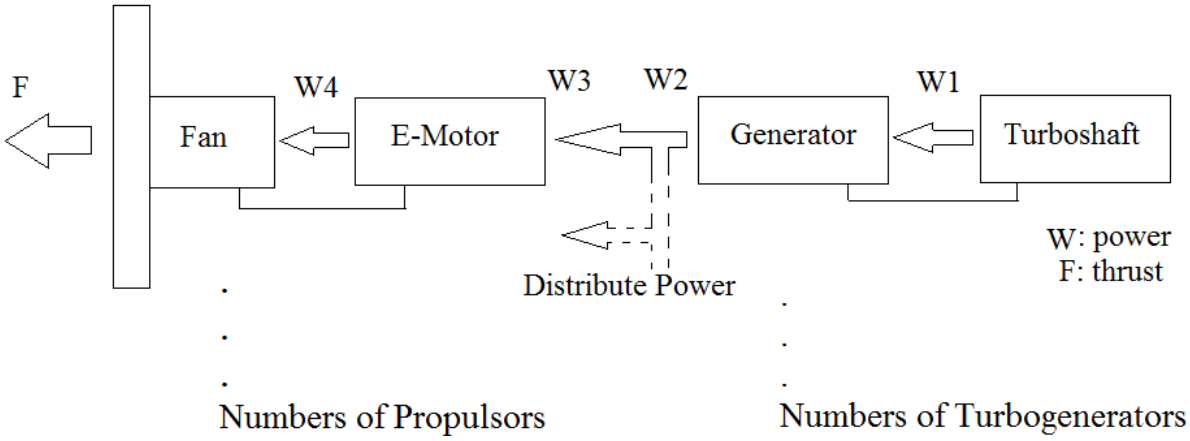

Figure 3.3 TeDP Drive Train

$$W_2 = \mu_{Generator} \times W_1 \tag{3-6}$$

$$W_3 = \frac{Num_T}{Num_F} \times \mu_{transmit} \times W_2 \tag{3-7}$$

$$W_4 = \mu_{E-Motor} \times W_3 \tag{3-8}$$

The rotational speed of the fan and the electric motor (E-Motor) is the same; the rotational speed of the generator and the turboshaft engine power turbine is the same. There are several methods to calculate engine thermo-cycle data. One of them is to build a 'big fan' turbofan engine. The fan mass flow area should match the total area of all propulsors and a gearbox is needed to match the fan rotation speed. The benefit of this method is that the traditional engine performance simulation program can be used directly. However, it is difficult to integrate BLI models. In this research, the core-engine and the propulsors array are modelled separately.

3.2.2 Propulsor Control Volume

In the podded case, the definition of the control volume for the engine is clear. The propulsive force created by the engine, therefore, can be calculated by the momentum difference of the Trefftz Plane and inlet freestream plane [58]. This propulsive force balances the bare airframe drag if the nacelle drag is neglected. However, for an embedded engine it is not possible to separate the influence of the airframe and the engine on the flow. The force on the control volume includes the flow from the start of the pre-compression zone to the Trefftz Plane, as Fig.3.4(a) shows. It contains not only the engine propulsive force but also the pressure force that comes from the airframe curvature. However, the disadvantage of using this CV is the unknown conditions of the flow that do not go through the engine, which should be accounted for.

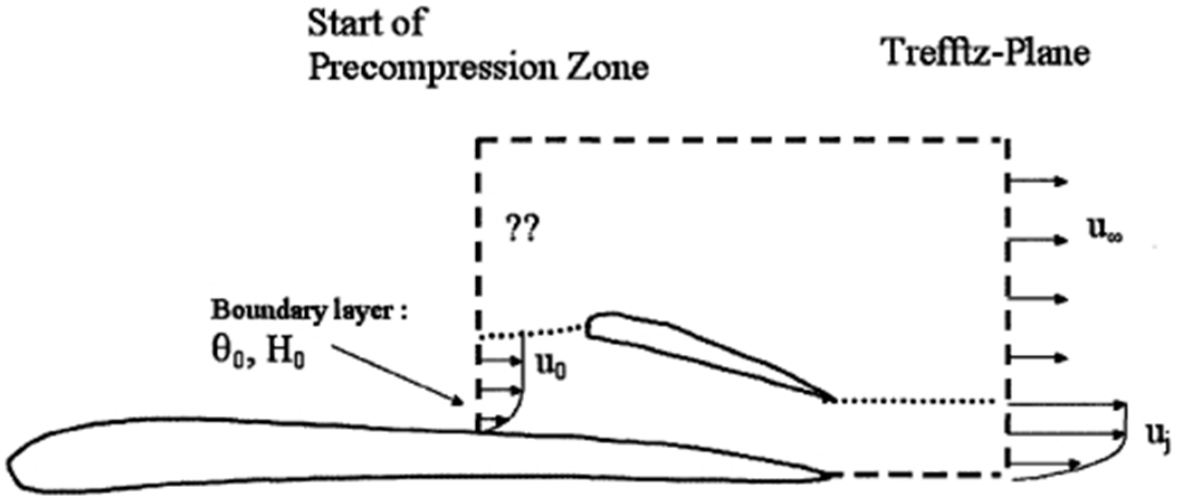

(a) Inner Control Volume

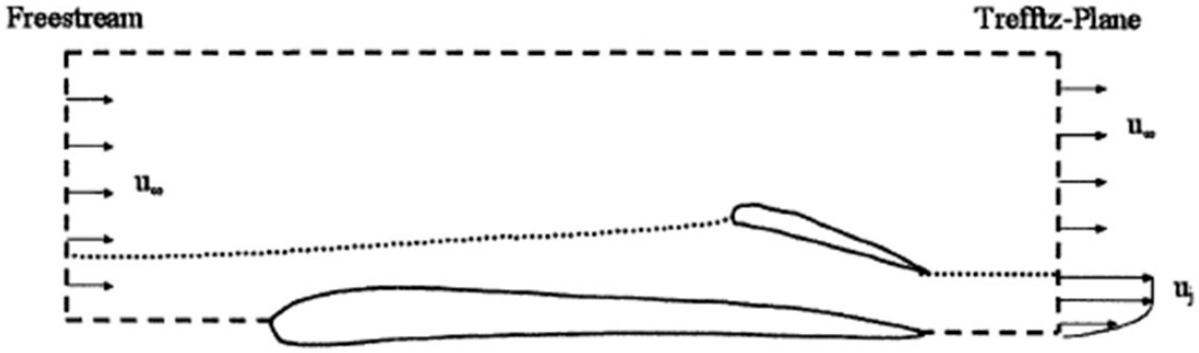

(b) Outer Control Volume

Figure 3.4 Control Volume for an Embedded Engine [52]

For Fig.3.4(b), the net thrust is:

$$T_N = \int \rho(U_j - U_\infty)U_j dA \tag{3-9}$$

This net thrust must balance the drag defined:

$$T_N = D_N = D_A + D_{nacelle} - D_w \tag{3-10}$$

In Eq.3.10, the D_A is the airframe drag, which is the thrust requirement of the N3-X aircraft; the $D_{nacelle}$ is the nacelle drag; and D_w is the ingested drag. Fig.3.5 shows their definitions.

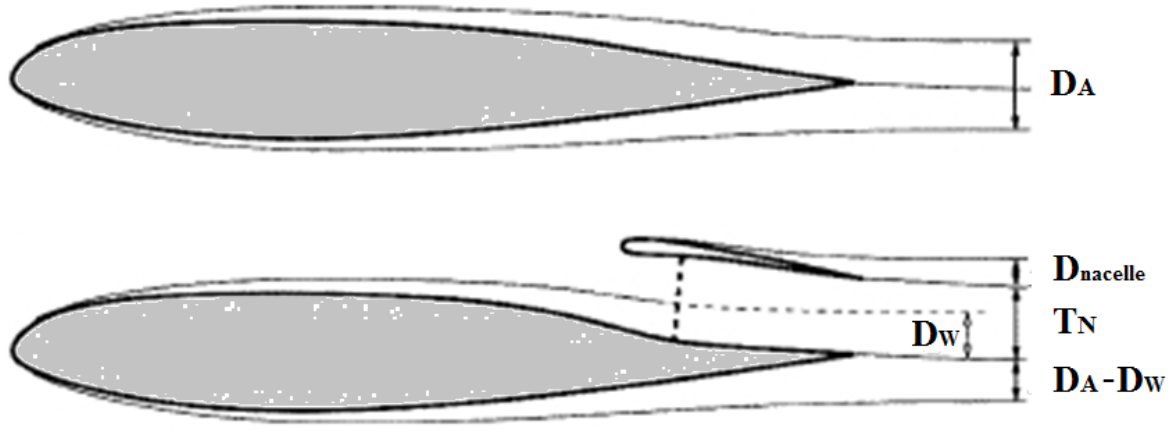

Figure 3.5 The Drag and Thrust Definition for an Aircraft with Embedded Engine with BLI

The ingested boundary layer flow contributes to the net thrust as the engine accelerates. If the friction that would occur downstream of the start of the pre-compression zone is neglected, the ingested drag can be calculated using a modified von Karman equation. [52]

$$D_w = \rho U^2 \theta b \left(\frac{U}{U_\infty}\right)^{H_{avg}} \tag{3-11}$$

In Eq.3.11, *b* is the span of ingested boundary layer, θ is the boundary layer momentum thickness, and H_{avg} is the average value of the boundary layer shape factor. NASA figured out that the ingested drag is equal to 7% of the total thrust requirement at DP. So the thrust produced by the propulsors at DP is approximate 120 KN. In this chapter, off design calculations were done without considering BLI. The way to model BLI for off-design calculation will be introduced in chapter 7.

3.2.3 Propulsor Module Design

The propulsor array is placed on the upper surface of the airframe near the trailing edge. The structure of one propulsor unit (Fig.3.6) consists of a fan, an E-Motor and a nozzle with shared nacelle. The most important function of this model is to figure out the number of fans, shaft speed and fan pressure ratio at DP.

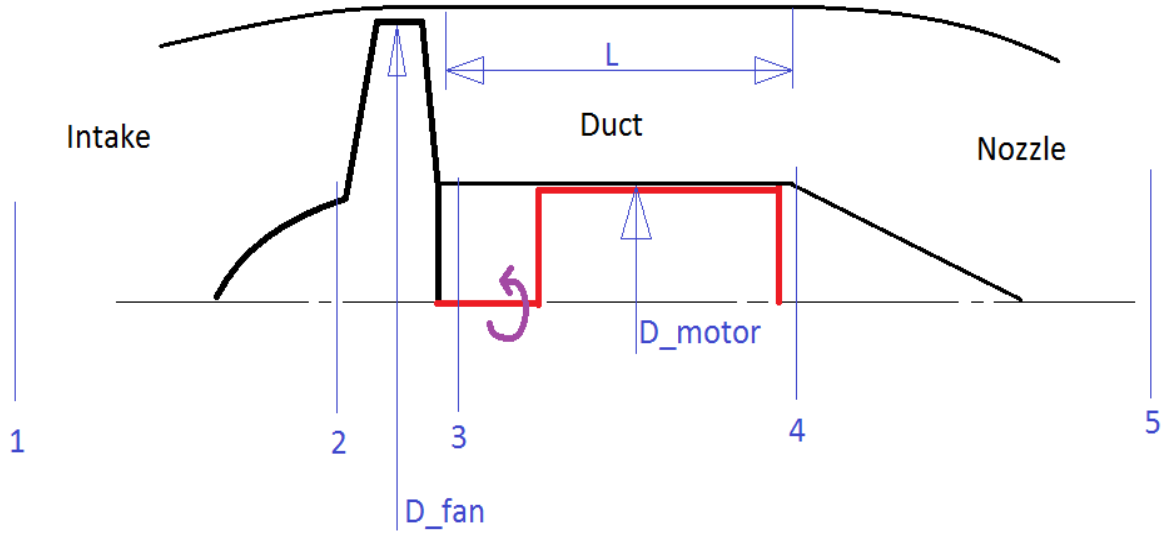

Figure 3.6 The Propulsor Modulus

Other propulsor design parameters are:

- Hub to tip ratio equals 0.3

- Dimension of fan nacelle equals fan diameter
- Motor diameter equals to fan hub diameter, but with a minimum diameter 300mm (12 in).
- Duct length equals half of the fan diameter, but with a minimum length 500mm (20 in).
- The duct is constant cross section
- Duct has constant inlet swirl of zero degree
- Duct Mach number is 0.3
- Material of duct: alumina
- Total length for the fans (based on inlet width): 60 ft to 65 ft (19m)
- Fan inlet width to fan diameter ratio: 1.125
- Fixed nozzle area, variable EM power output in order to change thrust produced by fans
- The number of fans

To satisfy a given design target, the number of fans is not unique. So the first step is to find the relation between the fan number, diameter, weight, fan tip loss and duct pressure loss. From reference 18, increasing the number of fans leads to:

- The total weight of propulsors reduced
- Fan diameter reduced
- Fan tip loss increase
- Fan bypass duct pressure loss increase

The total weight of the propulsors is reduced with increasing number of fans. So to maximise system thrust to weight ratio, the propulsors should be chosen as many as possible. However, more propulsors lead to smaller fan diameter, higher fan tip loss and duct pressure loss. So the number should be optimised as follows:

- There is a minimum requirement of fan diameter to guarantee enough space for the electric motor behind the fan. The maximum number of fans can be used to ensure fan diameter larger than this value is N1;
- The fan tip loss becomes more serious at small fans. The maximum number of fans that can be used at an affordable fan tip loss is N2;

- Small fans also cause high pressure losses in both the inlet duct and bypass duct, the maximum number of fans can be used within a suitable duct pressure loss is N3;

So Eq.3.12 can calculate the number of fans. Besides these three considerations, others can also be included in the equation to satisfy design requirements. After choosing the number of fans, the fan diameter can be calculated by Eq.3.13 where *L* is the total width of the propulsor array and *f* is the fan cap factor (the ratio of one propulsor module width to fan diameter).

$$\text{Number} = \text{Min.}(\text{N1}, \text{N2}, \text{N3} \ldots) \tag{3-12}$$

$$\text{Diameter} = \frac{L}{\text{N} \cdot f} \tag{3-13}$$

a. Fan shaft speed

The fan shaft speed is the other important design parameter. Increasing fan shaft speed reduces fan loading coefficient ($\Delta h/U^2$). However, fast shaft speed leads to fast fan tip speed, which mitigates fan efficiency at high level. In modern fan design with tip blade angle less than 65 degree, the maximum fan tip Ma, Ma_t, is between 1.4 and 1.8 [68]. The other important factor that should be considered is the motor performance; this means the motor can provide enough power and torque under this shaft speed. In this chapter, performance of the motor is not considered. The shaft speed for different PPR, in this chapter, can be calculated by the fan tip speed limitation given by NASA (Fig.6 in reference 32). In following chapters, the fan DP shaft speed will be calculated from the fan tip Ma, which is assumed equal to 1.6.

b. Propulsor Fan pressure ratio (PPR or FPR)

Meeting NASA's N+3 goals requires a propulsion system with high overall efficiency. Material and design improvements allow higher overall pressure ratio and higher burner exit temperature, which improve the thermal efficiency. The propulsive efficiency, however, is largely determined by the PPR. Lower PPR reduces the jet exit velocity, which improves propulsive efficiency, but also dramatically decreases the shaft speed. To choose a PPR, firstly, a group of PPRs should be examined to find its relation with TSFC. NASA research results (reference 19) show that the maximum shaft speed of PPR above 1.5 is too high and makes the direct electric

motor drive impossible [17]. PPR bellows 1.2 is also not attractive because of difficulty to recover inlet duct pressure loss. So the PPR of a TeDP system on HWB should be from 1.2 to 1.5.

c. Fan inlet duct design

The other special structure of propulsors is the air inlet duct, which is combined by the airframe upper surface and the nacelle. The duct is used to guide air to fans. The inlet can be divided into internal and external parts, which allows the inlet Ma and static pressure to be calculated. The critical parameter necessary to determine is the inlet height. If the inlet height is too high, the total drag and weight will increase. But if the height is not enough high, the duct pressure loss and flow noise would increase. One method is to assume the inlet height and capture height will be the same at design point with a pressure loss factor, $\Delta \mathrm{P}/\mathrm{P}$. The value of this factor equals to 2% in this chapter. It is much higher than the modern duct due to ingesting boundary layer. However, NASA also points out the value can be as little as 0.5% (reference [20]).

d. Propulsor weight model

The propulsor system contains the inlet duct, fans, duct, E-Motors, nozzles and nacelle. Because the inlet duct and nacelle are part of the airframe, in this weight model it is not necessary to consider them. Meanwhile, the nozzle is also assumed as part of the airframe. The total weight of all E-motors is assumed to increase linearly with the electric power. So changing the number of fans does not change their total weight. Therefore, the propulsor weight (except the motors) can be calculated by Eq.3.14.

$$\text{Propulsor total weight} = \text{Number of fans} \times (\text{weight of fan} + \text{weight of duct}) \tag{3-14}$$

$$weight\ of\ fan: W_{fan} = \frac{K_F (D_t)^{2.7}}{(AR)_{x,r}^{0.5}} \cdot \left(\frac{\delta_t}{\delta_{t,ref}}\right)^{0.3} \cdot \left(\frac{U_t}{U_{t,ref}}\right)^{0.3} \tag{3-15}$$

$$\text{weight of duct} = \text{weight of casing} + \text{weight of acoustic lining} \tag{3-16}$$

$$W_{casing} = \pi D_D L_D \rho_D t_D \tag{3-17}$$

$$W_{Lining} = \pi[(LD_h)_{inner\ wall} + (LD_h)_{outer\ wall}]\rho_{wall}t_{wall} + \pi\left(\sum_{i=1}^{N_R} L_R\, D_{R,i}\right)\rho_R t_R \quad (3\text{-}18)$$

Where:

- D_t is fan tip diameter
- N:number of stages
- AR=(average blade height)/(average blade chord)
- σ_t:rotor blade tip solidity
- U_t:tip speed
- D is diameter
- L is length
- ρ is density
- T is thickness
- D: duct casing
- R: splitter ring

In my model:

- AR=2.5
- σ_t=1.25
- (σ_t)_ref= 1.25
- (U_t)_ref= 350
- N=1
- K_F=135
- No splitter ring
- Duct casing thickness is 1.3mm
- Wall thickness is 1mm
- ρ is 2770 kg/m

For example, if the weight of one core with cooling system is assumed 5000 kg and total weight of the motors is 3200kg, at PPR=1.3 with 16 propulsors the overall weight of the system is approximately 15200 kg.

3.2.4 Propulsor DP Cycle Calculation

Step 1: calculate ambient conditions.

ambient static temp. $$t_0 = 288.15 - 0.0065 \times alt \quad (3\text{-}19)$$

ambient static pressure $$p_0 = 101325 \times (1 - 0.0000226 \times alt)^{5.2} \quad (3\text{-}20)$$

air density $$\rho_0 = 1.226 \times (1 - 0.00226 \times alt)^{4.256} \quad (3\text{-}21)$$

sound speed $$a_0 = \sqrt{rRt_0} \quad (3\text{-}22)$$

Step 2: calculate intake conditions

ambient total temp. $$T_0 = t_0(1 + \frac{r-1}{2} Ma^2) \quad (3\text{-}23)$$

ambient total pressure $$P_0 = p_0 \left(1 + \frac{r-1}{2} Ma^2\right)^{\frac{r}{r-1}} \quad (3\text{-}24)$$

intake inlet total temp. $$T_1 = T_0 \quad (3\text{-}25)$$

intake inlet total Pt. $$P_1 = P_0 \times R_{Pt} \quad (3\text{-}26)$$

intake inlet Ma $$Ma_1 = Ma \times R_{Ma} \quad (3\text{-}27)$$

Step 3: calculate fan stage conditions

fan inlet total temp. $$T_2 = T_1 \quad (3\text{-}28)$$

fan inlet static temp. $$t_2 = T_2/(1 + \frac{r-1}{2} Ma_1^2) \quad (3\text{-}29)$$

fan inlet total Pt. $$P_2 = P_1 \times (1 - intake\ pressure\ loss) \quad (3\text{-}30)$$

fan exit total temp. $$T_3 = T_1 \times PR^{\frac{r-1}{\eta_{poly} r}} \quad (3\text{-}31)$$

efficiency change: $$\eta_{isen} = \frac{PR^{\frac{r-1}{r}} - 1}{PR^{\frac{r-1}{\eta_{poly} r}} - 1} \quad (3\text{-}32)$$

fan exit total Pt. $$P_3 = P_2 \times PR \quad (3\text{-}33)$$

Step 4: nozzle calculation

The nozzle needs to be checked if it is chocked. Supposing that the static pressure at the nozzle exit is equal to ambient static pressure, the exit gas Ma can be calculated.

nozzle exit static Pt. $$p_5 = p_0 \quad (3\text{-}34)$$

nozzle exit total Pt. $$P_5 = P_4 = P_3 \times (1 - duct\ pressure\ loss) \quad (3\text{-}35)$$

nozzle exit Ma. $$Ma_5 = \sqrt{\frac{\left(\frac{P_5}{p_5}\right)^{\frac{r-1}{r}} - 1}{\frac{r-1}{2}}} \quad (3\text{-}36)$$

Then, checking the exit Ma:

if $Ma_5 \geq 1$ $$Ma_5 = 1 \quad (3\text{-}37)$$

else $$Ma_5 = Ma_5 \quad (3\text{-}38)$$

nozzle exit total temp. $$T_5 = T_4 = T_3 \quad (3\text{-}39)$$

nozzle exit static temp. $$t_5 = \frac{T_5}{1 + \frac{r-1}{2} Ma_5^2} \quad (3\text{-}40)$$

nozzle exit static Pt. $$p_5 = \frac{P_5}{\left(1 + \frac{r-1}{2} Ma_5^2\right)^{\frac{r}{r-1}}} \quad (3\text{-}41)$$

jet velocity $$V_j = Ma_5 \times \sqrt{rRt_5} \quad (3\text{-}42)$$

nozzle pressure ratio $$NPR = \frac{P_5}{p_0} \quad (3\text{-}43)$$

nozzle coefficient

$$C_V = (-0.00000005) * NR\text{^}6 + 0.00000412 * NPR\text{^}5 - 0.00012692 * NPR\text{^}4 + 0.00192109 * NPR\text{^}3 - 0.01434825 * NPR\text{^}2 + 0.03787371 * NPR + 0.94732668 \quad (3\text{-}44)$$

Step 5: calculate the mass flow and nozzle area

If the nozzle is not chocked:

mass flow

$$\dot{m} = \frac{T_N}{C_V(V_j - V_0)} \quad (3\text{-}45)$$

nozzle area

$$A_N = \frac{W}{V_j \rho_5} \quad (3\text{-}46)$$

If the nozzle is chocked, the thrust due to nozzle static pressure ratio needs to be considered. In this case, it needs an iterative process to find out mass flow. First of all, guess a nozzle area, A, then the mass flow can be calculate:

mass flow guess

$$\dot{m}_{guess} = \frac{\frac{T_N}{C_V} - (p_5 - p_0)A}{V_j - V_0} \quad (3\text{-}47)$$

nozzle are

$$A_N = \frac{\dot{m}_{guess}}{V_j \rho_5} \quad (3\text{-}48)$$

Iterate till the guess are, A, is equal to calculated nozzle are A_N, the calculation process is:

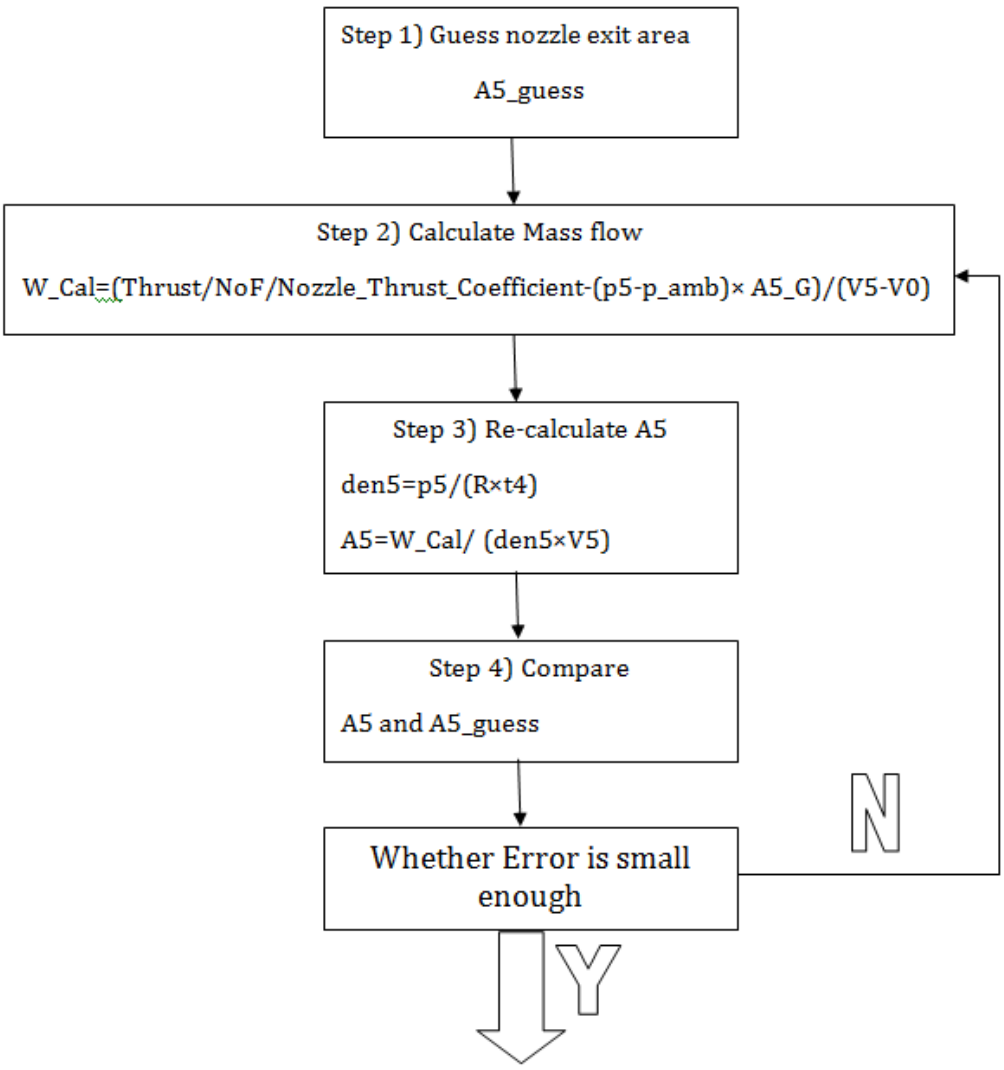

Figure 3.7 Flow Chart of Calculating Mass Flow If Nozzle Chocked

Step 6: calculate the fan power

fan power $$Power = \dot{m}C_p(T_3 - T_2) \quad (3\text{-}49)$$

fan tip diameter $$D = \sqrt{\frac{4\dot{m}}{\pi\rho_2 V_2(1-HTR^2)}}$$ where HTR=hup to tip ratio (3-50)

3.2.5 Propulsor Off-Design Calculation

In this chapter, BLI is not considered for off design calculation (chapter 6 will introduce the off design method with BLI). More detailed works of BLI off design methodology will be introduced in following chapter. The fan operating point changes

with ambient conditions including pressure, temperature, inlet Ma and the power available to drive the fan. In addition, as a whole system, the mass flow flowing through intake, fan and nozzle should be the same and matched with the fan power available [57, 64]. In order to find out the exact operating point on the fan map for each off design case, an iterative process is required.

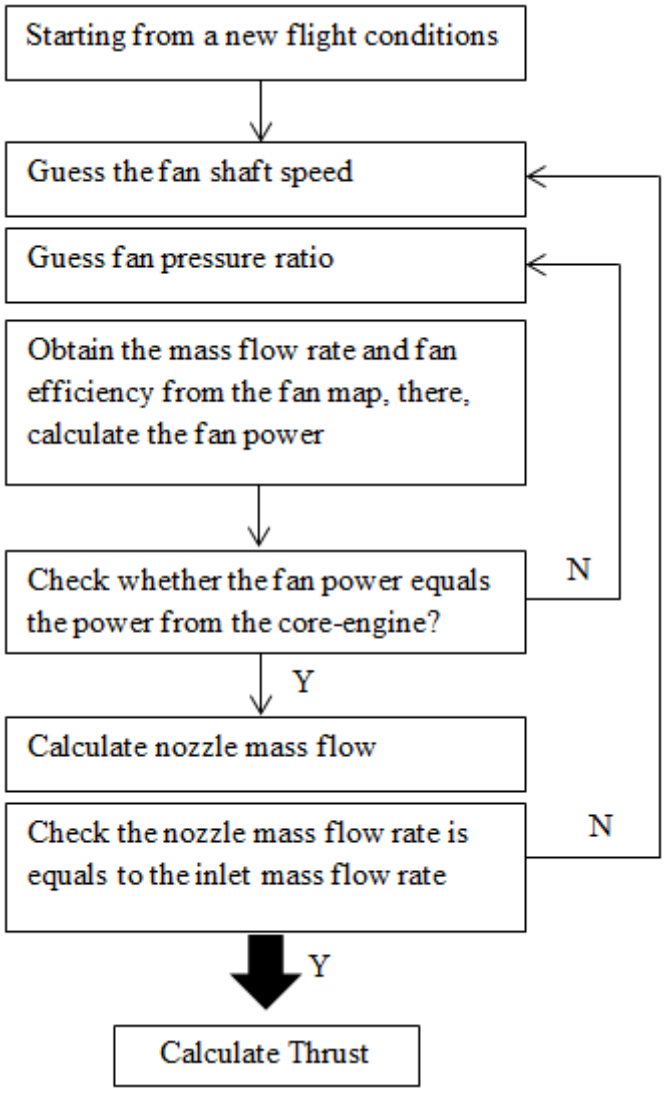

Figure 3.8 Flow Chart of The Iterative Process For Fan Off-design

3.2.6 Electric Motor

To apply the off design method, the motor performance curve is needed to obtain the shaft speed. For example, if by changing the TET, the core-engine free turbine power changes then the motor power changes. The power-rotating curve is needed to calculate its shaft speed. The modelling will be introduced in chapter 6. In this chapter, we assumed that the motor can work at any rotating speed. So the propulsor shaft speed can be optimised without considering the motor performance. The only link between the turbogenerators and the propulsors array is the power.

3.2.7 Core-engine Modelling Methodology

A turbogenerator comprises of a turboshaft engine and a superconducting generator. To design the generator, we can assume a constant working efficiency, $\eta_{generator}$, which equals to the ratio of electric power to mechanical shaft power form the power turbine. The impacts of its performance on the system design will be discussed in following chapter. The design methodology of the turboshaft engine is similar as the traditional design method. One of the most important considerations is the power it produces, which should be large enough to power the propulsors array. The design of the compression system should guarantee at different operation conditions that the compressor exit temperature (T3) and burner exit temperature (T4) should be at least 100K lower than the maximum values. This determines its overall pressure ratio. The shaft speed of the power turbine equals to the shaft speed of generator and the power turbine can operate within a very narrow range of efficiencies near the peak efficiency at each running line. Turbomatch was used to model the core turboshaft engine. Fig.3.9 shows the configuration.

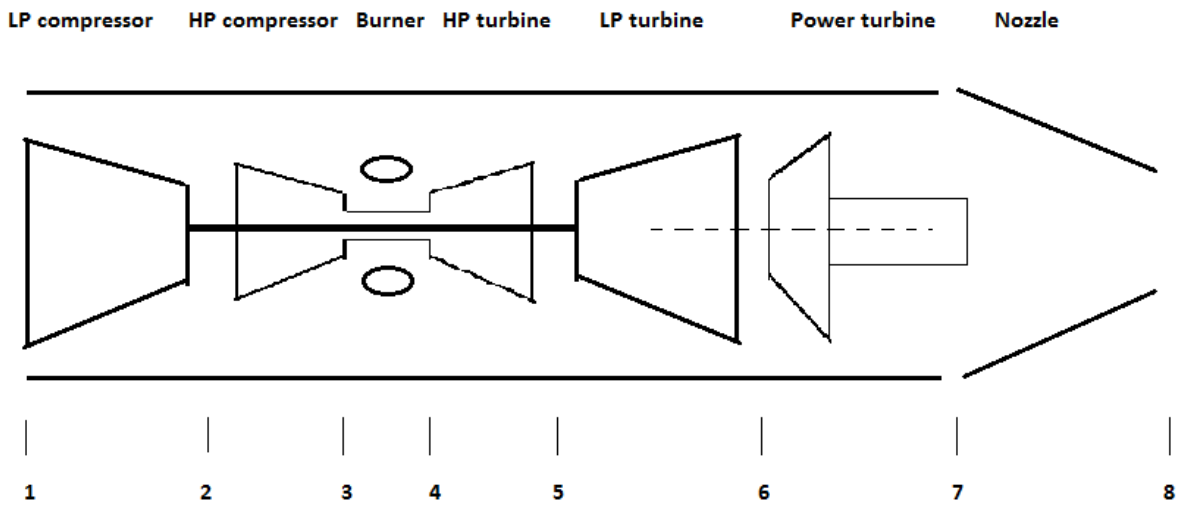

Figure 3.9 The Turboshaft Engine Modulus

3.2.8 Overall Modelling Methodology

The TeDP system model includes three major parts: the core turboshaft engine model, the propulsor model and the BLI model. Fig.3.10 shows how there three models connect to each other.

The first step is guessing the propulsor power and then calculating the fan diameter, fan shaft speed and the number of propulsors that should be used. After that, the mass flow rate of the propulsor can be calculated in order to produce enough thrust at design point. After obtaining the mass flow, propulsor inlet condition should be recalculated due to BLI and iteration is needed to ensure that under this boundary layer inlet condition, the thrust produced by the propulsors is equal to the design requirement. The next step is utilising Turbomatch to find the fuel consumption and to check whether the requirements are satisfied. If not, change the design propulsor PPR. Finally, thrusts and fuel consumptions at take-off, rolling take-off and top of climb should be calculated to test whether they meet the design targets.

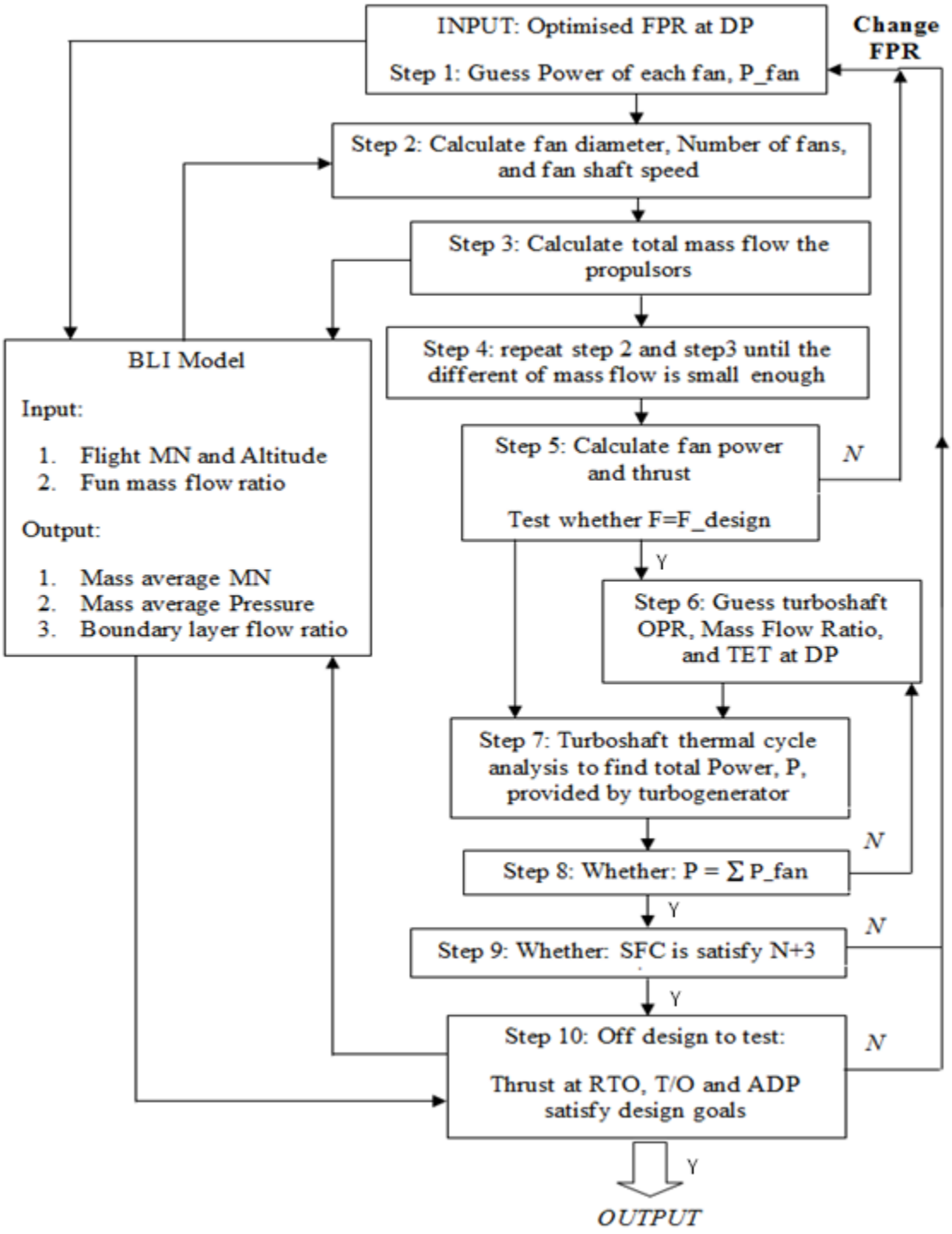

Figure 3.10 Engine Thermodynamic Cycle Calculation Procedure

3.3 Propulsor Design Point Analysis

3.3.1 Number of Fans

A turboshaft-driven TeDP system with propulsor fan pressure ratio equals 1.3 was chosen to give an example of how to obtain the optimum number of propulsors. The propulsors array should produce 120 KN thrust at design point, so increasing the number of propulsors reduces the thrust of individual propulsor. Fig.3.11 shows the weight of the propulsors array reduces with the increment of the number of propulsors. Fig.3.12 shows the total inlet width of the propulsors array increase with the propulsor number. In this case, the allowable width is 19.4 meters. So the number of propulsors cannot exceed 16. Fig.3.13 shows that the fan diameter reduces with the increment of propulsor number. The fan should be designed with a diameter larger than 1 meter so the number of propulsors cannot exceed 18. Fig.3.14 shows the fan shaft speed at different number of fans to satisfy the fan tip speed limitations. It has been proved that the other benefit of increasing the number of propulsors is that of increasing its shaft speed. In summary, the optimum number of propulsors equals to 16 at PPR 1.3. In this case, its fan diameter equals 1.06 meters; its shaft speed equals 4536 RPM, and the propulsors array inlet width equals 19.2 meters.

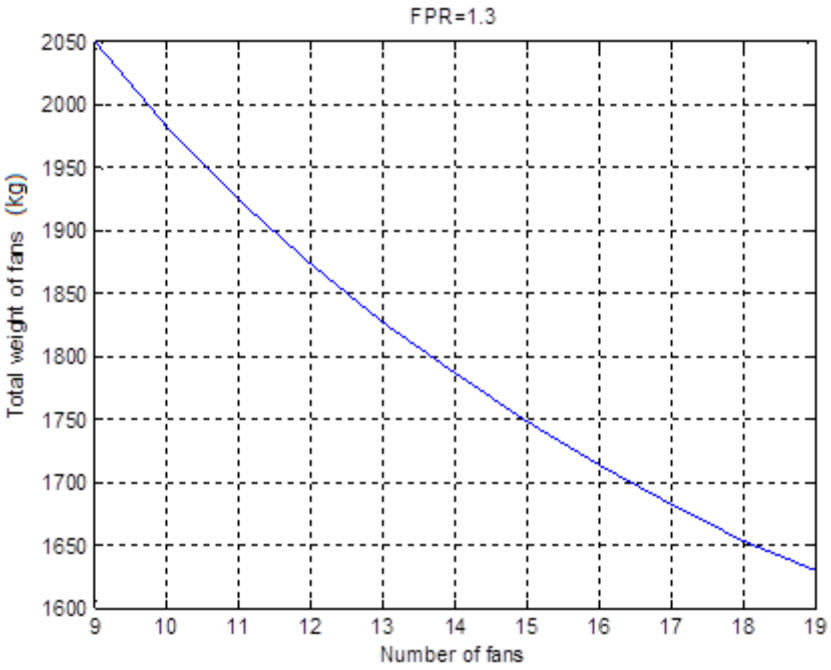

Figure 3.11 Propulsors Array Weight at Different Number of Fans (PPR=1.3)

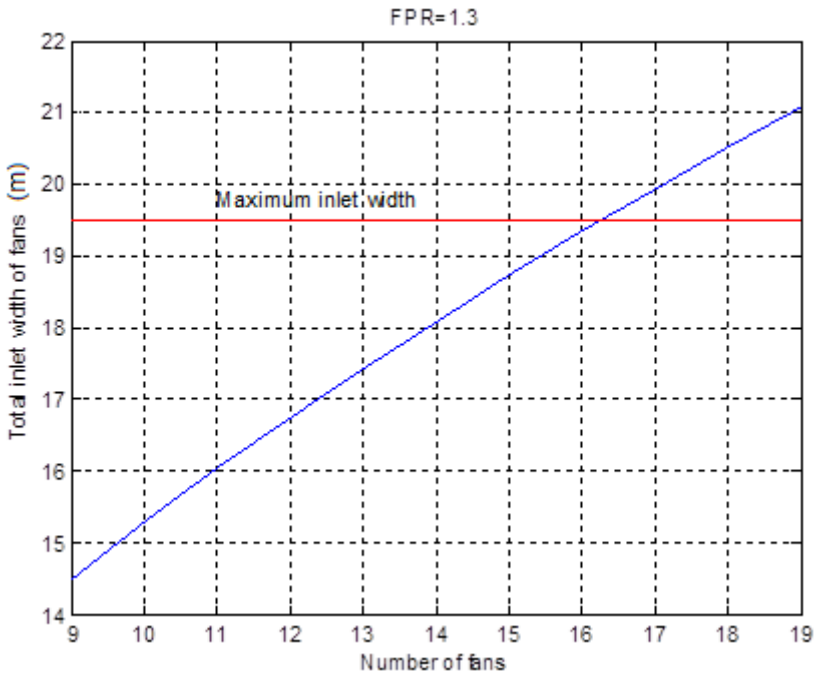

Figure 3.12 Total Inlet Length vs. Number of Fans at PPR=1.3

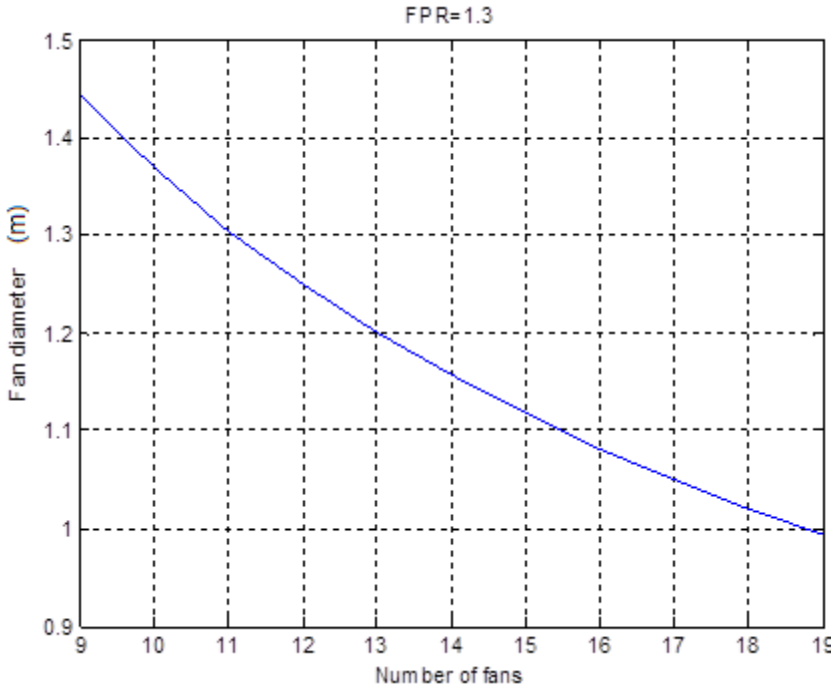

Figure 3.13 Fan Diameter vs. Number of Fans at PPR=1.3

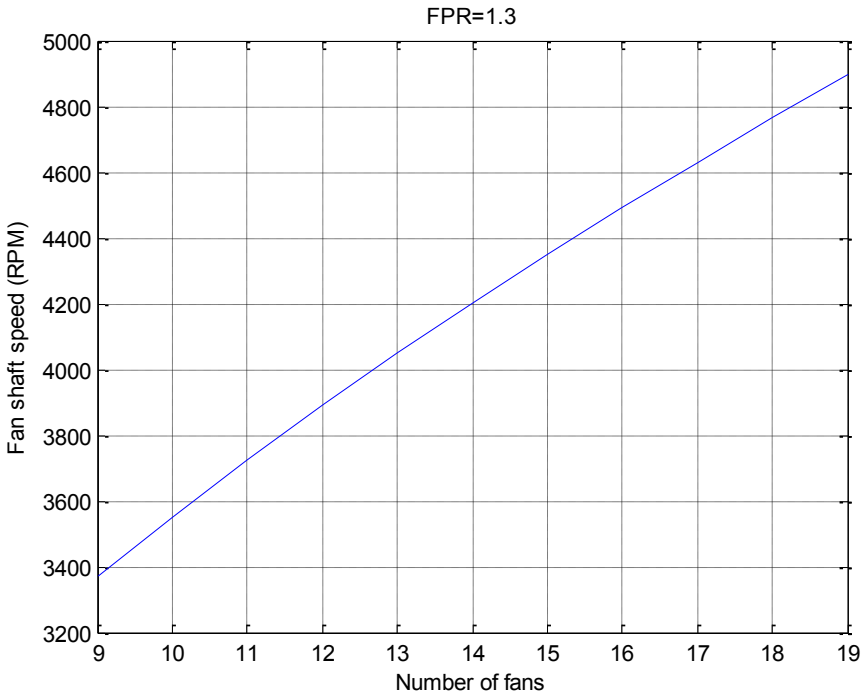

Figure 3.14 Shaft Speed vs. Number of Fans at PPR=1.3

Table 3.3 shows the propulsor DP parameters from PPR=1.2 to 1.5.

Table 3.3 Propulsor DP Parameters at Different PPR

PPR	1.2	1.25	1.3	1.35	1.4	1.45	1.5
number of propulsor	12	14	16	17	14	13	12
Inlet width, m	1.61	1.37	1.20	1.10	1.15	1.15	1.15
Fan diameter, m	1.44	1.22	1.06	0.98	1.02	1.02	1.02
Fan tip speed, m/s	209.09	238.96	268.83	298.70	328.57	358.44	388.32
Fan shaft speed, rpm	2644	3525	4536	5650	5947	6287	6778

Fig.3.15 compares the results from NASA. The differences come from the different number of fans we used. In our model, the fan diameter cannot be smaller than 1 meter. This is because there should be enough space after the fan stage to fix an electric motor, and we assumed the minimum motor diameter is 0.3 meters. So if the

fan diameter is too small, the duct pressure loss after the fan stage will increase. The difference of the TSFC comes from the different tools we used to model the core-engine. However, the differences are within 5%.

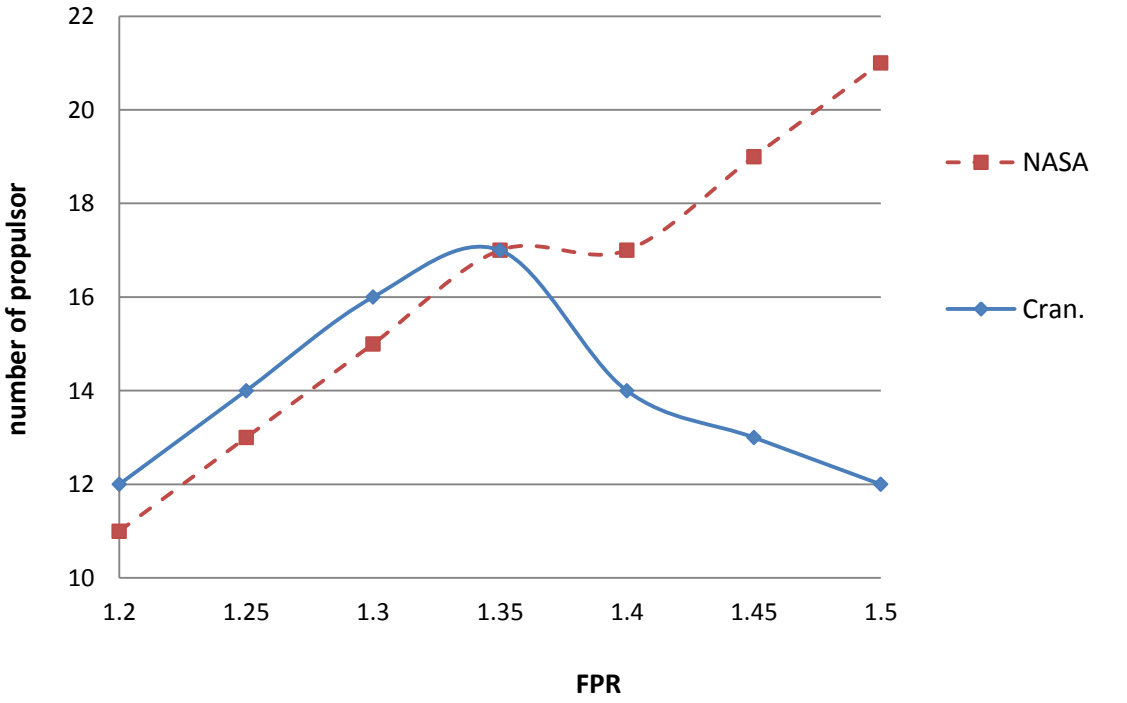

(a) Number of Propulsors

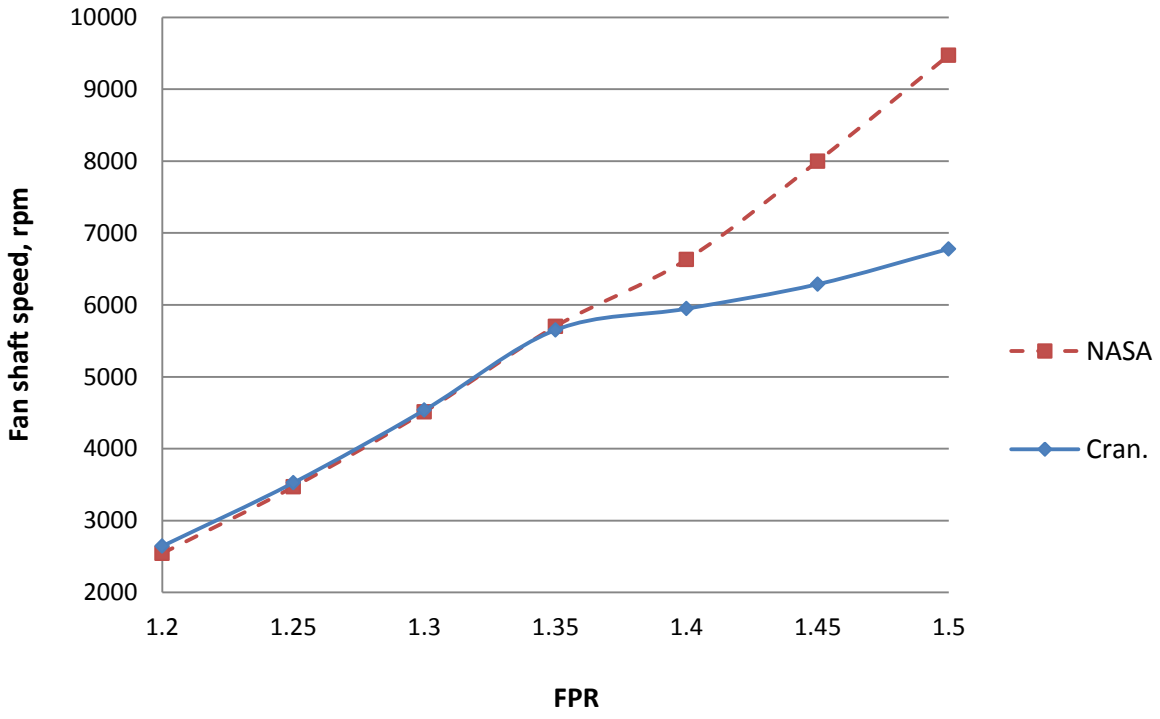

(b) Fan Shaft Speed

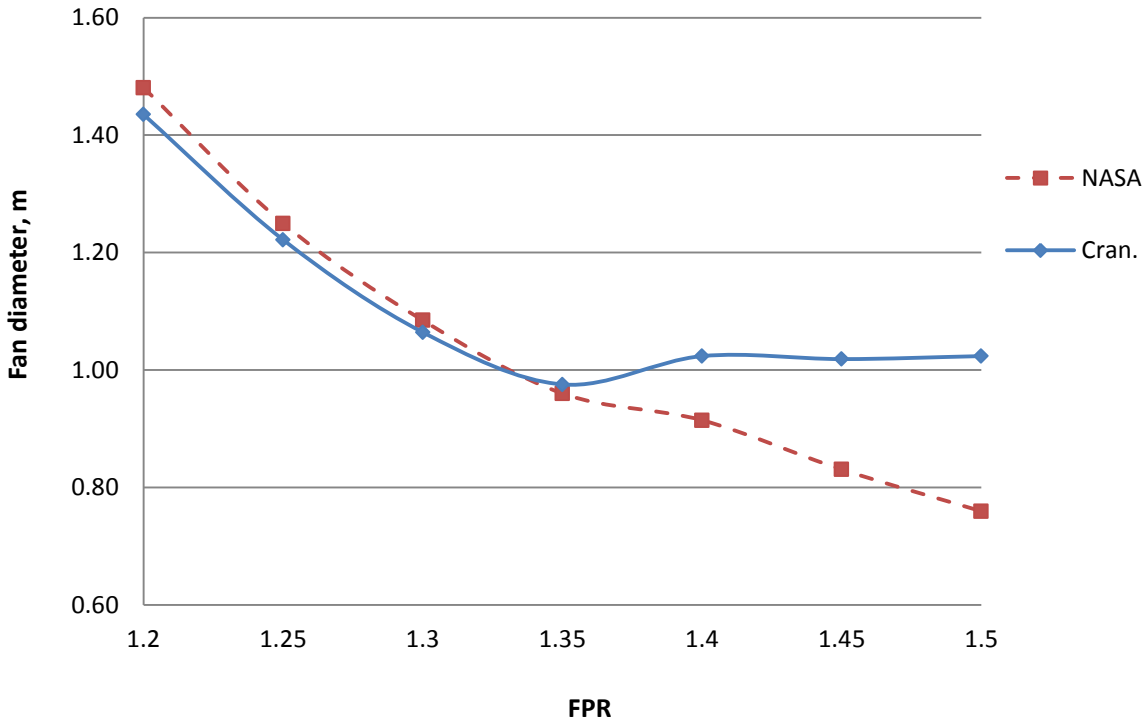

(c) Propulsor Fan Diameter

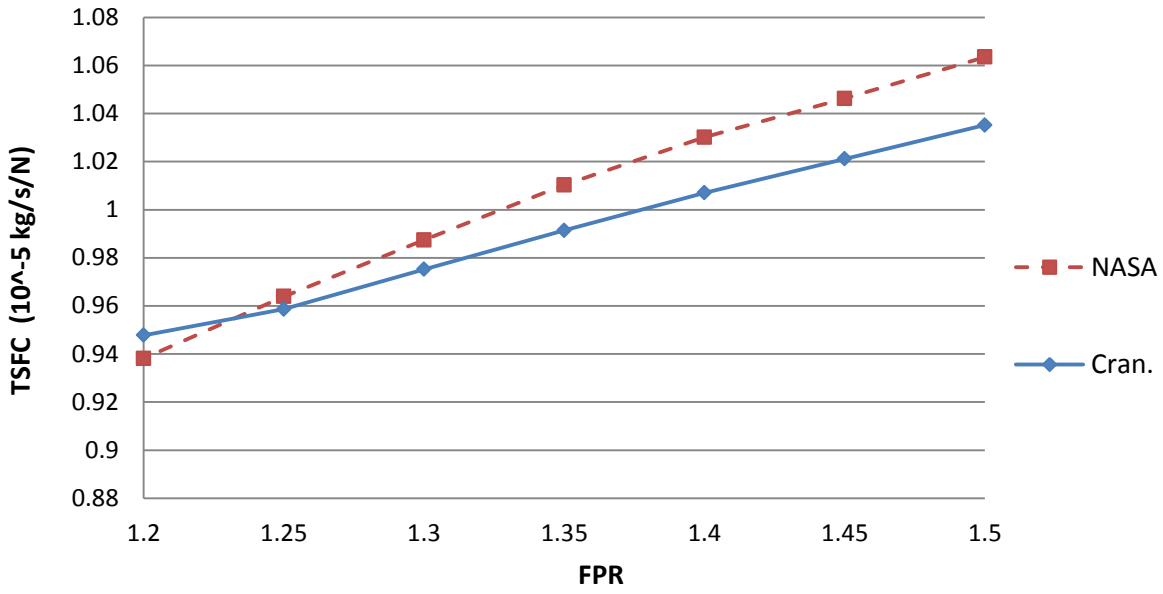

(d) TSFC at DP

Figure 3.15 Comparison with NASA's Results

3.3.2 Thermodynamic Cycle Results

A design fan pressure ratio of 1.3 was selected to explore the performance of the TeDP system.

Table 3.4 Engine Cycle Results Comparison (NASA data from reference 19)

	NASA	Cranfield
Number of fans	15	16
DP		
Thrust (kN)	74.09	80.64
TSFC (mg/s/N)	9.91	9.66
OPR	75	79.8
PPR	1.3	1.3
TET (k)	1811.1	1811.1
Generator power (MW)	8.35	9.17
Motor power (MW)	1.113	1.12
W_Propulsors (kg/s)	809.58	844.18
ROT		
Thrust (kN)	301.4	276.21
T3	1005.56	917.78
T/O		
Thrust (kN)	551.89	432.95
TET (k)	1922.22	1903.18

3.4 Sensitivity of Fuel Consumption to the TeDP System Design Assumptions

This section presents the results of a sensitivity analysis of the fuel consumption to reductions in some key technology assumptions. These include the pressure loss and propulsor fan efficiency drop due to ingesting boundary layer and cooling loss. Also, the reasons why a TeDP with thrust comes from both the propulsor arrays and core-engines will be developed in following chapter.

3.4.1 Propulsor Intake Pressure Loss

The manner in which the inlet and engine designs are integrated plays a key role in determining the degree to which propulsion system and aircraft operational goals are ultimately achieved in the production model. The fundamental challenge for engines ingesting boundary layer fluid is the non-uniform velocity profile of the air entering the engine, which causes serious loss of operability. So the flow should be mixed well before entering the propulsor. NASA assumed the flow mixes well before entering the propulsors. However, intake distortion will cause pressure drop. A loss factor, LF, was introduced in order to express its efficiency. The loss factor of a TeDP system is a function of inlet distortion and flight condition; it describes the total pressure loss due to BLI. . NASA indicated that with advanced intake duct design the duct pressure loss with BLI can be as small as 0.5%.

$$\mathrm{LF} = 1 - \mathrm{P}/\mathrm{P}_{\mathrm{noloss}} \tag{3-51}$$

Fig.3.16 highlights the TSFC benefits promised by using BLI in aircraft design. However, if the pressure loss exceeds 3% the benefits will be eliminated, especially at lower pressure ratio. Although the configuration with mixing loss is still more efficient than the non-BLI configuration, as losses increase, the benefit of BLI system relative to a non-BLI system decreases. So if the intake pressure losses are sufficiently high, HWB with podded propulsor configuration may be preferable.

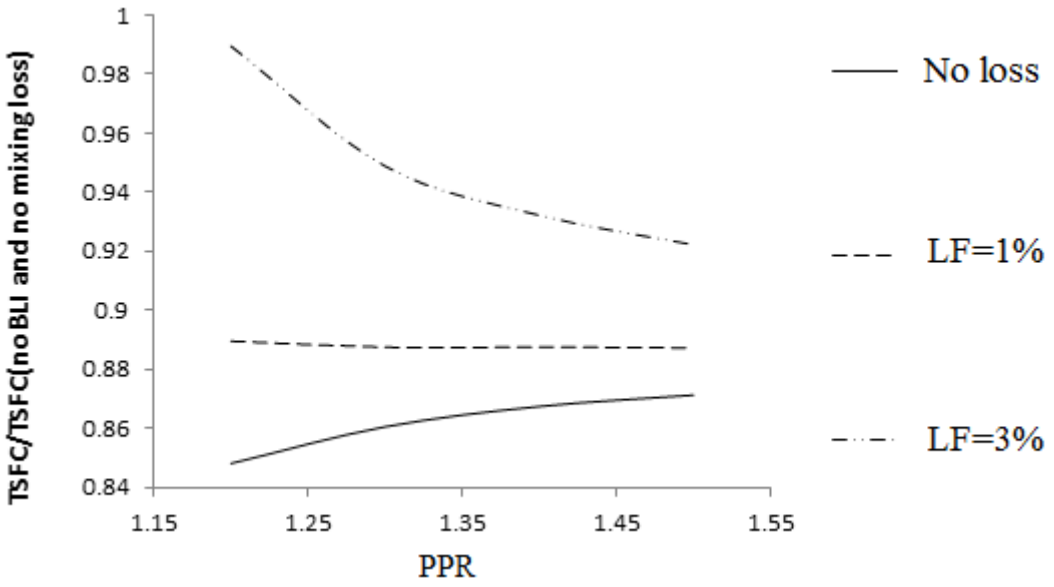

Figure 3. 16 Effect of Intake Total Pressure Loss

3.4.2 Propulsor Fan Efficiency

Fig.3.17 shows the TSFC at different propulsor fan pressure ratios. Reducing fan polytropic efficiency increases fuel consumption, especially at high propulsor fan pressure ratio. At PPR=1.3, a 2% reduction of the fan efficiency causes 1.7% increase of the TSFC.

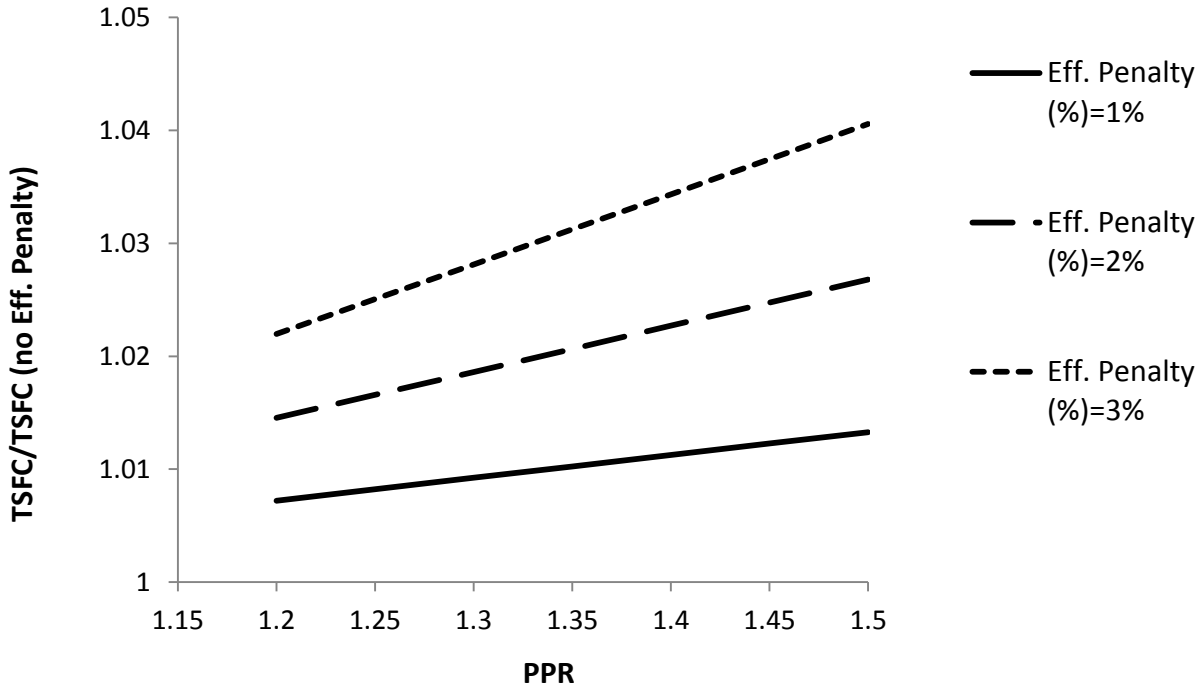

Figure 3.17 Fuel Consumption Change at Different Fan Efficiency Penalty

3.4.3 Cooling Losses

Superconducting machines were used due to their higher working efficiency. However, one of the challenges is the ultra-low operating temperature, which is usually not higher than 70 K. To maintain this low temperature, advanced cooling system is needed. In above-mentioned model, the power to drive the cooling system or the losing power in cooling process, was regarded as part of energy loss of the electrical system. And because the efficiency was assumed constant, the extra power needed for cooling system at some operating conditions, such as RTO, T/O, etc., was ignored. Fig.3.18 examined this problem at RTO. Cooling losses, here, refer to the additional power used for cooling.

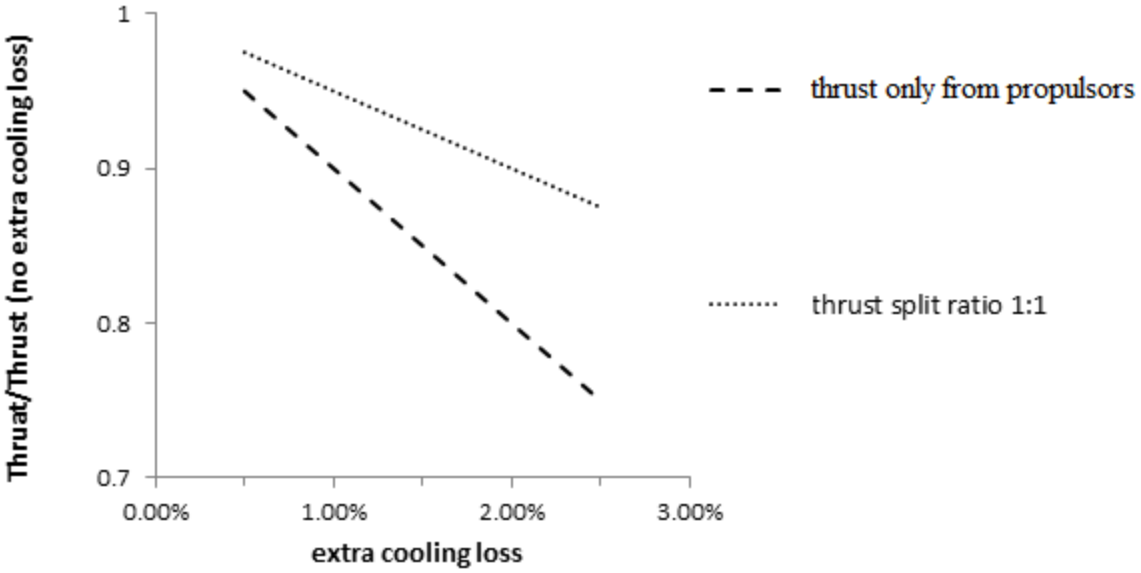

Figure 3.18 Thrust ratio vs. Cooling Losses at RTO

Thrust is reduced linearly with extra cooling losses. Taking the N3-X as example, if the TeDP extra cooling losses were higher than 0.5%, the thrust would fail to meet the requirements. There are numerous methods to solve this problem; one of them is by using liquid hydrogen (LH2). Hydrogen has a boiling point of 23 K at 2 atm, boiling hydrogen is therefore capable of cooling superconductors. In this case, LH2 would flow from the tank to motors, generators and other superconducting devices. Then power converters could be used to heat up the LH2 before entering the burner. LH2 as the energy source and superconducting machines have a very good synergy and represent one of the most promising technologies in future. However, the volume of fuel tank for LH2 would become larger, and evaporating the LH2 would cause airframe vibrations.

Another method is to replace the turboshaft engine with an engine where part of the turbine power is used to drive generator and the rest goes to produce thrust. In this case, thrust is produced by both turbogenerators and propulsors array. The extra cooling losses only reduces the propulsors' thrust, so excessive total thrust reduction was inhibited. For example, in Fig.3.18, if half of the thrust at RTO was produced by the cores, the system would bear 1% cooling losses.

One of other important design parameters is the electrical system weight. The weight of propulsor reduces with the increasing number of fans, which means the distributed propulsion system has the potential to achieve a lighter ultra-high bypass ratio

engine. Since the present chapter concentrates on the thermal and performance analysis of a distributed propulsion system, the weight of electric motors, superconducting generators, and cooling system are not considered here. However, when assessing the overall design of a distributed propulsion system the weight of the additional components and their implications must be accounted for. Especially in the case of a blended wing body configuration powered by distribution propulsion where the novelty of the concept system configuration and the resulting weight becomes very important. For example, an estimation of the total weight of electric system of a TeDP system would be around 5,000 to 10,000 kg. The final value depends on the number of propulsors, fuel type, cooling method, as well as the power of turbogenerator. Given the additional weight, which is similar to that of a conventional propulsion system, future studies should concentrate on these issues and address their implications on the overall design and performance. It is true that in the case of large mass penalties, the benefits of superconducting distributed propulsion system would be largely diminished. Detailed analysis will be introduced in following chapters.

3.5 Discussion

The BLI improves TSFC at all the range of examined FPRs, especially at low FPRs. This improvement benefits the TeDP on N3-X, which has ultra-high bypass ratio and low FPR. However, mixing loss, or distortion, in the intake duct largely reduces the benefit. Ingesting boundary layer increases propulsive efficiency but on the other hand, leads to higher distortion, which causes lower fan efficiency. Considering the above situations, in future TeDP system design, detailed CFD simulations of intake duct flow are needed to find a BLI ratio with small inlet distortion.

Different from podded engine configuration, concepts like the HWB with TeDP system, where the engine inlets and airframe are closely coupled, will make it very difficult to analyse components isolated from one other. The highly integrated inlet and airframe of such concepts could have significant impact on the propulsion system performance. In order to reduce the drag of pylons, HWB will allow the boundary layer developed forward of the engine face to be ingested by the inlet. Thermal cycle analysis showed benefits on fuel consumption. However, the total inlet pressure distortion seen by the propulsor fan could be detrimental to its operating

characteristics, which were not issued in this chapter. In future studies, impacts of propulsor inlet distortion should be analysed. Advanced CFD tools are needed to model the inlet flow behaviour and its impacts on engine performances.

The other issue of propulsion system airframe integration is its significant impacts on engine noise. N+3 highlighted a strict noise reduction goal for future aircrafts. For example, the position of engine, the inlet duct, and the jet exhaust plume; the number of propulsors, which are needed to be analysed in order to reduce the noise as much as possible.

In this chapter, the method to design a TeDP system for NASA N+3 Airplane was given. However, most of the design parameters were from NASA's assumptions, these included the BLI ingestion model and turbogenerator concept. In chapter 4, a new method to model the impacts of ingesting boundary layer will be given. This model will be used to analyse impacts of BLI on TeDP system DP performances. The TeDP system design point performance and off-design performance analysis by our own tools will be introduced in chapter 5 and 6.

3.6 Conclusion

1. The TeDP system design method put forward in this chapter was built on a hybrid wing body airframe; however, this method can also be used on other airframe. The first step was to determine the number of turbogenerators and propulsors. Turbogenerators were used to produce power to drive fans, so for a maximum allowed TET, OPR and mass flow ratio, its shaft work was calculated. The number of turbogenerators was found to meet fan power requirements. The number of fans or propulsors was affected by many other factors, which both come from engine design and airframe design. In short, satisfying all design constrains, the number of propulsors should be chosen as high as possible.
2. Changes in design FPR for a given thrust level influence the fan number and diameter. Higher FPR leads to an increased number of fans that can be chosen, but wth higher fuel consumption and smaller fan hub diameter. Lower FPR has lower fuel consumption and noise level, but reduced maximum fan shaft speed and the difficulty to recover inlet duct pressure loss. So for future TeDP system, the FPR should larger than 1.2 but smaller than 1.5.

3. A TeDP system developed in this chapter to power the NASA N+3 airplane has the following design parameters:

   Propulsors unit:

   - Number of propulsors: 16
   - Fan diameter: 1.06 meters
   - Inlet mass flow rate at DP: 83.1 kg/s
   - PPR: 1.3 @ DP
   - Motor power requirement: 1.74 MW @ DP and 2.69 MW @ T/O
   - Thrust: 119 KN @ DP and 432.95 KN @ T/O

   Each core-engine (turboshaft-driven two should be used):

   - OPR: 74.8 @ DP
   - TET: 1811K @ DP
   - Inlet mass flow rate at DP: 22.3 kg/s
   - Power turbine power: 14.2 MW @ DP and 22 MW @ T/O

4. The benefit of BLI reduced with increased intake pressure loss. The loss increased with increasing BLI ratio at all FPR range, and especially at low FPR. So if the intake pressure losses are sufficiently high, a podded propulsor configuration may be preferable. The other problem caused by BLI is the fan efficiency drop. So a model to figure out the impacts of propulsor intake distortion due to BLI should be built.
5. Extra power for cooling is needed at some operating condition such as RTO and T/O. If the losses are too high, a TeDP will fail to produce enough thrust. Moreover, in this chapter, impacts of BLI were not considered in off-design performance.
6. Although, there are technical challenges, the use of TeDP system with BLI on N3-X airframe offer an opportunity for reduced fuel consumption compared to podded propulsion system.

Chapter IV

A Preliminary Method to Model Boundary Layer Ingestion of the TeDP System

Ingesting boundary layer (BLI) by fans in propulsion system improves the propulsive efficiency. However, inlet flow distortion dramatically eliminates these benefits. This chapter puts forward a method to deal with BLI and examines their impacts on the turbofan performance at engine design point. At all examined fan pressure ratios, boundary layer ingesting improved fuel consumption. However, the benefits predicted by the new method are lower than previous predictions. NASA's predicted 7-8% of fuel saving for the N3-X aircraft comes from BLI. However, it is a challenge to meet this goal due to inlet distortion.

4.1 Introduction

It has long been known in the field of marine propulsion that the propulsive efficiency is improved when fluid from the wake of the craft is used as part or all of the propulsive steam. Because with wake ingestion, the power expended can actually be less than the product of the forward speed and craft drag. The benefit of boundary layer ingesting (BLI) comes from re-energizing the aircraft wake, which enables less kinetic energy to be wasted. Fig.4.1 illustrates physical concepts of podded engine and BLI engine by using two idealized configurations. The podded engine shows the situation with no BLI, and the BLI engine shows a situation with 100% of boundary layer (or wake) ingested by the engine.

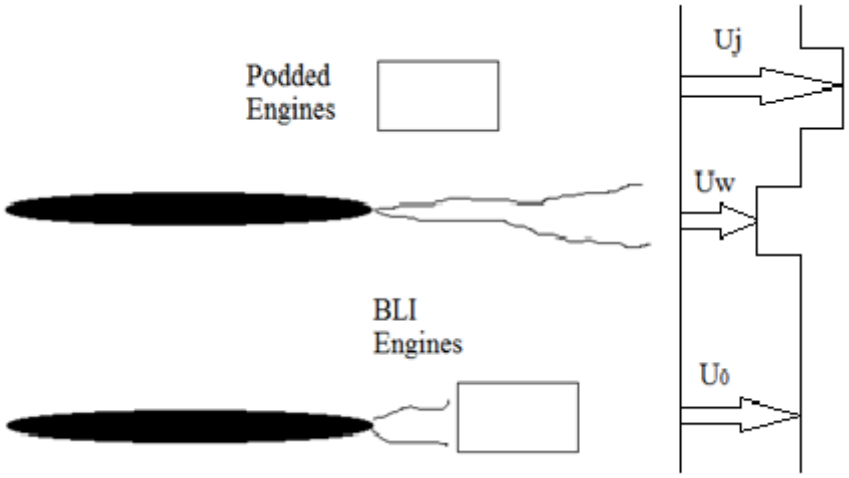

Figure 4.1 Idealized Configuration of Podded Engines and BLI Engines [52]

With podded engine, the flow entering the engine has a velocity of U_o. The engine accelerates the flow to *U*j to recover the momentum deficit by the airframe drag. The *Uw* is an average velocity in the aircraft wake. So the engine thrust, Fn, and mechanical power ratio, P, are, (if we assume $U_j - U_o = U_o - U_w$) :

$$Fn = \dot{m}(U_j - U_o) = \dot{m}(U_o - U_w) \tag{4-1}$$

$$\mathrm{P}_{podded} = \frac{\dot{m}(U_j^2 - U_o^2)}{2} = \frac{Fn}{2}(U_j + U_o) \tag{4-2}$$

For the BLI case, if all the boundary layer was ingested and the engine increases the wake velocity from *Uw* to *Uj,* in this case, $U_j = U_o$. So:

$$Fn = \dot{m}(U_j - U_w) = \dot{m}(U_o - U_w) \tag{4-3}$$

$$\mathrm{P}_{BLI} = \frac{\dot{m}(U_j^2 - U_w^2)}{2} = \frac{Fn}{2}(U_w + U_o) \tag{4-4}$$

Since *Uj>Uw,* the power needed for the podded engine to produce the same thrust is higher than the BLI engine. The above arguments, although idealized, capture the benefit of BLI on fuel saving. However, directly ingesting boundary layer flow would dramatically increase the inlet flow distortion [44,45, 69], which leads to fan efficiency drop, fan surge margin drop, serious vibration, and total pressure losses [46,47,50,61,62]. So the main purpose of this chapter is to build a method to model inlet flow distortion and estimate its impacts on fuel saving.

4.1.1 Aims of this chapter

- Summarise the methods to model BLI
- Introduce a new method to model BLI for the TeDP system
- Apply the new method to the TeDP system with BLI and compare the results with previous predictions
- Assess the risks associated with the using of BLI

4.2 Previous Works

There are numbers of methods to model BLI. Fig.4.2 shows the control volume of one engine with boundary layer ingesting developed by NASA.

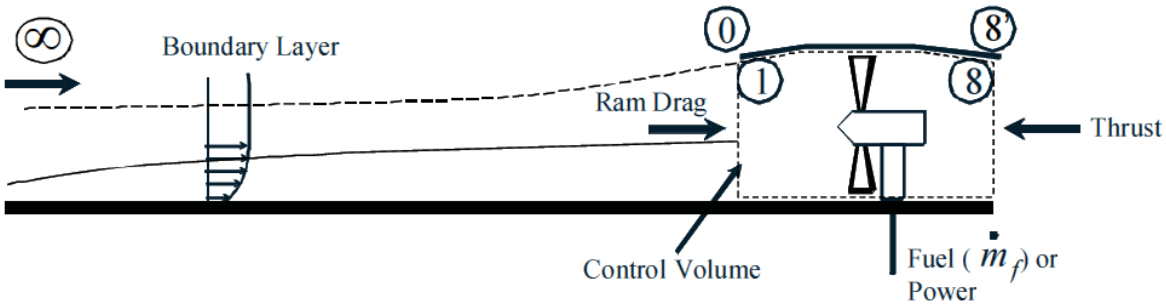

Figure 4.2 The Analysed Control Volume of Propulsion System with BLI [32]

In this case, Felder [32] gave the expression of net thrust:

$$Thrust\ (net) = \left(\dot{m}_1 + \dot{m}_f\right)U_8 - \dot{m}_1 U_1 + (p_8 - p_{8'})A_8 - (p_1 - p_0)A_1 \tag{4-5}$$

$$P_1 = P_0 \times R_{Pt} = \sum_0^i (m_i P_i) \,/\, \sum_0^i m_i \tag{4-6}$$

$$Ma_1 = Ma_0 \times R_{MN} = \sum_0^i (m_i Ma_i) \,/\, \sum_0^i m_i \tag{4-7}$$

In Eq.4.5, p_0 is the atmospheric static pressure, p_1 is the intake duct inlet static pressure, p_8 is the nozzle exit static pressure, and $p_{8'}$ is the nozzle exit ambient pressure. The inlet average total pressure and Mach number can be calculated by Eq.4.6 and Eq.4.7. P1 and Ma1 are the mass average intake total pressure and Ma. A profile of the mass-average Ma and P was calculated from the boundary layer

profiles. The mass average Ma and P for each distance "i" in the profile was calculated from the Eq.4.6 and Eq.4.7, where mi is the mass flow through the i*th* segment of the boundary layer, MAi is the Mach number in the i*th* segment, and Pi is the total pressure in the i*th* segment. Based on NASA's data, if the inlet height of Propulsor was chosen, to achieve the same thrust requirements, those two parameters are function of propulsor fan pressure ratio (PPR), so through 4th order simulation (initial data from NASA's thesis), we can find: (where the R_{Pt} is the mass average inlet total pressure ratio (defined by Eq.4.6) and R_{Ma} is the mass average inlet Mach number (defined by Eq.4.7)).

$$R_{Pt} = 0.3182 * PPR\text{^}4 - 1.5995 * PPR\text{^}3 + 3.0778 * PPR\text{^}2 - 2.8415 * PPR + 2.0419 \quad (4\text{-}8)$$

$$R_{Ma} = 0.3182 * PPR\text{^}4 - 1.5914 * PPR\text{^}3 + 3.0857 * PPR\text{^}2 - 2.9806 * PPR + 2.1335 \quad (4\text{-}9)$$

Both equations are only suitable from FPR 1.15 to 1.5.

Smith [60] carried out a detailed analysis of axisymmetric un-ducted propeller ingesting a wake using an actuator disk. He assumed the conditions were incompressible flow, no viscous force or mixing, no circumferential distortion, and the wake keeps its profile across the propeller. This method used stream line to express the flow on radial direction. Fig.4.3 shows the model he used: a wake air passing through the actuator disk propulsor.

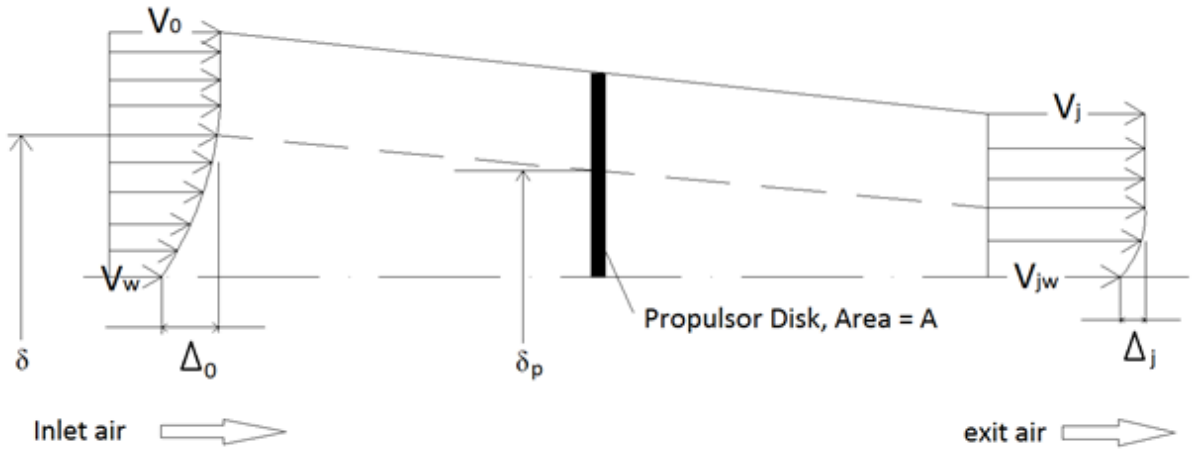

Figure 4.3 Smith Propulsor Ingesting Wake Model

In the model, he assumed the wake fluid maintains its identity and its viscous shear stresses are neglected. He defined a wake recovery factor, R (By Eq.4.10). R is greater than zero for two reasons: the propulsor adds more energy to the fluid, that approaches it with lower axial velocity and even if the wake fluid got the same energy from the propulsor as did the rest of the propulsor stream, its axial velocity defect would be reduced so as to keep the same kinetic energy defect. He also assumed the R in his analysis was kept the same value for all wake streamlines.

$$R = 1 - \frac{V_j - V_{jw}}{V_0 - V_w} \tag{4-10}$$

He also defined a power saving coefficient, PSC, as the ratio of the difference between the propulsive power with and without BLI to the power necessary to propel the body whose drag is to be ingested.

$$PSC = \frac{P_p' - P_p}{V_0 D/\eta_p'} \tag{4-11}$$

Where P_p' is the propulsor power without BLI; P_p is the propulsor power with BLI; η_p' is the propulsive efficiency without BLI; D is the drag, and V_0 is the fight velocity

Eq.4.11 tells us that to ingest a certain drag, *D*, an equal thrust must be provided to propel it. In one case its wake goes through the propulsor, and in another case it does not. The power will be less when the wake is ingested. The PSC was defined in terms of propulsive powers. As we know, when the wake is not ingested, thrust and power can be described by following equations:

$$T' = \frac{\rho}{2} A({V_j'}^2 - V_0^2) \tag{4-12}$$

$$P_p' = \frac{1}{2} T'(V_j' + V_o) \tag{4-13}$$

Substituting Eq.4.12 and Eq.4.13 into Eq.4.11, the power saving coefficient becomes:

$$PSC = \frac{V_j' - V_j}{V_j' + V_0}\frac{T}{D} + \frac{V_0(2-R)}{V_j' + V_0}\left[\frac{V_j}{V_0} - 1 + R(1-K)\right] \quad (4\text{-}14)$$

Where K is the Pseudo energy factor, defined by Eq.4.15

$$K = \frac{BL\ energy\ thickness}{BL\ momentum\ thickness} = \frac{\int_0^\delta \frac{V_w^2}{V_0^2}\left(1 - \frac{V_w}{V_0}\right)dA}{\int_0^\delta \frac{V_w}{V_0^2}\left(1 - \frac{V_w}{V_0}\right)dA} \quad (4\text{-}15)$$

He found the power saving increases with the propulsor disk loading, and the benefit can be in the 20% range in some cases. The power saving with wake ingestion is greatest for small propulsors, such as propulsors with high thrust-loading coefficients. Moreover, he found the power saving is greatest when the form factor of the wake being ingested is high.

Longley and Greitzer [74] put forward a parallel stream method for a 2D analysis of BLI. They represented the non-uniform inlet velocity by two uniform streams of different stagnation pressure and velocity, and assuming no mixing losses between these two streams. These two streams have the same height. After passing the fan, both streams reached the same static pressure. They found that the BLI benefit increased with increasing ratio of ingested boundary layer. Their calculation process can be described as follow:

Step 1: obtain the boundary velocity profiles.

Step 2: use two uniform streams, with the same height, to present the velocity profile. These two streams have no pressure distortion; velocity should be calculated by Eq.4.16:

$$V = \frac{\int_0^t \rho V dt}{\int_0^t \rho dt}, where\ t\ is\ the\ height\ of\ one\ steam \quad (4\text{-}16)$$

Step 3: guess pressure ratio of one stream and calculate the pressure ratio of the other stream. These two streams have the same fan exit static pressure, which can be calculate by Eq.4.17 and Eq.4.18. In Eq.4.18, the Ma is the Mach number through the fan stage.

$$P_{exit} = P_{in} \times FPR \tag{4-17}$$

$$p_{exit} = P_{exit} / \left(1 + \frac{r-1}{2} Ma^2\right)^{\frac{r}{r-1}} \tag{4-18}$$

Step 4: calculate the thrust in order to obtain the PSC.

However, the problem of this method is that the working points of both streams cannot be guaranteed in the same fan running line. That is because, there is no total temperature difference and the rotating speed of the rotator is the same. The working points of each stream should be in the same fan running line. In short, this method can be described by Fig.4.4. In the figure, two fans are used to compress each stream in order to let them reach the same exit static pressure.

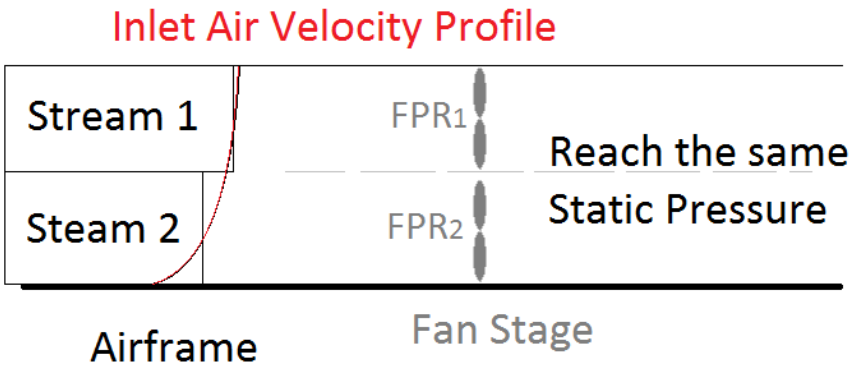

Figure 4.4 Parallel Stream Method Model

Parallel compressor models have been widely used to model compressor response to inlet distortion. The concept considers the circumference of the compressor to be divided into two flow regions: one with the relatively low velocity such as would exit behind a distortion inducing screen and one of relatively high velocity. The compressor performance in each region is assumed to be obtained from uniform flow operation at the local value of inlet velocity. It is further assumed that circumferential cross flow within the compressor is negligible and that the exit static pressure is uniform. The total pressure distortion is attenuated by the compressor because of the difference in the pressure ratio between the high and low velocity regions. The limit of stability (stall point) of the distorted compressor is predicted to occur when the low velocity region reaches the uniform flow (undistorted) compressor stall point.

The resultant performance at stall is calculated as the area average of the two regions.

Fig.4.5 illustrates the method. Consider a circumferential segment as it approaches the compressor. In the presence of a non-uniform inlet total pressure, circumferential static pressure gradients exist at the compressor inlet which redistribute the flow and can alter the flow velocity and direction of that segment. Proceeding through the compressor, the circumferential non-uniform static pressure can cause further flow redistribution, particularly when ‘stagnant’ air cavities exist external to the compressor flow path. This redistribution will result in a different amount of airflow in the segment at different axial locations within the compressor. Finally, the exit static pressure may not be uniform so it is necessary to know the angular displacement of the segment as it traverses the compressor in order to apply the proper downstream boundary condition. But to apply the parallel compressor method, one of the assumptions is that the two sections reach the same static pressure.

Multiple-segment parallel compressor model expands the basic parallel compressor theory by using multiple parallel segments to provide a detailed definition of the circumferential flow field. The flow rate in each segment is determined from its boundary conditions (inlet total pressure, total temperature and exit static pressure) and the compressor’s performance within that segment in a manner quite similar to classic parallel compressor. The concept of using multiple parallel segments, however, is much more complex than the multiplication of the classic calculation. The complexity arises from two dimensional flow effects and from unsteady flow effects caused by the relative motion of rotor blades through the distorted flow region.

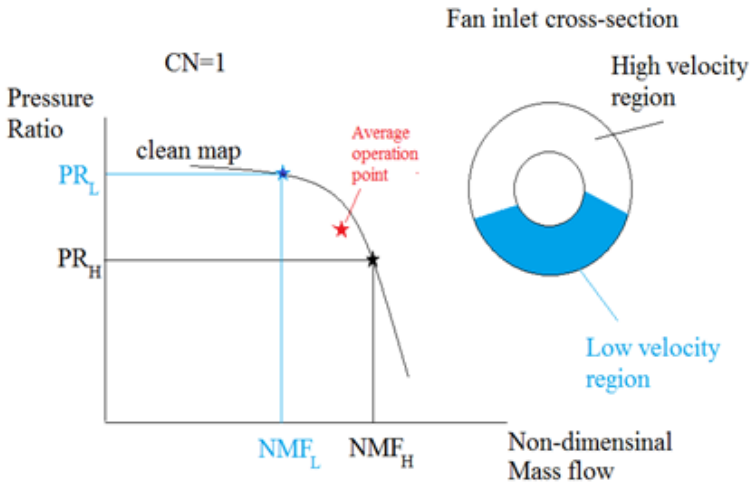

Figure 4.5 Parallel Compressor Method

Another method given by Plas [75] is called Integral Boundary Layer Method. This method is similar to Smith's method. She assumed the flow shape factor keeps, H^* defined by Eq.4.19, the same after the fan. And also found the BLI benefit increases with increasing ratio of ingested boundary layer. She also found at very low ratio of inlet boundary layer, the power saving ratio would become negative.

$$H^* = \frac{\int_0^{\delta}\left(1-\frac{\rho u}{\rho_0 u_0}\right)d\delta}{\int_0^{\delta}(1-\frac{u}{u_0})\frac{\rho u}{\rho_0 u_0}d\delta} \tag{4-19}$$

In her model, she assumed the flow can be represented by a boundary layer and an inviscid stream of uniform properties at any duct location. The static pressure is uniform across the duct and only integral descriptions of the boundary layer are needed. The effect of boundary layer was estimated by putting a heat exchanger through the duct, as Fig.4.6 shows. She used exponential decay of the pressure difference between the freestream p1 and the wall p2, over a distance based on the boundary layer thickness. The pressure field due to the heat exchanger was reflected in an extra term in the integral momentum equation and the scheme worked well. However, for fan modelling, this approach is more difficult to apply due to the identification of the appropriate wall pressure and length scales.

The way to calculate the fan pressure rise is, firstly, by assuming an ideal fan without any losses and deviations. The stagnation pressure rise can only be calculated on

an overall basis, i.e. based on the corrected flow. The next step is to calculate the pressure and temperature rise in the inviscid part of the flow based on the corrected mass flow for this stream, and to let the pressure rise in the boundary layer come out of the calculation. The static pressure downstream of the fan is calculated from the inviscid flow characteristics. Finally, fan power should be obtained by Eq.4.20:

$$Power = \dot{m}C_p(T_{exit} - T_{inlet}) \tag{4-20}$$

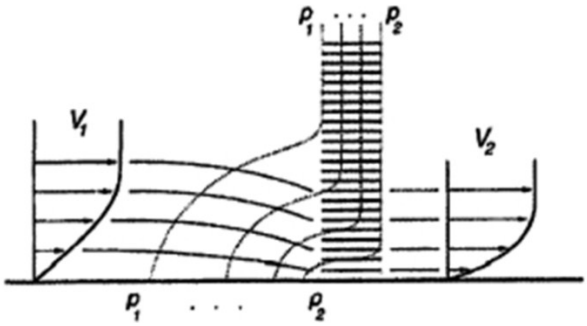

Figure 4.6 Pressure Field Contours and Streamlines for a Boundary Layer Approaching a Heat Exchanger, from [4]

The integral model is useful because, firstly, it shows the same trends of the power saving coefficient as the parallel compressor models. Secondly, it demonstrates that inlet pressure recovery is not decreased with BLI. Thirdly, it shows the importance of the downstream blockage in setting the performance of the propulsion system with BLI. If the distortion is not attenuated enough, BLI is not beneficial.

Liu and Eddie [39] introduced a 2-dimensional integral method. This method simplified the 3D CFD simulation to a 2D problem. Fig.4.7 shows their computational domain. Based on their computational domain, Eq.4.21 to Eq.4.23 can be converted in order to calculate the force and velocity through a fan blade. The detailed method was introduced in the reference 37.

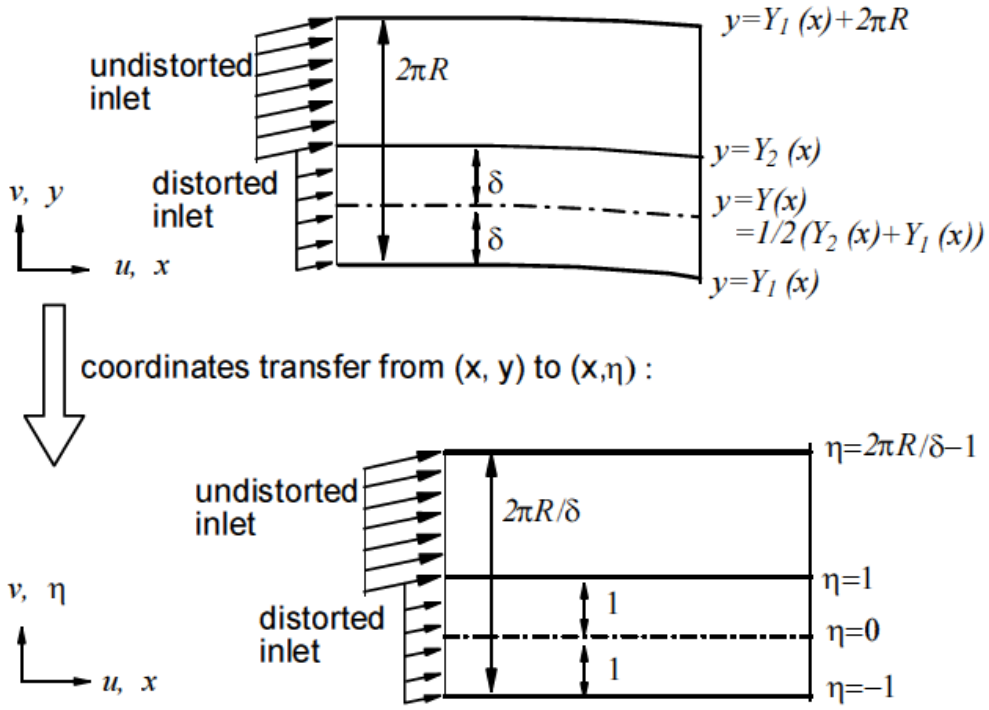

Figure 4.7 2D Integral Method by Liu and Eddie [39]

The inlet flow is described by the following equations:

$$\frac{\partial u}{\partial x}+\frac{\partial v}{\partial x}=0 \tag{4-21}$$

$$\frac{\partial}{\partial x}(u^2)+\frac{\partial}{\partial y}(uv)+\frac{\partial}{\partial x}\left(\frac{p}{\rho}\right)=F_x \tag{4-22}$$

$$\frac{\partial}{\partial x}(uv)+\frac{\partial}{\partial y}(v^2)+\frac{\partial}{\partial y}\left(\frac{p}{\rho}\right)=F_y \tag{4-23}$$

Besides these methods, 3-dimensional (3D) analysis, including streamline curvature [72] and 3D CFD simulation, and experimental methods can be used to model BLI.

Comparison of different methods to model BLI

Group 1

The methods in this group need detailed information of the fan blade shape, so it is not suitable for preliminary design for a TeDP system.

	Smith Method	3D Method
✓	• Convenience to use • Calculation can be done without using computer	• Precise
×	• More suitable for un-ducted fan • Cannot address the effects of intake distortion due to the BLI	• Time consuming • Need large computer sources

Group 2

The methods in this group don't need detailed information of the fan blade shape, so it is suitable for preliminary design for a TeDP system.

	Parallel Stream Method (PSM)	Parallel Compressor Method (PCM)
✓	• Suitable to model redial distortion	• Widely used method
×	• It is a 2D modelling method to address BLI • Maybe neglect impacts of inlet distortion	• Fan map needed

The difference of the PSM and the PCM:

To use the PSM, the mass flow ratios of each stream are known, therefore, their pressure ratio can be calculated by their exit static pressure.

To use the PCM, the mass flow ratios of the two sections are un-known, therefore, the fan map is needed to obtain the pressure ratio.

4.3 Approach to Assess BLI

In recent years inlet pressure distortion and its effect on compressor stability have received much attention. Great amounts of effort have been expended on distortion testing, correlation of distorted inlet conditions with compressor surge, and evolution

of models to predict the reaction of the compressor to distortion. In most cases the distortion is a combination of circumferential and radial gradients, especially of high ratio BLI propulsion system. Directly BLI system has ultra-high inlet distortion, so finding a new way to estimate its impacts becomes important for preliminary engine design.

The difficulty of direct modelling BLI comes from non-uniform inlet (inlet non-uniform total pressure and velocity). Distorted inlet leads to non-uniform pressure rises through the fan blade. So it is difficult to calculate the flow exit total pressure and temperature directly. To solve this problem, the new method makes the following three assumptions:

1. No inlet total temperature distortion

Total temperature is a way to estimate the total energy. As we know, for a flow of gas without heat transfer and external work, the total temperature is constant. Boundary layer is caused by viscous force between the wall and flow itself, the heat transfer between the wall and the flow is limited. So the inlet process can be assumed isentropic. 3D CFD simulations also show there is slightly total inlet temperature difference with well-designed inlet duct [40]. This assumption indicates that all the inlet flow sections are working in the same non-dimensional speed line if the compressor rotational speed is the same. So once the corrected mass flow of the inlet flow section is obtained, the pressure ratio can be found on the compressor map.

2. Uniform exit static pressure

This assumption indicates that all the flow sections reach the same static pressure after a compressor stage (fan blade), therefore flows mixed well before entering the nozzle.

3. Constant intake duct total pressure loss

Propulsor inlet pressure loss is caused by both the boundary layer itself and the intake duct. The total pressure loss of BLI is caused by the effects of viscosity of a surface. The pressure drop only happens within the boundary layer flow. The intake duct pressure loss is caused by the intake duct itself, which includes its shape, size, and length. In the chapter, total pressure losses due to the inlet duct are assumed

constant, therefore, changing the ratio of ingested boundary layer does not change the intake duct total pressure losses. Modern intake ducts have duct losses less than 1%. Considering the additional losses due to BLI, 1.5% propulsor intake total pressure losses was used in this chapter.

4.3.1 Modelling methodology

STEP 1:

The modelling of the inlet was divided into external and internal diffusion. This allows the inlet throat Ma and pressure to be calculated. However the critical parameter necessary to determine the inlet conditions is not the physical inlet height of the intake duct, rather it is the height of the capture sheet (named 'capture height') of air as measured at the point just before any external diffusion begins. The inlet height and the capture height will be the same as the design point. However, during off-design analysis, the capture height was varied such that the air flowing through a sheet of that height contains the mass flow required by the propulsors.

The first step of the method is to use a uniform flow to describe the boundary flow. Therefore, it has lower velocity. For example, Fig.4.8 describes a velocity profile (blue line) from the upper surface of the airframe to the 'capture height' of the intake duct (1 meter). The uniform flow (red line) is used to represent the boundary flow; its velocity should be calculated by following Eq.4.24, which is the mass conservation equation.

$$\dot{m} = \rho AV = \int \rho V(A) dA \tag{4-24}$$

Where the A is the area, V is the velocity and ρ is the density; if it is a 2-D problem as Fig.4.8 shows, the average velocity equals:

$$V = \frac{1}{h}\int_0^h V(y)dy = \int_0^1 V(y)dy \tag{4-25}$$

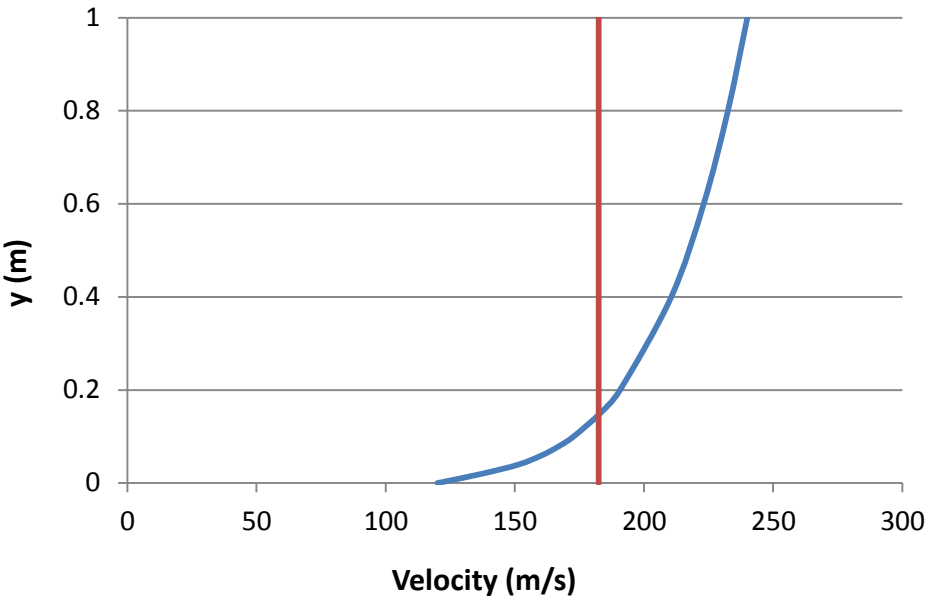

Figure 4.8 Inlet Velocity Profile

Inlet average total temperature, pressure of the uniform flow can be calculated by the following equations:

$$T_{inlet} = T_1 = const. \tag{4-26}$$

$$Ma = V/\sqrt{rRt_{amb}} \tag{4-27}$$

$$P_{inlet} = p_{amb}\left(1 + \frac{r-1}{2}Ma^2\right)^{\frac{r}{r-1}} \tag{4-28}$$

Now, the definition of the FPR is the pressure rise of the uniform flow through the fan stage. However, this pressure ratio is NOT the actual pressure ratio of the fan stage by ingesting the boundary layer. It describes the pressure ratio if the fan was ingesting a uniform flow with lower inlet velocity. The actual pressure ratio of the fan stage is named propulsor pressure ratio (PPR. So the FPR and the fan stage polytropic efficiency used in the following section refer to the value of the mapping point (or the DP at the new map).

Exit conditions of the uniform flow should be calculated by the following equations:

$$P_{exit} = P_{inlet} \times FPR \tag{4-29}$$

$$T_{exit} = T_{inlet} \times FPR^{\frac{r-1}{\eta_{poly} r}} \tag{4-30}$$

Then a defaulted fan map from the Turbomatch should be mapped to a new fan map, as fig.4.9 shows. The new map design point (or mapping point) should equals to the values obtained by Eq.4.24 to Eq.4.30. So the design point of the new map is the working point of the average uniform flow. In short, the first step (Fig.4.9) develops a fan map from a defaulted fan map in Turbomatch, and the new map design point should be obtained by using the uniform flow approximation. The new map will be used in the second step.

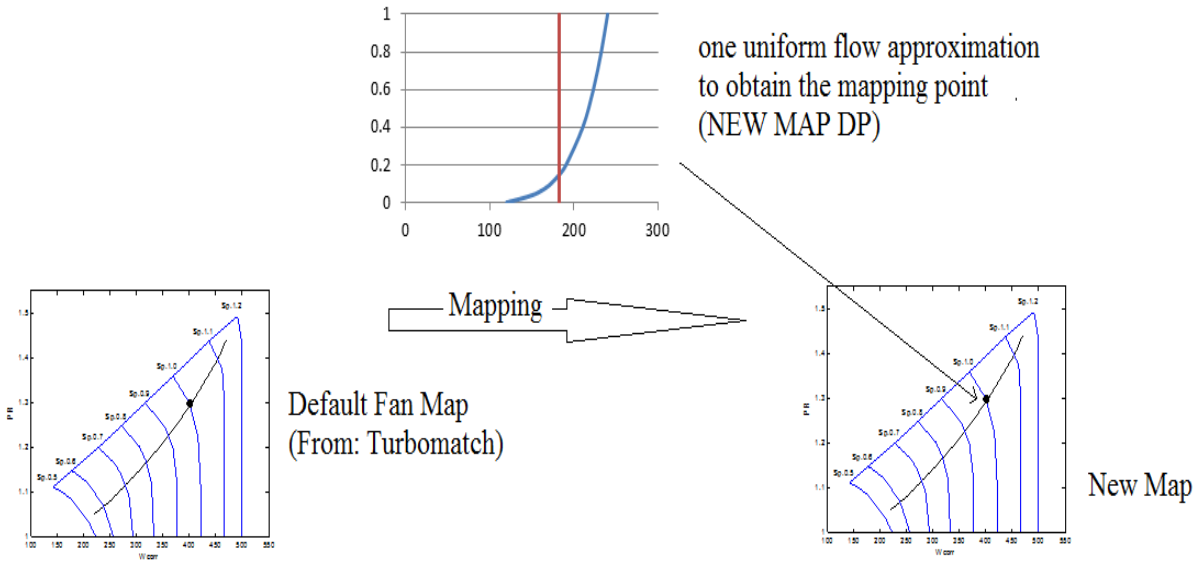

Figure 4.9 The Step 1 Procedure

STEP 2:

The second step is to use two uniform sections to describe the non-uniform velocity profile. For example, two sections, one with relative high velocity and one with low velocity, were used to describe the velocity profile in the Fig.4.8. The height of the low velocity section is '*a*' meter and the height of the high velocity section is *1-a* meter (Fig.4.10).

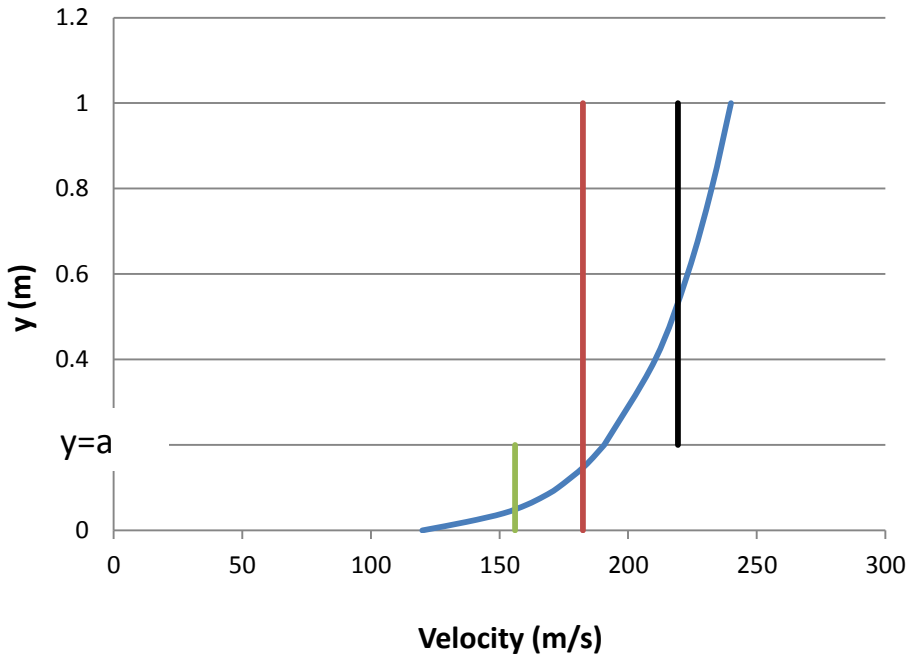

Figure 4.10 Two Streams Approximation

- High velocity section (black line), from y=a to y=1, average velocity can be calculated by Eq.4.31; inlet total pressure can be calculated by Eq.4.26 to 4.28

$$V_H = \frac{1}{h-a}\int_a^h V(y)dy = \frac{1}{1-a}\int_a^1 V(y)dy \tag{4-31}$$

- Low velocity section (green line), from y=0 to y=a, average velocity can be calculated by Eq.4.32; inlet total pressure can be calculated by Eq.4.26 to 4.28

$$V_L = \frac{1}{a}\int_0^a V(y)dy \tag{4-32}$$

After obtaining the velocity, total inlet pressure and temperature, corrected mass flow rate of each section can be calculated. Because there is no inlet total temperature difference, and the rotating speed of the fan blade is the same, the working points of both sections are in the same running line. For example, the working point of the uniform flow in the first step (red line in Fig.4.10) is the design point of the new fan map and because the total inlet temperature and the fan shaft speed are the same, the two sections (in step 2) should work in the same working line (CN=N/$\sqrt{T}$=const.) as the uniform flow. Pressure ratio of each section can be found in the fan map, as fig.4.11 shows.

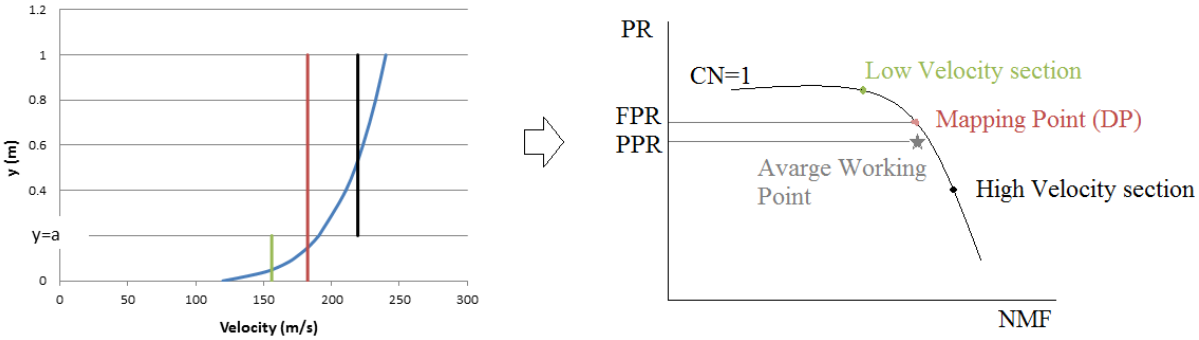

Figure 4.11 The Step 2 Procedure

STEP 3:

The third step is to calculate the mass flow rate of each section (the value of a). In the second step, for example, the height of the low velocity (a) is an un-defined parameter; its value can be from 0 to 1. Once obtained the value of a, the mass flow rate of each section can be calculated. Iteration (Fig.4.12) is needed in order to ensure both streams reach the same static pressure after the fan stage.

Propulsor pressure ratio (PPR) is defined by Eq.4.33:

$$PPR = \frac{\dot{m}_L}{\dot{m}} PR_L + \frac{\dot{m}_H}{\dot{m}} PR_H \tag{4-33}$$

Propulsor polytropic efficiency is defined by Eq.4.34:

$$\eta = \frac{\dot{m}_L}{\dot{m}} \eta_L + \frac{\dot{m}_H}{\dot{m}} \eta_H \tag{4-34}$$

Static pressure should be calculated by the following steps:

1. Calculate the fan exit total temperature, T3, and total pressure, P3; by the pressure ratio and polytropic efficiency obtained from the map.
2. Assume the axial velocity through the fan stage keeps the same, and thus the exit static temperature equals is:

$$t = T - \frac{V^2}{2C_p} \tag{4-35}$$

3. Calculate the exit Mach number, and thus the static pressure

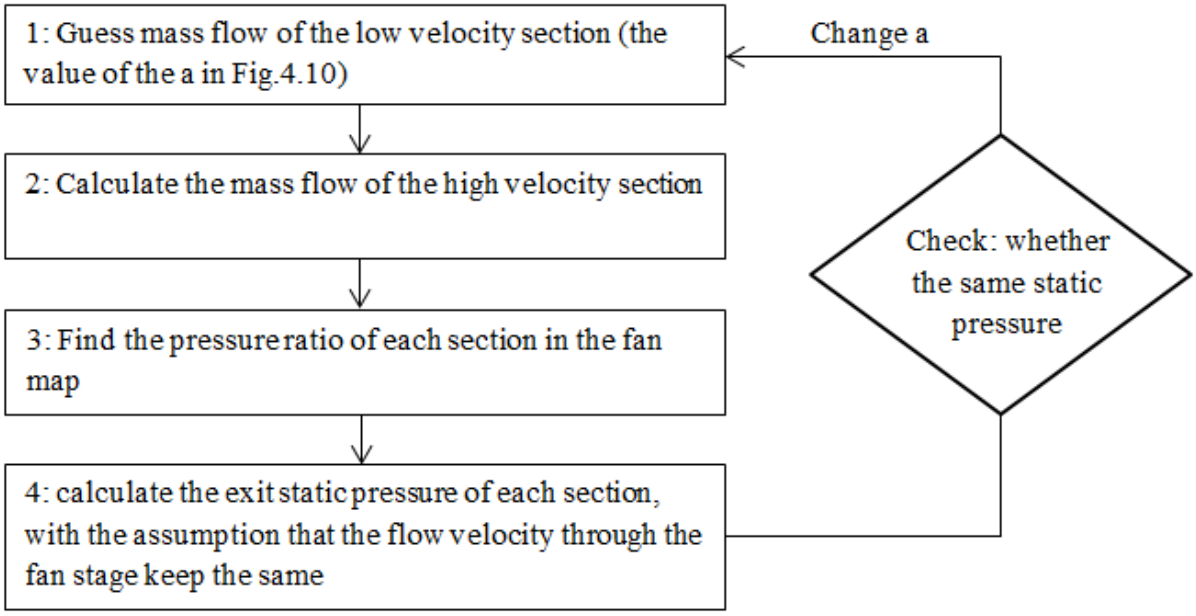

Figure 4.12 The Step 3 Procedure

STEP 4:

Finally, all the flows mix well (uniform nozzle inlet total temperature and pressure) before entering the nozzle. The nozzle inlet total temperature equals:

$$T_4 = \frac{\dot{m}_L}{\dot{m}} T_{3,L} + \frac{\dot{m}_H}{\dot{m}} T_{3,H} \tag{4-36}$$

Where, the subscript 3 is the fan exit, 4 is the nozzle inlet, *L* is the low velocity section, *H* is the high velocity section

The mixing process can be described by Fig.4.13:

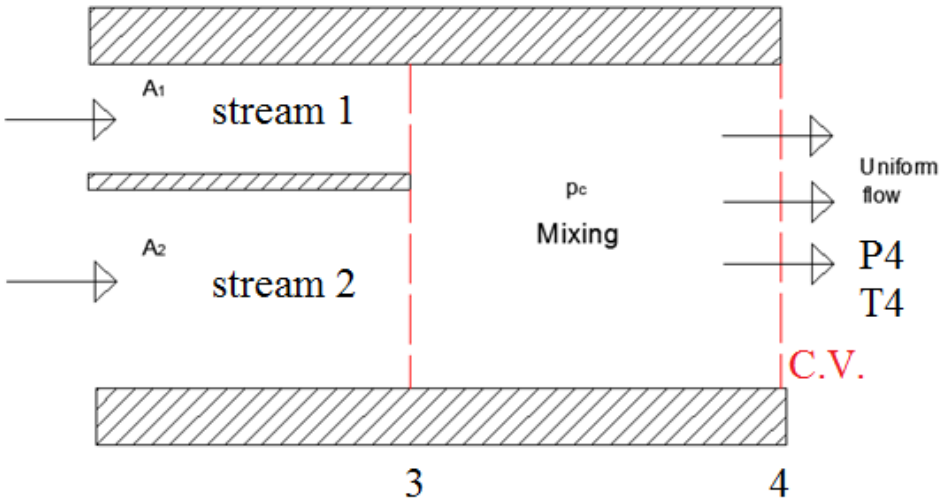

Figure 4.13 The Mixing Process (step 4)

Two streams each with their own stagnation pressure and temperature, mix to uniform static pressure, p_c. Eq.4.36 describes the energy conservation in the control volume. Eq.4.37 is the momentum conservation through the control volume.

$$p_c(A_L + A_H) + \dot{m}_L V_L + \dot{m}_H V_H = p_c A_4 + (\dot{m}_L + \dot{m}_H) V_4 \tag{4-37}$$

If the duct is straight and no cross area change:

$$V_4 = \frac{\dot{m}_L V_L + \dot{m}_H V_H}{\dot{m}_L + \dot{m}_H} \tag{4-38}$$

Then, calculate the static nozzle inlet temperature by Eq.4.35 and the Ma, and therefore the total pressure. This new method has the following two pressure ratios and polytropic efficiencies for the propulsors:

- FPR, Polytropic Efficiency: the mapping pressure ratio and Eff., or the DP PR and polytropic efficiency of the clean map
- PPR, Mass average Polytropic Efficiency: the propulsor working PR and polytropic efficiency

4.4 Sample Calculation

The N+3 airplane, introduced in chapter 3, was used in this section. Design parameters of the core-engine were kept the same as the NASA's TeDP system. Propulsor FPR and polytropic efficiency (the mapping PR and Efficiency) equals to the NASA's design values [19]. Seventh power low (Fig.4.8) was used to describe the inlet velocity profile of the boundary flow; moreover, we assumed the profile keeps the same for all the propulsors. The propulsor intake capture height at different FPRs should be obtained to ensure the inlet mass flow equals to the NASA's results.

Comparing to the NASA's BLI modelling method (Fig.4.14), the new method estimates lower pressure ratio and polytropic efficiency, and the differences increase with the increment of the FPR. That is because, to produce the same amount of thrust, the mass flow of the propulsors reduces with the increment of FPR and this leads to lower capture height. Reducing the capture height increases the ratio of ingested boundary layer and therefore increases the intake distortion.

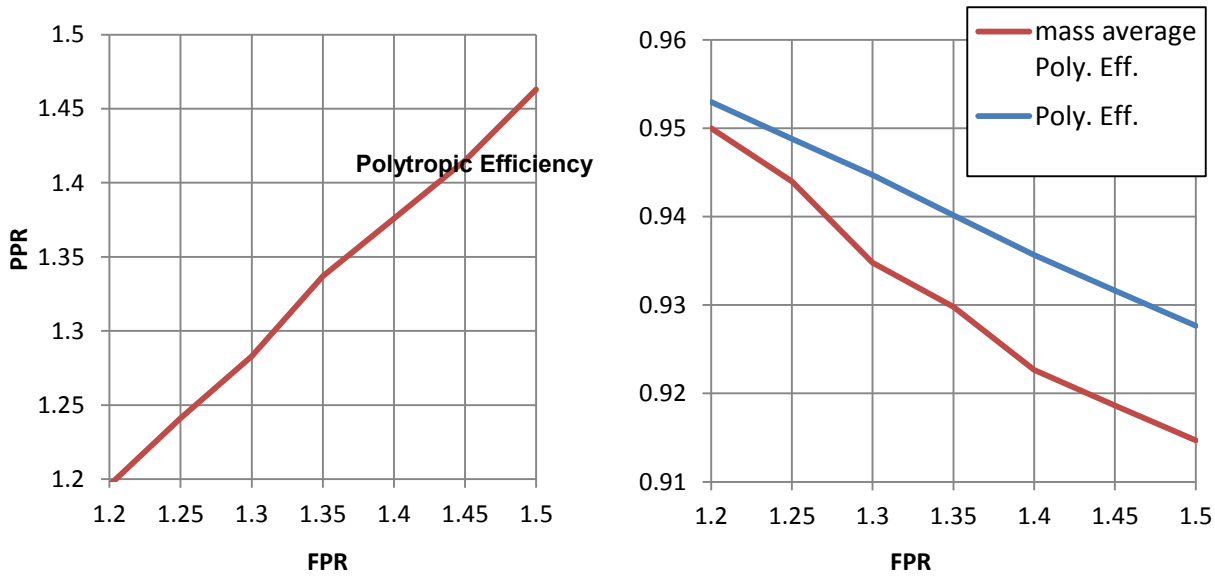

(a) (b)

Figure 4.14 PPR and Mass Average Poly. Efficiency at Different FPRs

Fig.4.15 compares the TSFC by using the new method. BLI benefits the system. However, intake distortion reduces the benefits, especially at high FPR with high ratio of boundary layer.

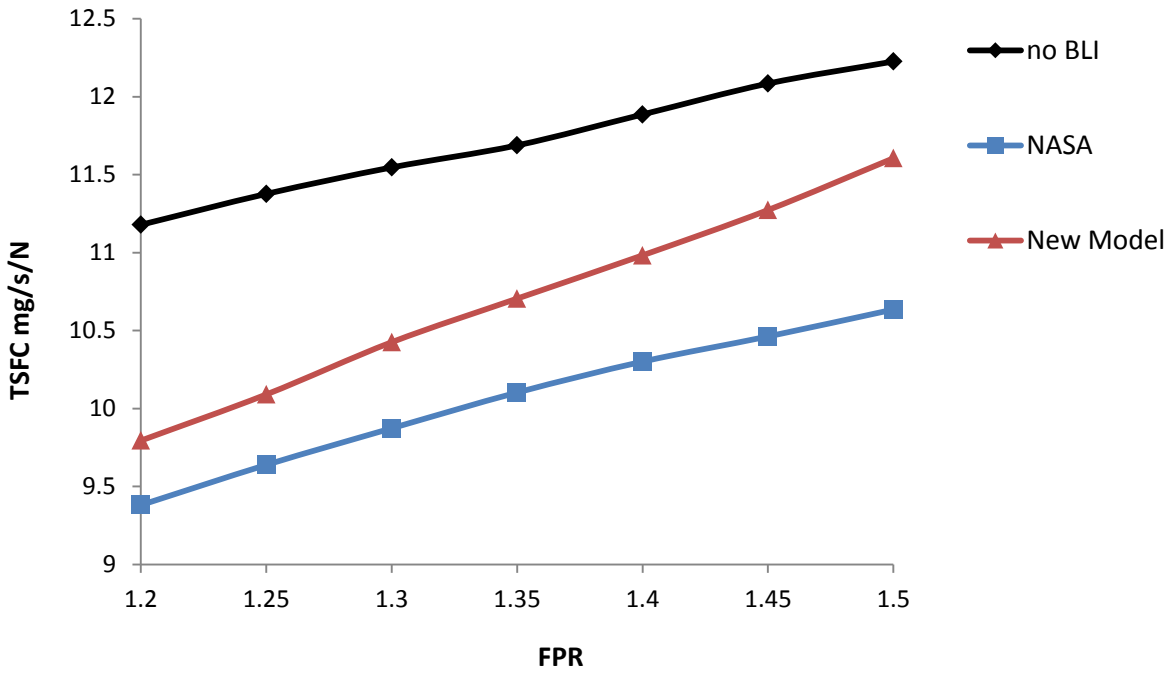

Figure 4.15 Comparison of TSFC

4.5 Future Work

4.5.1 Distorted Map Concept

The method developed in section 4.3.1 can be used to estimate the impacts of BLI at design point. However, for off-design calculation, distorted fan map concept, which refers to a fan map obtained by considering inlet distortion, should be used. The distorted fan map refers to the fan running lines with BLI. In section 4.3.1 step 1, a defaulted map was mapped by the one uniform stream approximation method. This new map (used in step 2) is the clean map. Fig.4.16 illustrates the running line (non-dimensional rotating speed equals to 1) of the clean map, the mapping point in this line, and its mass average working point. Through changing the nozzle area, or with another method, the uniform flow can move in the clean map from the mapping point to other point. For example, if we reduce the inlet mass flow rate without changing the shaft speed and flight condition, the uniform flow working point moves from the mapping point to the black point in the Fig.4.16. A mass-average working point can also be obtained by the same steps (step 2-4). By summarising all the mass-average points, the new running line is called the distorted map. The distorted map refers to

the actual working point if the fan stage ingests boundary layer flow. The distorted map is obtained with the velocity profile of the inlet flow. Therefore, for different boundary layer inlet conditions, the distorted fan map is different.

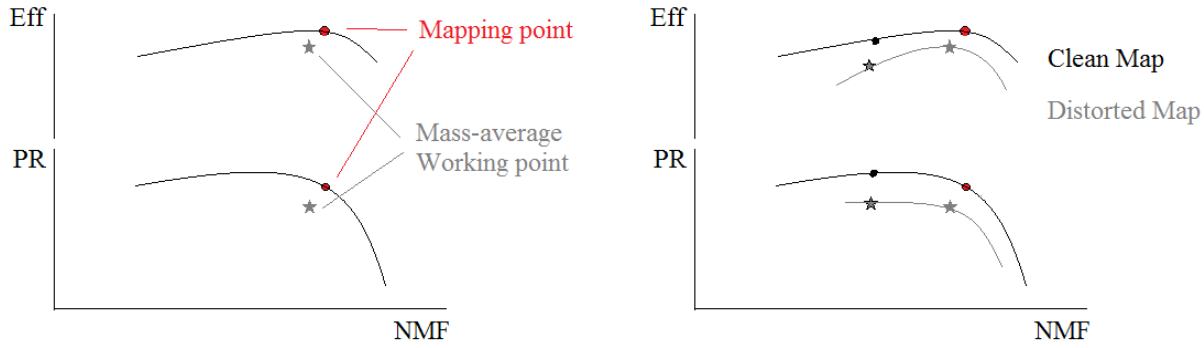

Figure 4. 16 The Distorted Map at None Dimensional Rotating Speed = 1

However, it is difficult to obtain a useful distorted map based on the clean map from Turbomatch. That is because the information provided by the defaulted Turbomatch compressor map is limited. The program cannot converge at most of examined off-design conditions. Future works should address this problem.

4.5.2 Multi-streams Method

The new method is a 2-D approximation for modelling BLI by using a number of parallel streams in order to increase the accuracy. One of the ideas, multi-streams method, is described below. Firstly, numbers of small parallel streams are used to present the propulsor un-uniform intake velocity profile, as Fig.4.17 shows. Secondly, all the streams are assumed to reach the same static pressure after the fan stage. Thirdly, we assume that all the flow mixed well with each other before entering the nozzle. The number of the streams should be large enough so that the non-square streams near the boundary can be neglected. The potential problem of using this method comes from the assumption that all the streams reach the same static pressure. CFD simulation (provided by Flouriot, L.) shows that the fan exit static pressure is non-uniform. So whether more precise results can be obtained by increasing the number of parallel streams is still not clear.

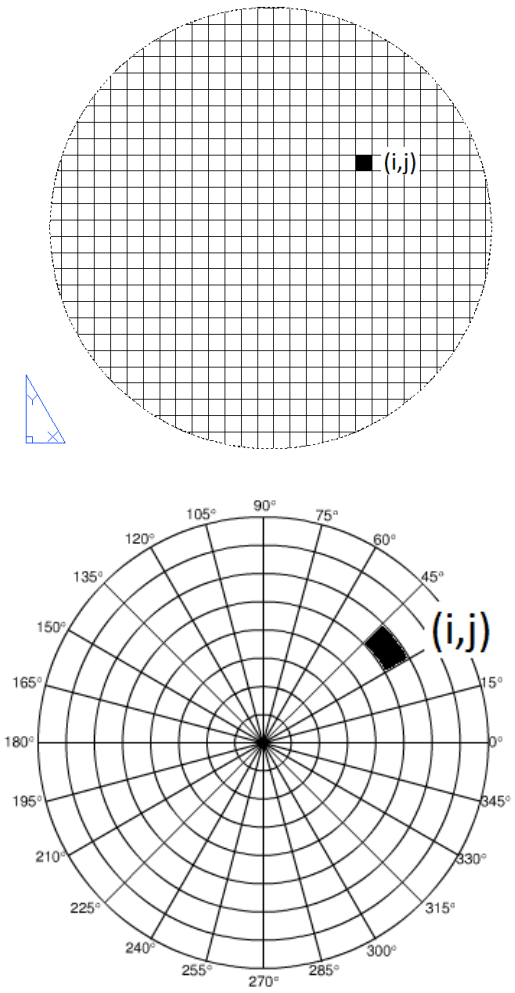

Figure 4.17 Multi-stream Method, X-Y coordinate and θ-r polar coordinate

Area:

$$\pi r^2 = \sum\sum (x_{i+1} - x_i)(y_{i+1} - y_i)$$

$$= \sum\sum (\theta_{i+1} - \theta_i)(r_{i+1}^2 - r_i^2)$$

No intake total temperature difference:

$$T_{ij} = T_o$$

Mass flow of the stream (i, j):

$$\dot{m}_{ij} = \rho V_{ij}(x_{i+1} - x_i)(y_{i+1} - y_i)$$

$$= \rho V_{ij}(\theta_{i+1} - \theta_i)(r_{i+1}^2 - r_i^2)$$

All the streams reach the same fan exit static pressure:

$$p_{exit} = const.$$

4.6 Discussion

NASA's plan on meeting the plans of next generation commercial airplane for 2030 is through combining the Blended Wing Body aircraft and the distributed propulsion system. Distributing an array of propulsors that ingest a relatively large mass flow directly produces an 8% fuel burn saving relative to today's aircraft. BLI achieves a 7-8% fuel burn saving as expected. However, these BLI benefits are very sensitive to inlet distortion; if the fan pressure loss and efficiency drop due to inlet distortion are too high, BLI should not be used.

This new way estimated lower benefits of BLI than NASA's prediction, especially at high FPRs. What's more flow mixing losses were not considered in this model. Greitzer [52] estimated mixing losses of boundary flow of BWB airframe (which is similar to the airframe NASA used) which caused 2-4% reduction in total inlet pressure, which means, the BLI benefits offered less than 2% fuel burn saving.

The BLI benefit associated with turbojet engine or similar types of propulsors such as the turbogenerator without a directly attached fan seems to be almost negligible, and therefore it is not desirable to ingest boundary layer flow from the airframe for the turbojet-like engines. In addition, any significant flow distortion associated with the boundary layer flow entering the inlet may propagate through the engine compressor and will lower the compressor efficiency and hence the thermodynamic efficiency of the engine.

Finally, the current analysis is still being refined, and the equations used in the above analysis are currently limited to propulsion system at subsonic speed without intake shock wave. In the future, the analysis may include the analysis for propulsion system with shock wave ahead of inlet in viscous flow and even a supersonic propulsion system. Based on the current analysis, the electric fan propulsion system seems to show promising results for subsonic aircraft in reducing aircraft fuel burn through the use of lower pressure ratio fans and the airframe boundary layer ingesting.

4.7 Conclusion

1. The method developed in this chapter take into account the impacts of intake distortion. At all the examined pressure ratios, BLI causes about 0.8-1.3% reduction on the fan exit total pressure and 0.7-1.1% reduction on the fan polytropic efficient. The final values depend on the ingested boundary layer ratio, the fan working pressure ratio and the flow inlet conditions.
2. The new method to model BLI is based on clean fan map and propulsor inlet flow conditions, but independent of blade shape. So it is suitable for primary TeDP design with BLI.

3. Sample calculation showed that BLI benefits the overall fuel consumption but the benefits are lower than NASA's predictions, especially at high propulsor pressure ratios.
4. NASA's plans of next generation commercial airplane for 2030 require 50% fuel reduction, and they estimated that 7-8% of fuel savings come from BLI. However, it is a challenge to achieve this goal.

Chapter V

Design Point Analysis of Distributed Propulsion System with Boundary Layer Ingesting

The performance benefits of boundary layer ingestion in the case of air vehicles powered by distributed propulsors have been documented and explored extensively by previous studies. However, the increased inlet flow distortion and system total weight would dramatically reduce the expected benefits. In this chapter, a new TeDP system (turbofan-driven TeDP) modulus on the N3-X airframe has been developed. It includes two turbofan core-engines (each drives a free power turbine) and a propulsors array, therefore both the core-engines and the propulsors unit produce thrust. Secondly, a parametric and quasi-two dimensional studies at component and at system level are carried out so that the effects of these two aerodynamic issues over the system performance can be assessed. The figure of merit in this study is the TSFC and the system parameters examined are: thrust split between propulsors and engines, capture height and the core engine parameters. Preliminary results found optimum configurations at around 50-90% thrust split ratio, when installation effects were neglected. The final value depends on the propulsor intake pressure losses and the BPR of the TeDP system.

5.1 Introduction

To improve vehicle performance enough to satisfy NASA's N+3 goals, the HWB airframe designed for N+2 was used but the propulsion system should be replaced by turboelectric distributed propulsion (TeDP) system. A concept currently analysed by NASA is N3-X shown in Fig.5.1. This vehicle utilises low pressure electrically driven fans powered by electric generators driven by turboshaft engine. The fans of the N3-X configuration are put in a continuous nacelle across the upper/rear surface

of the HWB aircraft and the two turbogenerators, each composed by a turboshaft engine and a superconducting generator, are mounted in the wingtip. This concept has been analysed in previous chapters.

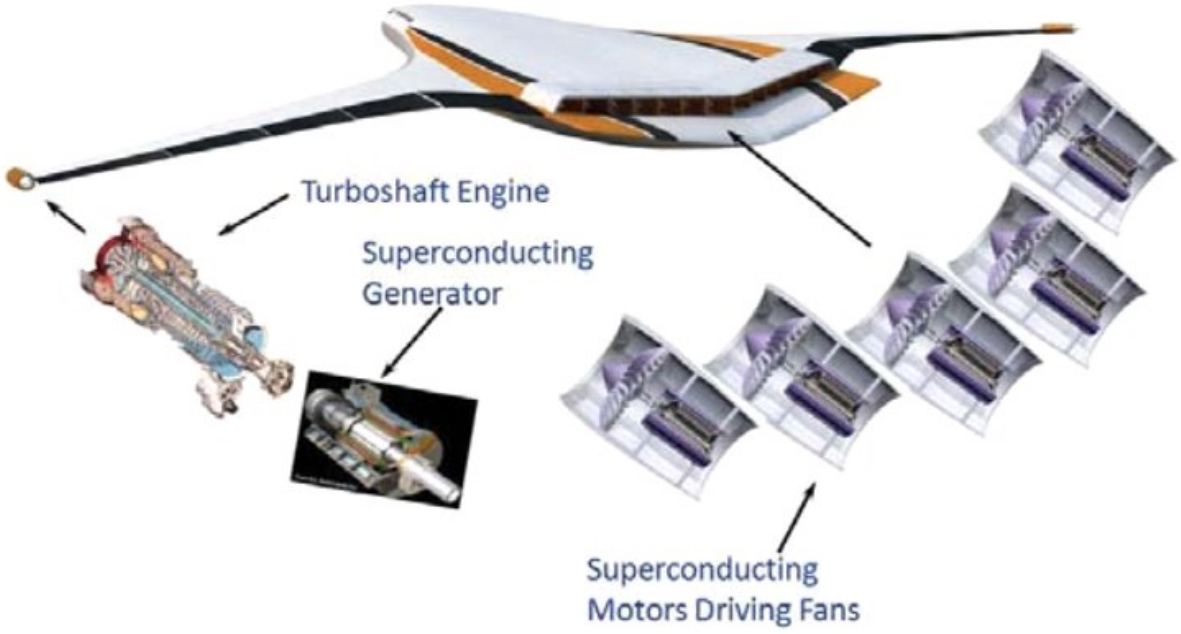

Figure 5.1 N3-X vehicle and a schematic of its TeDP system [20]

TeDP system is a new kind of turbofan engine. This new design utilises a number of small fans to replace the big fan in a turbofan engine, which enables ultra-high bypass ratio with acceptable engine size. However, aerodynamic integration issues are associated with BLI as increased inlet distortion and intake pressure losses dramatically affect fan performance and hence mitigate the benefits[15,22,25,27]. This chapter aims to assess the effects of the aerodynamic integration issues over fan performance using parametric and quasi-two dimensional (parallel compressor) approaches. Then the influence of these effects is taken into account in the system analysis, where different propulsion architectures are examined.

5.1.2. Aims of this chapter

- Introduce the new TeDP system
- Use thrust split ratio (TSR) as the way to characterise the TeDP system
- Figure out the impacts of TSR on engine design point performance

- Figure out the impacts of BLI on the TeDP system with different TSR
- Find the optimised propulsor pressure ratio of a TeDP system
- Exam the impacts of core-engine bypass ratio and fan pressure ratio on TeDP system performance
- Provide TeDP design information and guidance
- The case study of the N3-X Aircraft

5.2 Modelling Methodology

5.2.1 Overall system model

Fig.5.2 is the system modulus; this system contains two parts: two core-engines and the propulsor unit. The core-engine includes a turbofan engine and a free power turbine. Power from the power turbine is transferred to propulsor unit electrically. The inlet air of the core-engine is freestream flow, but the inlet air of the propulsors is partly boundary layer flow. The core-engine contains the fan stage (1 to 2), the compressor stage (2 to 3), the combustor (3 to 4), the HPT stage (4 to 5), the LPT stage (5 to 6), a free power turbine (6 to 7) and two nozzles (core nozzle: 7 to 8; bypass nozzle: 2 to 8). The propulsor has the fan stage (I to II) and its nozzle (II to III). The generator can also be connected to the LPT directly. This configuration does not have the free power turbine. There is no significant difference between these two configurations at DP.

Table 5.1 highlights some key parameters and their definition. Thrust split ratio, which equals the ratio of the propulsor thrust to the total thrust, is used as the way to characterise the TeDP system. This gives a good idea of what the engine will look like, since the size of the core and the size of the propulsors are roughly proportional to the thrust they produce.

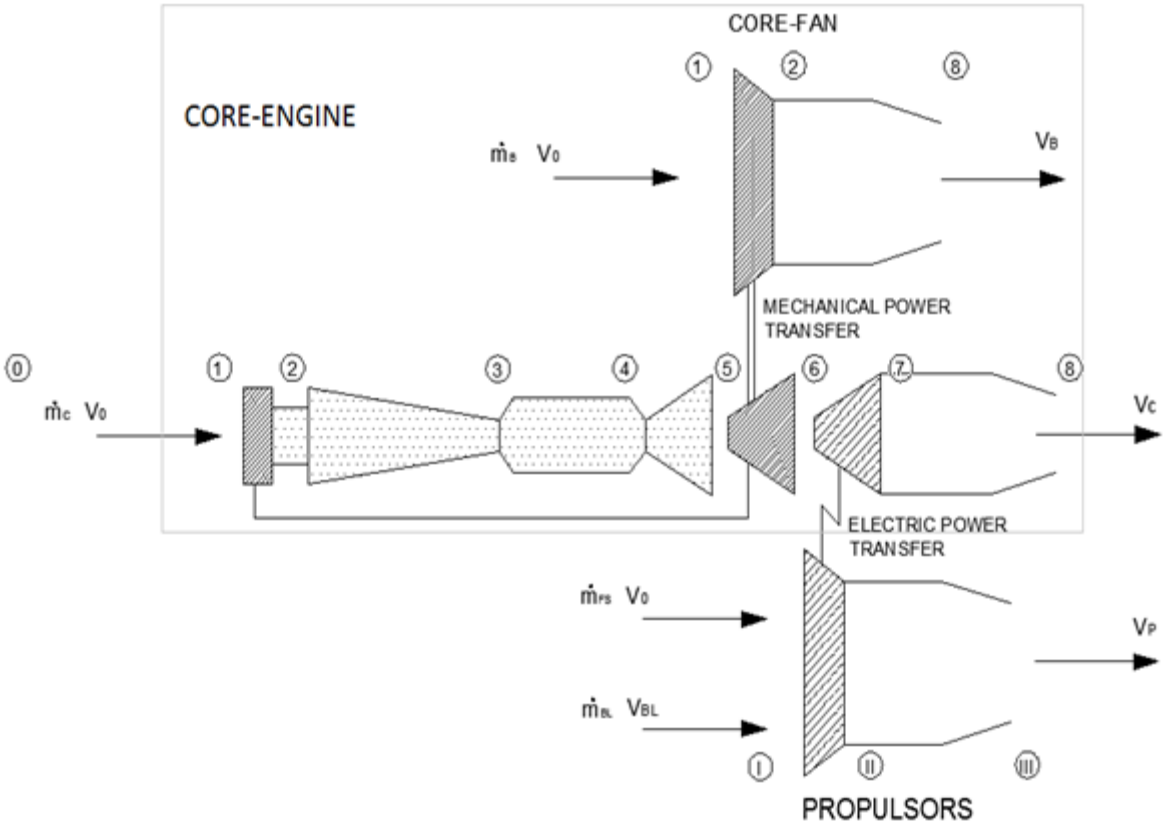

(a) Overall system modulus with one core-engine

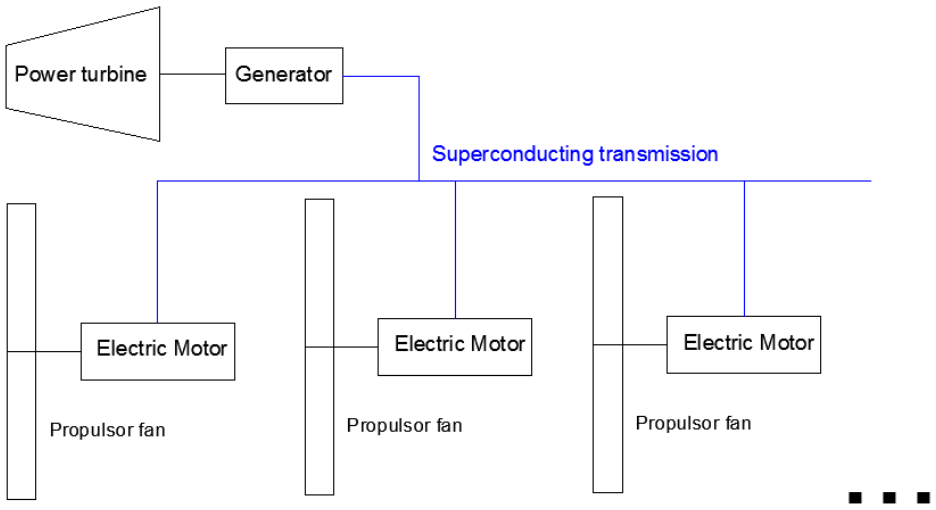

(b) Electric system modulus

Figure 5.2 The TeDP System Modulus

Table 5.1 System Parameters Definition

Parameter	Definition
Core-engine bypass ratio	$BPR = \frac{\dot{m}_B}{\dot{m}_c}$
Core-engine fan pressure ratio	$cFPR = \frac{P_2}{P_1}$
Propulsor fan pressure ratio	$PPR = \frac{P_{II}}{P_I}$
Thrust split ratio	$TSR = \frac{N \times F_P}{F_N}$
Total thrust	$T_N = 2 \times F_{CE} + N \times F_P$

Performance of the core-engine was simulated by TURBOMATCH, a gas-turbine performance simulation program developed by Cranfield University. The overall pressure ratio (OPR=74.8) and turbine entry temperature (TET=1811K) are kept the same. So the turbofan engine compressor pressure ratio equals to the OPR divided by FPR. The efficiency of the electric system was assumed constant at any working conditions. In this chapter, the efficiency was assumed equal to 0.999.

The propulsors are deliberately positioned on the upper rear surface of the airframe to ingest the boundary layer. The total inlet width of the propulsors unit is 16 meters. So the intake area of the propulsor unit equals the intake capture height times the width. The propulsor fan diameter is assumed equal to the intake capture height, and the hub-tip ratio equals to 0.3.

5.2.2 BLI modelling methodology

The method developed in chapter 4 was used. The common intake duct of the propulsors unit in the N+3 airframe has a rectangular cross section and the inlet velocity profiles of different propulsors don't have too much difference. So the other assumption is that the inlet air conditions of each propulsor are the same. This is not a strong assumption, because impacts of applying different inlet air velocity profiles

at the intake on overall system fuel consumption are less than 2% (results will be shown in next section). This assumption simplified a 3D problem to a 2D problem and dramatically reduced the calculation time. Fig.5.3 shows the control volume of one propulsor. At design point, the flow velocity profiles at position 0 and 1 are the same. Improved seven power law Eq. (Eq.5.1) was used to describe the inlet velocity profile. In Eq.5.1, δ is the boundary layer thickness and U_∞ is the freestream air velocity; μ is the dynamic viscosity and δ is the boundary layer thickness, and x is the length defined in Fig.5.3.

$$\frac{U}{U_\infty} = 0.9865 \times \left(\frac{y}{\delta} + 0.1\right)^{\frac{1}{7}} \tag{5-1}$$

$$\delta = 4.91x/\sqrt{Re_x} \tag{5-2}$$

$$Re_x = \rho U_\infty x/\mu \tag{5-3}$$

The inlet fuselage length, x, of each propulsor is different; therefore their inlet velocity profiles are different. In this chapter, the boundary layer thickness is assumed the same for different propulsors in order to simplify the calculation. Final results show that its impacts on final fuel consumption are small, because the boundary layer thickness does not vary too much.

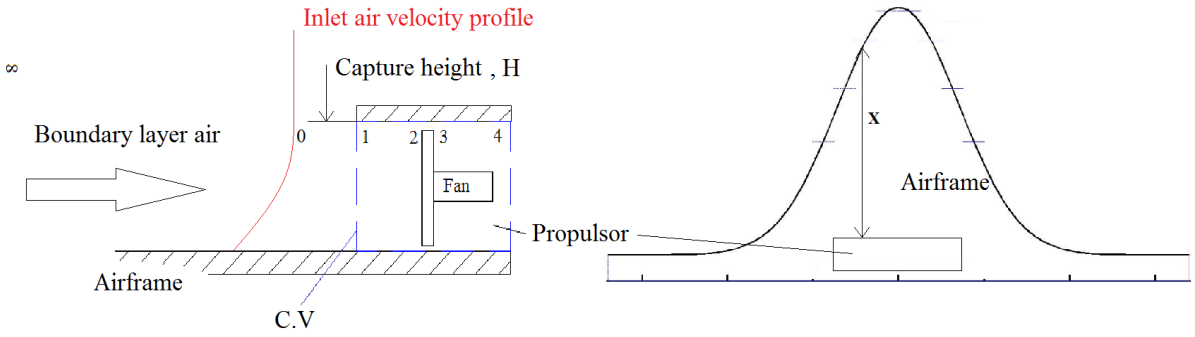

Figure 5.3 Propulsor Position and The Control Volume Definition

5.2.3 Calculation procedure

The overall calculation program has two parts: the propulsor and the core-engine. In the thesis, the TeDP system was designed to power N+3 airplane, which required 119KN (26750lbf) thrust at DP. The thrust was produced by both the propulsors unit and the two core-engines. The inputs of the propulsor calculation model includes:

thrust split ratio (TSR) and capture height (H). TSR define the thrust produced by both parts; capture height defines the propulsor inlet mass flow rate and the inlet conditions. Propulsor pressure ratios can be calculated in order to produce the required thrust, and thus the propulsor power can be calculated. The propulsor power is varies with the capture height, lower capture height leads to higher PPR, and thus reducing the propulsive efficiency. Higher capture height improves propulsive efficiency, but makes it difficult to recover the intake pressure losses. So the optimised capture height should achieve the lowest fan power.

Inputs of the core-engine includes: core-engine bypass ratio and core-engine fan pressure ratio. After obtaining the propulsor power and core engine thrust requirement, overall fuel consumption can be calculated. Fig.5.4 shows the calculation procedure. Table 5.2 lists other design parameters. 7% air from high pressure compressor exit flow was used to cool high pressure turbine blades. Core engine intake pressure losses are 0.5%.

Table 5.2 DP parameter values

Component	Parameter values
Propulsor fan	$\eta_{poly} = 0.9325$ hup/tip = 0.3 fan face Ma = 0.64
Core engine fan	$\eta_{poly} = 0.9325$
Core engine compressor	$\eta_{poly} = 0.9325$
Cooling air from compressor exit	7%
Turbine	$\eta_{poly} = 0.93$
Power turbine	$\eta_{poly} = 0.924$

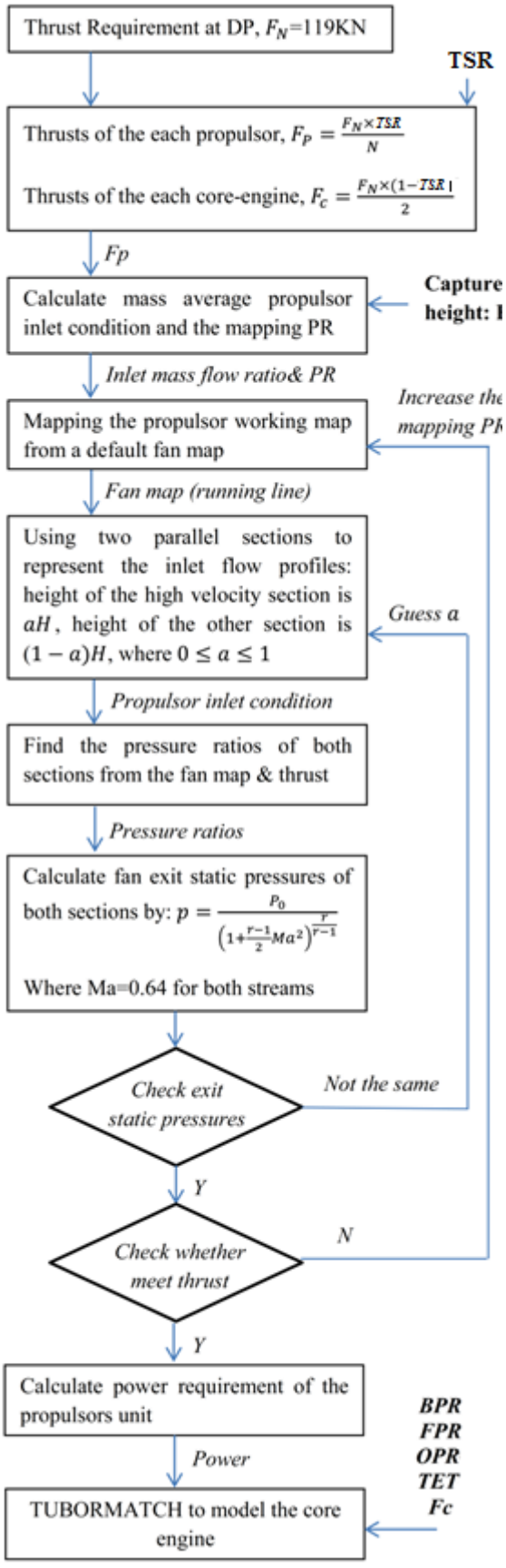

Figure 5.4 The Calculation Procedure

- Step 1

Calculate the thrust requirements of both the propulsors unit and the core engine.

$$F_P = F_N \times TS \tag{5-4}$$

$$F_C = F_N - F_P \tag{5-5}$$

- Step 2

Input data: intake capture height, *H*

Calculate the inlet mass flow ratio

$$\dot{m} = \rho \times H \times L \times V \tag{5-6}$$

Where *L* is the propulsor intake width and *V* is the average intake velocity

- Step 3

Calculate propulsor fan inlet conditions: inlet average total pressure and pressure

- Step 4

Calculate the propulsor pressure ratio to satisfy the thrust requirement

- Step 5

Using the pressure ratio and the inlet mass flow rate to map a default fan map

- Step 6

Using parallel compressor method to calculate the PPR and the thrust

- Step 7

Check the thrust whether meet the requirements, if not, increase the mapping pressure ratio in Step5 and iterate until the required thrust is met and then calculate the fan power

- Step 8

Core-engine modelling by Turbomatch

5.2.4 Sample calculation

NASA N+3 airplane requires 119 KN at design point (Altitude=30000ft & Ma=0.84), 60% (TSR=60%) of the total thrust produced by the propulsors. The total pressure loss of the propulsor intake duct is 2%. Two core-engines are used, each has a turbofan engine (BPR=15, OPR=74.8, and TET=1811k@DP) and a superconducting generator (Eff=0.99).

$$F_P = F_N \times TS = 119 \times 0.6 = 71.4 \text{ KN} \tag{5-7}$$

$$F_C = F_N - F_P = 47.6 \text{ KN} \tag{5-8}$$

The next step is to calculate the inlet mass flow rate at different intake capture heights. For example, if H=0.1, the inlet mass flow rate can be calculated by the following equation:

$$\dot{m} = 16 \times \int_0^H \rho V dy = 16 \times \int_0^{0.1} 0.9865 \rho U_\infty \left(\frac{y}{1} + 0.1\right)^{\frac{1}{7}} dy \tag{5-9}$$

Where ρ is the air density and U_∞ is the flight velocity

After obtaining the mass flow ratio, parallel compressor method is used to find the propulsor fan pressure ratio (PPR) in order to satisfy the thrust requirements. So the propulsor power can be calculated:

$$P = \dot{m} C_P \Delta T = \frac{\dot{m} C_P T_{inlet} \left(PPR^{\frac{r-1}{r}} - 1\right)}{\eta_{isen}} \tag{5-10}$$

Next, the fan power at different capture height must be found which consists in finding the very H to achieve lowest fan power. Fig.5.5 shows the results with 2% intake pressure loss. The lowest power is 20.194 MW with H=0.7.

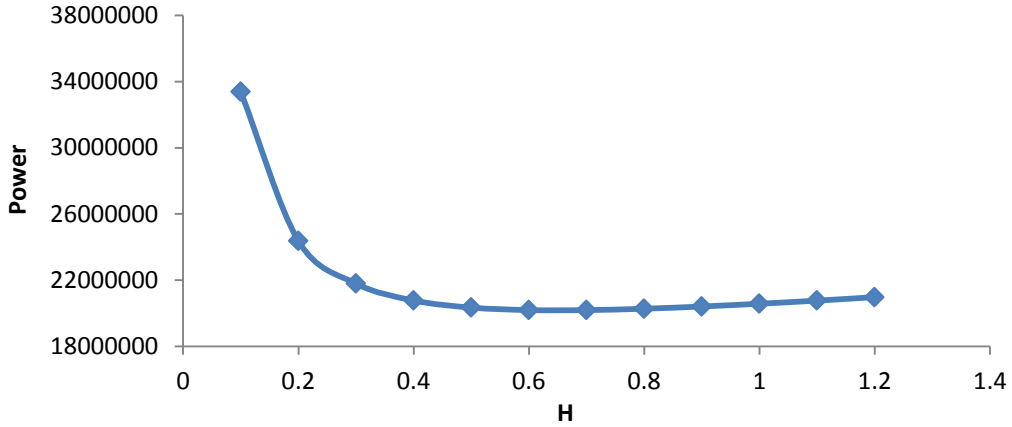

Figure 5.5 Fan Power of Different Capture Heights at TSR=60%

Then, the power is used as the input data of the core-engine model (the power of the free power turbine). Turbomatch should be used to obtain the TSFC. Fig.5.6 shows the results. The lowest TSFC achieved at core turbofan engine FPR equals to 1.22.

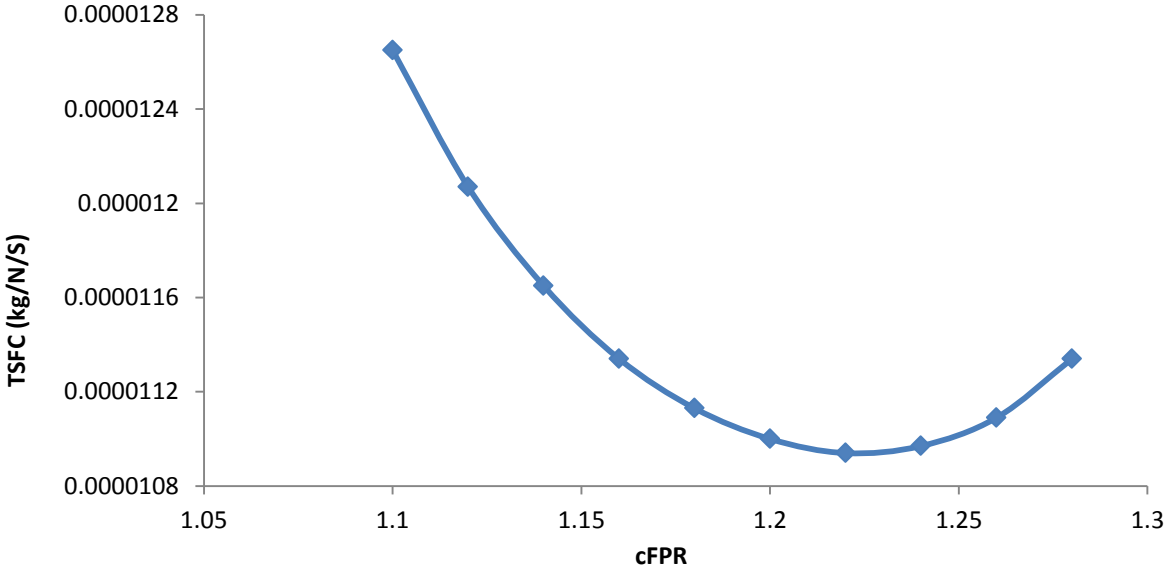

Figure 5.6 TSFC of the TeDP System (H=0.7, TSR=0.6)

So the lowest TSFC@DP of a TeDP system with TSR=0.6 has the following design parameters:

- Propulsor capture height, H=0.7
- Propulsor average pressure ratio, PPR=1.247
- Propulsor intake pressure loss, PL=2%
- Core turbofan engine bypass ratio, BPR=15

- Core turbofan engine fan pressure ratio, c FPR=1.22
- Core turbofan engine overall pressure ratio, OPR=74.8
- Core turbofan engine turbine entering temperature, TET=1811 K

The following step is to change the TSR and to repeat the calculation process; Fig. 5.6 shows the propulsor power requirement at other TSR values. The y-axis value, defined by Eq.5.11, equals to the power divided by the corresponding minimum power of 2% pressure loss at the specific thrust split ratio.

$$y-axis = \frac{Power\ (TS = a)}{Minimum\ Power\ (TS = a\ \&\ 2\%PL)} \tag{5-11}$$

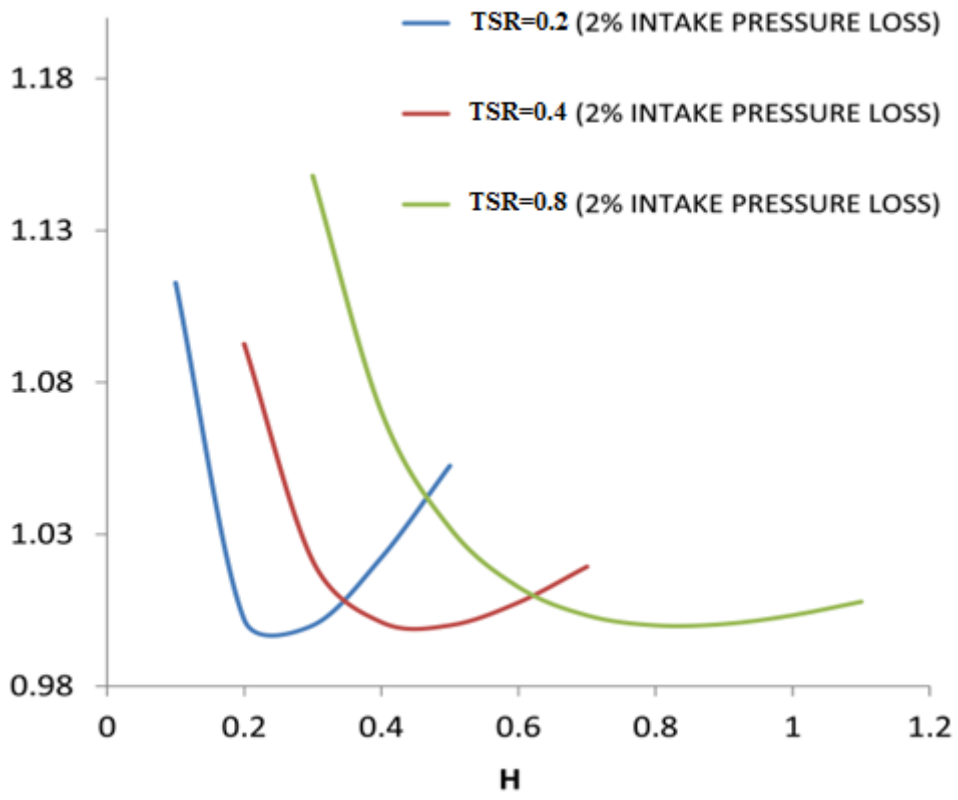

Figure 5.7 Power Requirements at Different Capture Height

At different thrust split ratios, there is a capture height to achieve minimum power requirement. This is because, at very small capture height, large ratio of power should be used to recover the velocity drop due to BLI. With the increasing of capture height, the benefits of ingesting boundary layer overweigh its kinetic energy loss. However, if we keep increasing the height, energy losses due to intake

pressure losses become serious, thus increasing the power again. However, if there are no intake pressure losses, the power will keep reducing with the increase of capture height but the amount of improvement declines as capture height increases. Table 5.3 lists the capture height and its corresponding PPR at different TSR to achieve lowest power with 2% intake pressure losses.

Table 5.3 Propulsor Optimised Capture Height and PPR at Different TSR (2% Duct Pressure Loss)

TSR	H	PPR
0.2	0.3	1.193
0.4	0.5	1.231
0.6	0.7	1.247
0.8	0.8	1.293
0.99	1.0	1.290

The capture height to achieve lowest power increases with the increasing value of thrust split ratio. At high thrust split ratio, more thrust should be produced by the propulsor by either increasing propulsor pressure ratio or capture height. Higher pressure ratio leads to higher exit jet velocity and thus lower propulsive efficiency. So capture height should be increased at higher thrust split ratio.

The next step is to find the specific fuel consumption (TSFC, kg/s/N) at each TS. The inputs include the minimum power for this TS, the core engine BPR (=15) and its FPR. Fig.5.8 shows the results with 2% propulsor intake pressure losses. There is a FPR for each thrust split ratio that achieves the lowest TSFC. That is because as the FPR increases, for a given bypass ratio and OPR turbofan engine, the propulsive efficiency rises and the TSFC falls. However, increases in FPR lead to higher bypass jet velocity but lower core jet velocity, and thus lower thermal efficiency. Fig. 5.8 illustrates the lowest TSFC at different TSR and table 5.4 summarises the corresponding cFPR and PPR. In this section, a BPR=15 turbofan engine was chosen to power the TeDP system. At take-off, if the electric system and the cooling

system are not efficiency enough, most of the thrust should be provided by the turbogenerator. Therefore, using high BPR core-engine can improve the fuel consumption. However, at DP, the fan pressure ratio of the turbofan engine is low especially at higher thrust split ratios. This means the turbofan engine bypass air produces almost no thrust at DP. What's more, to guarantee enough space for the generator, using high BPR turbofan engine will dramatically increase the size of the turbogenerator. In short, high BPR turbofan-driving TeDP system probably is not suitable to power the N3-X airplane.

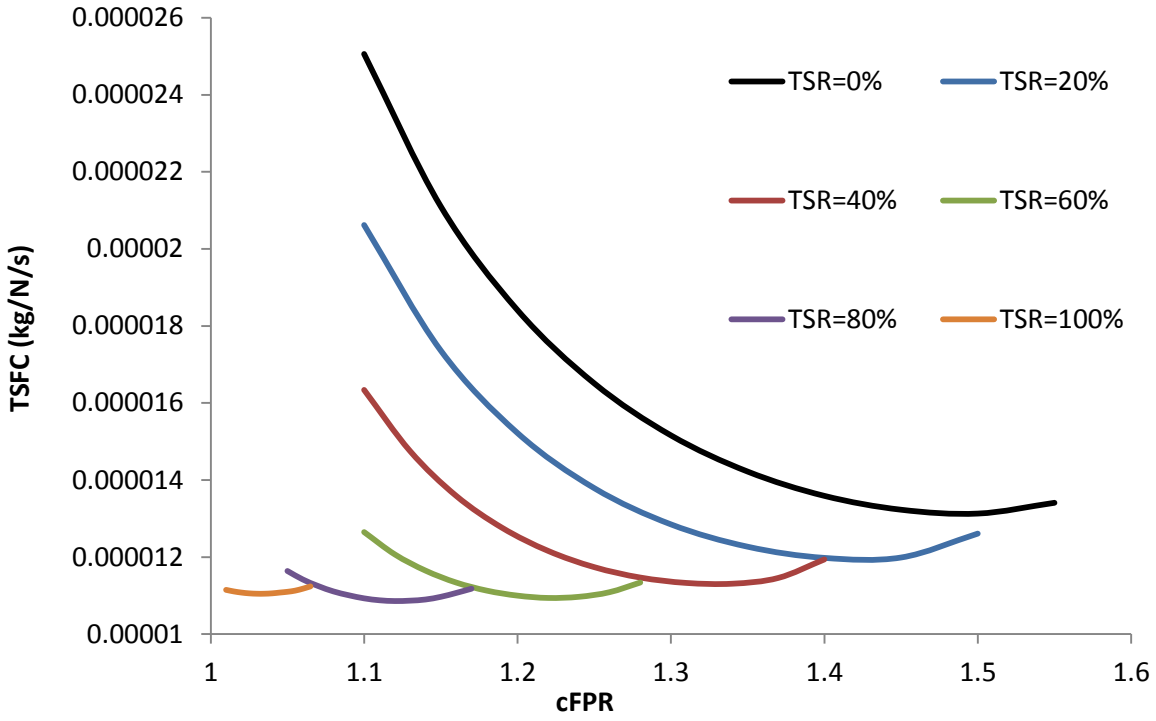

Figure 5.8 TSFC at Different TSR and Core Engine FPR (BPR=15, Propulsor Duct Loss 2%)

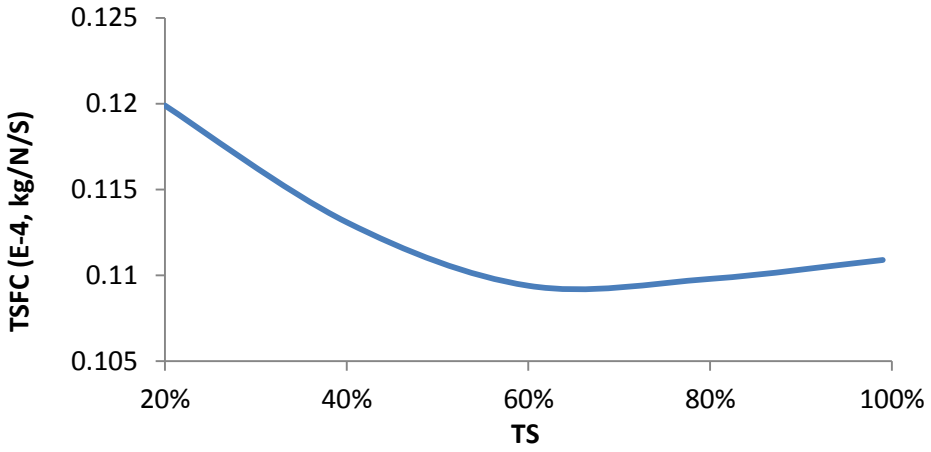

Figure 5.9 The Lowest TSFC at different TSR

Table 5.4 Optimised Design Parameters at Different TSR (BPR=15, Propulsor Duct Loss 2%)

TSR	H	PPR	cFPR	TSFC (e-4, kg/N/s)
0.2	0.3	1.193	1.4	0.1198
0.4	0.5	1.231	1.325	0.1131
0.6	0.7	1.247	1.225	0.1094
0.8	0.8	1.293	1.12	0.1098
0.99	1.0	1.290	1.03	0.1109

From the results, the 60% TSR TeDP system offers the lowest TSFC. The cFPR reduces with the increment of TS. That is because the increment of TSR reduces the core-engine thrust. This leads to lower bypass jet velocity. It is difficult to have a turbofan engine with its fan pressure ratio lower than 1.25. So for the BPR 15 TeDP system, the optimised configuration probably has TSR between 40% and 60%.

5.3 Results and Analysis

5.3.1 Impacts of BLI

Fig.5.10 compares the TSFC with or without BLI. BLI improved the overall fuel consumption at all the examined conditions, especially at high thrust split ratios. The TSFC reduced from 6% at 20% TSR to 11% at 100% TS. The propulsor duct pressure losses for both cases (with or without BLI) are 2%. So the results can only prove that if the propulsor duct pressure losses are the same, ingesting boundary layer benefits the fuel consumption. As we know, ingesting boundary layer leads to additional intake pressure losses. A well-designed inlet duct without boundary layer should have pressure losses lower than 0.5%. Other negative effect of BLI is the fan efficiency drop due to the fan inlet distortion.

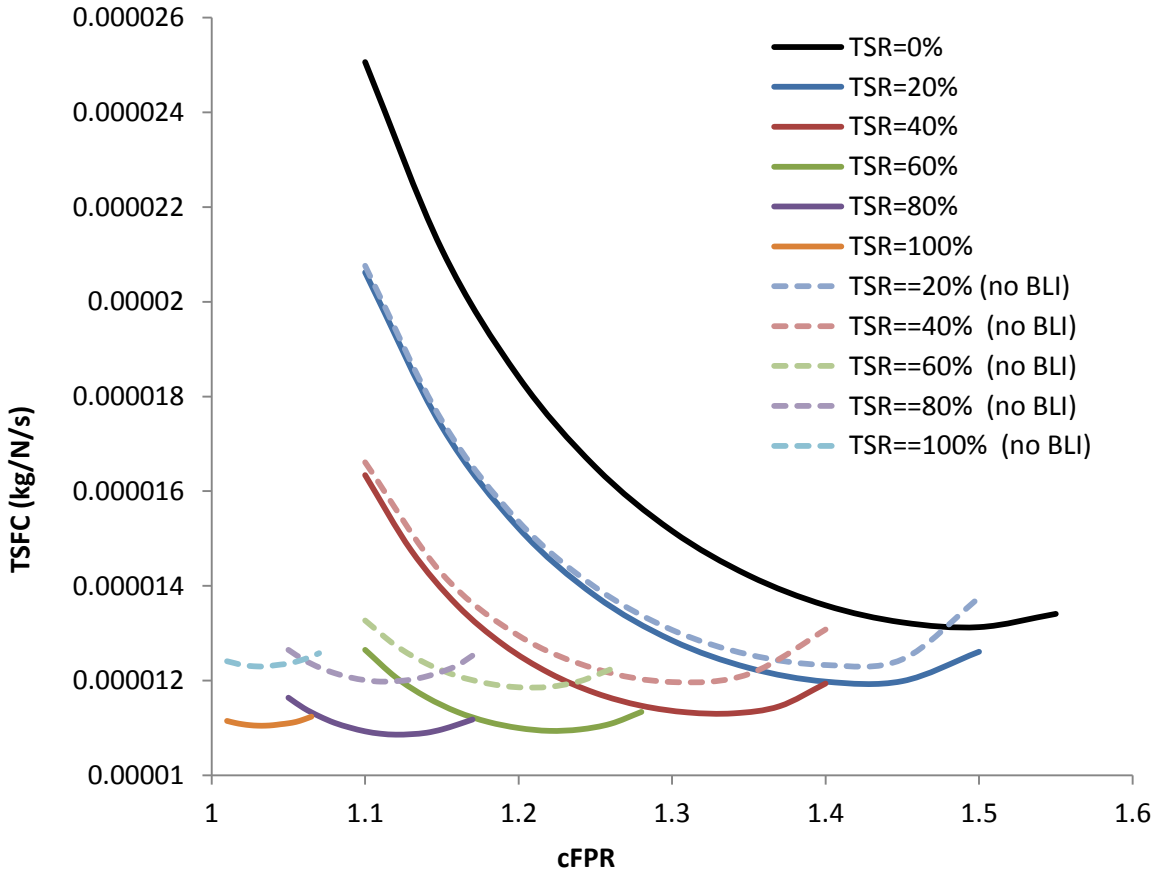

(a)

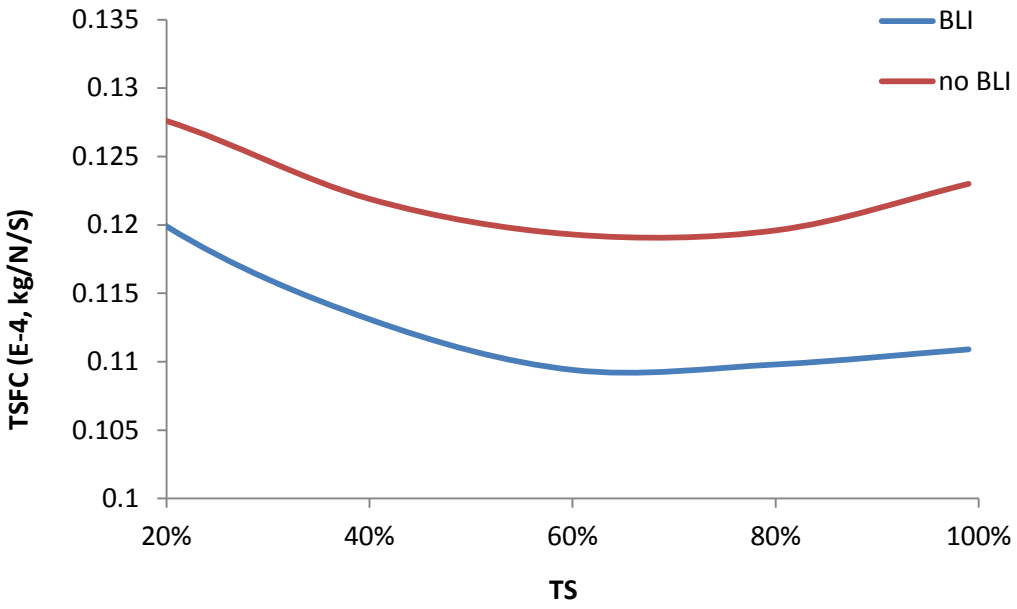

(b). Lowest TSFC achieved at different TSR ratios

Figure 5.10 TSFC at Different TSR and Core Engine FPR with/without BLI

Fig.5.11 compares the four different engine configurations. Two BLI cases are shown with 2% and 4% of propulsor duct pressure loss; One BLI case with 2% propulsor duct pressure loss and 5% fan efficiency drop; One non-BLI system with 0.5% propulsor pressure loss. Although the configuration with BLI is more efficient than the alternative non-BLI configuration, as losses increase, the benefit of the BLI system decreases. If the propulsor intake duct pressure losses or the propulsor fan efficiency penalty is sufficiently high, a podded configuration may be preferable.

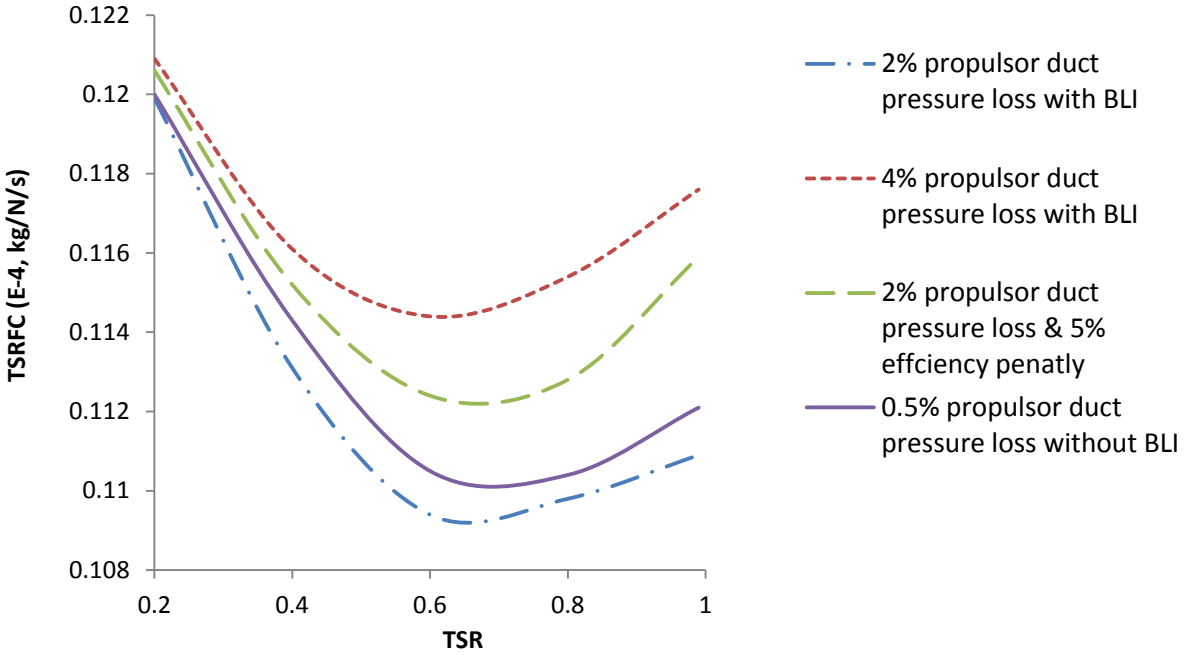

Figure 5.11 Effects of Propulsor Duct Pressure Losses and Other Inefficiencies

The propulsors unit was assumed to be positioned in a continuous array across the upper rear surface of the fuselage section with the inlet as close to the trailing edge as possible. The propulsor array forms a wide V shape with the bottom of the V at the centre line and the arms moving forward to follow the trailing edge. In this chapter, to simplify the problem, we assumed that the inlet boundary profiles of each propulsor are the same. However, the inlet air profiles of each propulsors are different, especially the boundary layer thickness. In Fig.5.12, the black dash line is the optimised propulsor capture height for the TeDP system with 50% higher inlet BL thickness. The blue dashed line is the corresponding propulsor power. There is no significant difference on the propulsor power for different intake boundary layer thickness. However, the optimised propulsor capture height increases, especially at high TS. The inlet boundary layer thickness of the propulsors array becomes thicker as the propulsor approaches the centre; this means that the optimised capture height of the propulsor in the centre should be higher than the propulsors on both sides. Fig.5.13 gives one of an intake designs concept for future studies. The disadvantage of the design is the structure complexity. Future studies should figure out its advantages and disadvantages. To simplify the modelling process, in this chapter, the capture height of each fan unit is assumed constant.

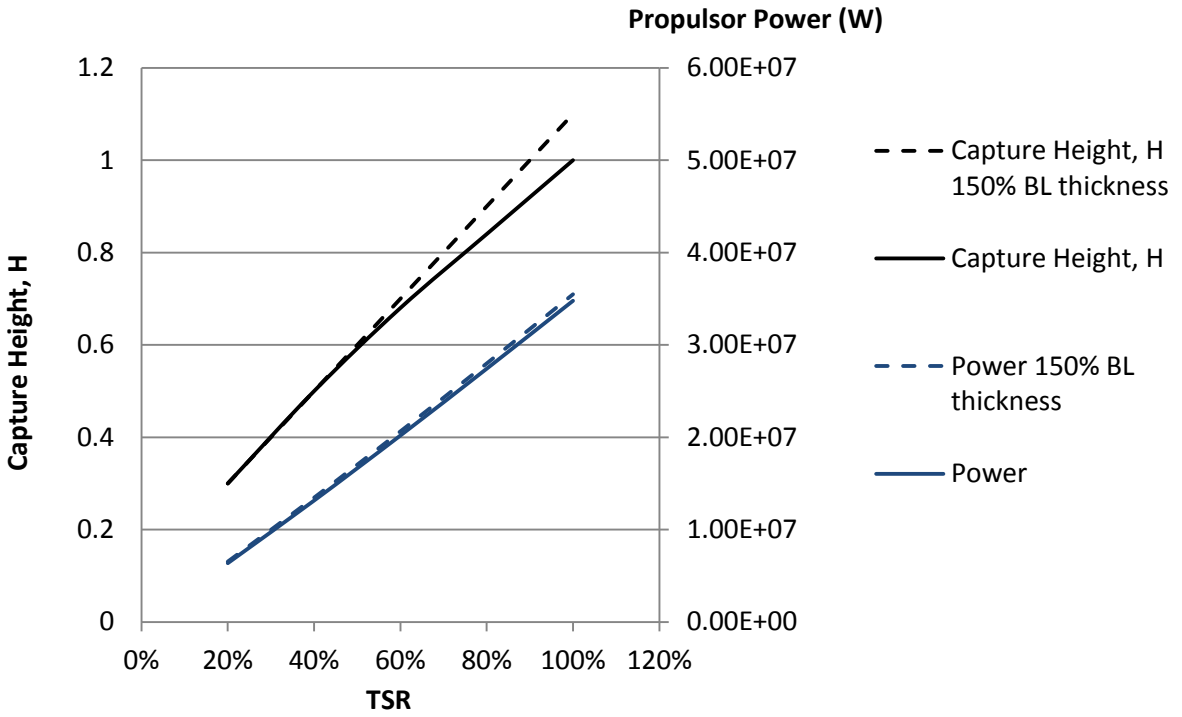

Figure 5.12 Optimised Capture Height and Propulsor Power with BLI for different BL Thickness

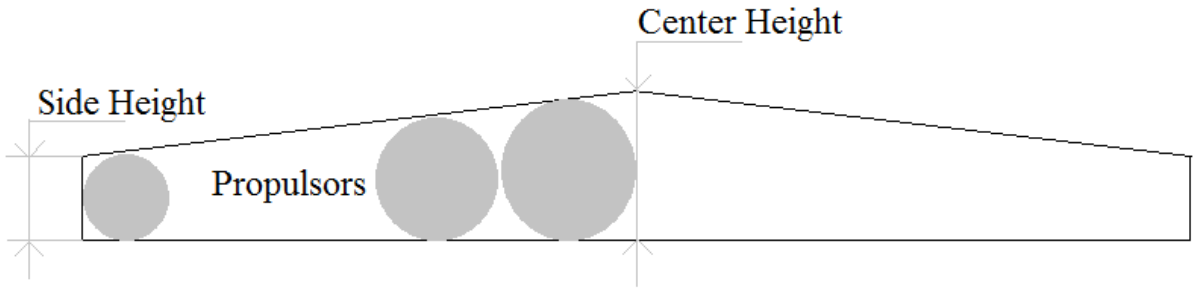

Figure 5.13 Propulsors Array Inlet Duct Shape

5.3.2 Impacts of core-engine BPR

The core engine has a turbofan engine, a power turbine and a superconducting generator. The core engine BPR refers to the ratio of the mass flow rate of turbofan engine bypass duct to the mass flow through its high pressure compressor. Higher BPR can improve propulsive efficiency. The rate of improvement with BPR decreases as BPR rise, and eventually the increased penalty associated with the drag of the nacelle outweighs the benefits predicted for the bare engine. In addition, an increase in BPR engine leads to an increase in engine weight. A turbofan engine of BPR15 was used in previous studies. However, lowest TSFC achieved with TSR

exceed 0.6. In these cases, most of the thrust is produced by the propulsors. Is it necessary to use such a high bypass ratio turbofan engine? Fig.5.14 compares the TSFC of two TeDP systems: one with BPR 15 and the other, 8.

At low TS, high BPR improves the overall fuel efficiency. That is because most of the fuel is consumed by the core engines and high BPR improves the propulsive efficiency. However, the benefits decrease with the increasing of TS. After TSR exceeds 0.6, low BPR TeDP system can get almost the same TSFC as the high BPR TeDP system. Moreover, low BPR TeDP system has smaller core engine nacelle, and thus reduces the core-engine weight. Additionally, the optimised core-engine fan pressure ratio of the low BPR TeDP system is higher than the high BPR TeDP system.

- High BPR TeDP system

This TeDP system usually has BPR of the core turbofan engine higher than 10. It is more suitable for low TSR TeDP system. Results show that it is not necessary to use it for high TSR TeDP system. It is because, in this case, the cFPR is too low and the improvement on the TSFC is not obvious.

- Low BPR TeDP system

This TeDP system usually has BPR of the core turbofan engine lower than 8. It is more suitable for high TSR TeDP system. The disadvantages are its sensitivity to the propulsor intake pressure losses and the performance of the electric system.

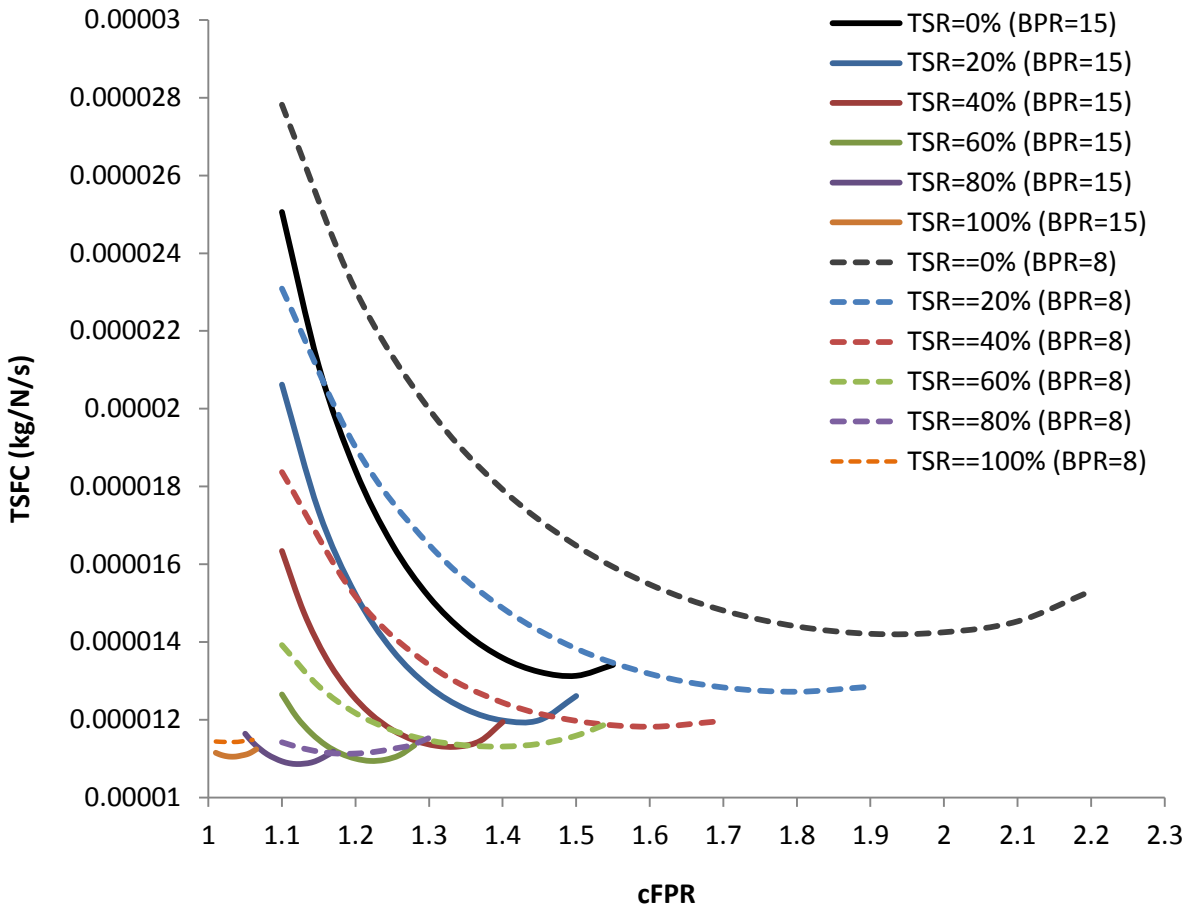

(a)

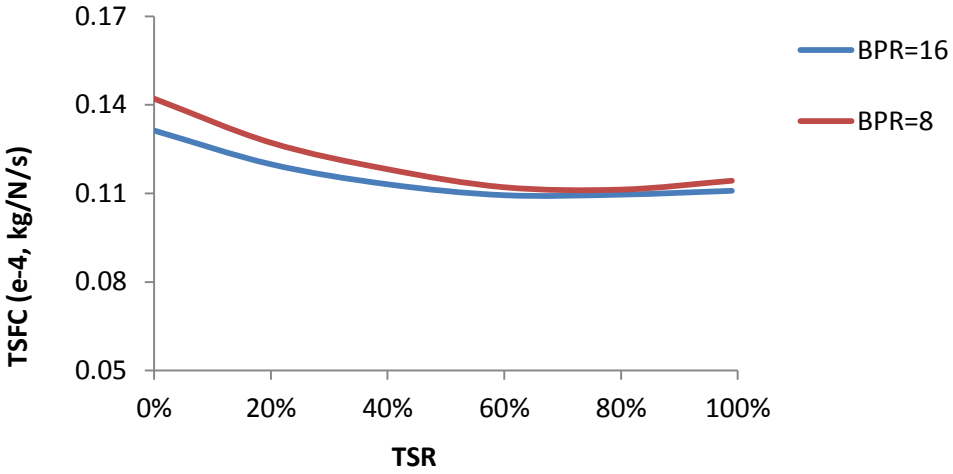

(b)

Figure 5.14 Comparison of Two TeDP Systems' TSFC: One with BPR 15, the Other Is 8

5.3.3 Constant propulsor intake height

The propulsors are put on the upper rear surface of the airframe; their intake is integrated into the airplane. Previous studies all assumed its height is a variable data, which is changed in order to achieve lowest propulsor power. However, the intake height should be chosen as small as possible, to reduce the airplane drag (which is assumed the same for different intake heights in previous studies). Meanwhile, it should be large enough to provide room for the fan stage. That is because, the fan stage is driven by an electric motor, and the diameter of the motor is usually larger than 0.3 meters [19]. If the hub tip ratio of the fan stage equals 0.3, the intake exit should be at least 1 meter high. So if the intake inlet height is too small, air flow will separate in the duct and cause serious distortion. In this section, the propulsor intake is designed with a constant capture height 1 meter and width 16 meters.

Fig.5.15 and Table 5.5 show the results. Its impacts on the PPR and FPR are small, but it increases the TSFC. That is because it is not the optimised capture height, therefore, the fan power increased.

Table 5.5 Design Parameters of the TeDP System with Constant Propulsor Capture Height

TSR	H	PPR	FPR	TSFC (e-4, kg/N/s)
0.2	0.3	1.193	1.4	0.1198
	1.0	1.067	1.4	0.1237
0.4	0.5	1.231	1.34	0.1131
	1.0	1.123	1.325	0.1161
0.6	0.7	1.247	1.22	0.1094
	1.0	1.184	1.225	0.1117
0.8	0.8	1.293	1.12	0.1098
	1.0	1.252	1.12	0.1109

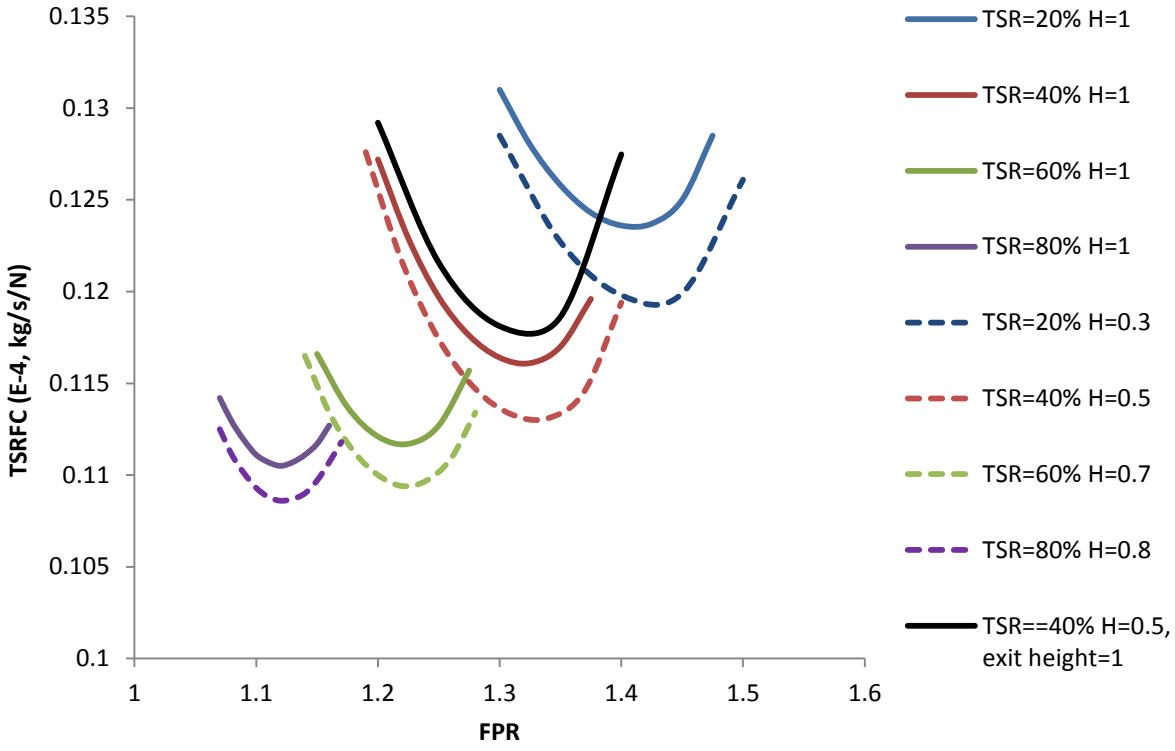

(a)

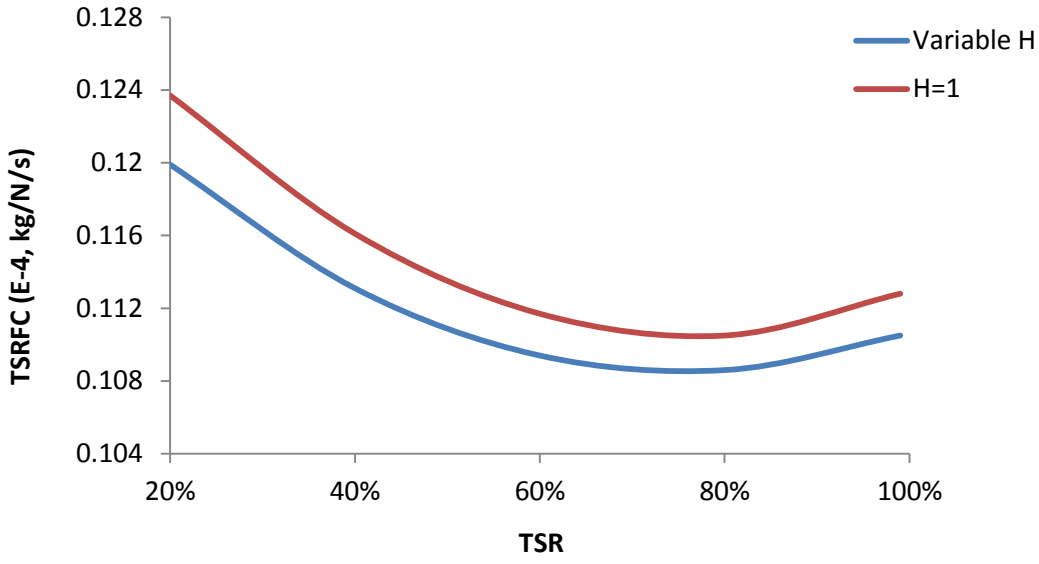

(b). Lowest TSFC achieved at different TSR ratios

Figure 5.15 TSFC of TeDP System with Constant Capture Height (H=1m)

In all the examined cases, the propulsor intake duct was assumed to have the same inlet and exit height. The black line in Fig.5.14 shows the other situation. The propulsor inlet duct has inlet height of 0.4 meter and exit height of 1.0 meter. Comparing to the straight duct, the divergent duct would have higher pressure

losses. If the pressure loss is 4% larger, the fuel consumption is higher than the TeDP system with 1 meter capture height. So the size of the electric motor and the intake duct shape are directly impacting the fuel efficiency of the TeDP system.

5.4 NASA N+3 case study

In 2009, a new airframe concept, N3-X, with TeDP system, was introduced at AIAA Aerospace Science Meeting. The N3-X aircraft is designed to carry a 53,574.8 kg payload 12200m at Mach 0.84. These mission requirements need 119 KN at design point (Altitude=30000ft & Ma=0.84). Previous studies examined its design point performance. However, the TeDP system is powered by a turboshaft engine. In this section, the turbofan-driven TeDP system developed in this chapter was used.

To guarantee enough space for the propulsor electric motor, its intake height should be larger than 1 meter. To increase the reliability of the TeDP system, the number of propulsors used should be as high as possible. So the total intake width should equal to the allowable value (16m). To recover the core engine intake pressure losses, its cFPR should be larger than 1.25, OPR (=74.8) and TET (=1811k) stay the same. Based on these assumptions, three low BPR TeDP systems were chosen to power the NASA N3-X aircraft.

Fig.5.16 and Fig.5.17 show the power and the PPR at different capture height and TSR ratios. From Fig.5.16, the lowest power of each TSR ratio was achieved at capture height equal to 1. The other benefit of choosing small capture height is the increased number of propulsors. That is because the propulsor fan diameter is more or less the same as the capture height. Fig.5.17 shows the PPR of each TSR ratio at different capture height. The PPR reduces with the increment of the capture height but increases with TSR ratios. For a ducted propulsor with common nacelle, a reasonable pressure ratio should be larger than 1.25 to recover the pressure losses. So the intake capture height of the propulsors unit equals one meter and the TSR ratio of the TeDP system should be larger than 80%.

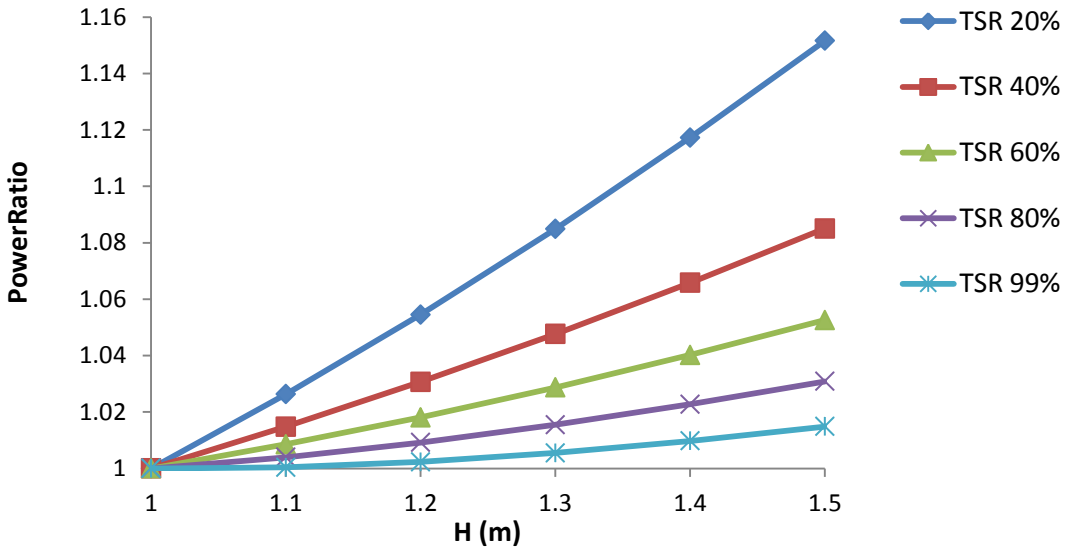

Figure 5.16 Propulsor Intake Height vs. PowerRatio (= Power/Power (H=1) @ each TS)

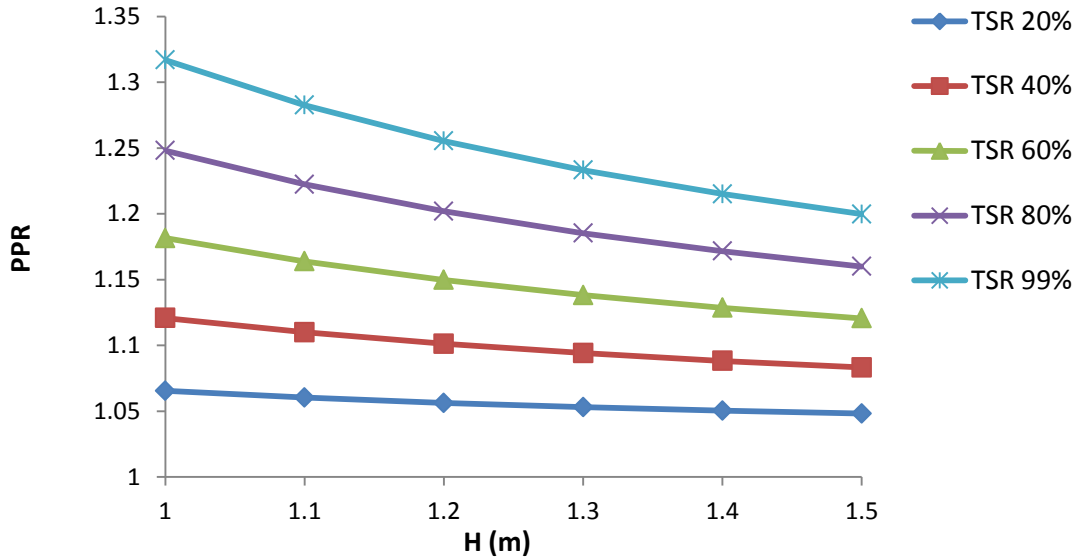

Figure 5.17 Propulsor Intake Height vs. PPR

Table 5.6 lists the PPR and power requirement at different TSR ratios with capture height equal to 1 meter. The PPR increases with the TS. The next step is to find the TSFC of each case. The core turbofan engine FPR should also be larger than 1.25. From the previous results, low BPR turbofan engines are more suitable for the high TSR ratio TeDP system. So turbofan engines with BPR of 1, 3 and 5 were chosen to power the TeDP system. Fig. 18 shows the results.

Table 5.6 PPR and Power of Different TSR with H=1m

TS	0.8	0.85	0.9	0.95	0.99
PPR	1.248	1.2655	1.2835	1.3018	1.3168
Power (MW)	28.819	30.699	32.603	34.53	36.088

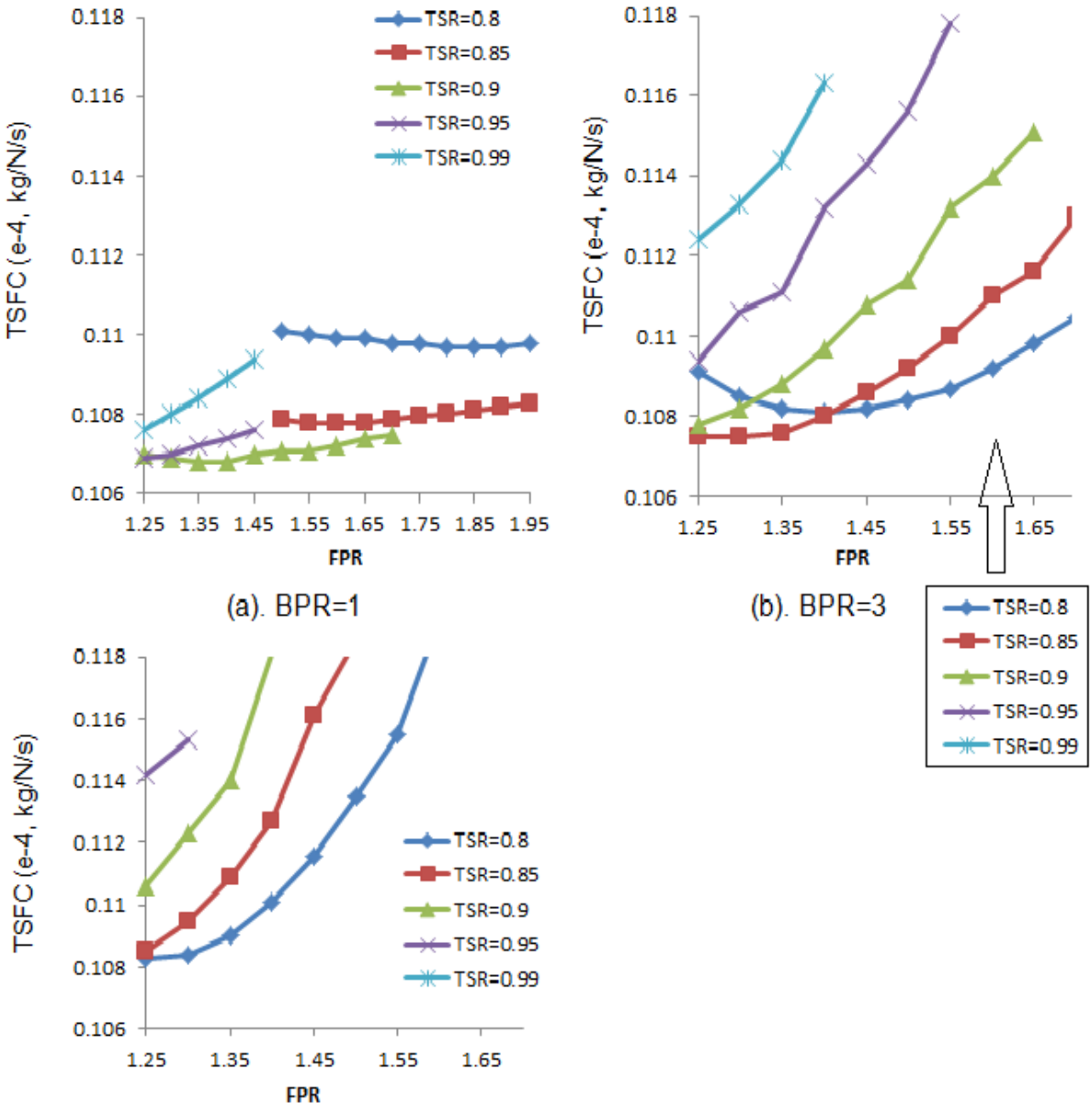

Figure 5. 18 TSFC vs. FPR of Different Core-engine BPR

From the results in Fig.5.18, with increasing core turbofan engine bypass ratio, the lowest TSFC is achieved at lower TSR ratio. At BPR=1, the lowest TSFC achieved at TSR ratio is bigger than 0.9 but for BPR=5, the lowest TSFC achieved at TSR ratio equals to 0.8. Overall, the lowest TSFC is achieved at BPR=1 and TSR=0.9. The other benefit of using low BPR engine is the reduction in core engine weight. In short, without considering the performance at off design conditions, the TeDP system for the N+3 airplane should be combined by propulsors and a low bypass turbofan core generator, or even a turbo-generator (core engine only provide power) as the NASA suggested.

Fig.5.19 and table 5.7 show the results of the lowest TSFC at examined thrust split ratios of different BPR. The FPR to achieve the lowest TSFC reduces with the increase of both the TSR ratio and core-engine BPR. Moreover, at lower TSR ratios, high BPR engines benefit overall fuel consumption. But for higher TSR ratios, low BPR engines are preferable. That is because the FPR should be higher than 1.25, for high BPR engines, their lowest TSFC is usually achieved with FPR lower than 1.25.

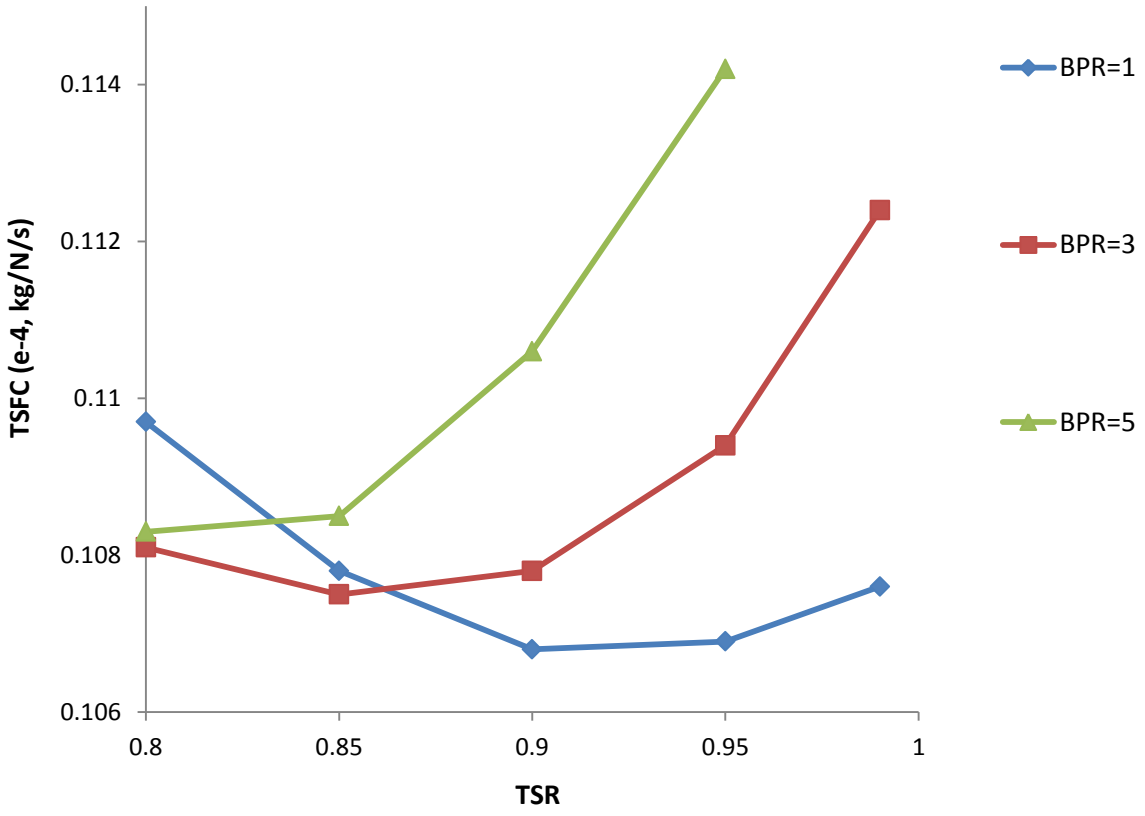

Figure 5.19 Lowest TSFC at Different TSR Ratios

Table 5.7 cFPR to get the Lowest TSFC

TS		0.8	0.85	0.9	0.95	0.99
cFPR	BPR=1	1.85	1.6	1.4	1.25	1.25
	BPR=3	1.4	1.3	1.25	1.25	1.25
	BPR=5	1.25	1.25	1.25	1.25	

In short, in this case study, the TeDP should be designed with the following data (@DP):

- TSR= 0.9
- BPR=1
- cFPR=1.4
- PPR=1.28
- OPR=74.8
- TET=1811

5.5 Discussion

The work in this thesis has demonstrated that there are fuel burn benefits to be gained from applying BLI to a blended wing body airframe. To achieve these benefits, performances of the superconducting systems are critically important. For example, at DP, power produced by the core–engine is transmitted to propulsors electrically, the transmission efficiency was assumed equal to 100% in the thesis. However, when utilising superconductivity, refrigeration is needed to maintain its ultra-low working temperature, which reduces the transmission efficiency. Moreover, the cooling power increased with the increase of TS. So, cooling losses reduce the optimised TS, especially on the TeDP system with high TS, in order to achieve lowest TSFC.

The use of gas-turbine-driven generators to supply electric power to motor driven propulsive fans adds considerable flexibility to the propulsion and vehicle architecture. As noted above, the electric components function as a gear box allowing the turbine engines to run at high speed, independent of the fan shaft speed. Beyond functioning as a simple gearbox, the electric components can function as a continuously variable ratio gear box with the addition of a solid state

power inverter. This would permit the turbogenerator power turbine and fan shaft speed to vary independently to yield best performance.

NASA's plan on meeting the plans of next generation commercial airplane for 2030 is through combining the Blended Wing Body aircraft and the distributed propulsion system. Distributing an array of propulsors that ingest a relatively large mass flow directly produces an 8% fuel burn saving relative to today's aircraft. BLI achieves a 7-8% fuel burn saving as expected. However, the benefits are very sensitive to the thrust split ratio, the propulsor intake pressure losses, inlet distortion, and efficiency of the superconducting system. If the cooling losses are high, a turbofan core engine, instead of a turboshaft engine (NASA's design concept), should be used. So both the propulsors and the core engine produce thrust, and the best TSFC is always achieved at TSR around 0.6 to 0.8.

The distorted inlet velocity and pressure profile used in the thesis is very simple and for a more special design problem, more detailed S-duct CFD simulation are needed. The duct should be designed carefully to avoid flow separation, which becomes more likely to happen with high ratio of boundary flow. Also, straight duct is not preferred, because it will increase the airframe drag.

The optimised capture height at each TSR ratio refers to the propulsor inlet duct capture height that achieves lowest fan power. The heights were obtained without considering the diameter of the propulsor fans and electric motor. For example, the optimised capture height at 0.2 TSR and 2% intake pressure loss is 0.3m, which means, the fan hub diameter is 9cm. In this case, it is difficult to find such a small motor, which should be positioned behind the rotor stage, to drive the fan. If the intake duct exit diameter was increased to provide more space for the motor, the ingested boundary layer flow would be more likely to separate and thus causing serious distortion problem.

Case study shows that optimised design parameters of the TeDP system are closely associating with technical levels. For example, in the case study, FPR cannot be lower than 1.25. That is because the FPR should be high enough to recover the duct pressure losses. So in this case, high BPR engine should not be used, due to its low optimised FPR. Low BPR engine or turboshaft engine should be used to increase the FPR. However, other factors will also impact the final result, such as the cooling

efficiency and the efficiency in transmitting the electric power. In this chapter, the efficiency was assumed the same for different TeDP system. However, the efficiency will reduce with the increase of power. Future studies should figure out these problems.

5.6 Future works

Different from podded engine configuration, concepts like the HWB with TeDP system where the engine inlets and airframe are closely coupled will make it very difficult to analyse components isolated from each other. The highly integrated inlet and airframe of such concepts could have significant impact on the propulsion system performance. In order to reduce the drag of pylons, HWB will allow the boundary layer developed forward of the engine face to be ingested by the inlet. Thermal cycle analysis at design point showed its benefits on fuel consumption. However, the benefits are sensitive to the inlet pressure distortion. Detailed analysis of the inlet distortion and its impacts on engine performances at DP are not issued in this thesis. In future studies advanced CFD tools should be used to model the inlet flow behaviour and its impacts.

One other challenge is the TeDP system overall weight analysis. It includes the weight of each propulsor, the superconducting transmission system, the electric motor, the cooling system and the core engines. For example, Brown [12] estimated that the total weight of the electric system of a TeDP system would be around 9,000 to 12,000 kg. The final value is dependent on the number of propulsors, fuel type, cooling method, as well as the power of the turbogenerator. Given the additional weight, which is similar to that of a conventional propulsion system, future studies should concentrate on these issues and address their implications on the overall design and performance. It is true that in the case of large mass penalties the benefits of superconducting distributed propulsion system would be largely diminished.

TeDP system off design analysis is critical, because enough thrust should be produced at take-off and top of the climb. The propulsor fan rotor of the TeDP system is driven by a motor, instead of a turbine. The challenge is to predict the off-

design performances of the motors and the way to match their performance with the fan. For example, whether the motor can drive the fan at RTO to produce enough thrust, and how to control the motor to produce more power, should be analysed. Moreover, how to decide the TSR at take-off condition, and what the relation of the TSR at DP with the maximum thrust the TeDP system can produce should be figured out.

5.7 Conclusions

Current high bypass ratio turbofan engines are reaching a higher limit of bypass ratio due to ground clearance and lower limit of fan pressure ratio. To explore lower fan pressure ratio with high shaft speed, a number of fans should be applied to replace one big fan. This thesis examined the concept of using superconducting generators and motors to transmit power from the core engines to distributed propulsors.

Firstly, a new TeDP system concept was introduced. It contains three major parts: the propulsors unit, the core engine, and the electric system. Power produced by the core-engines is transmitted to the electric motor driven propulsors. The thrust comes from both the propulsors unit and the core engines. Moreover, thrust split ratio (TS) is used to characterise the TeDP system, and the BPR of a TeDP system refers to ratio of the bypass flow of the core engine to its centre flow.

Secondly, the propulsors unit is put on the upper trailing surface of an airframe in order to ingest boundary layer. At all examined conditions, BLI reduces the fuel consumption, especially at high thrust split ratio. However, the benefits are sensitive to propulsor intake distortion. For example, if the intake pressure loss increased from 2% to 4%, the fan power will increase around 10%; and if the fan efficiency dropped 5%, it leads to 5% fan power increase.

Thirdly, for a propulsor intake duct with constant width, there is an optimised capture height to reach lowest fan power. This optimised height increases with the increase of TS. For the same TS, the height reduces with the increasing of intake pressure loss. Moreover, the height should be large enough to guarantee enough space for the electric motors.

Fourthly, the total propulsor inlet width is the sum of each propulsor inlet width. Its maximum span-wise distance available on the after upper fuselage section is constrained by the airframe. To design a TeDP system with low TS, the chosen propulsor inlet width should be as small as possible. But with high TS, the propulsor inlet width should always be reaching the maximum span-wise distance.

Finally, for low TSR TeDP system, high BPR turbofan engine should be used. For high TSR TeDP system, low BPR turbofan engine, or turboshaft engine, is preferable. At all the examined conditions, the lowest TSFC is always achieved with TSR higher than 0.6. So the TeDP system of high TSR with low BPR turbofan engine is the future research trend for the turbofan-driven TeDP system. In short, the new case study shows the TeDP system to power the N3-X airplane should have the following design parameters (@DP):

- Propulsors unit:
    - Intake width: 16 meters
    - Capture height: one meter
    - Fan efficiency: 0.94
    - PPR: 1.28
    - Inlet mass flow ratio: 1681.6 kg/s
    - Power requirement: 32.6 MW
    - Thrust: 108.53 KN
- Each core-engine (two should be used):
    - BPR: 1
    - OPR: 74.8
    - FPR: 1.4
    - Inlet mass flow ratio: 61.3 kg/s
    - TET: 1811K
    - Thrust: 5.97 KN
    - Power turbine efficiency: 0.93
    - Power turbine power: 16.5 MW

Chapter VI

Off Design Performance Modelling of the TeDP System and the Electric Components

The turboelectric distributed propulsion (TeDP) system with boundary layer ingestion (BLI) uses electricity to transmit power from the core turbine to a number of propulsors. This novel concept can increase bypass ratio and propulsive efficiency to achieve lower fuel consumption and noise. Different from the turbofan engines, the speed of the power turbine shaft is independent of the fan (in the propulsor) shaft speed. The electric system functions as a gearbox with arbitrary gear ratio. This allows the power turbine shaft speed be optimised without considering the fan tip speed limitation. In this chapter, the method to predict the propulsor off-design performance was developed, as well as the method to evaluate impacts of BLI. Then, the methods to analyse off-design performances of electric components, including the motor, the generator, the cryocooler and the inverter, were introduced, followed by the method to estimate their weights.

6.1 Introduction

The TeDP system has three major parts: the core engine (turbogenerator), the propulsors unit and the power transmit system. The core engine, which combined by a turboshaft engine and a generator, is put on the wing edge. It only ingests free stream air and its power turbine shaft speed is independent of the propulsors fan speed, thus Turbomatch (Cranfield Aero-engine Simulation Program) was used to model the core engine off design performance. Other programs, such as GasTurb, also can be used. The propulsors, combined by a motor and a fan, can be designed with method introduced before. However, at off-design operation points, how to match the performance of the motor and the fan is a challenge, because the motor is analysed by torque and power, and the fan is analysed by fan pressure ratio and

rotating speed [28]. So in this chapter, the method to model the motor's off-design performance (or how to match motor's performance with the fan) will be introduced first. The turboelectric approach requires that a number of new electric components are inserted into the aircraft propulsive drive train between the core-engines and the distributed fans. These components include superconducting generator, transmission lines, cooling system and motors. To achieve low flight weight at acceptable efficiency, most of the components must operate at very low temperatures. While electric transmission provides nearly unprecedented flexibility in aircraft design, a number of penalties of adding the new components must be evaluated. These include greater complexity and possible reliability issues, as well as the weight and inefficiencies introduced by the added components. Both of these additions require additional fuel burn, which subtracts from the expected benefits, so the electrical system must not be either too heavy or too inefficient [1]. Fig.6.1 shows a block diagram of the components in a turboelectric drive train.

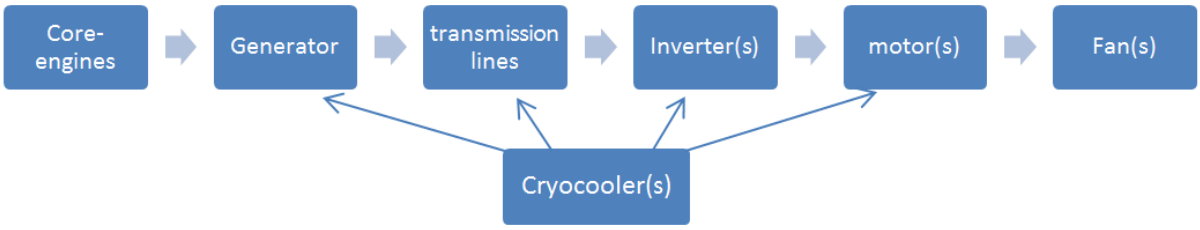

Figure 6.1 Components in a TeDP System

The generator, which is expected to have high power density, can be obtained only if the machines are fully superconducting. This requires that both its rotor and stator conductors are superconducting. To reduce power losses, the transmission lines also need to be superconducting. The inverter enables the motor and fan to operate at any desired shaft speed, which is independent of the generator shaft speed. Lightweight Cryocooler was used to maintain the low superconducting system running temperature. In this chapter, the methods to model performances of each electric component will be introduced. Then, their impacts on TeDP system performances will be analysed. Finally, a brief model to estimate their weight will be given.

6.2 Propulsor Modelling Methodology

As Fig.6.2 shows, one propulsor comprises a fan stage, a superconducting motor and the common nacelle and nozzle. The design point performance of the fan stage can be modelled by the method introduced in chapter 3. Motors are machines that convert electrical energy into mechanical energy using magnetic forces. When current is passed through a wire loop that lies in a magnetic field, a turning force, or torque, is created that causes the loop to rotate. In motors, this rotating motion is transmitted to a shaft. This rotational energy is then utilized for useful work in the form of mechanical power. Industrial motors are used for running pumps, fans, and compressors as well as in equipment involved in the handling and processing of manufactured materials. Marine propulsion motors are used to propel commercial vessels and warships. The basic features of modern conventional AC (alternating current) and DC (direct current) electric motors were first designed in the 1890s and the underlying technology has not been changed significantly in the past fifty years. Despite the lengthy period of time in which motors have been in development, motors are still far from being perfectly efficient converters of electrical to mechanical energy. The principal causes of power losses in motors come from the electrical resistance of the wire and from mechanical friction.

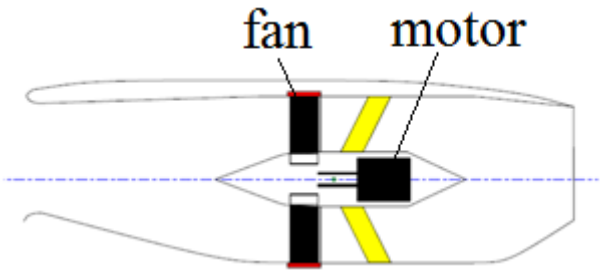

Figure 6.2 Propulsor with Superconducting Motor Driven Fan

6.2.1 Motor DP Modelling Method

Superconducting motors are new types of AC synchronous motors that employ HTS (high temperature superconductor) windings in place of conventional copper coils. Because HTS wire can carry significantly larger currents than copper wire can, these windings are capable of generating much more powerful magnetic fields in a given volume of space. Other benefits include lower first cost, lower operating cost, less

vibration and noise, and increased stability and reliability. Following equations can be used to calculate motor speed, horsepower and its torque. For superconducting motors, its efficiency equals to one.

$$\omega = \frac{120 \times Frequency}{number\ of\ motor\ winding\ poles} \tag{6-1}$$

$$HP = \frac{Voltage \times Current \times Eff}{746} \tag{6-2}$$

$$\tau = \frac{5252 \times HP}{\omega} \tag{6-3}$$

where, ω *is rotating speed; f* is supply frequency; N is number of motor winding poles; *HP* is horse power; *V* is Voltage; *I* is current; *Eff* is motor efficiency; τ is torque; the horse power is a unit of power equal to 746 watts

Fig.6.3 shows the motor performance map. Its maximum output power increases with the increasing of its shaft speed. After it reaches the maximum output power, increasing shaft speed will reduce its output power. Its output torque keeps constant before reaching the maximum output power. In this section, we assumed that if the rotating speed is large than the maximum output power shaft speed, the motor output power keeps constant due to the benefits of superconducting. Therefore, its output power can be calculated by Eq.6.4.

$$Power = \begin{cases} \frac{\omega}{\omega_M} \times Power_M\ , if\ \omega < \omega_M \\ Power_M\ , if\ \omega > \omega_M \end{cases} \tag{6-4}$$

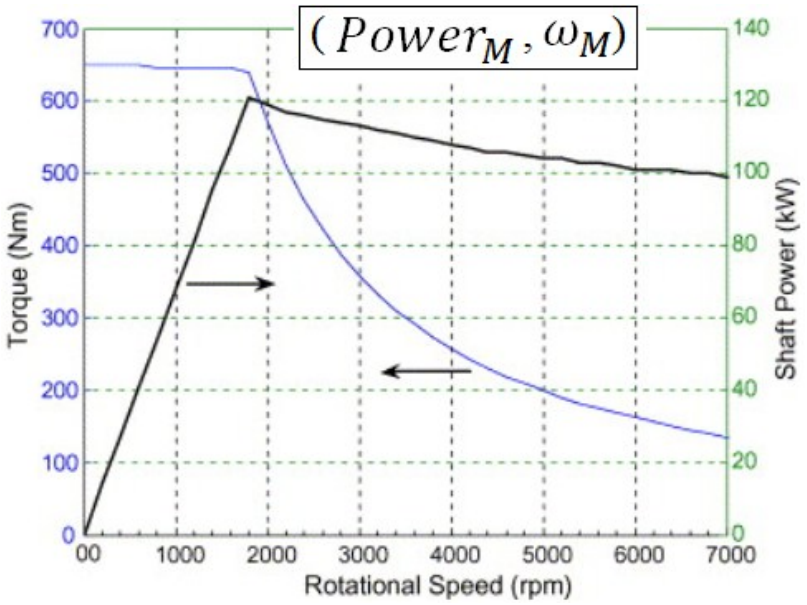

Figure 6.3 Motor Performance Map

Its performance map:

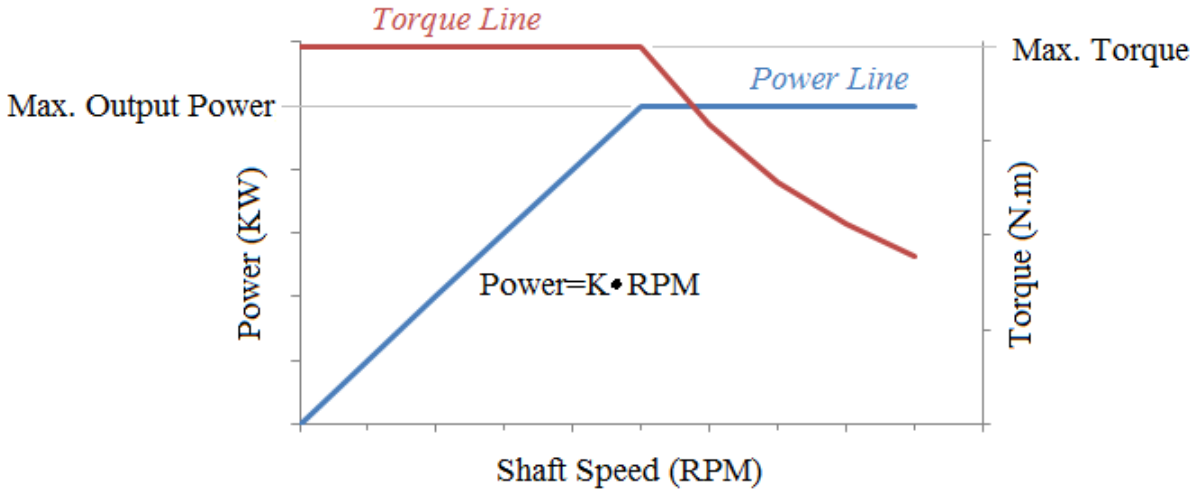

Figure 6.4 Superconducting Motor Working Map

$$K = Power_M/\omega_M \tag{6-5}$$

The number of motor winding poles should equals even number (i.e. 2, 4, 6, 8…). The winding poles should be chosen as small as possible to reduce the motor weight. If using four winding poles, its working frequency equals 133.3 Hz and the load torque equals 3228 N·m. If the working frequency should equals to 60 Hz or 120 Hz (international grid standard), the motor speed can only equals:

- 1800 RPM, 4 winding poles, 60 Hz

- 3600 RPM, 2 winding poles, 60 Hz
- 3600 RPM, 4 winding poles, 120 Hz
- 7200 RPM, 2 winding poles, 120 Hz

However, the values obtained from the motor without superconducting technologies. Advanced superconducting motors maybe work at variable frequency, therefore, future studies should figure out this question. The superconducting motor is used to drive the fan stage in a propulsor. It's working rotating speed is limited by both the load torque and the fan tip speed limitation. Increase rotating speed can reduce the fan loading coefficient but lead to higher fan tip speed and lower output torque. So, at design point, the motor working efficiency and the number of its winding poles should be optimised to satisfy the fan tip speed limitation (the max. rotating speed to satisfy fan tip speed limitation can be calculated by Eq.3.18) and motor output torque requirement (defined by Eq.6.6). This torque is the motor output torque, not the motor maximum output torque at the very rotating speed. The motor works only if the output torque is smaller than its maximum output torque. Maximum output torque is dramatically high in superconducting motor [5], so to analyse its performance, we can assume the motor's torque is large enough. Therefore, if the motor can produce enough power, it can produce enough torque.

$$\tau = \dot{m} C_p \Delta T / \omega \tag{6-6}$$

where,$\dot{m}$ is one propulsor inlet mass flow, ΔT is the air total temperature different through the fan stage

The motor should be put behind the fan stage, as Fig.6.2 shows; this means the motor diameter should be smaller than the fan hub diameter. For example, if the fan diameter is 1 meter and its hub-tip-ratio is 0.3, the maximum motor diameter is 0.3 meter.

6.2.2 Motor-Fan Performance Match

The superconducting motor can be designed based on the method introduced before at design point. However, at off-design operation points, the way to match the performance of the motor and the fan should be figured out. Because the motor is analysed by torque and power, but the fan is analysed by fan pressure ratio and

rotating speed. So in this section, the method to model the motor's off-design performance (or how to match motor's performance with the fan) will be introduced.

Motor, similar to an inner combustion engine, is widely used in automotive. As we know, if a car engine fails to provide enough torque, the engine vibrates or stalls. That is because the resistance force acting on the wheels is higher than the engine can provide. That is why we use lower gear when we start and accelerate the car. However, working situation of the propulsor used in the TeDP system is not the same as starting a car. Because the fan is not directly driving the airplane, but compressing the air in order to produce thrust. The motor won't stall before enough thrust is produced by the TeDP system. That means the torque of the motor at take-off, where the highest power is needed, can be kept the same as the torque at design point. Nevertheless, torque produced by electric motor is ultra-high [5]. Once the motor power is enough, the airplane can take-off. Thus, to match the motor performance with the fan stage, only the power needs to be considered. As long as the motor power does not exceed the generator power, it can be controlled by both its working voltage and current. The off-design performance of the fan is described by the fan map: FPR, rotating speed, inlet mass flow rate and efficiency. At any working point, the motor's power should be equal to the fan power. So:

$$Power\frac{\sqrt{\frac{T}{T_{sls}}}}{\frac{P}{P_{sls}}} = \frac{C_p}{Eff}\cdot CMF\cdot\left(PR^{\frac{r-1}{r}}-1\right)\cdot\frac{1}{NPER^2}\cdot T_{DP}\cdot\left(\frac{\omega}{\omega_{DP}}\right)^2 \tag{6-7}$$

$$CMF = \frac{\dot{m}}{A}\frac{\sqrt{T/T_{sls}}}{P/P_{sls}} \tag{6-8}$$

$$NPER = \left(\frac{\omega}{\sqrt{T_{inlet}}}\right)\div\left(\frac{\omega}{\sqrt{T_{inlet}}}\right)_{DP} \tag{6-9}$$

Where, T is the fan inlet total temperature; P is the fan inlet total pressure; ω is the shaft speed (rpm) T_{sls} equals 288.15K and P_{sls} equals 101300Pa

In Eq.6.7 the *Eff* is the fan efficiency. It refers to the ratio of the fan power to the motor power. Eq.6.10 describes the relationship with the fan isentropic efficiency. In

the equation, there is a working factor, *k*, which refers to the energy loss between the processes. Its value should be less than 0.5% with advanced mechanical designs [5]. In this section, its value was assumed equal to 0.5%. So the propulsor unit loses 0.5% power on the driven-shaft.

$$Eff = (1-k)\eta_{isen} \tag{6-10}$$

The non-dimensional power, NDP introduced by Eq.6.10, can be used to map the traditional fan map to a power based fan map. The new map shows the NDP at different CMFs and rotating speeds. The NDP enables the calculation of fan power with only inlet total temperature and pressure. Fig.6.5 shows the NDP map based on the results from chapter 3 at cruise. The benefit of using the new map for off-design calculation is it can include the motor maximum output power at different shaft speeds. The map directly shows the impacts of motor output power on the fan off-design performances.

$$NDP = \frac{Power}{C_p T}\frac{\sqrt{\frac{T}{T_{sls}}}}{\frac{P}{P_{sls}}} = \frac{CMF}{Eff}\left(PR^{\frac{r-1}{r}} - 1\right) \tag{6-11}$$

For example, in fig.6.5, if the motor maximum output power equals to 1.843 MW at 4460 RPM, the grey zone is the possible fan working zone to satisfy the motor power requirement. If the maximum output power increases to 3.68 MW at the same rotating speed, the fan can operate at both the red and the grey zone. The propulsor can change the shaft speed to change its running line. It can also change the nozzle area to change the working point through a running line. Fig.6.6 shows how the nozzle area changes in order to change the fan working point in a running line.

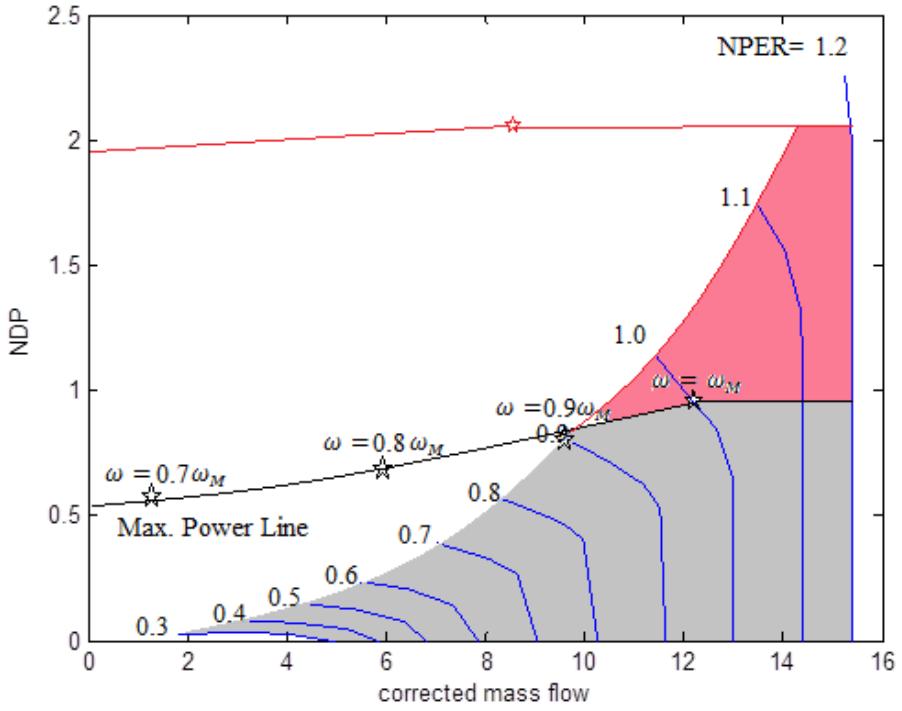

(a) NDP vs. CMF

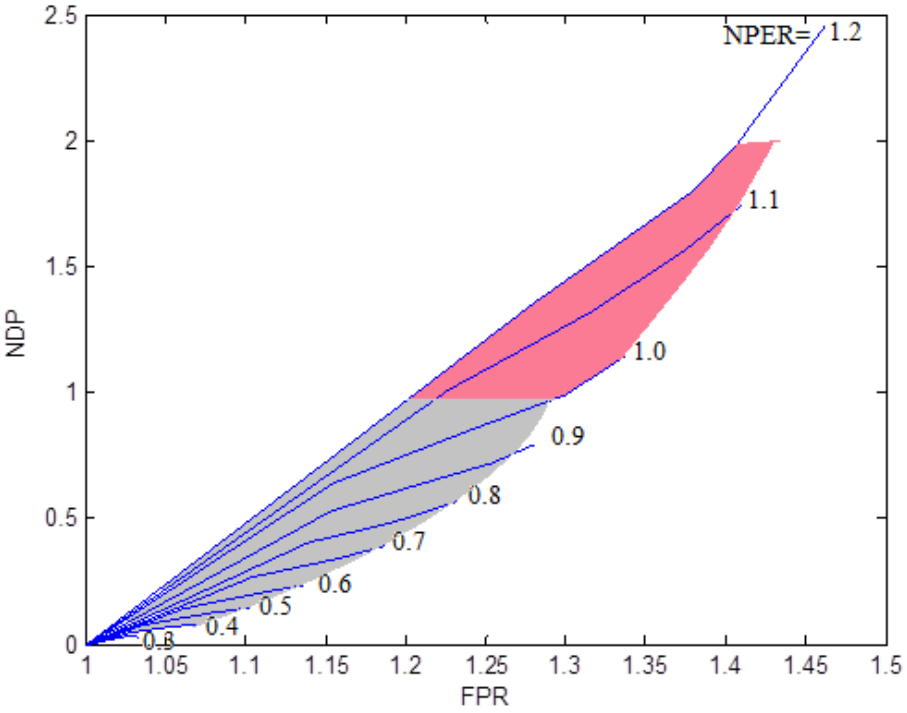

(b) NDP vs. FPR

Figure 6.5 Power Based Fan Map Example (data obtained from the TeDP system developed in Chapter 3 at cruise, with 16 propulsors and FPR=1.3@DP)

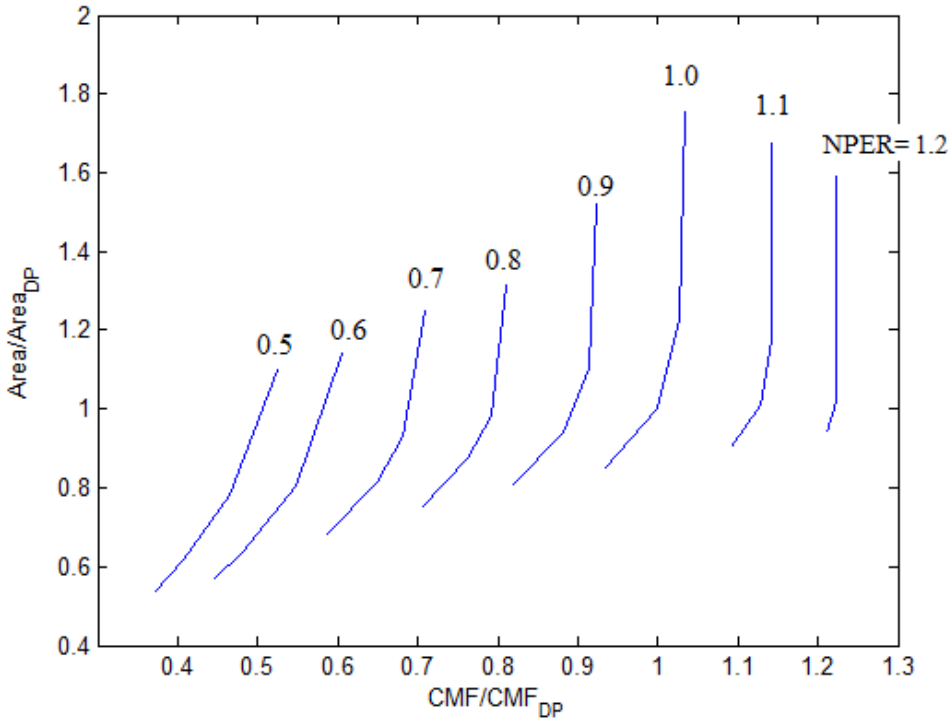

Figure 6.6 Nozzle Area (exit air fully expand to atmospheric pressure)

6.2.3 BLI Modelling Method

To evaluate the BLI impacts on off-design performance, the distorted fan map should be used to replace the clean fan map in Fig.6.7. The inlet air, therefore, can be described by a uniform flow. Its inlet condition can be calculated by Eq.4.24 to Eq.4.28. However, it is difficult to obtain a useful distorted map due to the limited data of the Turbomatch defaulted fan map, especially at lower shaft speed. That is because the clean fan map is not detailed enough. The program is difficult to converge when the uniform flow working point moves to the surge point. This largely reduces the surge margin of the new distorted map. So, future studies should address this problem. An alternative method is described below:

Step 1: the first step is obtaining the off-design working point without considering BLI; therefore, the inlet condition can be obtained by the flight conditions.

Step 2: obtain the inlet boundary velocity profile.

Step 3: calculate the capture height (*h in Fig.6.7*) by mass conservation.

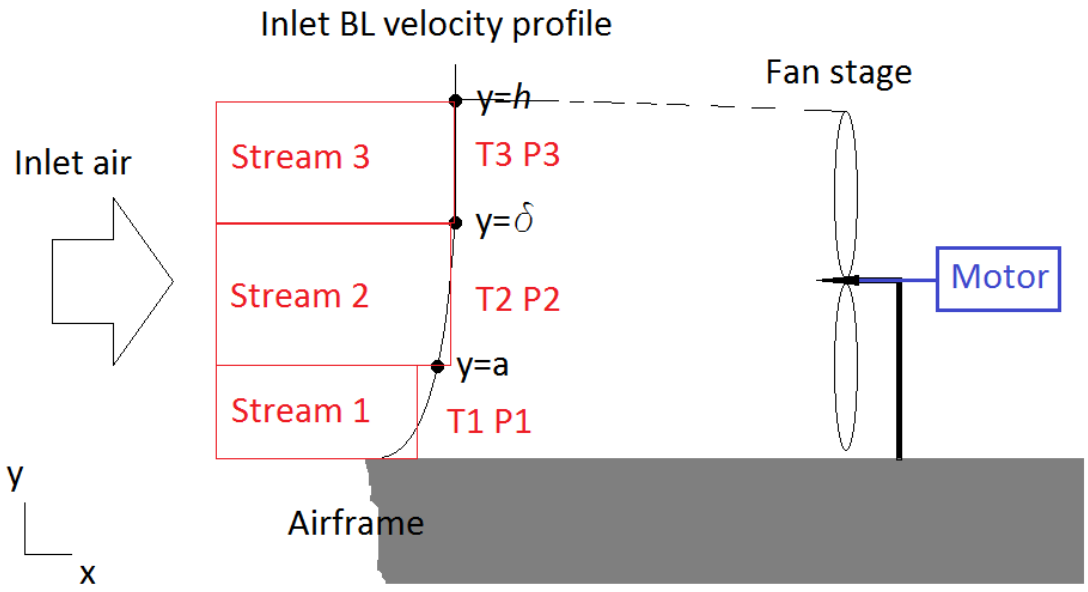

Figure 6.7 BLI Off-design Modelling Method

Step 4: use following way to describe the inlet boundary layer.

If the capture height (h) is smaller than the boundary layer thickness, use two parallel uniform streams to describe the inlet air and guess the height of stream 1 (y=a): stream 1 (from y=0 to y=*a*); steam 2 (from y=*a* to y=*h*), and $a = h/2$.

mass flow:

stream 1:

$$\dot{m}_1 = \int_0^a \rho V dA \tag{6-12}$$

average inlet velocity:

$$\bar{v}_1 = \frac{1}{A_1}\int_0^a V dA \tag{6-13}$$

average inlet Ma:

$$\overline{Ma}_1 = \frac{\bar{v}_1}{\sqrt{rRt_0}} \tag{6-14}$$

average inlet total pressure:

$$\bar{P}_1 = p_0\left(1 + \frac{r-1}{2}\overline{Ma}_1^2\right)^{\frac{r}{r-1}} \tag{6-15}$$

average inlet total temperature:

$$T_1 = t_0(1 + \frac{r-1}{2} Ma^2) \tag{6-16}$$

stream 2: mass flow:

$$\dot{m}_2 = \int_a^h \rho V dA \tag{6-17}$$

average inlet velocity:

$$\bar{v}_2 = \frac{1}{A_2} \int_a^h V dA \tag{6-18}$$

average inlet Ma:

$$\overline{Ma}_2 = \frac{\bar{v}_2}{\sqrt{rRt_0}} \tag{6-19}$$

average inlet total pressure:

$$\bar{P}_2 = p_0 \left(1 + \frac{r-1}{2} \overline{Ma}_2^2\right)^{\frac{r}{r-1}} \tag{6-20}$$

average inlet total temperature:

$$T_2 = T_1 \tag{6-21}$$

If the capture height is bigger than the boundary layer thickness, use three parallel uniform streams to describe the inlet air and guess the height of stream 1 (y=a): stream 1 (from y=0 to y=*a*); stream 2 (from y=*a* to y=*δ*); stream 3 (from y=*δ* to y=*h*); and $a = \delta/2$.

stream 3: mass flow:

$$\dot{m}_3 = \rho V_0 A_3 \tag{6-22}$$

average inlet velocity:

$$\bar{v}_3 = V_0 = Ma \times \sqrt{rRt_0} \tag{6-23}$$

average inlet Ma:

$$\overline{Ma}_3 = Ma \tag{6-24}$$

average inlet total pressure:

$$\bar{P}_3 = p_0\left(1 + \frac{r-1}{2}Ma\right)^{\frac{r}{r-1}} \tag{6-25}$$

average inlet total temperature:

$$T_3 = T_1 \tag{6-26}$$

Step 5: calculate the fan exit static pressure of the free inlet stream, with the assumption that its pressure ratio equals to the pressure ratio obtained in step 1.

Step 6: assume all the streams reach the same static pressure after the fan stage, and therefore, calculate their pressure ratio.

Step 7: calculate the nozzle inlet condition by the method introduced in chapter 4, therefore, the thrust and fan power.

6.2.4 Propulsor Off-design Calculation Flow Chart

Step 1: Once the electric motor was chosen, the method described in section 6.2.2 should firstly be used to obtain the allowable fan working zone in its fan map.

Step 2: Obtain the propulsor inlet flow velocity profile by the new flight conditions. This can be obtained by CFD simulation. However, due to lack of information, in this chapter we assumed the upper surface of the airframe is flat plate. Therefore, analytical method can be used to calculate the inlet velocity profile.

Step 3: Guess the propulsor fan shaft speed and its exit nozzle area. Therefore, obtain the propulsor inlet mass flow rate from the fan map.

Step 4: Calculate the propulsor capture height by the new inlet flow velocity profile in order to satisfy the mass conservation.

Step 5: The method described in section 6.2.3 should be used to calculate the fan power and the thrust.

Step 6: Repeat step 3 to 5 to find the minimum fan power to produce a targeted thrust; or the maximum thrust for a fan power.

Fig.6.8 shows the flow chart:

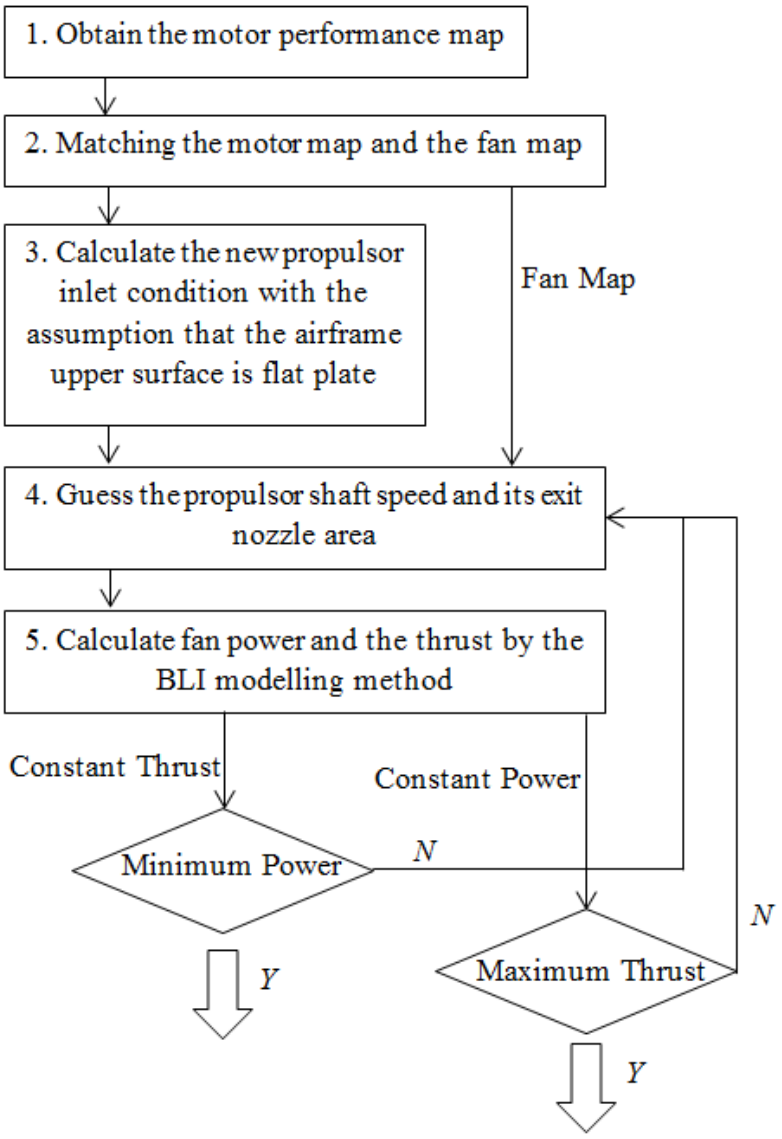

Figure 6. 8 Propulsor Off-design Calculation Flow Chart

6.3 Turbogenerator Driven-Engine Turbomatch Model

The turbogenerator, or the core-engine, is combined by a driving-engine and a superconducting generator. The driving-engine can be a turboshaft engine with a free power turbine, a turbojet engine with a free power turbine, or a turbofan engine with a free power turbine. Fig.6.9 shows models of the three core-engine modulus.

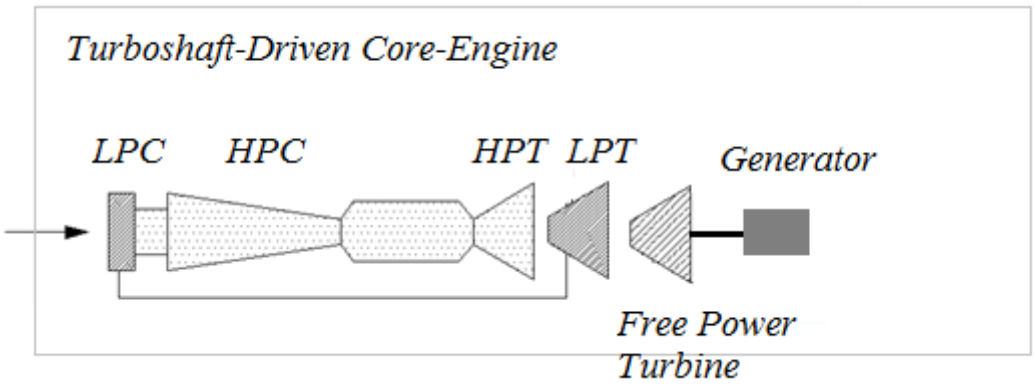

(a) Turboshaft-driven Turbogenerator

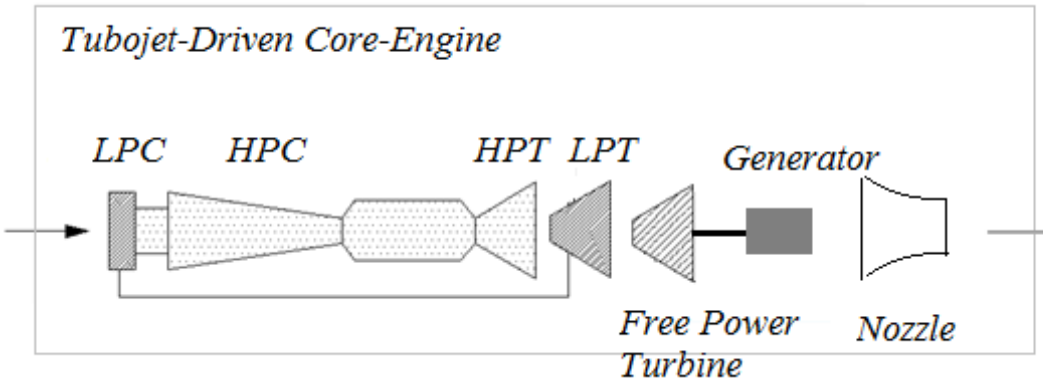

(b) Turbojet-drive Turbogenerator

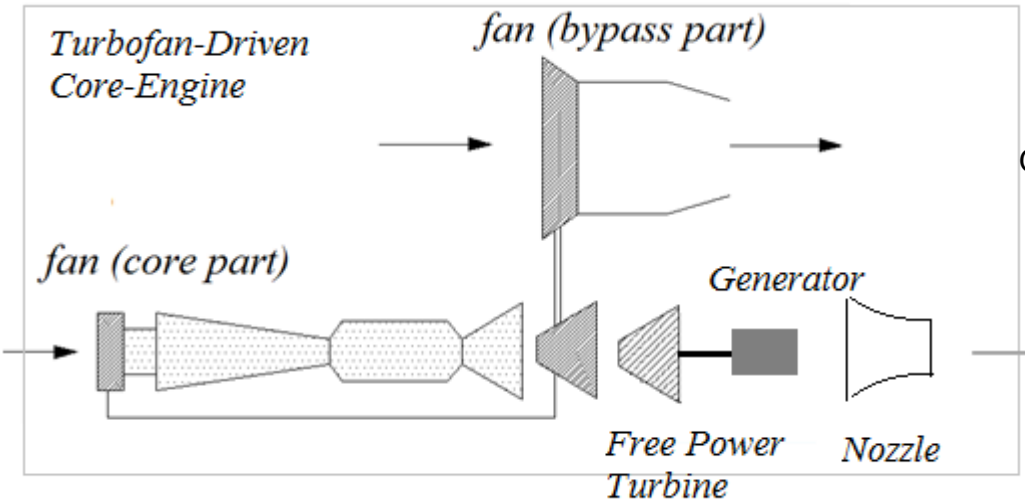

(c) Turbofan-driven Turbogenerator

Figure 6.9 Three Core-engine Concepts

- Turboshaft-driven Turbogenerator

For the turboshaft-driven model, the default Turbomatch turboshaft engine models can be used. Design parameters should be changed in order to match the design requirements. At off-design working points, the power can be obtained directly from the Turbomatch model.

Benefits:

- ✓ Lower core-engine weight
- ✓ Design simplicity for easy maintenance

Potential Problem:

- × Fuel consumption is sensitive to the intake distortion due to BLI
- × Heavier electric system, that is because powerful electric power system is needed to produce all the thrust. This leads to heavier motor, generator and cooling system

- Turbojet-drive Turbogenerator

For the turbojet-drive model, a new power turbine stage should be added before the nozzle in a default model. Its power should be equal to the electric power requirement.

Benefits:

- ✓ Lower core-engine weight
- ✓ Design simplicity
- ✓ Effective to control the weight of the electric system

Potential Problem:

- × Large noise from the core-engine
- × Relative higher fuel consumption due to the exit hot jet, especially at Take-off

- Turbofan-driven Turbogenerator

For the turbofan-driven model, a new power turbine stage should be added before the nozzle in a defaulted turboshaft engine model.

Benefits:

- ✓ Effective to control the weight of the electric system
- ✓ Relative lower fuel consumption, results in chapter 5 shows high thrust split ratio (>80%) with relative lower BPR offers best TSFC at design point.
- ✓ Relative lower core-engine noise

Potential Problem:

- × Structure complex
- × Heavier core-engine weight

To control the weight of the electric system, the motor power can be kept the same as at design point. For example, at T/O, the motor power is kept the same as at DP. The total electric power, therefore, is more-or-less the same. This dramatically reduces the total weight of the electric system. In this condition, the core-engine should produce the rest of the thrust to meet the requirement.

6.4 Superconducting Generator Modelling Methodology

In electricity generation, an electric generator is a device that converts mechanical energy to electrical energy. The source of mechanical energy is the core engine free power turbine. For the TeDP system under study, the generators should provide around 50,000 horse power. The generator was put inside the turbo-engine, thus its size should be as small as possible. Fig.6.10 shows the place to put the motor. This ultra-high power density can be obtained only if the machines are fully superconducting, which means both its rotor and stator are superconducting. However, the ‘superconducting’ machines of today typically have superconductors only in the rotor. So to model its performance, its efficiency, defined by Eq.6.27, should be assumed lower than 1. Research shows its efficiency can be as high as 0.9999 with superconducting technology. In this chapter, its efficiency was assumed equal to 0.999.

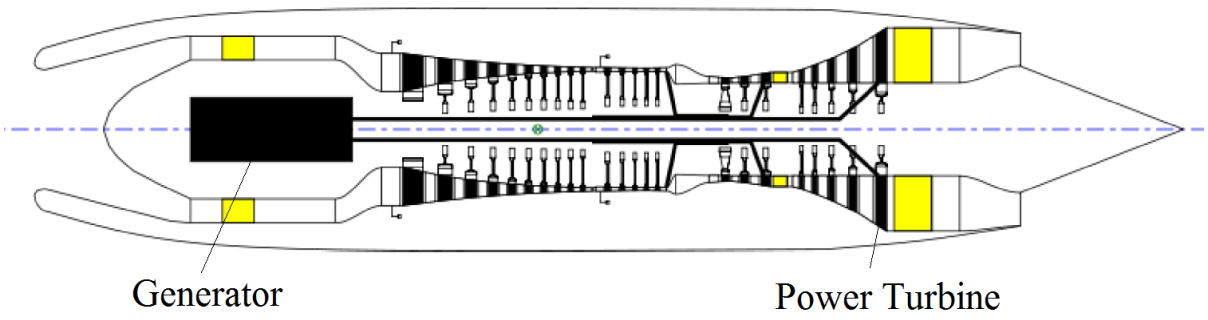

Figure 6.10 NASA's Core-engine Concept

$$Generator\ Efficiency = \frac{Electric\ Power}{Turbine\ Power} = \frac{Electric\ Power}{\dot{m}C_p\Delta T_{power\_turbine}} \quad (6\text{-}27)$$

The performance curve of the generator has no significant difference between the motor. It can be treated in exactly the same way as the motor. So its maximum output power should be at least equal to the sum of the motors maximum output power. Its shaft speed should be chosen to match the optimum speed of the power turbine in the core engine. The speed should high enough to reduce the power turbine weight. The electric drive provides the same advantage as a gear box in a turbofan engine. The ability to control motor and generator speed independently allows the generator to change its shaft load without changing its speed, or to change speed without changing its load.

There are two kinds of core-engine. The first is developed by NASA; the generator is driven by a turboshaft engine, therefore, all the power should be converted to electric power. In this case, the maximum output power of the generator should be obtained at take-off condition and the power turbine exit temperature should be kept as low as possible.

The other concept is the generator driven by a turbojet or turbofan engine, therefore the core-engine produces both the power and thrust. The reason to utilise this concept is to reduce the weight of electric components, including the generator, the motor and the cooling system. In this case, the maximum output power, which equals to the power at DP, of the motors is kept constant at different working points. The generators are not necessary working in a wide range of output power. The result is that the power turbine can operate within a very narrow range of efficiencies near its peak efficiency. For example, at take-off the motor power is the same as DP,

but the core-engine inlet conditions and burner exit temperature are different. This is because the shaft speeds of the motor and the generator are independent; the power turbine shaft speed can be kept the same as design point to maintain the same generator output power. If the turbojet engine was used, this could be achieved by changing the free power turbine pressure ratio. At take-off this leads to higher power turbine exit temperature, the nozzle should be used to transfer the power to thrust. If the turbofan engine was used, this should be achieved by changing the power ratio between the power turbine and the low pressure turbine. More power should go to the turbofan engine fan stage in order to produce more thrust by the core engine at take-off.

6.5 Cooling System Modelling Methodology

There are two cooling methods can be utilized in a TeDP system. The first one is using liquid hydrogen. Liquid hydrogen has a boiling point of 23 K at 2 atm [5]. Boiling it is therefore capable of cooling the electric system. The drawbacks of this method are increased fuel tank size and vapour shock in the fuel injection system. Due to the different thermal behaviour of liquid hydrogen, in this chapter, the system using LH2 was not analysed. The other method is using electrically driven Cryocooler to provide active refrigeration to pump the heat from the superconducting system. The heat should be rejected to the air and thus the sink temperature equals atmospheric temperature. Lower cooling power is required at high flight altitude, so the system should be designed based on take-off conditions, where the motors are fully loaded and the ground temperature is higher.

The method to model its performance is using a cooling power factor (CPF), defined by Eq.6.28, to calculate its power requirement. The factor is assumed change linearly with the motor power and the temperature difference between the atmospheric temperature and superconducting system working temperature. So if the factor at design point equals to 0.02, Eq.6.29 can be used to obtain its value at other flight condition. Fig.6.11 shows the values at different system operating conditions. Its value increases with the increasing of atmospheric temperature and motor power. The cooling power comes from the generator, so the power provides by the generators is the sum of the cooling power and motor power.

$$CPF = \frac{Cooling\ Power}{Total\ Electric\ Power} \tag{6-28}$$

$$CPF = CPF_{DP} \times \frac{Motor\ Power}{Motor\ Power\ @\ DP} \times \frac{t - 73}{t_{DP} - 73} \tag{6-29}$$

where, *t* is the atmospheric temperature; DP is condition at design point

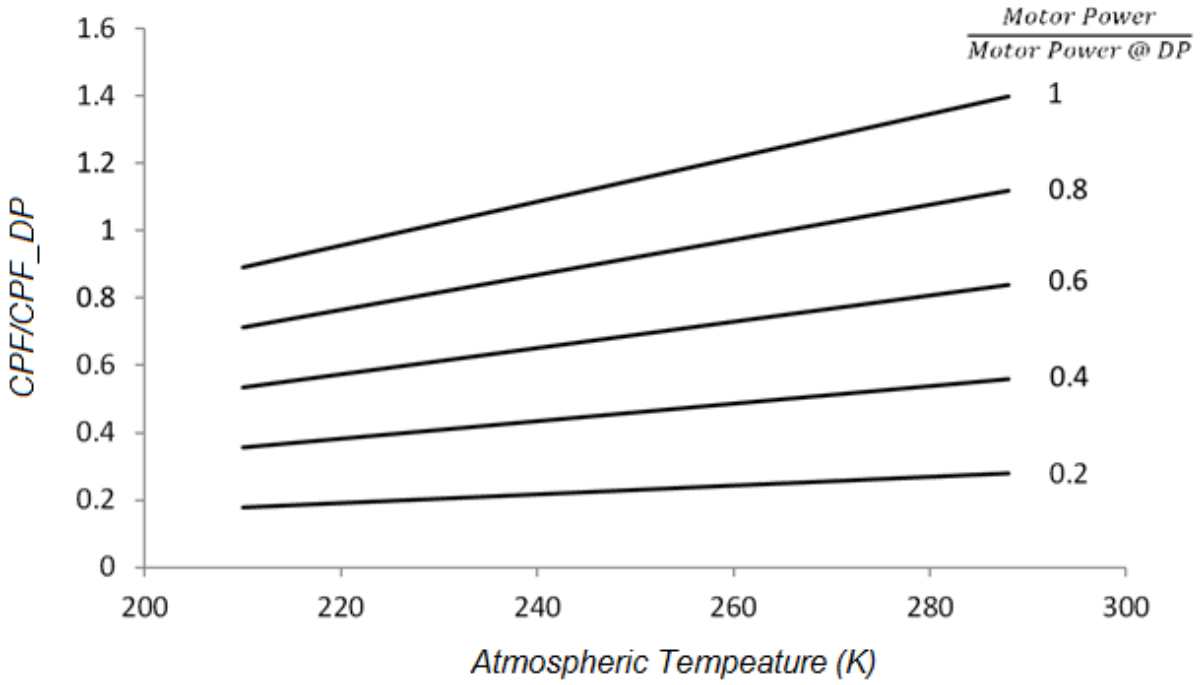

Figure 6.11 Cooling Factor Value at Different Flight Conditions

6.6 Weights of Electric Components

This section discusses the method to estimate the weight of the TeDP system electric components. The components to be discussed are the motors and generators, the cooling system, the superconducting transmission lines to distribute the power, and the inverters to allow the fan motor to change speed independently of the generator shaft speed. Due to lack of information, all the basic weight data are provided by Brown (2013) in the technical meeting between Cranfield and NASA (data also included in reference [5]).

6.6.1 Motor and Generator

There is no significant difference between a superconducting generator and a motor. So they can be treated in exactly the same way. A motor is combined by a rotor, which turns the shaft to deliver the mechanical power; a stator, usually has either wingdings or permanent magnets; and a commutator, which is used to switch the input of certain AC and DC machines consisting of slip ring segments insulated from each other and from the electric motor's shaft. Comparing the stator and rotor, the weight of the commutator can be ignored.

The material used to achieve superconducting is BSCCO (Bismuth strontium calcium copper oxide). It is a family of high temperature superconductors having the generalized chemical formula $\mathrm{Bi_2Sr_2Ca_{n-1}Cu_nO_{2n+4+x}}$. Its current density is a function of magnetic field and operating temperature. The BSCCO operating temperature, in our studied TeDP system, is kept constant. Moreover, the motor torque is quadratically changed with the current; the weight of motor's rotor is linearly changing with the BSCCO current density. In Eq.6.30, the power is the maximum motor output power.

$$W\_rotor \propto \sqrt{((Motor\ Power)/(shaft\ speed))} \tag{6-30}$$

Fig.6.12 shows the map to estimate motor rotator weight. In the map, the x-axis is the non-dimensional weight to power ratio; the y-axis is the non-dimensional power. This map shows how the weight of rotor changes with the motor output power and shaft speed. The weight of stator is assumed to change linearly with the weight of rotor. This means that the ratio of weight of the stator to weight of the rotor is constant. NASA's motor weight data can be used as the default data:

motor:

$$Power_{default} = 5.7\ MW;\ W_{default} = 78.5\ KG;\ \omega_{default} = 5000\ RPM$$

Generator:

$$Power_{default} = 39.2\ MW;\ W_{default} = 912\ KG;\ \omega_{default} = 3600\ RPM$$

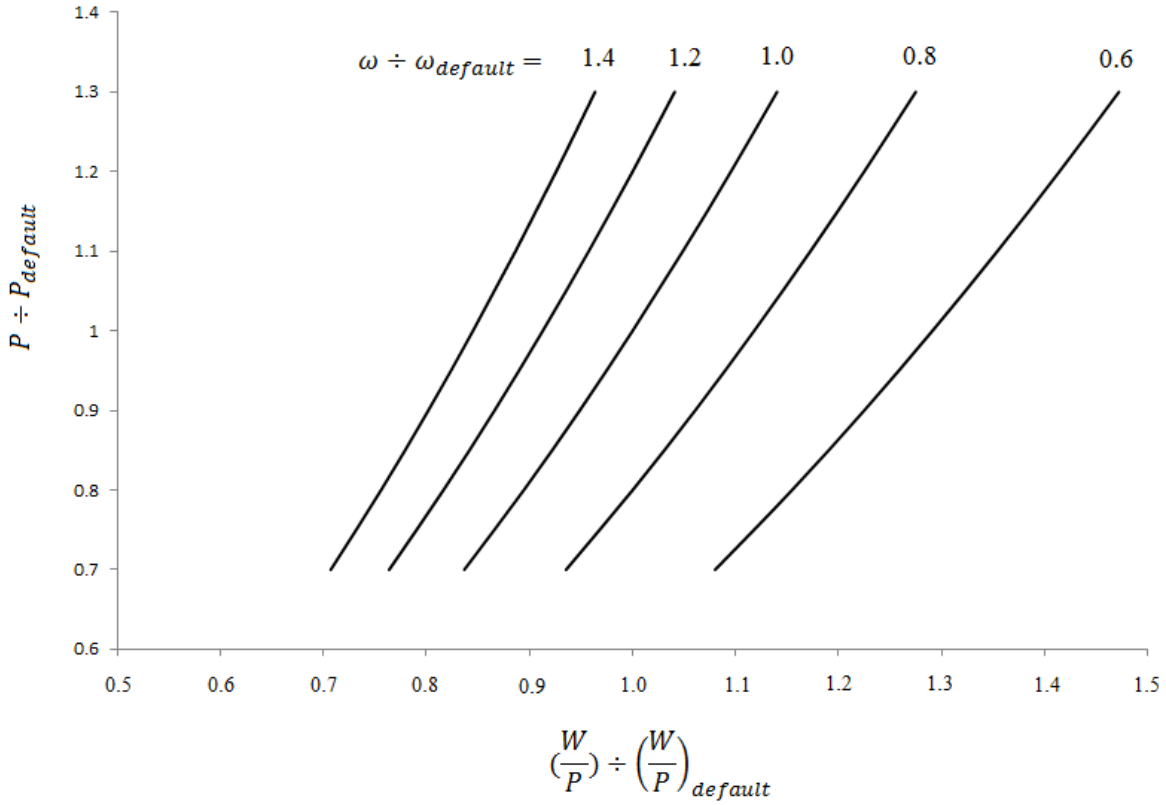

Figure 6.12 Motor Rotor Weight Map

6.6.2 Cryocooler and Inverter

Conventional solid-state switching power invertor is efficient and light. NASA's results show its weight is independent from the motor shaft speed and power. So we can assume the weight of an inverter equals 74.8 KG [5].

$$m_{inverter} = 74.8\ KG$$

The method to estimate cryocooler weight is, firstly, splitting the cooling system into two parts. The first part is used to cool motors and the second part is used to cool generators. Moreover, we assume their weights are linear changing with electric maximum output power.

motor part:

$$m^1 = (number\ of\ motors) \times \frac{Motor\ Power}{Motor\ Power_{default}} \times m^1_{default} \tag{6-31}$$

generator part: (6-32)

$$m^2 = (number\ of\ generators) \times \frac{Generator\ Power}{Generator\ Power_{default}} \times m^2_{default}$$

where, $m^1_{default} = 314\ KG$; $m^2_{default} = 1452.2\ KG$

6.7 Application of Methods to the Turboshaft-driven TeDP System Design for NASA N3-X Aircraft

In this section the turboshaft-driven TeDP systems will be developed and analysed in order to meet the NASA N3-X commercial aircraft plane. The TeDP system is powered by a turboshaft engine. Comparing to the turboshaft-driven core-engine, the turboshaft engine has lower electric system weight, but increases the weight of the core-engine. In this case, the NASA N3-X airplane was used. The TeDP systems have two core-engines. The propulsors unit is put on a common nacelle on the upper rear surface of the airplane. The allowable width is 20 meters, and the minimum propulsor fan hub diameter is 0.3 meters. According to the results in chapter 3, increasing the number of propulsors can reduce the total weight of the propulsors unit. So the propulsor fan (hub-tip-ratio equals 0.3) diameter is 1 meter.

Flat plate airframe upper surface is assumed to obtain the propulsor inlet boundary layer velocity profile. Seventh power low (Eq.5.1 to 5.3), therefore, can be used to describe the profile of the boundary layer. The fuselage length of the propulsors in this section was assumed equal to 35 meters.

6.7.1 Impacts of BLI

The turboshaft driven TeDP system developed in chapter 3 was used. This system has 16 propulsors and 2 core-engines. All the thrust comes from the propulsors unit. In chapter 3, impacts of BLI on the engine off-design performance were not considered. So, firstly, detecting its impacts by the method developed in section 6.2.3. RTO condition was chosen to evaluate impacts of BLI. The reason to choose RTO but not T/O condition is because at T/O the flight speed is equals to zero and

the boundary layer flow ingested by the propulsors is much smaller than the free stream flow. Table 6.1 shows the results.

Table 6.1 Impacts of BLI at RTO

	without BLI	with BLI
Inlet mass flow rate per propulsor (kg/s)	153.5	153.5
PPR	1.231	1.238
Fan polytropic efficiency	0.9473	0.9425
Total Thrust (KN)	288.21	289.83
Fan Power (MW)	2.688	2.583

The boundary layer thickness at RTO is 0.291m (the data obtained with the assumption that the airframe upper surface is flat plate) and the propulsor capture height is 1.51m. So the ratio of ingested boundary layer is 17.7%. BLI causes 1.23% reduction on propulsor pressure ratio and 0.51% reduction on fan efficiency. This leads to lower thrust and fan power. However, the power to thrust ratio increases. This means ingesting boundary layer flow can improve the fuel consumption of the TeDP system with the penalty of reducing the total thrust. Therefore inlet mass flow rate should be increased to ensure enough thrust is produced by the propulsors unit.

6.7.2 Motor Performance

According to the results in chapter 3, at Take-off, the maximum power the motor should provide is 2.693 MW at shaft speed equals 3930 RPM. Fig.6.13 (the black line) is its maximum output power at different shaft speed if the maximum power of the motor is the same at the take-off condition, and Fig.6.14 and Fig.6.15 are the fan maps. In the map, the grey zone is the possible working zone of the fan stage. However, in this case, if the fan shaft speed exceeds 3930 RPM, the motor fails to provide enough power. Therefore, the fan cannot work in the red zone in Fig.6.14.

To cover the red region, the motor should provide 60% more power at rotating speed equals 4704 RPM.

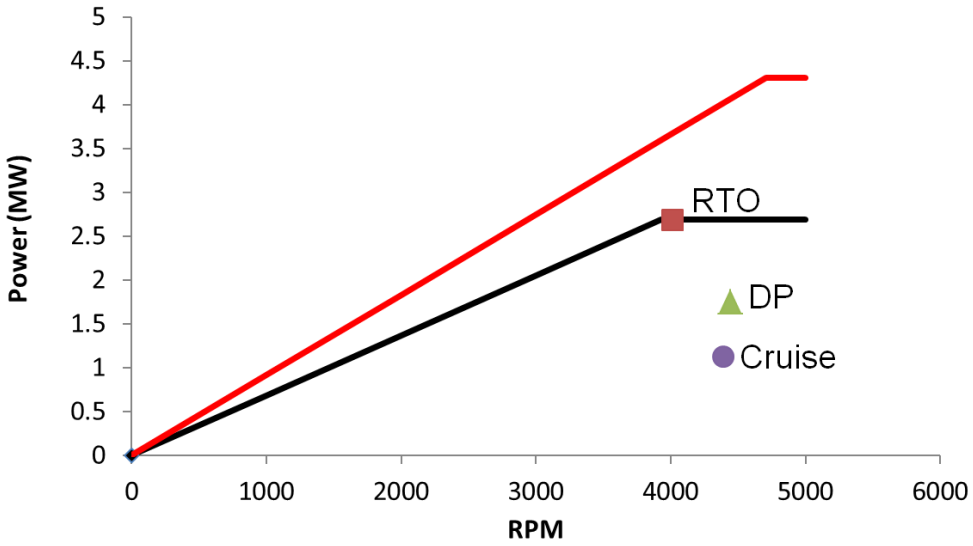

Figure 6.13 Motor Performance Map

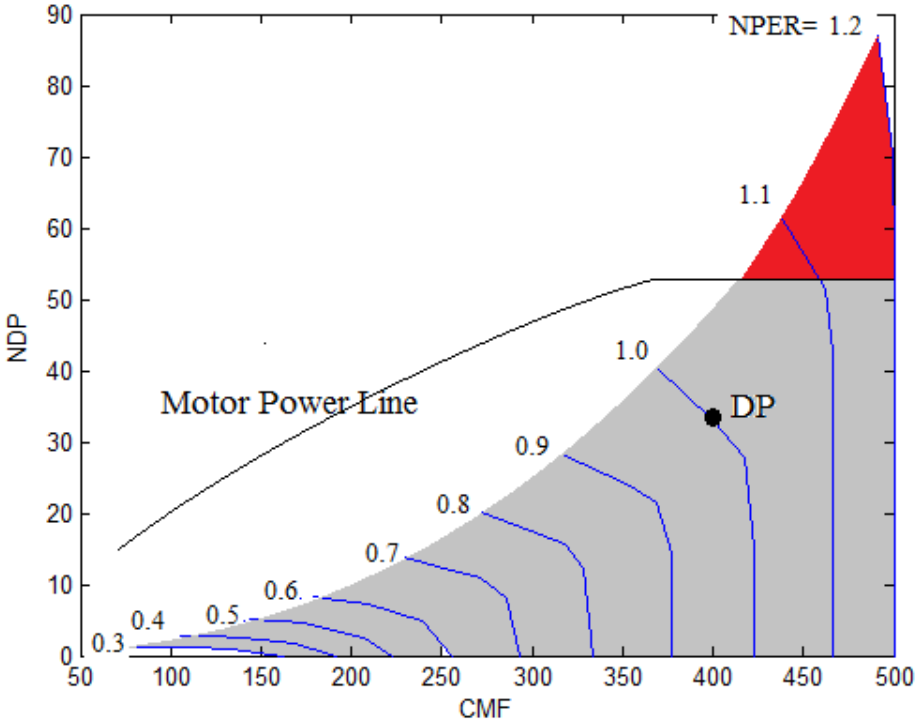

Figure 6.14 Power Based Fan Map for the Propulsor of the Turboshaft-driven TeDP system

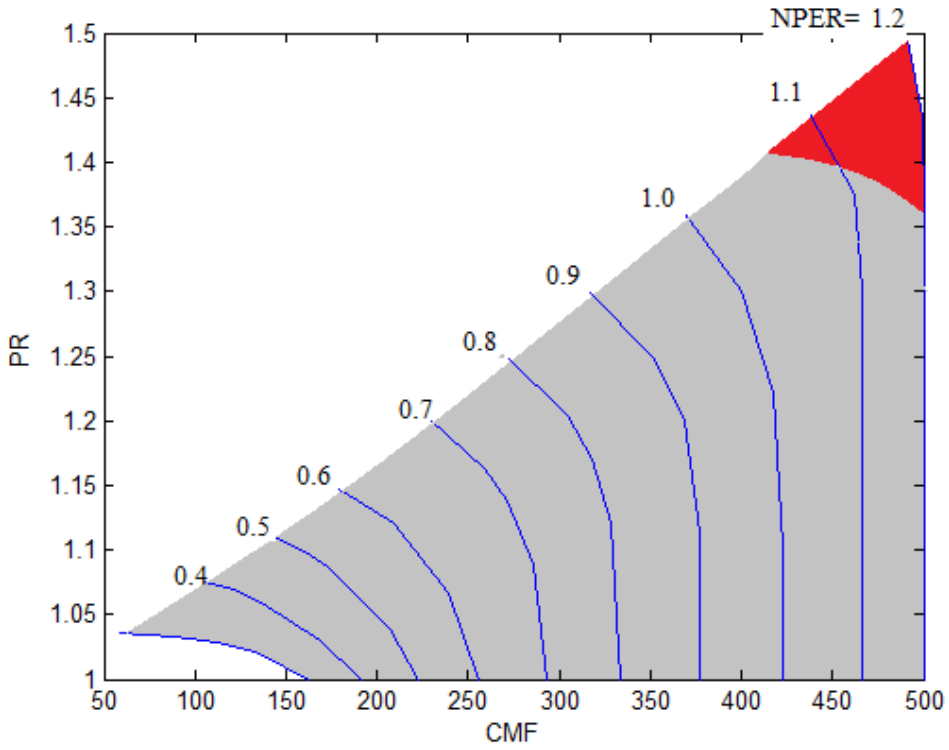

Figure 6.15 PR Based Fan Map

So the motor should have the ability to provide maximum 4.301 MW at 4704 RPM. This data should be used to calculate the motor weight. Its performance curve, therefore, is the red line in Fig.6.13.

6.7.3 Weight of Electric Components

- Motor

The motor has maximum output power is 4.301 MW at 4704 RPM. Based on the data in Fig.6.12, the weight of each motor is 70.3 KG.

- Generator

The generator should have maximum output power around 36.2 MW at 3600 RPM. The weight of each generator is 876.4 KG.

- Inverter

74.8 KG

- Cooling system

The motor part is 237 KG; and the generator part is 1341.2 KG. So its weight is 1578 KG.

The total weight of the electric system equals can be calculated by Eq.6.33.

$$Total\ weigh = number\ of\ propulsors \times (W_{motor} + W_{inverter}) + 2 \times W_{generator} + W_{cooling\ system} = 5652.4\ KG \quad (6\text{-}33)$$

So the total weight of the electric system of the turboshaft-driven TeDP system is 5652.4 KG. This value is obtained based on the model developed in last section. The final value is higher, because there are numbers of devices not included. The final value could be more than 7000 KG. In this model, the weight of the motor and the generator increases with the increasing of their output power. It was developed based on the data for an AC motor without superconducting technology. Superconducting motor, probably, can increase its output power without increasing the weight or increases less than the model predicted weight.

6.8 Application of Methods to the Turbofan-driven TeDP System Design for NASA N3-X Aircraft

In turbofan-driven TeDP system used in this section was developed in chapter 5. This TeDP system has a thrust split ratio of 90% at design point. The propulsors unit has 15 propulsors and their diameter is 1 meter. The motor should provide 2.17 MW (4500 RPM) power at DP. The main reason to utilize this concept is to reduce the weight of the electric system. That is because the motor reaches its maximum output power at DP. If the propulsors failed to produce enough thrust, the core-turbofan engine can produce the rest thrust.

6.8.1 Off Design Performance

Different from the turboshaft-driven TeDP system, the turbofan-driven TeDP system can produce thrust by two parts: the propulsors unit and the core-engine. Fig.6.16 is its maximum output power at different shaft speed, and Fig.6.17 is the power based fan map. Comparing to the turboshaft-driven TeDP system, its working zone is much smaller. However, it is not necessary to increase the motor maximum output power

to increase its working domain. That is because the core-engine can also be used to produce the thrust.

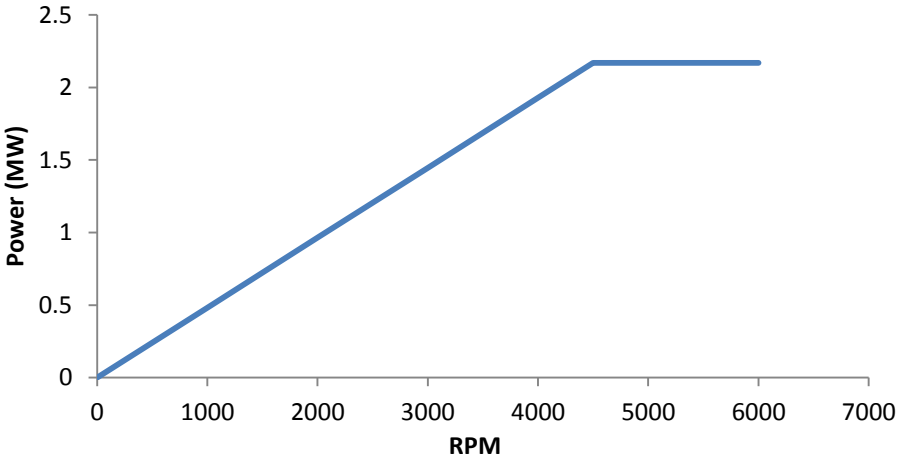

Figure 6.16 Motor Maximum Output Power at Different Rotating Speed

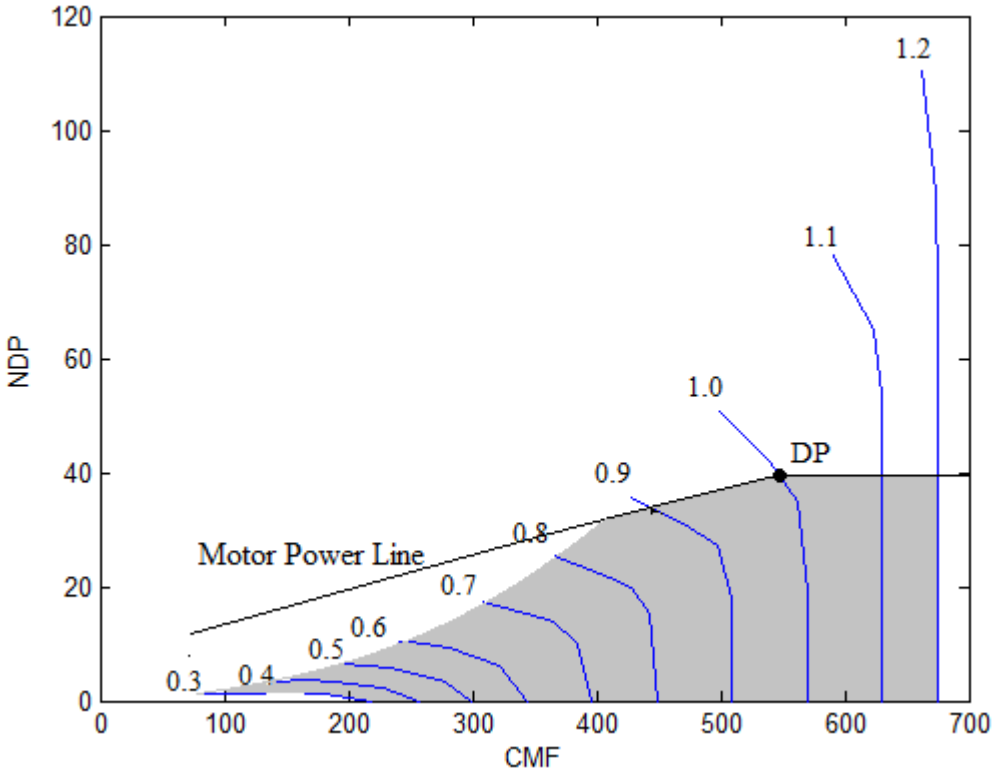

Figure 6.17 Power Based Fan Map for the Propulsor of the Turbofan-driven TeDP system

Table 6.2 list the propulsor performance at RTO.

Table 6. 2 RTO Performances

	without BLI	with BLI
Motor Power (MW)	2.17	2.01
Shaft speed (RPM)	4500	4168
PPR	1.275	1.263
Isentropic efficiency	0.933	0.929
Inlet mass flow rate per propulsor (kg/s)	91.52	91.52
thrust per propulsor (KN)	10.99	10.37
total thrust (KN)	288	288
Thrust split ratio	57.2%	54%

The thrust split ratio drops from 90% at DP to 57.2% at RTO without BLI and 54% with BLI. At T/O the TSR drops to 35.6% without BLI, but at cruise the TSR increases to 98% without BLI and 94.6% with BLI. We also found that the TSFC increases 14% at RTO and 9.3% at RTO comparing to the turboshaft-driven TeDP system. That is because the BPR of the turbofan engine is 1; this leads to lower propulsive efficiency. The RTO and T/O fuel consumption can be reduced by using high bypass ratio turbofan engine. But this is not attractive due to additional weight brings by the core-engine fan stage and nacelle.

The weight of the motor is 51 KG; the weight of the generator is 587.6 KG; the weight of the cooling system is 817.6 KG. Total weight of the electric system is 3504.8 KG. Comparing to the turboshaft-driven TeDP system, weight of electric system reduces around 2000 KG (approximately 35%).

6.9 Discussion

The turboelectric approach requires that a number of new electric components be inserted into the aircraft propulsive drive train between the core-engines and the distributed fans; these include superconducting generator, transmission lines, cooling system, and motors. Performances of each electric component, therefore, are critical to the TeDP system off-design performance. These include the motor performance curve, its maximum output power and shaft speed, its efficiency, as well as the cooling system efficiency.

Weight of the electric components is the other important factors. Because the additional weight brought by using the TeDP concept would largely diminish its benefits. In section 6.5, a simply model to estimate their weight was given. This model developed was based on the assumption that their weight increases with the increasing of the electric power, and the default data were obtained from NASA's results. However, advanced technologies or materials will keep developing; this leads to even higher power density of the electric system. In future studies, this is the major research objective.

Weight of the electric system of a Turbofan-driven TeDP system is approximately 35% (2000 KG) lower than the turboshaft-driven TeDP system. However, the turbofan engine will bring additional weight. If the turbofan-driven TeDP system weight (without out the electric system) is approximately 7000 KG (this is the weight of a turbofan engine, which can produce the same amount of thrust), replacing the turboshaft engine with a turbofan engine (BPR=1) will lead to 10% to 15% increment on the weight. So by using the turbofan-driven TeDP system offers 6-8% (650-750 KG) reduction on total weight. This reduction is relative small comparing to the total weight of the TeDP system. Moreover, if the weight of the superconducting motor, the generator or the inverter is smaller than the predicated value, the turboshaft-driven TeDP system may be lighter than the turbofan-driven TeDP system. In short, if the power density of the superconducting devices were high enough, turboshaft-driven TeDP is preferable to power the N3-X aircraft.

6.10 Conclusion

- Superconducting motor maximum power increases linearly with its rotating speed before reaching the maximum output power.
- The non-dimensional power, NDP is introduced by Eq.6.10, can be used to map the traditional fan map to a power based fan map. This map can be used to match the motor performance and the fan performance.
- The method to model off-design performances of a TeDP system with BLI is to use three (or two) parallel streams to describe the boundary air. One stream for free stream air (if it has), the others for boundary flow. The model further assumed all the streams reach the same static pressure after the fan to obtain the pressure ratio of each streams. It also assumed them mixed well before entering the nozzle. Propulsor Nozzle area needs to be changed to match the inlet mass flow ratio.
- Turbofan-driven TeDP system has the benefit on reducing weight of electric system.
- Two cooling methods, liquid hydrogen or cryocoolers, can be used in a TeDP system. Liquid hydrogen has a boiling point of 23 K at 2 atm [1]. Boiling it is therefore capable of cooling the electric system. The drawbacks of this method are increased fuel tank size and vapour shock in the fuel injection system. The disadvantage of using cryocoolers is the increment of propulsion system weight.
- BSCCO could be used as the superconducting conductor material. Its current density is a function of magnetic field and operation temperature.
- A motor comprises a rotor, a stator, and a commutator. Comparing the stator and rotor, the weight of the commutator can be ignored. The weight of the rotor increases with the increasing of motor power but reduces with the increasing of motor shaft speed. The weight of a stator increases linearly with the weight of the rotor.
- The inverter enables the motor and the generator to operate at any desired shaft speed. Its weight is independent with the motor shaft speed and power. So we

can assume the weight of an inverter is constant, which equals to 49.8 KG in this chapter.

- The method to estimate cryocooler weight is to split the cooling system into two parts: the first one is used to cool motors and the other is used to cool generators. The weight of both parts increases with the increasing of motor and generator maximum output power.
- If using the turboshaft-driven TeDP (introduced in chapter 3) to power the NASA N3-X airplane, the weight of its electric system is approximately 5,000 KG to 7,000 KG; if using the turbofan-driven TeDP (introduced in chapter 5), the weight of its electric system is approximately 4,000 KG to 5,000 KG.
- If the power density of the superconducting devices were high enough, the turboshaft-driven TeDP system should be chosen to power the N3-X aircraft.

Chapter VII

New Propulsor Concepts of Turboelectric Distributed Propulsion System

Turboelectric distributed propulsion system benefits from boundary layer ingestion. However, inlet flow distortion will dramatically eliminate these benefits, especially circumferential distortion. The negative effects come from the non-uniform flow ingested by the rotating fan. This chapter puts forward a novel propulsor conceptual design to solve these problems. The basic idea to eliminate negative effects of distortion is by moving rotor blades with a common rail instead of rotating by a shaft on the airframe surface but vertical to the air flowing direction. That is because differences of the inlet boundary layer profile in the blade moving direction are much smaller than other directions. Moving the blades to compress inlet air in this way can dramatically reduce negative effects of inlet circumferential distortion. Negative effects of radial distortion can be largely eliminated by advanced blade design.

The new propulsor is composed by three major parts: the electric motors, the common rail, and the blades. The blades are positioned on the electric motors-driven rail. The moving blades compress inlet air, which then passes through a stator stage and a common nozzle to produce thrust. The new propulsor can be embedded half of the moving blades (the lower part) into the airframe and ingests boundary layer by one intake duct. This propulsor is suitable for a large blended wing body airplane and it should be put on the upper rear surface of the airframe. Otherwise, the propulsor employs two intake ducts to ingest boundary layer flow from both the upper and lower surface of an airframe. After each duct, there is a stage with moving blades stage that compresses the ingested boundary air. This propulsor can also be used on tube and wing airplanes. In this case, the propulsor can be put at the back of the wings. Through analysis, the new propulsors have the potential to reduce cruise fuel

consumption up to 6%. In the end of the chapter, future research objectives are summarised as well as the technical challenges and risks.

7.1 Problem of Traditional Fan in Ingesting Boundary Layer Flow

The fan or propulsor here refers to the rotating machine, which was used to produce thrust. The fan consists of a rotating arrangement of vanes or blades which act on the air. The blades force the air to move in a parallel way to the shaft around which the blades rotate. The fans in TeDP system are powered by superconducting electric motors. Negative impacts of BLI come from the distorted inlet air, including non-uniform inlet velocity and total pressure. Fig.7.1 illustrates one fan inlet condition with high ratio of BLI. There is around 25% difference in the total pressure. So any high speed rotation blade working under this inlet condition would cause serious problem, such as vibration, efficiency drop, increased noise, and so on.

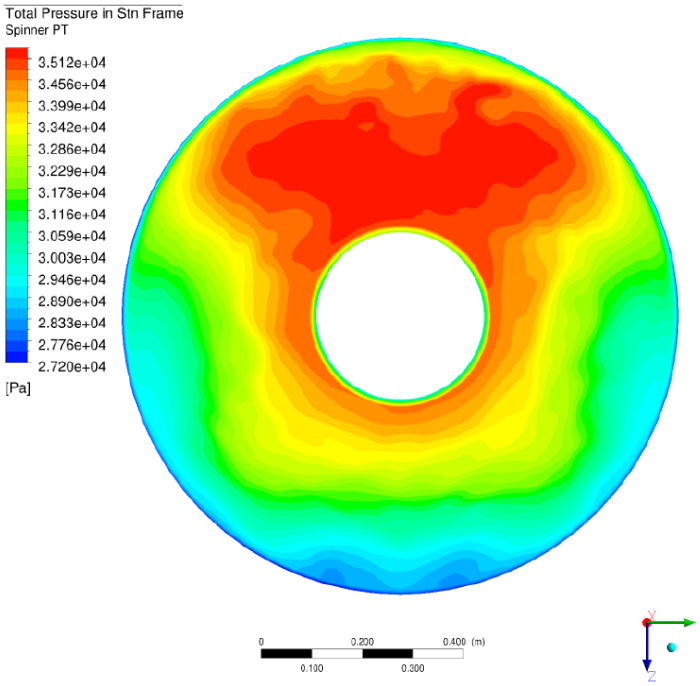

Figure 7.1 Total Pressure Contours [40]

In recent years, inlet pressure distortion and its effect on compressor stability have received much attention [65,66,70]. Great amounts of effort have been expended on distortion testing, correlation of distorted inlet conditions with compressor surge and

evolution of models to predict the reaction of the compressor to distortion. In most cases the distortion is a combination of circumferential and radial gradients, especially of high ratio BLI propulsion system.

Radial distortion is caused by non-uniform flow in the radial direction of the fan blade. Because of radial distortion, two effects occur; the one is the rotating stall at lower values of pressure coefficient and the other effect is the marked decrease of flow coefficient in the region of negative slop indicated by solid points for all stage groups. Negative impacts of radial distortion can be largely eliminated by advanced blade design. However, negative impacts of circumferential distortion, which refers to non-uniformity in the circumferential direction, are difficult to be reduced by changing the blade shape. Parallel compressor theory was widely used to model circumferential distortion. This method considers the circumference of the compressor to be divided into two flow regions: one of the relatively low velocities such as would exit behind a distortion inducing screen and one of relatively high velocity. The compressor performance in each region is assumed to be that obtained from uniform flow operation at the local value of inlet velocity. So no matter how well the fan was designed, the two regions can't work in the highest efficiency at the same time. Overall efficiency reduces with inlet circumferential distortion.

7.2 Design Methodology

7.2.1 Core engine

The core engine, which is used to produce power, is combined by a turbo-engine and a high speed generator. The turbo-engine can be either turbofan engine or turboshaft engine. If we use turboshaft engine, the shaft of the power turbine should be directly connected to the generator. In this case, all the thrust is produced by the propulsors unit. The other concept is to use a turbofan engine with a free power turbine where the power turbine is used to drive the generator. Thrust is produced by both the propulsors unit and the core engine. The benefit of this concept is its potential in reducing the weight of the cooling system. That is because, if all the thrust is produced by the propulsors, extra power is needed for cooling (maintain superconducting) at take-off. This leads to a larger and heavier cooling system.

Moreover, negative impacts of propulsor intake distortion are more serious if all the thrust is produced by the propulsors. However, the turbofan driven core engine has a bigger nacelle, which increases the weight. In this chapter, turbofan driven core engine is used to power the distributed system.

7.2.2 Airframe

The new propulsion system was designed to meet NASA's goals for future aircraft. In 2005, NASA released plans of next generation commercial airplane for 2030, with a cross-disciplinary effort on: reducing fuel consumption, aviation reliability, fundamental noise reduction and shorter take-off length. Comparing to the aviation with same capacity and cruise distance, the new aircraft with TeDP system should reduce at least 75% NOx emissions, 70% fuel burn, 55 dB noise and 50% take-off field length. The goals of noise reduction and shorter field length should be achieved by new aircraft designs together with the TeDP system. The conceptual aircraft design chooses a blended-wing-body type airframe. Fig.7.2 illustrates these aircrafts.

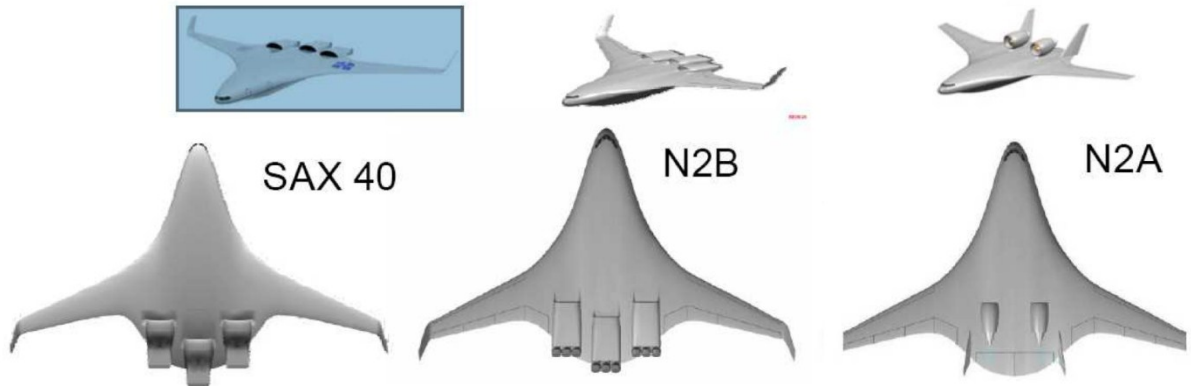

Figure 7.2 The CMI SAX40 and Boeing/NASA N2A and N2B Hybrid wing body Aircraft Concepts [17]

The benefits of the BWB airframe are the high lift-drag coefficient, which can dramatically reduce the field length, the potential on noise reduction by achieving full laminar flow at cruise and more, and the enabling of embedded engines. To utilise TeDP system, NASA gave their BWB airframe design: N3-X hybrid wing body airframe. The propulsors unit was put on the rear surface of the airframe with a common nacelle in order to ingest as much boundary layer flow as possible. In the thesis the N3-X is used.

7.2.3 Propulsors

Circumferential distortion happens with two prerequisites. The first one is un-uniform inlet flow. Because the propulsors need to ingest boundary layer to improve propulsive efficiency, it is difficult to change the inlet to make it becomes uniform flow. The other is the rotational machine itself. Because the rotating blades ingest un-uniform inlet flow, circumferential distortion must happen. To solve this problem, our method is replacing the rotating blades with rectilinearly-moving blades.

Boundary layer is the layer of fluid in the immediate vicinity of a bounding surface where the effects of viscosity are significant. Propulsors are put on the rear surface of an airframe. So if the blades are moving linearly and vertical to the flow direction, there is no big difference at different positions. Fig.7.3 shows this concept. The blades, instead of rotating, are moving through a common rail driven by two electric motors.

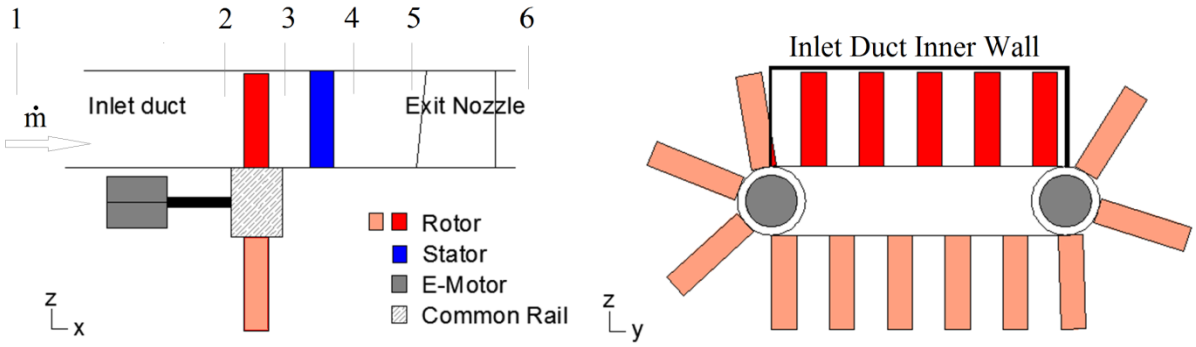

Figure 7.3 Propulsor Concept with Half Rotors Embedded into the Airframe

Six major parts combine the propulsor: the inlet duct, the rotor stage, the stator stage, the common rail, the electric motor and the exit nozzle. The common rail is driven by the two E-motors, which moves the rotor to compress the inlet air. The duct should be designed to reduce the distortion in y-direction. S-shape duct should be used to reduce airframe friction. As we can see in Fig.7.3, only the dark red blades of the rotor are under pressure and the propulsor unit must be embedded into the airframe to reduce its frontal area. So an S-duct can guide the inlet boundary flow, which comes from upper surface of the airframe, into the embedded propulsor. The rotor stage moves with the common rail. Half of the blades compress the inlet air and the other half of the blades are embedded into the airframe. One stator stage is installed after the rotor. The stator is needed only after the pressure stator blades

(dark red blades in Fig.7.3). The exit nozzle is used to accelerate exit the high pressure air in order to produce thrust.

Fig.7.4 illustrates the other installation concept. it has two separate inlet ducts: one ingests boundary flow from the upper surface of the airframe while the other one ingests boundary flow from the lower surface of the airframe. Both ducts can be either straight or S-shape, depending on its position, airframe design, and more factors. After the compression, both flows mix (at position 5 in Fig.7.4) before entering the nozzle. This concept needs to be embedded into the airframe so it should be put at the back of (inside and at the rear of) the airframe. However, because the second configuration needs to ingest boundary layer from both upper and lower airframe surface, it should be put in the back of (behind) the airframe.

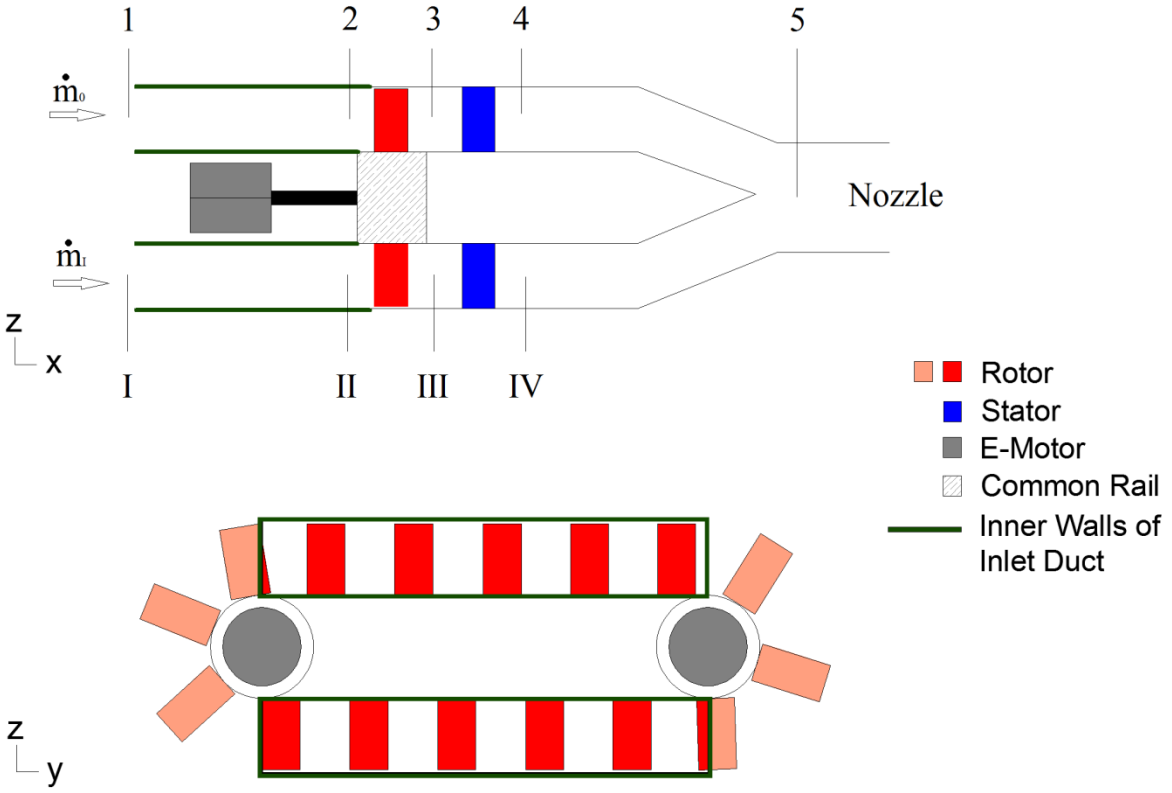

Figure 7.4 Propulsor Concept with two Intake Ducts

The design parameters need to be considered include the number of blades and its height, as well as the width of the propulsor (the distance between the axis of driven E-motors). To decide the blade height, not only the blade aerodynamic behaviour should be considered, but also the boundary layer ingestion. Because increasing the blade's height, more ratio of boundary flow can be ingested. For example, to ingest

the same amount of air, the propulsor can be designed longer but with lower blade height. This design can increase the ingestion of boundary layer to improve overall propulsive efficiency. The number of blades should be considered together with the propulsor width.

7.2.4 Design Methodology

Fig.7.5 illustrates the design methodology, which contains two parts: the airframe design part and the engine design part. In this thesis, the N3+X airframe was used and the new propulsors unit were put on the upper rear surface of the airframe, where NASA used to place 15 distributed fans. However, the design of the inlet duct of the propulsors should be considered because of inlet distortion. The goals check in Fig.7.5 (b) refers to check whether the new propulsor can reduce the negative impacts of inlet distortion. Fig.7.5 (a) shows the overall design flow procedure. The airframe design targets include airframe noise, aerodynamic behaviour, space, and etc[67,71]. Airframe design provides basic design parameters for engine design including engine size, its performance requirements, propulsor intake designing, etc. Overall engine design should guarantee that fuel burn, emissions and engine noise satisfy the targets. It is difficult to separate engine design from airframe design because of the highly integrated engine and airframe configuration. Major targets of Engine Performance Calculation are to find the fuel consumption and emissions at different working conditions. If the system failed to achieve the goals, the system should be redesigned. The final step is to check the overall airplane noise level. If failed, noise reduction technologies should be used firstly without changing the air foil or the propulsion system. Otherwise, the air foil and propulsion system should be redesigned in order to reduce noise.

The performance analysis in Fig.7.5 (b) includes the optimisation of the propulsor rotor pressure ratio, the number of propulsors as well as their position. In this case, a new design parameter, the propulsor quantity, is introduced. This is because in order to produce the same level of thrust with the same propulsor pressure ratio and inlet mass flow, the number of propulsors can either be low with large blades or high but with smaller blades. More detailed analyses should be carried out to figure out the benefits and drawbacks of increasing the number of propulsors. For example, by increasing the propulsor quantity, more boundary layer flow can be ingested.

However, more electric motors should be used, which increase total system weight. In short, the number of propulsors should be optimised.

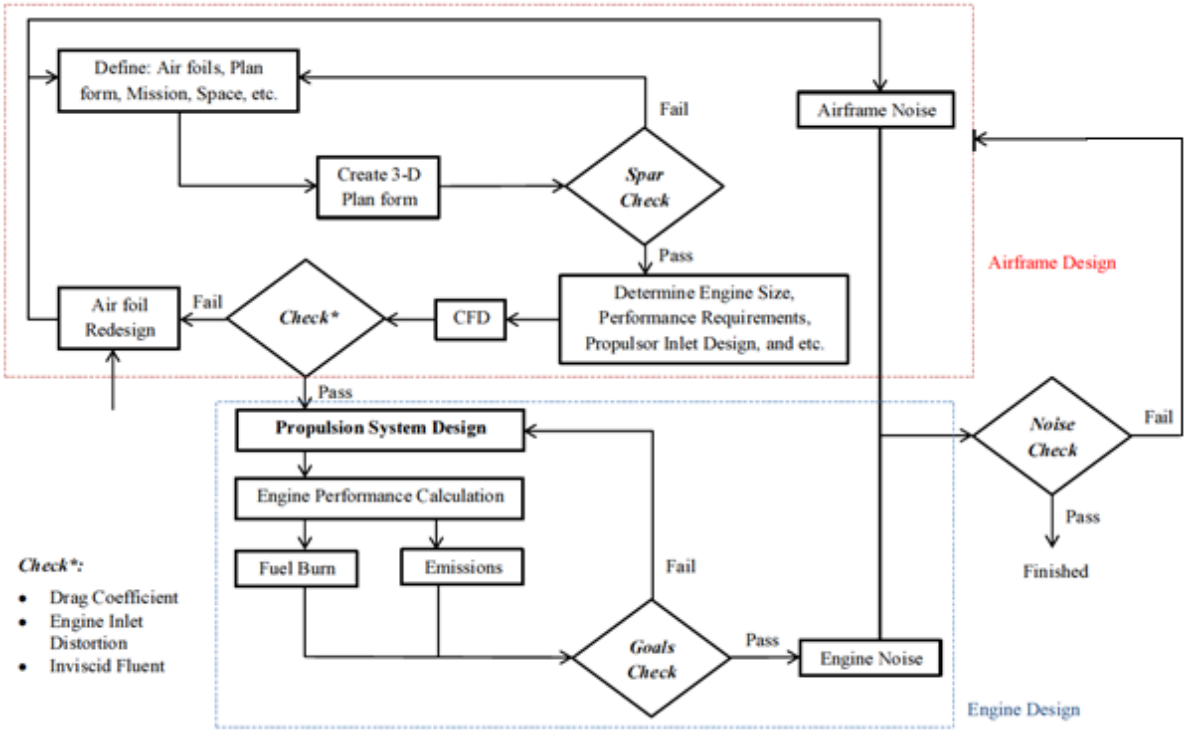

(a) Overall Flow Chart

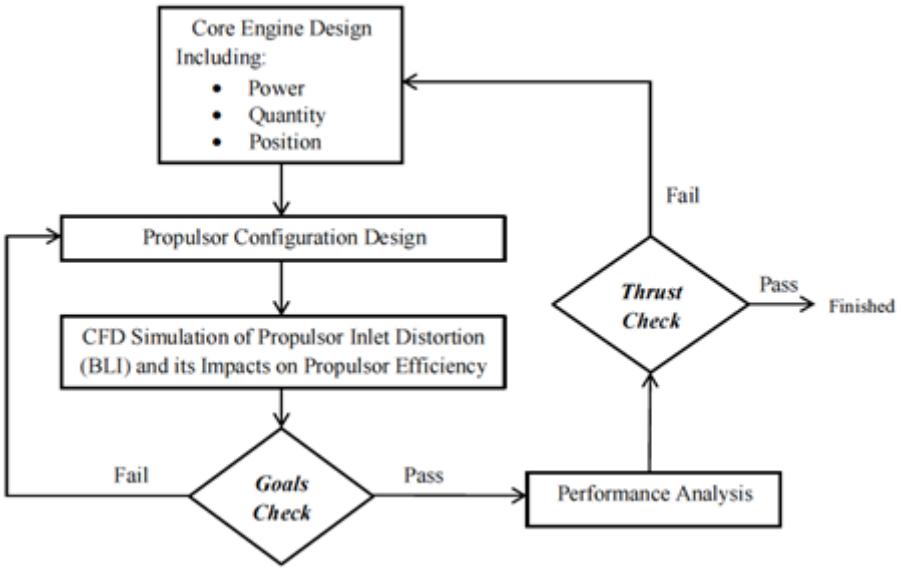

(b) Flow Chart of 'Propulsion System Design'

Figure 7.5 Suggest Design Methodology

7.3 Propulsor-Airframe Integration

Different from podded engine configuration, concepts like the HWB with TeDP system, where the engine inlets and airframe are closely coupled, will make it very difficult to analyse components isolated from one other. The highly integrated inlet and airframe of such concepts could have significant impact on the propulsion system performance. In order to reduce the drag of pylons, HWB will allow the boundary layer developed forward of the engine face to be ingested by the inlet. Thermal cycle analysis showed its benefits on fuel consumption. The other issue of PAI is the significant impacts on engine noise. N+3 highlighted a strict noise reduction goal for future aircrafts. For example, the position of the engine, the inlet duct, the jet exhaust plume and the number of propulsors must be analysed in order to reduce the noise as much as possible. In this section, only the way to install propulsors into an airframe is described, other important issues should be analysed in future.

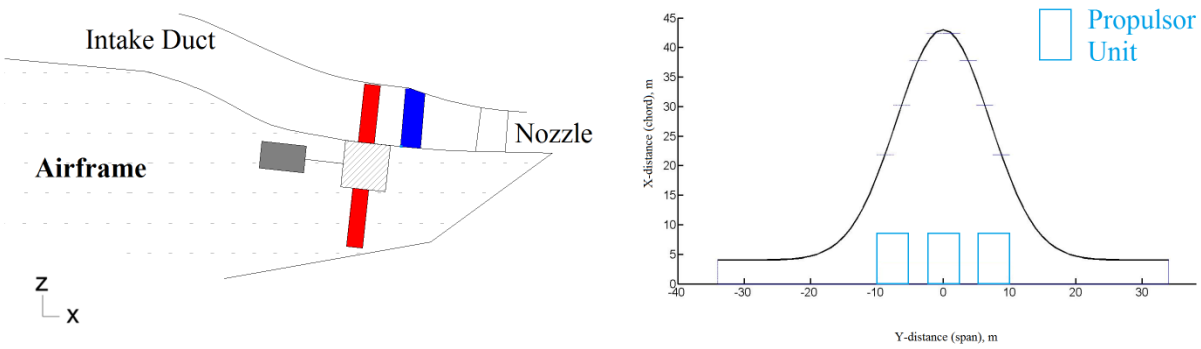

(a)

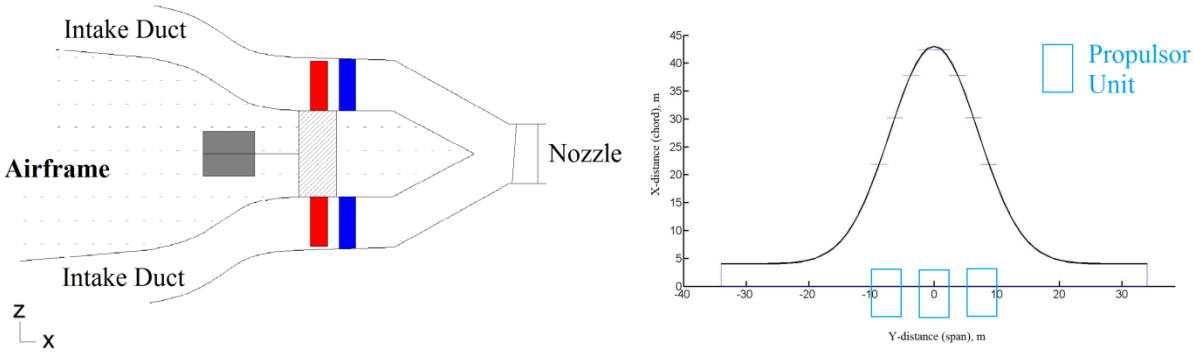

(b)

Figure 7.6 A HWB Airframe with the New Propulsor

In Fig.7.6 (b) the new propulsor should be put at the rail of the aircraft because the propulsor ingests streams from both upper and lower surface of the airframe and mixes them before entering the common nozzle. The shape of the inlet ducts is determined by the airframe. This kind of propulsor can also be used in tube-wing aircraft as Fig.7.7 shows. Turboshaft-driven core engine is more suitable for this application. This is because may be the size of the turbofan-driven core engine is too big to put under the wing.

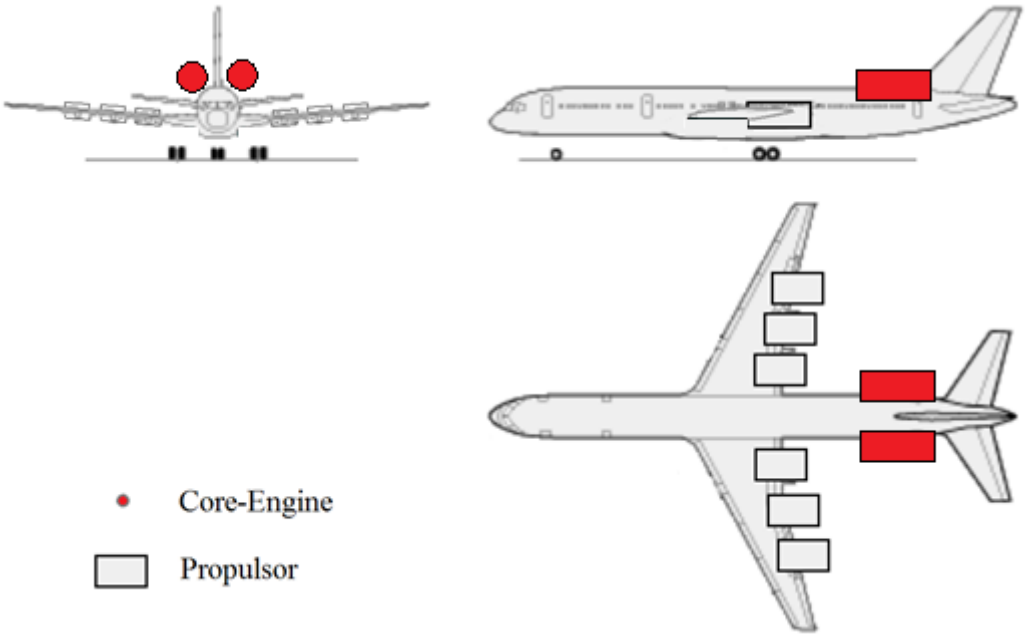

Figure 7.7 Tube-and-Wing airplane with the New Propulsor

7.4 New Propulsor Fuel Saving Potential Estimation

This part estimates the fuel saving potential of the new propulsors. The airplane used in this section is designed to carry a 53,570 kg payload 12200m at Mach 0.84.

A design fan pressure ratio of 1.3 with 15 fans and two turbogenerators was selected to explore a detailed thermal cycle performance of the traditional TeDP system. The method to model the impacts of BLI on the traditional TeDP system is by modelling the impacts of circumferential and radial distortion separately. Parallel compressor method is used to model the impacts of circumferential distortion and parallel stream

method is used to model the impacts of radial distortion. To address the benefits of BLI, a new parameter, fuel saving coefficient (Φ), is introduced as follow:

$$\Phi = \frac{TSFC_{no\ BLI} - TSFC}{TSFC_{no\ BLI}} \times 100\% \tag{7-1}$$

Φ gives us the amount of fuel that can be saved with BLI in order to produce the same amount of thrust at cruise. For example, if Φ equals 10% means that BLI offers 10% fuel reduction on cruise. The method to estimate fuel saving potential of the new propulsors is to find the negative impacts of both circumferential and radial distortion on the traditional propulsor. The new propulsors are designed to eliminate negative impacts of inlet distortion. So with well-designed propulsors the negative impacts of inlet distortion can be reduced as much as possible. Fig.7.8 shows the results. In the figure, NASA's method was used for the no distortion case; the parallel compressor method was used for the circumferential distortion case; the parallel stream method was used for the radial distortion case.

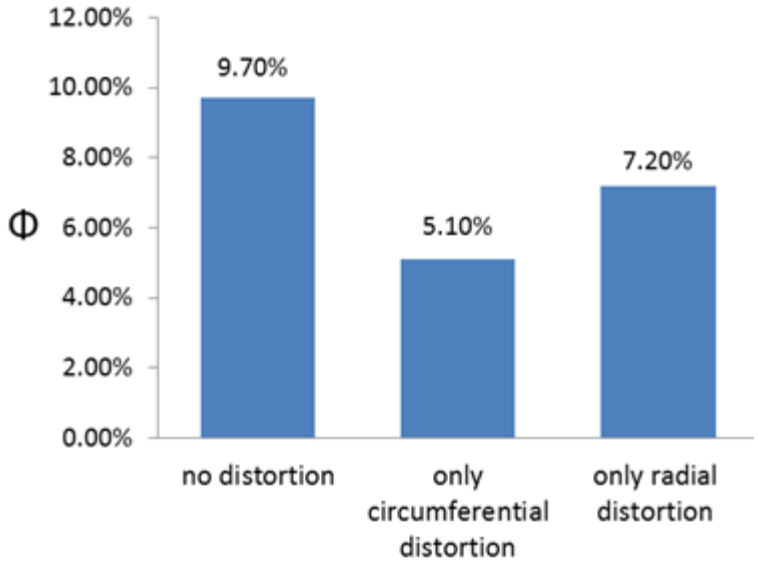

Figure 7.8 Fuel Saving Coefficient at different cases

BLI offers around 10% fuel reduction without considering negative impacts of inlet distortion. However, inlet distortion will reduce the benefit to 2.6%. In other words, 6.1% of BLI benefit on fuel saving is eliminated due to inlet distortion assuming everything else constant. So with careful design of the new propulsor, including intake duct design, blades design, and more parameters, BLI can improve fuel consumption up to 6%.

7.5 Advantages of the New TeDP System

Although a distributed propulsion system with a small number of core-engines driving numbers of propulsors could be applied to other vehicles, the concept is perhaps most suited to blended-wing-body aircraft. Nevertheless, the following possible advantages are identified:

- High fuel efficiency due to high effective engine bypass ratio. Effective bypass ratio is defined as the ratio of mass flow through all propulsors to mass flow through the core-engines.
- Improved propulsive efficiency due to BLI
- Decoupling of the propulsors from the power producing device. The turbine-driven generators (the core-engine) and the motor-driven propulsors can be located separately at the optimum locations. This can improve total airplane performance and operation.
- The speed of the power turbine shaft in the core engine is independent of the propulsor blades moving speed. The electric transmission system acts as a gearbox with an arbitrary gear ratio with an ultra-high efficiency. So this allows to optimise the shaft speed of the core turbine without considering the usual fan tip speed limitation
- Lower power losses because of using superconducting electric devices.
- The potential to reduce core-engine jet noise. This is because the generator extracts the maximum amount of energy to produce power instead of producing thrust, which leads to low exit velocity and temperature and thus reduces noise. Moreover, if the core engine noise is still too high, the position on an airframe can change without changing the propulsors location.
- Reduction of propulsor jet noise. This is because exhaust air of the propulsor has much lower temperature than the core engine. Separating the core engine and propulsors also enable lower temperature material be used for the propulsor nozzles.
- It allows propulsor power to be produced by devices other than a turbine. This improves overall system reliability. Because if the core engine failed, power to drive propulsors can come from other emergency devices, such as batteries.
- Concentrated power generator enables using of large, more efficiency turbo-machinery.
- Improved reliability working with high ratio of ingested boundary layer.
- Reduced airplane drag by ingesting the boundary layer.

However, using a TeDP system may also present some negative effects. The following possible drawbacks are identified:

- Higher weight. The generators, motors, conducting system, and cooling system add additional weight.
- Cooling problem. Low operating temperature (less than 100k) is needed to maintain superconducting. So a large amount of energy will be wasted to cool the electric system.
- High system complexity.
- Propulsor rotor blades air leakage. This is because same parts of the rotor stage are embedded into the airframe, which are not compressing the inlet air. So there is air leakage from the bypass duct to the airframe.

7.6 The Road Forward: Technical Challenges and Risks

NASA's N+3 goals require significant fuel burn benefits to be gained from applying ultra-high bypass ratio TeDP system, as well as BLI to all-lifting wing airframe. To achieve these benefits, the performance of the airframe, installation and propulsion system are all critically important. Furthermore, with boundary layer ingestion there is coupling between the airframe, installation and propulsion systems at all operating conditions of the engine and aircraft. There are also new mechanical, aerodynamic stability and acoustic issues, which should be considered during the conceptual, design process.

The work in this thesis puts forward a new conceptual design of TeDP system propulsor unit. Different from the rotating fan, the rotor blades are moving linearly in a common rail driven by E-motors. This conceptual design can significantly reduce the negative impacts of circumferential distortion. Meanwhile, a number of challenges must be faced to achieve the performance of these new propulsion systems. In this section, the areas that need attention to mitigate the risks presented by the challenges are described, as well as future research objectives and methodologies.

7.6.1 Engine Preliminary Design

The major issue concerning the engine preliminary design of an engine operating with boundary layer ingestion is the non-uniform flow compared to a podded engine.

Besides that, the distributed propulsors conceptual design brings another challenge; the number of propulsor units and core-engines that should be used. Furthermore, the mass flow rate of ingested boundary layer is associated with the propulsor capture height; in other words, the number of propulsors strongly impacts the propulsor intake conditions. These conditions not only include inlet mass flow rate but also the inlet total pressure and temperature as well as the propulsor efficiency. So the major design factors that should be considered include:

1. The number of Core-Engine
2. Core-Engine design parameters
3. The number of Propulsor Unit
4. Propulsor design parameters
5. Propulsor intake capture height
6. BLI conditions

7.6.2 Engine Off-design Operation

To minimise fuel consumption, the design of the boundary layer ingesting system has been targeted at cruise conditions. However, at off-design conditions, there is a different flow and thus leads to new flow field at propulsor inlet. This new inlet conditions bring total different inlet distortion, which directly impacts the performance of the new propulsors. Particular off-design conditions should be examined:

1. Take-off conditions
2. Top of climb conditions
3. Aircraft performance following numbers of propulsor unit failure, as well as a single core-engine failure
4. Rain and hail ingestion

7.6.3 Airframe Engine Integration

The highly integrated inlet and airframe of such concepts could have significant impact on the propulsion system performance. One of the major issues that should be considered is the intake duct design, which directly impacts the benefits of BLI. The propulsor mechanical integration is another complex design work. Its nacelle is a relatively small place where all demands of aircraft itself, power units and systems inner and outer aerodynamic, stress, weight, maintenance, controls, heat management, fuel system and electric power system meet together. Designers must find out the best trade-off among all these requirements. Typically, it is done by

means of iterative processes when all necessary information are collected, detailed, evaluated (trade-off) and finally processed into the power unit installation. In summary, the major research objectives include:

1. Development of design methodology for engine mechanical integration
2. Novel configuration with the propulsor on the airframe
3. Reliable design technology for aerodynamic engine/airframe integration
    a. Configuration impact on propulsion performances
    b. Innovative technologies and aerodynamic design methodology for air inlet and internal nacelle duct
    c. Aerodynamic design methodology of nacelle external shape
4. Engine and nacelle aero elastic integration

7.6.4 Components Performance Matching

Components performance matching here refers to performance matching of the mechanical system and the electric system. The propulsor rotor stages are driven by electric motors instead of turbines. So, performance of E-motors directly impacts propulsors, especially at off-design working conditions. The other research objective is the cooling system and its impacts on the overall system performance. Superconducting technology is used to transmit power from the core engine to numbers of propulsors. To achieve superconducting, refrigerating system is need to maintain low temperature, especially at take-off. This brings a new challenge of TeDP system design.

Although there are numbers of technical challenges, the use of the novel propulsors for TeDP systems appears to offer an opportunity for achieving substantial reduction in negative effects of inlet distortion, and thus improve fuel efficiency.

Chapter VIII

Conclusions and Future Work

Methods to design the TeDP system and to analyse its performances with BLI have been developed and tested. It includes the method to design the propulsors unit, the method to evaluate performances of both propulsors and core-engines; the method to modelling boundary layer ingesting and its impacts on engine performance; TeDP system design point and off-design analysis and electric components modelling methodology. The advantage is their applicability to boundary layer ingesting inlets and motor-driven propulsors. The methods have been applied to both the turboshaft-driven TeDP system and the turbofan-driven TeDP system. By comparing the performance and weight of these two types of TeDP system, some of the advantage and disadvantage of using them to power NASA N+3 Airplane have been identified. In addition to these, three novel propulsor concepts for TeDP system were introduced to eliminate negative effects of BLI. This chapter, firstly, summarises the work accomplished during the course of the research for this dissertation. Observations and conclusions based on the results of this work are also presented. Finally, recommendations for future works are given.

8.1 Conclusions

The objectives of this thesis include three main parts: the first objective has been to design a TeDP system for NASA N+3 Airplane, as well as to use existing tools to model its performances; the second objective is to evaluate impacts of ingesting boundary layer; the third one is to model the electric components and to estimate their weight.

8.1.1 TeDP System Design Method

The first step to design a TeDP system is to determine the number of core-engines (turbogenerators) and propulsors. Turbogenerator was used to produce power to drive fans, so for a maximum allowed TET, OPR and mass flow ratio, its shaft work can be calculated, and therefore, the number can be determined. To power the NASA N3-X Aircraft, two core-engines should be used. The number of fans or propulsors was influenced by many other factors, which both come from engine design and airframe design. We found that the total weight and fan diameter of the propulsors array reduce with the increasing number of propulsors for a constant propulsor fan pressure ratio. This also leads to increased propulsor array total inlet width. So to satisfy the minimum fan diameter and maximum inlet width limitation, the number of propulsors should be chosen as high as possible.

Propulsor fan pressure ratio is another vital design parameter. There is no simple answer for how to choose it. The value depends on the number of propulsors, the thrust requirements, and many others. Results show that the maximum shaft speed of PPR above 1.5 is too high and makes the direct electric motor drive impossible. On the other hand, PPR bellows 1.2 makes the fan fail to recover the intake pressure losses due to BLI. So the propulsor fan pressure ratio should be in the range of 1.2 to 1.5, and the value should be chosen as low as possible to improve the propulsive efficiency.

8.1.2 Boundary Layer Ingestion

Ingesting boundary layer by propulsors improves the propulsive efficiency. The benefit comes from re-energizing the aircraft wake, which enables less kinetic energy to be wasted. An optimistic estimation of direct ingesting boundary layer by the TeDP system on the NASA N3-X Aircraft offers 7-8% fuel burn saving relative to today's aircraft. However, these BLI benefits are very sensitive to inlet distortion. The method developed in chapter 4 found that, comparing to NASA's results, intake distortion due BLI causes 1.1% total pressure losses and 0.9% fan efficiency penalty at propulsor fan pressure ratio equals to 1.3. These makes the BLI offers less than 4% fuel burn saving. So without advanced intake flow control methods, ingesting boundary layer to reduce fuel consumption by 8% is a challenge.

8.1.3 Electric Components

The turboelectric approach requires that a number of new electric components be inserted into the aircraft propulsive drive train between the core-engines and the distributed fans. These components include superconducting generator, transmission lines, cooling system, inverters and motors. Their performances are critical to achieve the distributed propulsion concept. Traditional electric motor or generator fails to power the system, due to their low power to weight ratio. Superconducting technology must be used to achieve ultra-high power density and ultra-low power losses; therefore advanced cooling system is needed to maintain the low working temperature. This brings additional weight comparing to turbofan engines. Results showed the total weight of the electric components for a turboshaft-driven TeDP system would be around 5,000 KG to 8,000 KG. The final value is dependent on the number of propulsors, fuel type, cooling method, as well as the power of turbogenerator. On the overall design and performance, it is true that in the case of large mass penalties the benefits of superconducting distributed propulsion system would be largely diminished.

8.1.4 Turboshaft-driven and Turbofan-driven TeDP Systems

Two TeDP system concepts were developed in this thesis. The firstly is called turboshaft-driven TeDP system. Its core-engine only produce power and the propulsors array produce the thrust. This TeDP system has the lowest core-engine weight. However, its performance is sensitive to propulsor intake duct. Its weight of the electric system is the highest, especially the weight of the cooling system.

The turbofan-driven TeDP system has a turbofan driven turbogenerator. Its thrust comes from both the core-engines and the propulsors array. At cruise, more than 90% of thrust should be produced by the propulsors array; but at take-off, around 40-50% of thrust comes from the core-engines. This concept can reduce the weight of the electric components, especially the cooling system. Its drawbacks include structure complexity, higher core-engine weight, and higher fuel consumption during the take-off process.

So, if the future superconducting and cooling technologies are advanced enough, turboshaft-driven TeDP system should be chosen to power the N3-X aircraft. Otherwise, turbofan-drive

n TeDP system with low bypass ratio turbofan engine should be used.

8.2 Recommendations for Future Work

The thesis explained general methods to model a TeDP system on the NASA N3-X aircraft with BLI. These include the design point analysis, the off-design analysis, the BLI modeling, and etc. But this is only the first step of the project. Following comments give recommendations for the road forward.

8.2.1 Propulsor Intake Design with BLI

Embedded propulsors into the airframe enable the ingesting of boundary layer. Therefore, the propulsor intake interfaces directly with the internal airflow and the flow around the aircraft. This is why propulsor intake performance is so important in designing the TeDP system. The primary purpose of an inlet is to bring sufficient air to the engine or propulsor with minimum total pressure losses.[3] Its design parameters include the pressure recovery factor, propulsor location, exit distortion level requirement, noise requirements, and flow field interaction with the nacelle and airframe. The first stage of work has been done with Loic Flouriot [76]. We found S-duct used in BLI system benefit from reduced drag, size and weight. It also allows reduced ram drag and thus reduced inlet flow momentum. These advantages are closely related to inlet pressure recovery and acceptable level of engine inlet distortion level.

Main S-duct design parameters are the duct inlet area, outlet area, propulsor fan diameter, lip geometry, bended curvature radius, and the function of the duct center line [73]. Fig.8.1 shows the process of the design method. In the process, to create the 3D model by CATIA (A 3D CAD design software, Ref.80), the S-duct center line function should be defined firstly, and followed by cross sections though the center line (Fig.8.2). Fig.8.3 shows the structure of the S-duct. The duct has inlet height of 550 mm, and exit diameter of 1100 mm. Results shown the pressure recovery factor

is 0.92, which is much lower than what we expected. The low value comes from the impacts of boundary layer, and also comes from the chosen of the S-duct center line function, cross sections, as well as the lip geometry. So, future works should start from re-design the shape of the S-duct. It includes: re-define the center line function, re-design the duct lip geometry and re-design the cross-sections at different positions of the duct.

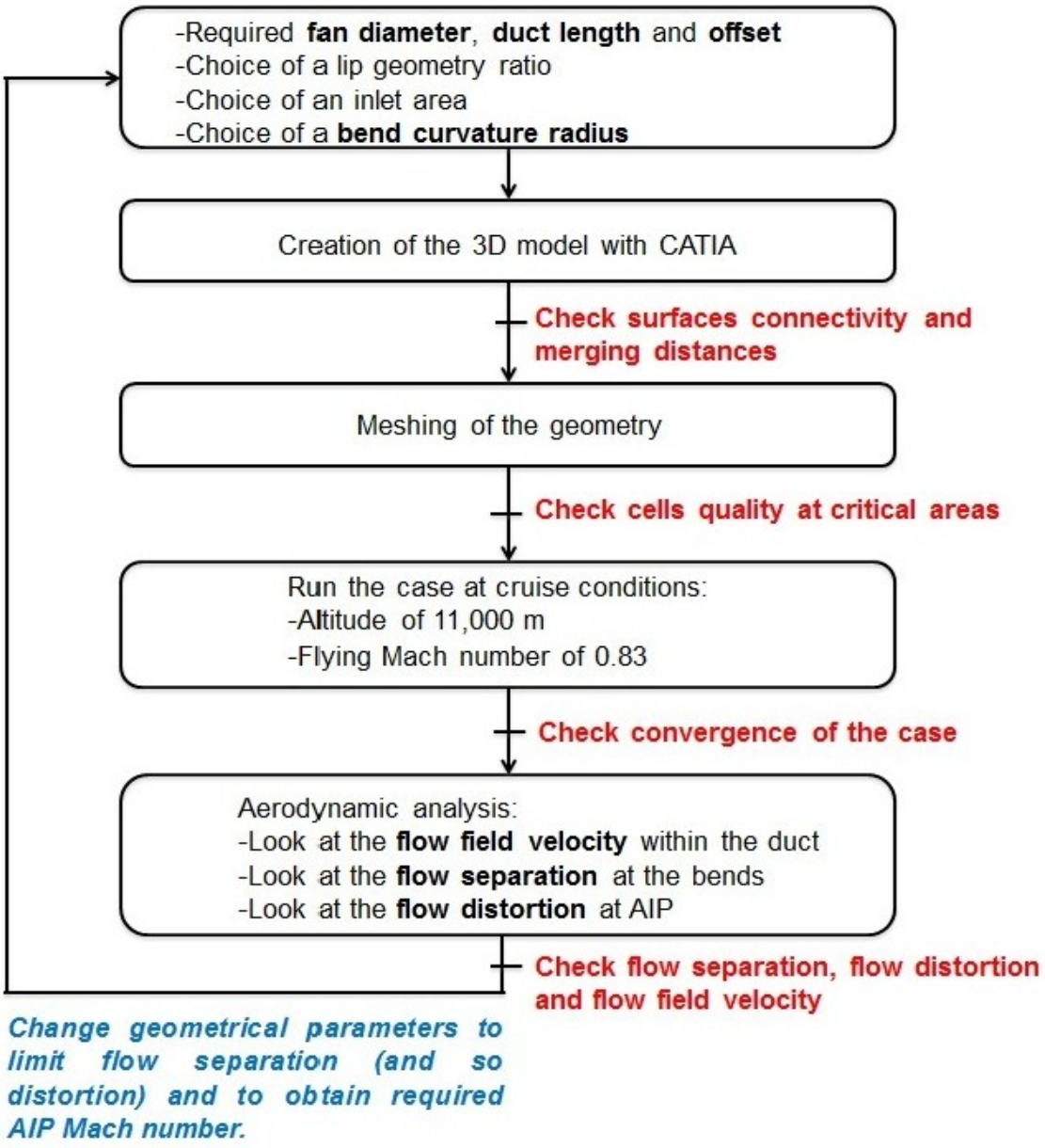

Figure 8.1 Propulsor Intake Design Method (Provided by Loic [76])

Flow distortion, refers to the intake exit flow distortion, is one of the other important parameters should be considered. NASA evaluated the maximum acceptable level of distortion is DC(60)=0.05 (DC(60) is the distortion parameter defined in Ref.81).

However, they found it is impossible to satisfy this constraint at aerodynamic design point with BLI. So they increased the value to 0.1 [78]. The DC(60) value obtained for the duct is 0.16, which is higher the acceptance value. A solution to this could be the use of vortex generators, which could be placed just before the bend of the duct. Previous studies [79] show by adding well designed vortex generators, distortion level can be reduced by 80%. So an advice for next step would be the designing of the S-duct with vortex generators.

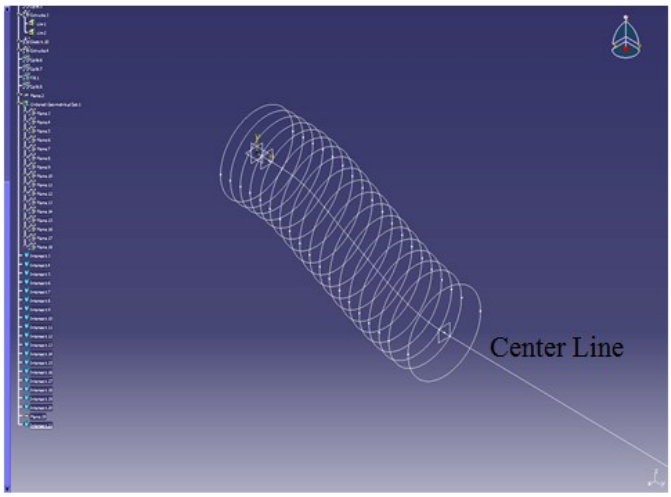

Figure 8.2 S-duct Design Cross Sections through the Centre Line (Provided by Loic) [76]

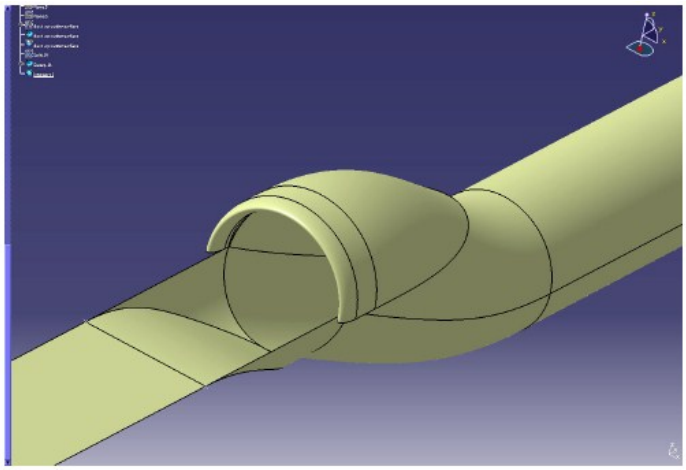

Figure 8.3 S-duct Geometry (Provided by Loic) [76]

8.2.2 Distortion Propagation through the Fan Stage

Distortion propagation refers to a three-dimensional (3D) distortion transfer calculation through a fan stage. The purpose is to include a detailed CFD simulation of the distortion transfer across the fan stage to estimate impacts of BLI. For the 3D problem, the model must address the following questions:

- What is an appropriate way to describe the inlet flow
- How to include the impacts of exit nozzle area
- How to design fan blade stage
- Which CFD model should be used
- What is the appropriate calculation domain

Fig.8.4 shows the computational domain. The code, therefore, requires the geometry of the duct, the shape of the fan stage, the number of blades, the shaft speed, and the inlet stagnation temperature and pressure profiles. Body force analysis can be employed to carry out the calculation. The other issue concerns the flow downstream of the fan. The flow exits through a choked nozzle. An ideal nozzle (no losses) can be assumed to obtain the momentum flux at the Trefftz Plane. The ideal nozzle is assumed in which each stream tubes expand independently without interaction with the rest of the flow down to atmospheric pressure.

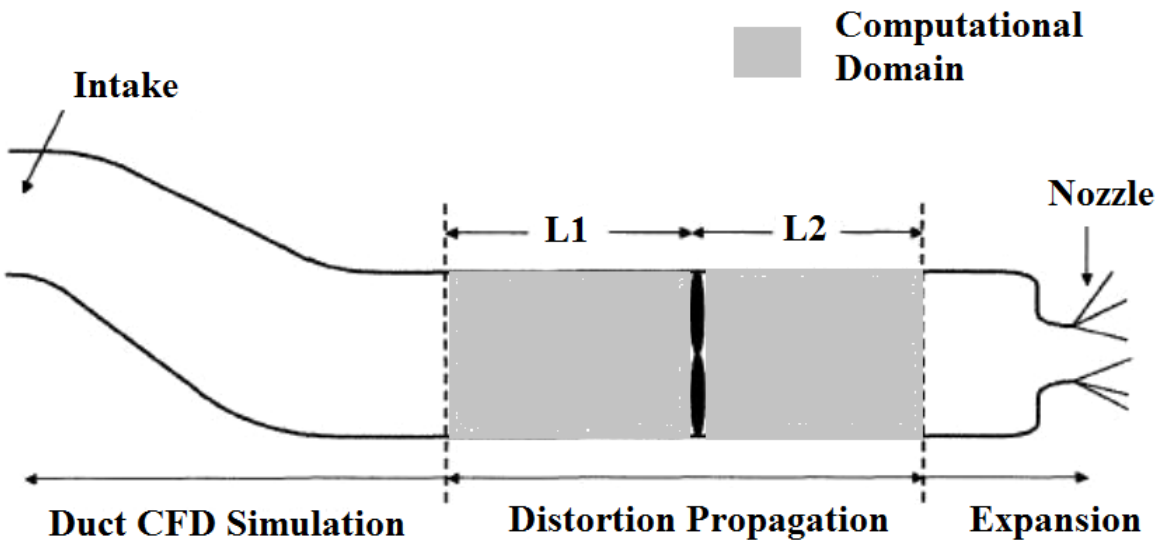

Figure 8.4 Sketch of the Simulation Domain for the Propulsor

8.2.3 Noise

The TeDP system developed by NASA targets three main objectives: reduced fuel consumption, emissions, and noise. So a model should be built to estimate the noise of the system on the N3-X aircraft. Regulations on noise are especially targeting at take-off and landing due to the proximity of habitations from airports. So there are three reference points for the noise measurements:

- Sideline: the microphone is placed on a parallel line at 450 meters from the center-line of the runway

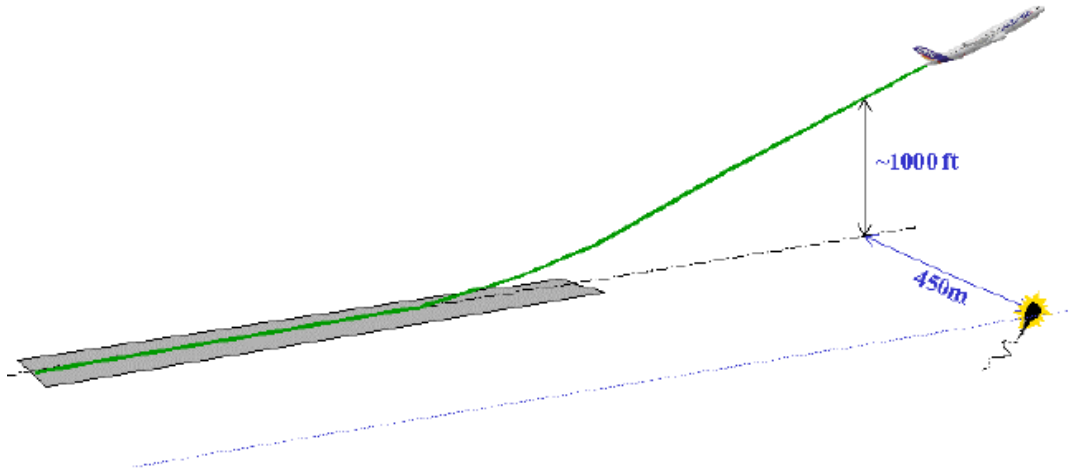

Figure 8.5 The Sideline Measure Point (Provided by C. Thomas) [77]

- Take-Off: the microphone is placed on the center-line of the runway, at a point 6,500m from the start of the rolling take-off.

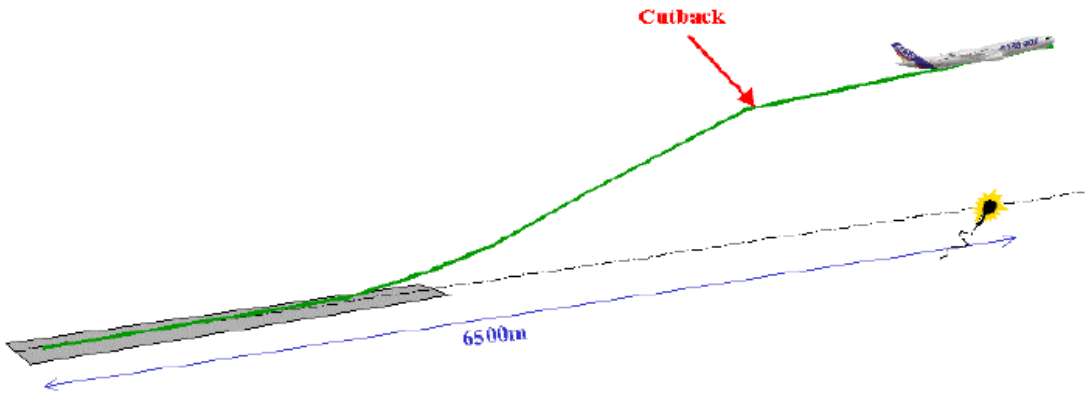

Figure 8. 6 The Take-off Measure Point (Provided by C. Thomas) [77]

- Approach: the microphone is placed at a point 2,000 meters from the threshold on the center-line of the runway.

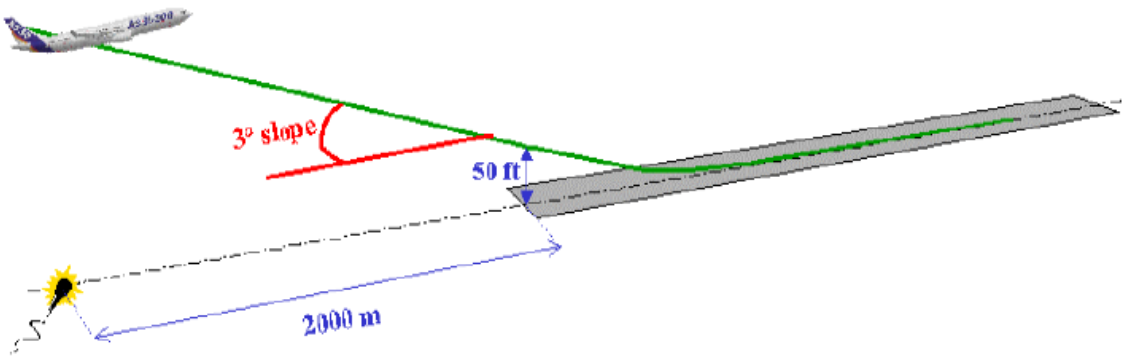

Figure 8. 7 The Approach Measure Point (Provided by C. Thomas) [77]

The Cranfield noise estimation code can be used in this sense. However, the code needs substantial effort to improve calculation of the intake, especially the intake is ingesting boundary layer. The first stage of work has been done with Thomas [77]. In our model, we chose RTO point as the main noise modeling point. Three different Turboshaft-driven TeDP systems (one with 14 propulsors, one with 15 propulsors, and one with 16 propulsors) were used. We found rearward fan noise is the main source of the propulsor noise. The noise level is independent with the number of propulsors, but increases with the increasing of propulsor fan pressure ratio. We also found that without using noise reduction methods, it is difficult to achieve the NASA's targets. However, in this study, the results for BLI were not precise. So, future works should address this problem.

8.2.4 Weight and Alternative Fuel

The weight estimation methods used in this thesis were based on correlations of current engines and motors. In such a way, the results were somewhat questionable for future propulsion system, especially for the superconducting devices and cooling system. The total weight of a propulsion system plays a key role in evaluating the system performances. Future studies should address this issue. The weight should include the weight of all the electric system, the cooling system, the core-engines, the propulsors, the engine nacelle, or even the fuel tank.

Liquid Hydrogen (LH2) has been proved to be an alternative fuel for propulsion system. The benefits include high power density, low emissions, and its ability to work as the cooling media for the TeDP system. Its disadvantages are its cost and the low energy density per volume. LH2 could be used in gas turbine without any

real change to the turbo-machinery [29], but the combustor and fuel system must be changed. Future studies should figure out these changes, as well as impacts on engine performances.

8.2.5 System Reliability Analysis

Many significant advances in technology have been applied to the TeDP system. These advanced technology improvements can be applied to achieve increased performance, useful life and reliability. However, comparing to the turbofan, new components have been added to the propulsion system. These include the free power turbine, the generator, the inverter, the cooling system, and the motor. So the firstly step is to analyze the reliability of these devices. Then, build a reliability block diagram for the TeDP system. Fig.8.8 shows a simplified example.

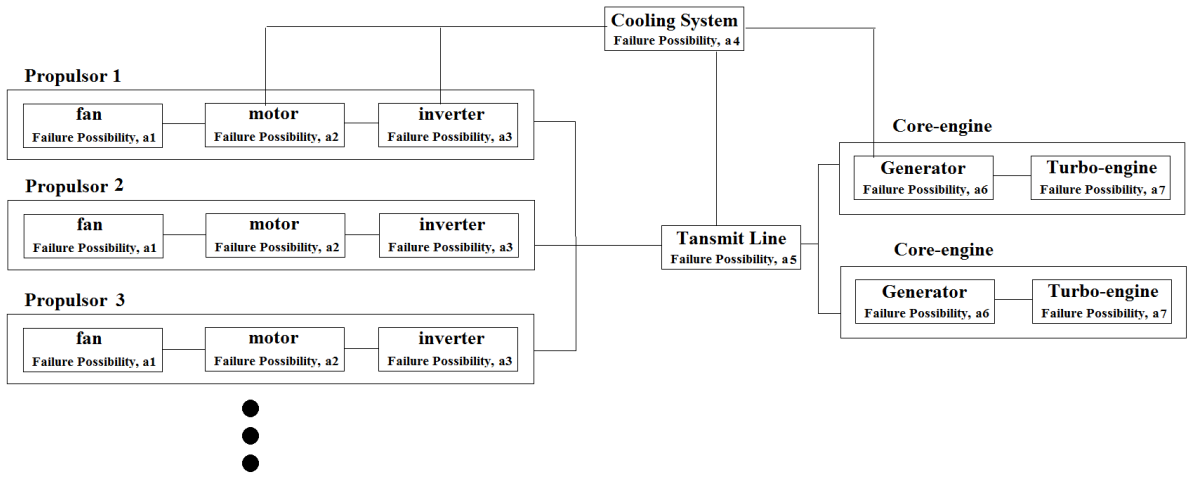

Figure 8.8 Reliability Block Diagram for the TeDP System

In this case, the possibility of both the core-engines are working under good conditions equal to:

$$[1-(1-a6)(1-a7)]^2 \tag{8-1}$$

The possibility of all the propulsors are working under good conditions equal to:

$$[1-(1-a1)(1-a2)(1-a3)]^N \tag{8-2}$$

Where *N* is the number of propulsors

So, without considering the cooling system, the overall system failure ratio is:

$$1 - [1 - (1 - a1)(1 - a2)(1 - a3)]^N \times (1 - a5) \times [1 - (1 - a6)(1 - a7)]^2 \qquad (8\text{-}3)$$

Eq.8.3 shows to improve reliability of the system, individual components should be improved as much as possible. Other method is reducing the number of propulsors. The cooling system is not included; this is because the failure of the cooling system won't directly cause the failure of the TeDP system. However, it will dramatically reduce performances of all the superconducting devices. Future studies should find method to merge the cooling system to the Eq.8.3 and evaluate how its failure connecting the failure of other components.

References

1. *A. Schilling et al. (1993). "Superconductivity above 130 K in the Hg–Ba–Ca–Cu–O system". Nature 363 (6424): 56. Bibcode:1993 Natur.363..56C.*
2. *Air Travel - Greener by Design: The Technology Challenge, (2001), , Greener by Design.*
3. *Alford, J. S., Davies, D. P. and Young, L. C. (19.), Inlet Duct - Engine Airflow Match and Compatibility for Supersonic Aircraft, 586C, SAE, USA.*
4. *Bibliographic data: GB720394 (A) — 1954-12-22, URL: http://worldwide.espacenet.com/publicationDetails/biblio?CC=GB&NR=720394 [cited 26 August 2013]*
5. *Brown, G. V. (2011), Weights and Efficiencies of Electric Components of a Turboelectric Aircraft Propulsion System , AIAA 2011-225.*
6. *C.A, Luongo, P.J, Masson, T, Nam, "Next generation more-electric aircraft: a potential application for HTS superconductors", IEEE, No.6, October 2008.*
7. *Chue, R., Hynes, T. P., Greitzer, E. M., Tan, C. S. and Longley, J. P. (1989), "Calculations of inlet distortion induced compressor flow field instability", International Journal of Heat and Fluid Flow, vol. 10, no. 3, pp. 211-223.*
8. *CLEANSKY, Clean Sky Annual Implementation Plan 2011, URL: http://www.cleansky.eu/ [cited 26 August 2013]*
9. *Costi, F. (2012), INVESTIGATION ON BOUNDARY LAYER INGESTION EFFECTS ON A DUCTED AXIAL FAN FOR A DISTRIBUTED PROPULSION SYSTEM, MSc thesis, Cranfield University.*
10. *Crichton, D., Xu, L. and Hall, C. A. (2007), "Preliminary Fan Design for a Silent Aircraft", ASME, vol. 129, pp. 184-191.*
11. *Curnock, B., Yin, J., Hales, R. and Pilidis, P. (2001), "High-bypass turbofan model using a fan radial-profile performance map", Aircraft Design, vol. 4, no. 2–3, pp. 115-126.*
12. *Dang, T. Q. and Bushnell, P. R. (2009), "Aerodynamics of cross-flow fans and their application to aircraft propulsion and flow control", Progress in Aerospace Sciences, vol. 45, no. 1–3, pp. 1-29.*
13. *Dardis, W. and Mayhew, E. (1992), An Acceptance Process for the Evaluation of Inlet Distortion, AIAA 92-3918.*
14. *de la Rosa Blanca, E., Hall, C. A. and Crichton, D. (2007), "Challenges in the Silent Aircraft Engine Design", AIAA 2007-454, Jan. 2007, Reno, Nevada, 45th AIAA Aerospace Sciences Meeting and Exhibit, .*
15. *Denton, J. D. (1993), "Loss Mechanisms in Turbomachines", Journal of Turbomachinery, vol. 115, no. 4, pp. 621-656.*
16. *Douglas, J. F., Gasiorek, J. M. and Swaffield, J. A. (1995), Fluid Mehanic, 3rd ed, Longman Scientific & Technical.*

17. *Felder, J. L., Kim, H. D. and Brown, G. V. (2009), "Turboelectric Distributed Propulsion Engine Cycle Analysis for Hybrid-Wing-Body Aircraft", AIAA-2009-1132, presented at 47th AIAA Aerospace Sciences meeting, 5-8 January 2009, Orlando, Florida, USA, .*
18. *Fielding J. P. and Smith, H. Blended Wing Body Preliminary Design Study. Aerospace Vehicle Design Postgraduate Project, Aerospace Design Group, Cranfield University.*
19. *Felder, J. L., Kim, H. D. and Brown, G. V. (2011), "An Examination of the Effect of Boundary Layer Ingestion on Turboelectric Distributed Propulsion Systems ", AIAA-2011-300, 4-7 January 2011, Orlando， Florida, 49th AIAA Aerospace Sciences Meeting including the New Horizons Forum and Aerospace Exposition, .*
20. *Felder, J. L., Tong, M. T. and Chu, J. (2012), Seneitivity of Mission Energy Concumption to Turboelectric Distributed Propulsion Design Assumptions on the N3-X Hybrid Wing Body Aircraft, AIAA 2012-3701.*
21. *Fleming, J., Anderson, J., Ng, W. and Harrison, N. (2005), Sensing and Active Flow Control for Advanced BWB Propulsion-Airframe Integration Concepts, NASA/CR-2005-213919.*
22. *George C. Asbby, (1987), Investigation of The Effect of Velocity Diagram Parameters on Inlet Total-Pressure Distortions Through Singh-Stage Subsonic Axial-Flow Compressor, CR-53745, NASA.*
23. *Gohardani, A. S., Doulgeris, G. and Singh, R. (2011), "Challenges of future aircraft propulsion: A review of distributed propulsion technology and its potential application for the all electric commercial aircraft", Progress in Aerospace Sciences, vol. 47, no. 5, pp. 369-391.*
24. *Hall, C. A. and Crichton, D. (2005), "Engine And Installation Configurations For A Silent Aircraft", 17th International Symposium on Airbreathing Engines, .*
25. *Harry, D. P. and Lubick, R. J. (1955), Inlet-Air Distortion Effects on Stall, Surge, and Acceleration Margin of A Turbojet Engine Equipped with Varable Compressor Inlet Guide Vanes, NACA RM E54K26.*
26. *Hileman, J. I., Spakovszky, Z. S., Drela, M. and Sargeant, M. A. (2007), "Airframe Design for Silent Aircraft", Vol. AIAA-2007-453, Jan. 2007, Reno, Nevada, 45th AIAA Aerospace Sciences Meeting and Exhibit, .*
27. *Hirai, K., Kodama, H., Nozaki, O., Kikuchi, K., Tamura, A. and Matsuo, Y. (1997), Unsteady Three - Dimensinal Analysis of Inlet Distortion in Turbumachinery, AIAA 97-2735.*
28. *Hostetler, G. W. (1965), Prediction of Off Design Performance of Multistage Compressor, , United States Navy.*
29. *Jackson, A. J. B. (2009), Optimisation of aero and industrial gas turbine design for the environment, Cranfield PhD Thesis.*
30. *Kawai, R., Brown, D., Roman, D. and Olde, R. (Oct. 2008), Acoustic Prediction Methodology and Test Validation for an Efficient Low-noise Hybrid Wing Body*

Subsonic Transport, NASA Contract NNL07AA54C, Phase 1 Final Thesis PWDM08-006A.

31. *Kim, H. D. and Berton, J. J. (2006), Cruise-Efficient, Low-Noise, Short-Takeoff-and-Landing Vehicle Studied for the Revelutionary System Concepts for Aeronautics Project, , Revolutionary System Concepts for Aeronautics, NASA, USA.*
32. *Kim, H. D. and Felder, J. L. (2011), "Control Volume Analysis of Boundary Layer Ingesting Propulsion Systems With or Without Shocked Wave Ahead of the Inlet", 4-7 Jan., 49th AIAA Aerospace Sciences meeting, Orlando, Florida, .*
33. *Kim, H. D., Berton, J. J. and Jones, S. M. (2006), "Low Noise Cruise Efficient Short Take-off and Landing Transport Vehicle Study", Vol. AIAA-2006-7738, Sep. 2006, Wichita, Kansas, 6th AIAA Aviation Technology, Integration and Operations Conference (ATIO), .*
34. *Kim, H. D., Brown, G. V. and Felder, J. L. (2008), "Distributed Turboelectric Propulsion for Hybrid Wing Body Aircraft", July 2008, London, United Kingdom, 9th International Powered Lift Conference, UK, .*
35. *Leifsson, L., Ko, A., Mason, W. H., Schetz, J. A., Grossman, B. and Haftka, R. T. "Multidisciplinary design optimization of blended-wing-body transport aircraft with distributed propulsion", Aerospace Science and Technology, , no. 0.*
36. *Lewis Research Center. Aircraft propulsion. NASASP-259, Proceedings of a conference held at NASA Lewis Research Center, Cleveland, Ohio, November 18-19, 1970.*
37. *Liu, C., Doulgeris, G., Laskaridis, P. and Singh, R. "Thermal cycle analysis of turboelectric distributed propulsion system with boundary layer ingestion", Aerospace Science and Technology, , no. 0.*
38. *Liu, C., Doulgeris, G., Laskaridis, P. and Singh, R. (2013), "Thermal cycle analysis of turboelectric distributed propulsion system with boundary layer ingestion", Aerospace Science and Technology, vol. 27, no. 1, pp. 163-170.*
39. *Liu, N. Y. and Eddie Ng, Y. K. (2007), Compressor instability with integral methods, SpringerLink.*
40. *Lugo, V. M. (2010), Effects of Boundary Layer Ingestion and Thrust Vectoring in Distributed Propulsion, MSc thesis, Cranfield, UK.*
41. *Lytle, J. K. (2000), The Numerical Propulsion System Simulation: An Overview, NASA TM-2000-209915, USA.*
42. *Mason, P. G., Brown, G. V., Soban, D. S. and Luongo, C. A. (2007), "HTS machine as enabling technology for all-electric airborne vehicle", Supercond. Sci. Techno, vol. 20, pp. 748-756.*
43. *Masson, P. J., Soban, D. S., Brown, G. V., and Luongo, C. A. , "HTS Machines as Enabling Technology for All-Electric Airborne Vehicles," Superconductor Science & Technology, 20 (2007) 748–756.*
44. *Mazzawy, R. S. and Banks, G. A. (1976), Modeling and Analysis of the TF30-P-3 Compressor System with Inlet Pressure Distortion, NASA CR-134996.*

45. *Mazzawy, R. S., Fulkerson, D. A., Haddad, D. E. and Clark, T. A. (1978), F100(3) Parallel Compressor Computer Code and User's Manual Final Thesis, NASA CR-135388.*

46. *Melick, H. C. (1973), Analysis of Inlet Flow Distortion and Turbulence Effects on Compressor Stability, NASA CR 114577.*

47. *Milner, E. J. (1977), ANALYTICAL PREDICTION OF THE PERFROMANCE AND STABILITY OF A J85-13 COMPRESSOR WITH DISTORTED INLET FLOW, NASA TM X-3515.*

48. *NASA (ed.) (2008), NPAA Customer Desk User's Guide, .*

49. *Nichol, C. L. (2008), Silent Aircraft Initiative Concept Risk Assessment, NASA/TM-2008-215112.*

50. *Owen, A. K. (1992), A Comprarison of Predicted and Measured Inlet Distortion Flows in a Subsonic Axial Inlet FLow Compressor Rotor, NASA TM-105427.*

51. *Perkins D. BWB dual-fan system assessment. NASA internal study, 2004.*

52. *Plas, A. P., Sargeant, M. A., Madani, V., Crichton, D., Greitzer, E. M., Hynes, T. P. and Hall, C. A. (2007), "Performance of a Boundary Layer Ingesting (BLI) Propulsion system", Vol. AIAA 2007-450, 8-11 Jan. 2007, Reno, Nevada, AIAA, .*

53. *Randall, L. M. (1986), Importance of Air Induction System Design to Supersonic Aircraft, , USA.*

54. *Reyle W. Aircraft. United Kingdom Patent, 1,066,360; 1967.*

55. *Sagerser, D. A., Lieblein, s. and Krebs, R. P. (1971), Empirical Expressions for Estimating Length and Weight of Axial Flow Components of VTOL Power Plants, E-6191, NASA, Cleveland, Ohio, USA.*

56. *Schetz, J. A., Hosder, S., Dippold, V. and Walker, J. (2010), "Propulsion and aerodynamic performance evaluation of jet-wing distributed propulsion", Aerospace Science and Technology, vol. 14, no. 1, pp. 1-10.*

57. *Serovy, G. K. and Anderson, E. W. (1959), Method for Predicting Off-Design Performance of Axial-Flow Compressor Blade Rows, NASA TN D-110.*

58. *Shahrokhi, K. A. and Davis, M. W. (1995), Application of a Modefied Dynamic Compression System Model to a Low Aspect Ratio Fan: Effects of Inlet Distortion, AIAA-95-0301.*

59. *Sirignano, W. A. and Mehring, C. (1999), Review of Theory of Distortion and Disintegration of Liguid Steam, AIAA 99-3641.*

60. *Smith, L. H. (1991), Wake Ingestion Propulsion Benefit, AIAA-91-2007-CP.*

61. *Spakovszky, Z. S., van Schalkwyk, C. M., Weigl, H. J., Paduano, J. D., Suder, K. L. and Bright, M. M. (1999), "Rotating Stall Control in a High-Speed Stage With Inlet Distortion: Part II -- Circumferential Distortion", Journal of Turbomachinery, vol. 121, pp. 517-524.*

62. *Spakovszky, Z. S., Weigl, H. J., Paduano, J.D. van Schalkwyk, C.M., Suder, K. L. and Bright, M. M. (1999), "Rotating Stall Control in a High-Speed Stage With Inlet*

Distortion: Part I -- Radial Distortion", Journal of Turbomachinery, vol. 121, pp. 510-516.

63. *Superconductivity, URL: http://en.wikipedia.org/wiki/Superconductivity/ [cited 28 August 2013]*
64. *Taylor, J. B. (1967), Inlet duct-engine exhaust nozzle airflow matching for the supersonic transport, AIAA-67/574, AIAA, USA.*
65. *Tesch, W. A. and Steenken, W. G. (1976), Blade Row Dynamic Digital Compressor Program, NASA CR-134978.*
66. *Veres, J. P. (2009), Axial and Centrifugal Compressor Mean Line Flow Analysis Method, AIAA-2009-1641.*
67. *Wakayama, S. and Kroo, L. (1995), "Subsonic Wing Planform Design Using Multidisciplinary Optimization", Jul.-Aug, vol. 32, no. Journal of Aircraft, pp. 746-753.*
68. *Walsh, P. P. and Fletcher, P. (2004), Gas Turbine Performance, 2nd ed, Blackwell Science Ltd, United Kingdom.*
69. *Wenzel, L. M. and Blaba, R. J. (1977), Analysis of Dynamic Inlet Distortion Applied to a Parallel Compressor Model, NASA TM X-3522.*
70. *Won, M. J. (1990), Sear Level Static Calibration of a Compact Multimission Aircraft Propulsion Simulator With Inlet Flow Distortion, NASA TM-102838.*
71. *Xu, L. P. and Hall, C. A. (2006), "Preliminary Fan Design For a Silent Aircraft", vol. 129, no. Journal of Turbomachinery, ASME, pp. 184-191.*
72. *Yin, J., Hales, R., Pilidis, P. and Curnock, B. (2001), 2-Shaft High-Bypass Ratio Turbofan Performance Calculation Using A New 2-D Fan Model, AIAA 2001-3302.*
73. *Zlavog, G. and Eversman, W. (2008), "Turbofan duct liner design/optimization: A statistical method", Journal of Sound and Vibration, vol. 313, no. 3–5, pp. 433-448.*
74. *Longley, J.P. and Greitzer, E.M., 'Inlet Distortion Effects in Aircraft Propuslion System Integration' AGARD, pp. 6-1-6-18*
75. *Plas, A.P. 'Performance of a Boundary Layer Ingesting Propulsion System'(2006), MIT Master Final Thesis.*
76. *Flouriot, L. (2012), A CFD Simulation of an Inlet S-duct Used with Distributed Propulsion and Boundary Layer Ingestion, Cranfield MSc thesis, School of Engineering, Cranfield University.*
77. *Thomas, C. (2012), Impact of the Boundary Layer Ingestion on the Noise Generated by Distributed Propulsion Concept, Cranfield MSc Final Thesis, School of Engineering, Cranfield University.*
78. *Rodriguez, D. L., "A MULTIDISCIPLINARY OPTIMIZATION METHOD FOR DESIGNING BOUNDARY LAYER INGESTING INLETS," No. AIAA 2002-5665, American Institute of Aeronautics and Astronautics, 2002, Symposium on Multidisciplinary Analysis and Optimization.*
79. *Waithe, K. A., "Source term model for VG vane in N-S computer code," No. AIAA-2004-1236, American Institute of Aeronautics and Astronautics, January 2004. The 42nd AIAA Aerospace Sciences Meeting and Exhibit.*

80. CATIA-Wikipedia*, the free encyclopedia,* Available from: <http://en.wikipedia.org/wiki/CATIA>. [25 March 2014]

81. Plumley, R.E. (1990). *Unsteady Compressor Distortion Response and Compressor Instability*, MIT Master Thesis, School of Aeronautics and Astronautics, Massachusetts Institute of Technology, pp.19.